UNIVERSITAT DE BARCELONA

Composition, remodeling and dynamics of the CPEB RNP

Manuel Cañete Ríos

Aquesta tesi doctoral està subjecta a la llicència ***Reconeixement- NoComercial – CompartirIgual 4.0. Espanya de Creative Commons***.

Esta tesis doctoral está sujeta a la licencia ***Reconocimiento - NoComercial – CompartirIgual 4.0. España de Creative*** **Commons**.

This doctoral thesis is licensed under the ***Creative Commons Attribution-NonCommercial-ShareAlike 4.0. Spain License***.

Universitat de Barcelona
PhD Thesis

Composition, remodeling and dynamics of the CPEB RNP

Manuel Cañete Ríos

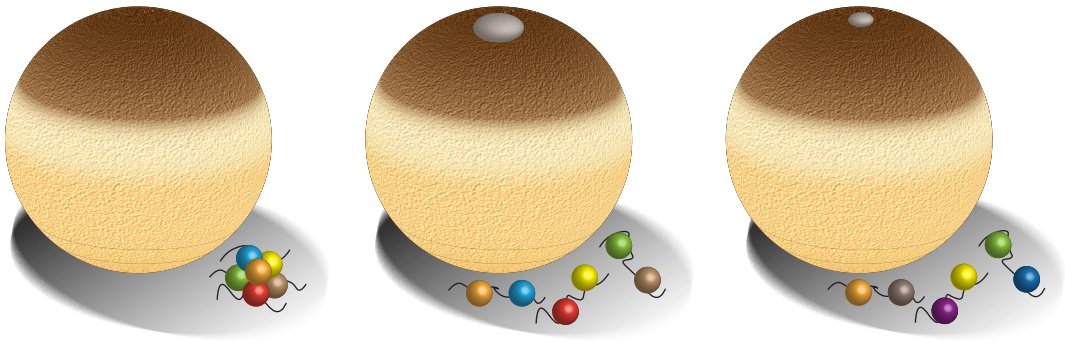

Barcelona, November 2020

UNIVERSITAT DE BARCELONA

IRB BARCELONA
INSTITUT DE RECERCA BIOMÈDICA

UNIVERSITAT DE BARCELONA
FACULTAT DE BIOLOGIA
PROGRAMA DE DOCTORAT GENÈTICA

Composition, remodeling and dynamics of the CPEB RNP

Memòria presentada per Manuel Cañete Ríos per optar al grau de doctor per la Universitat de Barcelona.

Aquesta tesi ha estat realitzada sota la direcció del Dr. Raúl Méndez a l'Institut de Recerca Biomèdica de Barcelona.

Raúl Méndez	Gonzalo Fernández-Miranda	Gemma Marfany	Manuel Cañete
Director de tesi	Co-director de tesi	Tutora de tesi	Doctorand

Barcelona, 2020

A mis padres...

七転び八起き

Japanese proverb

Contents

List of abbreviations **i**

Abstract **v**

Introduction **1**

mRNAs: at the crossroads of gene expression 3

The Central Dogma of Molecular Biology 3

pre-mRNA nuclear processing 4

mRNA features 7

Translation: from the message to the product 10

Translation initiation 10

Translation elongation 12

Translation termination and ribosome recycling 12

Bridging the edges: the closed-loop model 14

Translational control of gene expression 15

Global control of gene expression 16

mRNA-specific control of gene expression 17

mRNA localization 19

Mechanisms of mRNA decay 21

Prunning the 3'-end: mRNA deadenylation 22

Cytoplasmic polyadenylation 24

Translational control by the CPEBs 27
The CPEB family of proteins 27
The cytoplasmic polyadenylation element 29
CPEBs role in translational repression 31
CPEBs role in translational activation 35
CPEBs and phase separation 37
Principles of phase separation 37
Phase separation and disease 41
State-of-the-art of CPEBs phase separation 42

Research aim and objectives **45**

Results **49**

Development of a BioID protocol for frog oocytes 51
Extensive biotinylation is achieved after 40h incubation . . . 51
On-bead digestion facilitates release from streptavidin columns 53
Data analysis and hits selection 55
CPEB1 repression complex in stage VI oocytes 58
BioID of wild-type CPEB1 58
CPEB1 repression complex formation requires RNA binding 64
CPEB1 potentially recruits repression factors through the NTD 67
CPEB1-4 share a core of interactors in stage VI oocytes 70
CPEB1 activation complex in maturing oocytes 74
Sequence analysis suggests different features for the CPEBs 78
CPEB1 biomolecular condensation in vivo 81
CPEB1 forms round cytoplasmic foci in U-2 OS cells 81
CPEB1 foci are formed by liquid-liquid phase separation . . . 86
Comparison of CPEB1-4 phase separation properties 90
CPEB2 and CPEB3 phase separate in U-2 OS cells 90

CPEB1-4 NTDs have different propensity to undergo phase separation 93
CPEBs co-localize in the same biomolecular condensates . . . 95
CPEB1-4 droplets move differently within the cytoplasm . . 101

Discussion **105**
Revisiting CPEB1-mediated translational control 107
Novel players in CPEB1-mediated repression 107
Liquid-liquid phase separation ensures CPEB-mediated repression 110
Extensive modification of CPEB mRNP factors ensures the switch to translational activation 112
Phase separation exerts evolutionary pressure on CPEBs 116
CPEBs phase separate in the oocyte as clients of other factors 117
CPEB1-4 may not be redundant in stage VI oocytes 118
Limitations and perspectives 121
Limitations studying the CPEB mRNP composition and remodeling 121
Limitations in the study of the CPEB mRNP dynamics . . . 122

Conclusions **125**

Materials and methods **129**
Cloning strategies and RNA production 131
Cloning, subcloning and mutagenesis 131
In vitro transcription and polyadenylation 132
Oocyte manipulation and samples immunoblotting 135
Oocyte obtention, microinjection and enucleation 135
Immunoblotting 136
BioID approach methods 137

Identification of endogenously biotinylated proteins 137
BioID labeling and affinity purification 139
Mass spectrometry of BioID samples 140
BioID data analysis 141
Validation of BioID candidate proximal proteins 142
Cells manipulation 142
Cell culture and transfection 142
Cell harvesting 143
Cell fixation and mounting 144
Imaging methodologies 144
GFP distribution in fixed cells 144
Co-localization 145
Fixed cells image analysis 145
Live cell imaging 146
Fluorescence recovery after photobleaching 146

References **149**

Appendix **181**
Appendix I: BioID tables 183
Appendix II: Cloned CPEB1-4 sequences 199

Acknowledgements **201**

List of abbreviations

2'-O-Me	2'-O-methylation
4E-BPs	4E-binding proteins
A site	acceptor site
APA	alternative polyadenylation
ARE	AU-rich elements
ATP	adenosine triphosphate
AurkA	Aurora Kinase A
BFDR	bayesian false discovery rate
BioID	proximity-dependent biotinylation assay
BirA	biotin ligase
BSA	bovine serum albumin
CBC	cap-binding complex
Cdk1	cyclin-dependent kinase 1
cDNA	complementary DNA
CDS	coding sequence
CLIP	cross-linking immunoprecipitation
co-IP	co-immunoprecipitation
CPE	cytoplasmic polyadenylation element
CPEB	cytoplasmic polyadenylation element-binding protein
CPSF	cleavage and polyadenylation specificity factor
CstF	cleavage stimulation factor
CTD	C-terminal domain
Da	Dalton
DAPI	4,6-diamidino-2-phenylindole
DAZL	deleted in azoospermia-like protein
DMEM	Dulbecco's modified eagle medium

DNA	Deoxyribonucleic acid
E site	entry site
eEF	eukaryotic elongation factor
eIF	eukaryotic initiation factor
ER	endoplasmyc reticulum
eRF	eukaryotic release factor
ERK2	extracellular signal-regulated kinase 2
FBS	fetal bovine serum
FC	fold-change
FDR	false discovery rate
FRAP	fluorescence recovery after photobleaching
GEF	guanine nucleotide exchange factor
GFP	green fluorescent protein
GLD2	germ-line determinant 2
GTP	guanosine triphosphate
GV	Germinal vesicle
GVBD	Germinal vesicle breakdown
HA	hemagglutinin
HEX	hexanucleotide
hnRNP	heterogeneus nuclear ribonucleoproein
HRP	horseradish peroxidase
IDP	intrinsically disordered protein
IDR	intrinsically disordered region
IP	immunoprecipitation
IRES	internal ribosome entry site
LC	liquid chromatography
LCD	low-complexity domain
LLPS	liquid-liquid phase separation

lncRNA	long non-coding RNA
m6A	N6-methyl-adenosine
m7G	7-methyl-guanosine
MBE	Musashi-binding element
MBS	Modified Barth's Saline
MI	metaphase I
MII	metaphase II
miRISC	microRNA-induced silencing complex
miRNA	microRNA
MoRF	molecular recognition feature
mRNA	messenger RNA
mRNP	messenger ribonucleoprotein
MS	mass spectrometry
nt	nucleotides
NTD	N-terminal domain
Orb	oo18 RNA -binding protein
ORF	open reading frame
P site	peptidyl site
PABP	poly(A)-binding protein
PAGE	polyacrylamide gel electrophoresis
PARN	poly(A)-specific ribonuclease
PAS	polyadenylation signal
PB	processing body
PBE	Pumilio-binding element
P-body	processing body
PBS	phosphate buffer saline
PCR	polymerase chain reaction
Pg	progesterone

PI	prophase I
Plk1	Polo-like kinase 1
poly(A)	polyadenosine
PONDR	predictor of natural disordered regions
pre-mRNA	precursor mRNA
PTM	post-translational modification
RBP	RNA-binding protein
RNA	ribonucleic acid
RNAPII	RNA-polymerase II complex
RNP	ribonucleoprotein
RRM	RNA recognition motif
SAINT	significance analysis of interactome
SDS	sodium dodecyl sulphate
Ser	serine
SG	stress granule
SLiM	short linear interaction motif
snRNP	small nuclear ribonucleoprotein
SUMO	small ubiquitin-like modifier
TCS	translational control sequence
tRNA	transfer RNA
uORF	upstream open reading frame
UTR	untranslated region
WB	western blot

Abstract

Xenopus laevis oocytes are transcriptionally silent cells that require hormone stimulation for maturing into fecundation-competent eggs. Meiosis resumption underlying oocyte maturation is governed by sequential waves of protein synthesis, which in these cells is promoted by cytoplasmic polyadenylation, a mechanism that has been mostly studied for the CPEBs. CPEBs are a family of RNA binding proteins that can both promote translational repression in quiescent cells and translational activation in maturing oocytes. This dual activity has been shown to be regulated by post-translational modifications that impact on their interactome, stability and aggregation properties.

Several studies have addressed the composition of the CPEB complexes in stage VI oocytes and their remodeling upon hormone stimulation. However, these studies show inconsistent and mutually exclusive results. In this regard, we have tailored an adaptation of the BioID methodology to identify the *in vivo* interactors of the CPEBs in both contexts. With this approach we have established novel links between the CPEBs and machineries associated to miRNA translational control, adenosine methylation and the CCR4-NOT complex. In addition, we show that all four CPEBs have a similar interactomic landscape in stage VI oocytes, though they have also interesting specificities.

To add another layer of complexity, we have characterized the phase separation properties of the four CPEBs, a principle that is becoming increasingly relevant in all the processes regulating gene expression. We have found that CPEB1 has clearly different LLPS properties compared to CPEB2-4, even though these three paralogs have also different material properties that need to be further addressed. We propose that these differences explain why there are four CPEBs with non-redundant functions in higher organisms.

Our findings pave the way for more specific research focused on the potential links between the CPEBs and other master translational regulators, both in repression and activation, as well as provide a starting point for a deeper understanding on how the composition and material properties of a condensate impact translational control.

Introduction

mRNAs: at the crossroads of gene expression

The Central Dogma of Molecular Biology

A living organism is described as an open system that uses the gradients found in the environment to create imperfect replicates of itself (Prigogine et al., 1972). This definition of life already associates the biological processes characteristic of any living organism (metabolism, growth, adaptation, reproduction...) with a flux of information. For biological systems, as for modern societies, information is the most valuable resource and, consequently, mechanisms have been developed for its writing, storing, reading, transfer, surveillance and even hijacking.

Although it may be surprising for people my age, who have grown up in the boom of the post-genomic era, what we all know as the Central Dogma of Molecular Biology was defined not so many years ago (Crick, 1970). The Central Dogma establishes a flux of information that has allowed us to understand the molecular mechanisms underlying several experimental observations (Horowitz et al., 1945) as well as it has served as a framework for the development of fundamental models that are broadly accepted nowadays.

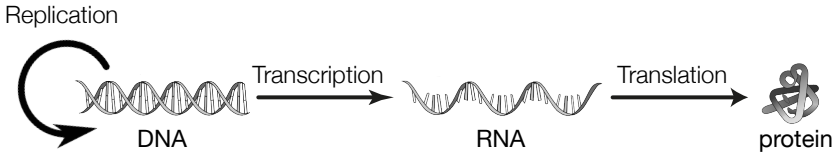

Figure 1: Central Dogma of Molecular Biology. The Central Dogma establishes the flux of information from DNA to proteins. Although it has been revisited several times since its definition (i.e. incorporating non-coding RNA molecules), it stills serves as a conceptual framework for gene expression.

As a consequence of the development of Molecular Biology techniques such as the well-known PCR, there has been an eruption in the last years of valuable experimental data

regarding the control of gene expression at the genomic and transcriptomic level. Some instances of this are public research projects like the Human Genome Project, the ENCODE Project and the 1000 Genomes Project, which have permitted the identification and characterization of important transcription factors and their cognate binding sites, transcription enhancers and start sites, chromatin architecture and modifications and also the identification of genetic variants that explain biological variability and disease.

Despite the advances in this field, historically less effort has been devoted to better understand the processes downstream RNA synthesis. In the recent years though, thanks to the development of methodologies including RNA immunoprecipitation, ribosome profiling, CLIP, RNA interactome capture..., post-transcriptional control of gene expression has been more broadly studied in a variety of contexts (cancer, inflammation, metabolism, memory acquisition...).

In this first section we will focus on the mRNA molecule, specially on its synthesis and processing in the nucleus as well as the molecular features that characterize it.

pre-mRNA nuclear processing

Transcription and the main pre-mRNA processing steps are physically and functionally coupled (Zhao, 2002; Soop, 2003). This coupling is mediated by the C-terminal domain (CTD) of the largest subunit of the RNA polymerase II complex (RNAPII), which acts as an interaction hub for several transcription and mRNA processing factors (Fong, 2001; Buratowski, 2005). While an mRNA is being transcribed it is concomitantly associated with mRNA binding proteins that will determine its processing, nuclear export, subcellular localization, translation and stability (Aguilera, 2005). Overall, maturation of a pre-mRNA involves its 5'-end capping, splicing and 3'-end cleavage and polyadenylation. Importantly, correct pre-mRNA processing is critical for generating stable and functional mRNAs (Ghosh and Lima, 2010).

The first step in pre-mRNA processing occurs as soon as the first 22-25 nucleotides of the nascent mRNA emerge from the exit channel of the RNAPII complex (Aguilera, 2005). At this moment, the RNA molecule is capped in three sequential steps by the Hce1 and Hcm1 enzymes with the well-known 7-methyl-guanosine cap (m7GpppRNA) (Moteki and Price, 2002; Ramanathan et al., 2016). The m7G cap, which is essential for recognition by the cap-binding complexes in the nucleus and the cytoplasm, contributes significantly to mRNA splicing (Edery and Sonenberg, 1985), nuclear export (Goodfellow and Roberts, 2008; Carmody and Wente, 2009), translation (Shatkin and Manley, 2000; Fischer, 2009) and stability (Shimotohno et al., 1977).

Even though it can also occur uncoupled to transcription (Kornblihtt, 2004), it is well established that the removal of introns from the pre-mRNA and the subsequent ligation of the flanking exons, a process called splicing, occurs co-transcriptionally (Kotovic et al., 2003). Indeed, the nuclear cap-binding complex (CBC) favors the assembly of the splicing-commitment complex on the cap proximal intron by facilitating the recruitment of the small nuclear ribonucleoprotein (snRNP) core spliceosome components, such as U1 snRNP. Remarkably, the deposition of the exon-junction complex on the spliced molecule has a vital contribution to the formation of mRNPs and marks the mRNA for downstream processing steps (Wahl et al., 2009).

Genome-wide studies estimate that 90-95% of human genes undergo some level of alternative splicing. This process is a ubiquitous regulatory mechanism of gene expression that allows the generation of more than one unique mRNA species from a single gene (Papasaikas et al., 2015), as it can make mRNA species differ in their untranslated regions or coding sequence by mechanisms that involve exon skipping, use of alternative splice sites, choice between mutually exclusive exons and intron retention (Baralle and Giudice, 2017). Alterative splicing of mRNA molecules can have also an impact on mRNA stability, localization and/or translation.

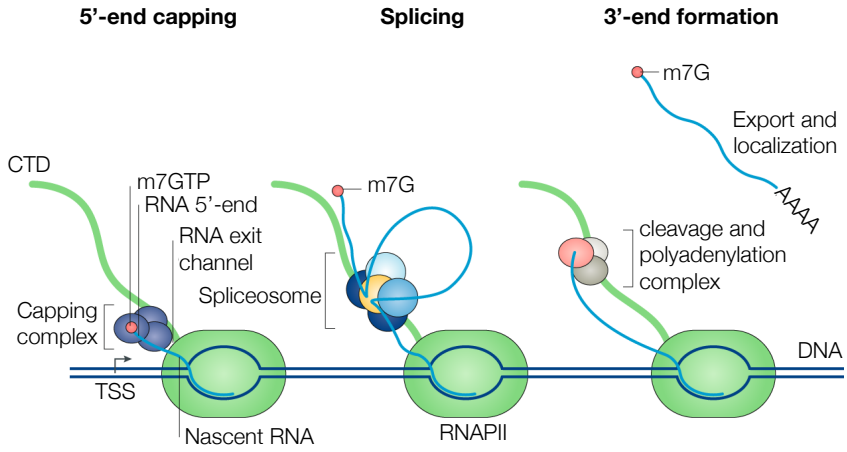

Figure 2: Nuclear pre-mRNA processing. While an mRNA is being transcribed, it is concomitantly modified in its 5'- and 3'-ends by capping and cleavage and polyadenylation. Also, introns and alternatively spliced exons are removed and the mRNA is coated with proteins that will determine its stability, localization and fate. Picture adapted from Desterro et al. (2020).

The last step in pre-mRNA maturation is 3'-end processing. With the exception of replication-dependent histone transcripts (Marzluff et al., 2008), the maturation of eukaryotic mRNA 3'-ends involves an endonucleolytic cleavage followed by synthesis of a 250 nucleotides-tail onto the upstream cleavage product in a template independent manner (Millevoi and Vagner, 2010; Eckmann et al., 2011; Jurado et al., 2014). The assembly of the 3'-end processing complex begins with the cooperative interaction of the CPSF and CstF complexes with the hexanucleotide or polyadenylation signal (PAS) (Proudfoot, 2011) and the downstream sequence element, a U/GU-rich region, respectively. Importantly, the formation of this complex also relies on the CTD of the RNAPII complex and the capped 5'-end (Darnell, 2013). Notably, polyadenylation impacts on many aspects of mRNA metabolism, especially transcription termination, mRNA stability, nuclear export and translation.

Similar to the combinatorial potential of alternative splicing, alternative polyadenylation (APA) is also extensively used to regulate gene expression. In fact, around 50-

70% of human genes have been found to encode multiple transcripts derived from APA (Di Giammartino et al., 2011; Elkon et al., 2013). Alternative usage of poly(A) signals can either generate transcripts with 3' untranslated regions (UTRs) of different length, when APA occurs at the 3' end, or can even produce different protein isoforms, when the selected PAS is located in internal introns/exons. Consequently, alternative polyadenylation as well has an impact on mRNA localization, stability and translation (Bava et al., 2013).

Finally, RNA molecules can also be post-transcriptionally modified by a collection of more than 100 distinct chemical modifications (Machnicka et al., 2012). The addition or removal of these chemical moieties is reversible, highly dynamic and context-dependent, forming what is known as the epitranscriptome. RNA modifications can occur in the base, the ribose or both, and have been shown to affect RNA stability, function and translation by direct and indirect mechanisms (Kuge, 1998). Direct effects are mediated by changes in the physicochemical properties of the RNA molecules, which can trigger restructuration of their secondary structure, while indirect effects are mediated through increased or reduced affinity for a certain group of RNA binding proteins, the modification readers (Liu et al., 2015; Zhao et al., 2017).

mRNA features

The mature mRNA can be dissected into two untranslated regions, at the 5'- and 3'-ends, and the coding sequence in between. Importantly, an mRNA is neither a linear nor a naked molecule, for it is coated by a plethora of RNA binding proteins (RBPs) throughout its lifetime and it is also able to acquire secondary and tertiary structures, altogether vital for determining its fate. It is important to mention that the 3'-UTR of an mRNA is the only region that is not swept by the ribosome, as there is no scanning through this region in normal conditions.

The 5'-end of most of the eukaryotic mRNAs, with the exception of the few mitochondrial genes (Montoya et al., 1981), harbors not only the 5' cap but also an untranslated sequence, with a median length of 53-218 nucleotides, that works as a loading platform for the ribosome. Ribosomes recruited to the mRNAs scan the 5'-UTR sequences until they reach the start codon, though genes with an extremely short 5'-UTR can undergo translation by scanning-free initiation (Mignone et al., 2002; Haimov et al., 2015).

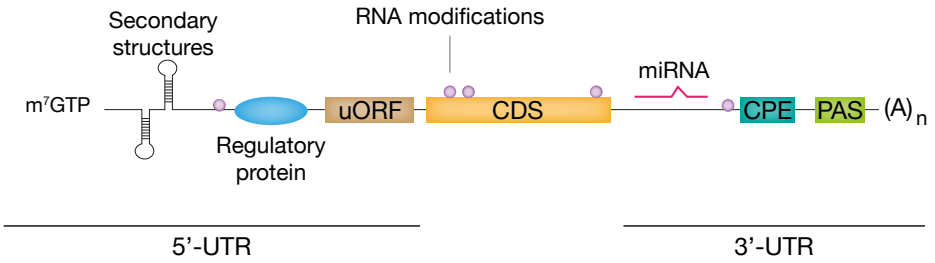

Figure 3: Collection of mRNA features. The untranslated regions of an mRNA are hubs of regulatory elements, secondary structures and chemical modifications. The integration of these signals decides the fate of the transcript.

Highly structured 5'-UTRs, containing folded domains such as hairpins, RNP complexes, RNA G-quadruplexes or pseudoknots, impair the recruitment of the ribosome required for cap dependent translation (Leppek et al., 2018). Interestingly, other folded regions (i.e. internal ribosome entry sites or IRES) can favor cap-independent translation in contexts where cap-dependent translation is impaired (Holcik and Sonenberg, 2005) . The 5'-UTR is also a platform for RBPs and long non-coding RNAs that can control the translational status of their cognate mRNAs . In addition, RNA modifications at the 5'-UTR such as N^6-Methyladenosine (m^6A) can favor cap-dependent translation mediated by eIF3 (Zhao et al., 2017), and other possible mechanisms (Kuge, 1998), in certain cellular contexts. It is also worth mentioning the existence of upstream open reading frames (uORFs), which generally inhibit translation by limiting the access of ribosomes to the main start codon (Zhang et al., 2019).

As it is the case for the 5'-UTR, there has been an increase in 3'-UTR length during the development of higher organisms, suggesting a role for both of them in the regulation of biological complexity (Mayr, 2016, 2017). 3'-UTRs mediate in the regulation of mRNA localization (Martin and Ephrussi, 2009), stability, translation (Mendez and Richter, 2001) and, more recently described, protein-protein interactions (Ma and Mayr, 2018), largely by AU-rich elements and miRNA binding sites (Barreau, 2005; Bartel, 2009). These *cis* elements are recognized by RBPs in a sequence- or structure-dependent manner and recruit effector proteins that will determine the fate of the mRNA. Remarkably, the composition of RBPs bound to the 3'-UTR is dynamic and context-dependent.

Importantly, alternative splicing and alternative cleavage and polyadenylation generate mRNAs with different 3'-UTR length that can regulate differentially their fate (Bava et al., 2013). Notably, differentiated cells in later developmental stages tend to express mRNAs with longer 3'-UTRs, whereas highly proliferating cells tend to generate shorter ones (Ulitsky et al., 2012).

On the other hand, the coding sequence (CDS) is the only region that is translated into a protein sequence. Even though it does not have *cis* elements described to mediate in the regulation of the mRNA life, in the last years several studies have demonstrated that codon composition of the CDS can have an impact on the translation rate (Komar, 2009; Pechmann and Frydman, 2013; Schuller and Green, 2018). Recent works suggest that the coding region is also a platform for RNA modifications such as m^6A, 5-hydroxymethylcytosine, pseudouridine and 2'-O-methylation, which have been described to have a potential role in the regulation of mRNA processing, stability and translation (Roundtree et al., 2017).

Now that we have a nuanced view of a messenger RNA, we will dedicate the following section to translation, the process by which these messengers serve as templates for protein synthesis.

Translation: from the message to the product

Translation of an mRNA represents the final step in the gene expression pathway and is used to fine-tune protein levels in time and space. In the cell, mRNAs are generally distributed between an actively translated and a non-translated pool in the cytoplasm.

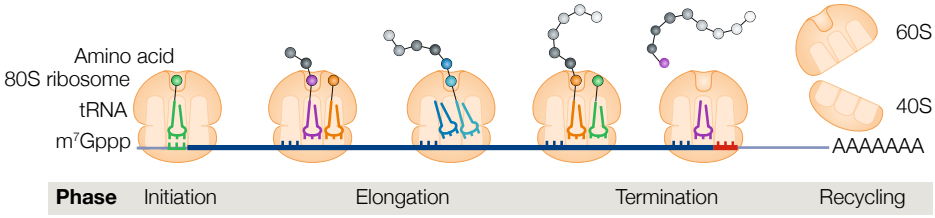

Figure 4: Overview of mRNA translation. The main steps in translation are initiation, elongation and termination. The proteins participating in each step are different and, specially for translation initiation, tightly regulated. Figure adapted from Schuller and Green (2018).

Translation initiation

There are several models for translation initiation, from cap-dependent translation to cap-independent mechanisms that rely on mRNA structural features (IRES), RNA modifications (m6A) or trans-acting factors (eIF3) (Leppek et al., 2018). For this section we will just focus on cap-dependent translation.

Translation initiation involves the positioning of an elongation-competent 80S ribosome at the start codon (AUG) . In the case of cap-dependent translation, the small ribosomal subunit (40S) assembles with the eukaryotic initiation factors eIF1, 1A, 3 and 5, and the ternary complex (composed of the initiator methionyl-tRNA (Met-tRNAi) and the GTP-bound form of eukaryotic initiation factor 2 (eIF2)) to form the 43S pre-initiation complex (Gebauer and Hentze, 2004; Hinnebusch and Lorsch, 2012; Shatsky et al., 2018). This complex associates with the 5'-cap structure by the interaction between eIF3 and the eIF4F protein complex, which contains the cap-binding protein eIF4E, the DEAD-box helicase eIF4A and the scaffolding protein eIF4G. Importantly,

eIF4G also interacts with poly(A)-binding protein (PABP), which in turn is bound to the poly(A) tail, and it is believed to cause the pseudocircularization of the mRNA molecule (Gallie, 1991). Though still in debate (Adivarahan et al., 2018; Khong and Parker, 2018), this conformation enhances ribosome recruitment, mRNA stability and ribosome recycling and provides a spatial framework in which the 3'-UTR binding factors can regulate translation initiation.

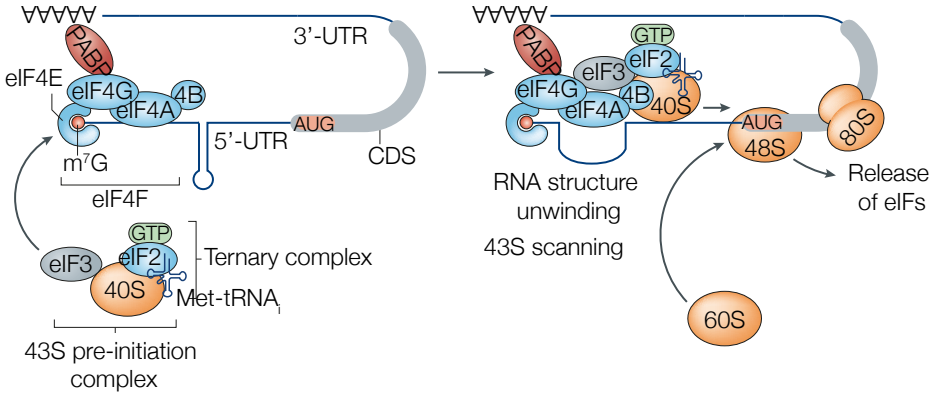

Figure 5: Overview of translation initiation. Cap-dependent initiation requires the formation of a 43S pre-initiation complex and its association with the eIF4F complex. Then, the 43S complex scans along the 5'-UTR until it reaches the start codon, which allows recruitment of the 60S subunit to form the 80S complex. Figure adapted from Leppek et al. (2018).

Once assembled, the 43S pre-initiation complex scans along the 5'-UTR in an ATP-dependent manner until it reaches and identifies the start codon (AUG) in an optimal context (Kozak, 2002). Binding of the 43S complex to this codon results in the formation of a stable complex known as the 48S initiation complex. Upon binding of the tRNA with the AUG, eIF2-bound GTP undergoes hydrolysis catalyzed by the GTPase-activating protein eIF5, which is necessary for the recruitment of the 60S subunit to form the 80S complex. This hydrolysis induces the release of most of the initiation factors, including eIF2-GDP, leaving the initiator tRNA base-paired with AUG at the P-site. Finally, GTP hydrolysis of eIF5B is stimulated by the ribosome and renders it competent for protein synthesis (Jackson et al., 2010; Hinnebusch and Lorsch, 2012).

Translation elongation

During elongation, ribosomes move processively along the mRNA molecule, codon by codon, synthesizing the encoded protein one aminoacid at a time (Schuller and Green, 2018). Translation elongation happens in three sequential steps: tRNA selection, peptide bond formation and translocation of the mRNA-tRNA complex. First, the codon-matching aminoacyl-tRNA is loaded into de A site of the ribosome by the eukaryotic elongation factor 1A GTPase (eEF1A) in a ternary complex with GTP (Carvalho et al., 1984); then, the peptide bond linking the nascent polypeptide with the aminoacid at the A site is formed by a nucleophilic attack assisted by eIF5A, hence transferring the growing peptide chain to the A site (Beringer and Rodnina, 2007). Translocation of the mRNA-tRNA complex to the next codon is assisted by the eEF2 GTPase, which allows the repetition of the elongation cycle until the ribosome reaches the stop codon (Shao et al., 2016).

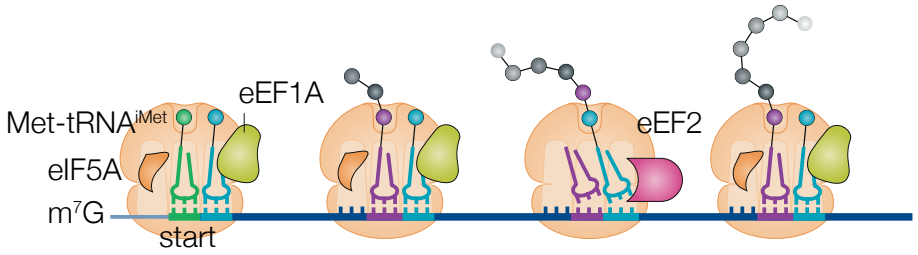

Figure 6: Overview of translation elongation. Elongation of the peptide sequence is mediated by a fully-competent 80S complex. This process consists of three sequential steps: tRNA selection by eEF1A, peptide bond formation by a nucleophilic attack and mRNA-tRNA translocation by eEF2. Figure adapted from Schuller and Green (2018).

Translation termination and ribosome recycling

Translation termination begins when the ribosome encounters a stop codon in the A site, a process that is assisted by the eukaryotic release factor 1 (eRF1), which has a strikingly similar shape to that of a tRNA and is also bound by the GTPase eRF3 (Song et al.,

2000; Schuller and Green, 2018). Upon engagement of the eRF1-eRF3 complex with the ribosome, eRF3 dissociates following GTP hydrolysis, which in turn poises eRF1 to coordinate a water molecule at the peptidyl-transferase center, thus hydrolyzing and releasing the nascent peptide from the peptidyl-tRNA and, ultimately, from the 80S ribosome (Frolova et al., 1999; Dever and Green, 2012).

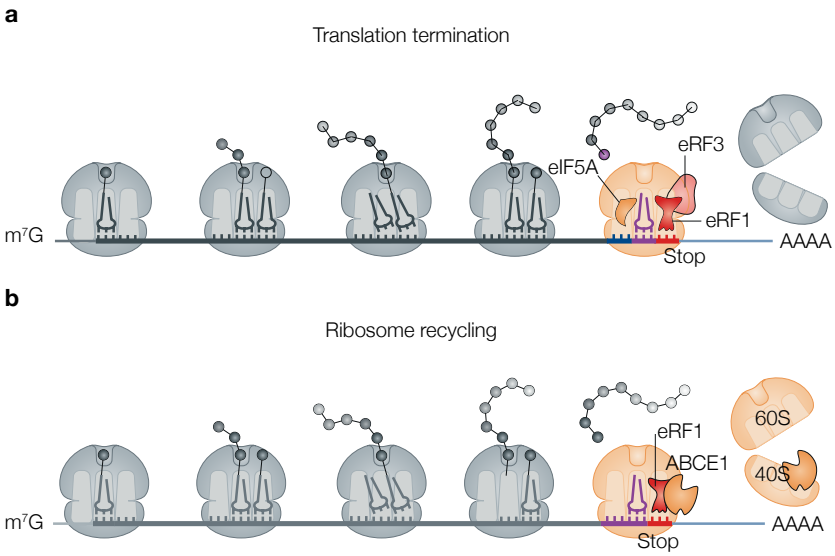

Figure 7: Overview of translation termination and ribosome recycling. (a) When the 80S complex encounters a stop codon, eRF1 hydrolyses and releases the nascent peptide assisted by eRF3-mediated GTP hydrolysis. (b) Ribosome recycling required for new rounds of translation is mediated by the ATPase ABCE1. Picture adapted from Schuller and Green (2018).

Once translation termination has been completed, the 80S complex containing a deacylated tRNA in the P site must be recycled into its 40S and 60S subunits. Ribosome recycling is attained by ABCE1, which uses the force generated by ATP binding and hydrolysis to dissociate the ribosomal subunits, assisted by eRF1 (Pisarev et al., 2010). Interestingly, ABCE1 could also have a role coupling translation termination with ribosome recycling in yeasts, as it stimulates peptidyl hydrolysis by eRF1 (Shoemaker and Green, 2011). Finally, the mRNAs and tRNAs must also be removed from the 40S subunit, potentially through the activity of ligatin or DENR proteins.

Remarkably, ABCE1 has been shown to interact with several initiation factors, and genetic depletion of this gene in yeast impairs the assembly of pre-initiation complexes. Therefore, it is likely that ABCE1 has an important role in connecting the sequential processes of ribosome recycling and translation initiation, which would underscore the importance of the pseudocircularization step required for translation to be initiated (Dong et al., 2004; Andersen and Leevers, 2007).

Bridging the edges: the closed-loop model

As mentioned earlier, the translation initiation factor eIF4G simultaneously binds eIF4E and PABP, hence linking the two ends of an mRNA molecule (Gallie, 1991). These interactions promote the pseudocircularization of the mRNA, which is suggested to stimulate translation initiation (by recruitment of eIF3 and eIF4A and increasing the interaction of eIF4E with the cap), inhibit decapping and assisting in ribosome recycling (Amrani et al., 2008; Sonenberg and Hinnebusch, 2009; Jackson et al., 2010; Tomek and Wollenhaupt, 2012). Remarkably, adoption of the closed-loop conformation would be facilitated by polyadenylation, as poly(A) strengthens the binding of PABP to EIF4G (Wells et al., 1998).

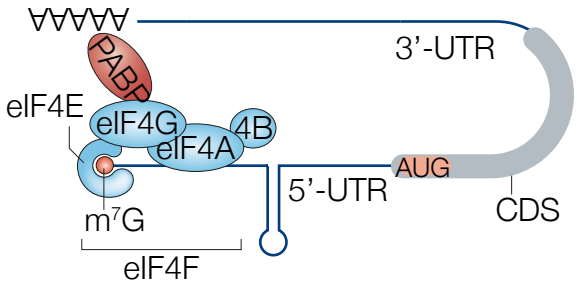

Figure 8: Closed-loop model conformation. Pseudocircularization of the mRNA has been postulated to play an important role in translation initiation. This conformation is attained by the interaction of both ends of the mRNA: on the 5'-end side the cap-binding complex eIF4E-eIF4G and on the 3'-end the poly(A) tail and PABP. Picture adapted from Leppek et al. (2018).

Despite the evidences for these interactions and the observations of circular conformations, specially *in vitro*, there are also works that compromise the validity of this model (Adivarahan et al., 2018; Khong and Parker, 2018). The more recent conception proposes a transient nature for the closed-loop conformation (once the ribosome has been recruited), which would conceal the fact that these interactions favor translation initiation with the fact that they haven't been observed *in vivo* and are not indispensable for cells. Alternatively, this model could also apply to only a subset of mRNA molecules. Nonetheless, it is important to stress that the integrity of the closed-loop conformation is allegedly a target of a number of factors that stimulate or inhibit translation (Stebbins-Boaz et al., 1999; Kim and Richter, 2006; Minshall et al., 2007).

We will dedicate the following section to the mechanisms that eukaryotic cells have developed for controlling gene expression by fine-tuning translation.

Translational control of gene expression

In eukaryotes, the nucleus physically separates transcription from translation, which has permitted the development of a complex post-transcriptional control system, largely absent in prokaryotes. The long lifetimes of the eukaryotic mRNAs, generally from hours to days, is another feature that allows tuning of translation rates and yields. Notably, global gene expression analyses in mammalian cells have revealed that translation efficiency is the best predictor of protein expression, thereby underscoring the importance of this last step in the gene expression flux.

It is vital to stress that, while almost every step of mRNA translation is target for regulation, translation initiation is the rate-limiting process and also the most complex one, hence being the main target for translational control mechanisms. For this reason, we will mainly focus on the regulation at this crucial step.

We will distinguish between those mechanisms that affect globally to translation and those that have an impact only on the translational status of a smaller set of genes. Other important aspects of translational control such as mRNA localization, decay and poly(A) tail length dynamics will be discussed as well.

Global control of gene expression

Global control of translation is generally attained by changes in the phosphorylation status of initiation factors or their regulators (Gebauer and Hentze, 2004; Hinnebusch and Lorsch, 2012), though proteolysis is implicated in some cellular contexts as well, such as viral infections or apoptosis (Sonenberg and Hinnebusch, 2009).

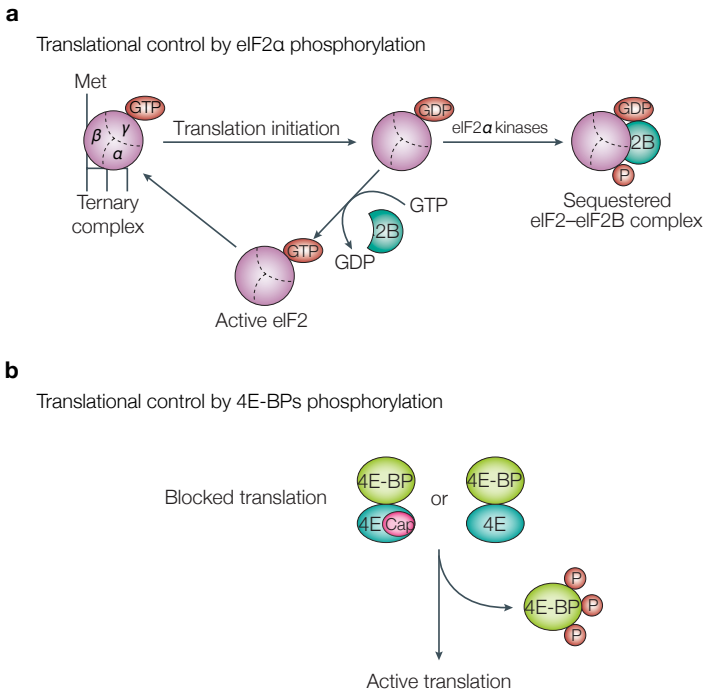

Figure 9: Global control of gene expression. (a) Global translation shut-down can be achieved through phosphorylation of eIF2α, which reduces the availability of this factor for the formation of functional ternary complexes. (b) Global translation activation can be attained by phosphorylation of 4E-BPs, which increases the availability of eIF4E for binding the cap of translationally active mRNAs . Picture adapted from Gebauer and Hentze (2004).

The best-characterized examples are phosphorylation of eIF2α and 4E-binding proteins (4E-BPs). Phosphorylation of eIF2α subunit (by kinases such as PERK, HRI, PKR and GCN2) reduces the dissociation rate of eIF2 with eIF2B, which has GEF activity, thus impairing the reconstitution of functional ternary complexes required for new rounds of translation initiation (Rowlands et al., 1988; Jackson et al., 2010). On the other hand, hyperphosphorylation of 4E-BP proteins (for example by the mTOR cascade in response to insulin) increases the availability eIF4E, thus favoring its interaction with eIF4G, required for the cap-mediated recruitment of the 43S pre-initiation complex (Pause et al., 1994; Gingras et al., 1999).

During the last decade, regulatory mechanisms that don't act at the initiation step have also been described, especially for the elongation phase. As an example, phosphorylation of eEF2 by the eEF2 kinase inhibits its activity by preventing it from binding to the ribosome, thereby affecting its translocation and, ultimately, translation elongation. This kind of regulation will ensure that, under conditions where energy availability is compromised, it is not dedicated to protein synthesis, as well as it also warrants that translation can be rapidly reversed upon return to homeostasis (Kaul et al., 2011; Roux and Topisirovic, 2012).

mRNA-specific control of gene expression

Control of the expression of certain mRNA subsets is essential for the life of complex organisms. Again, most of the mechanisms described to regulate translation of specific mRNAs impact on translation initiation, though more recent work is unraveling the control of the elongation step.

The association of the 43S pre-initiation complex with specific mRNAs is controlled by some aforementioned 5'-UTR features (IRES, pseudoknots, hairpins…) as well as RNA-binding proteins (Gebauer and Hentze, 2004; Leppek et al., 2018). RNA-binding

proteins controlling translation initiation can exert their function by steric hindrance in the cap-proximal region, as it is the case for IPR1/2 inhibiting the translation of the ferritin mRNA (Muckenthaler et al., 1998), or by interfering with the eIF4F complex, as it is the case for the repressor protein Cup with the unlocalized *nanos* mRNA (Nelson et al., 2004). Remarkably, translation initiation can also be inhibited after 43S recruitment: hnRNPK and hnRNPE1 have been observed to prevent the binding of the 60S ribosomal subunit at the start codon of the *LOX* mRNA (Ostareck et al., 2001).

Interestingly, global reduction of translation initiation can favor the translation of a subset of genes that share presence of a number of uORFs in their 5'-UTRs before the main open reading frame (ORF), as it is the case of the *ATF4* mRNA. Translation of *ATF4* is enhanced upon endoplasmyc reticulum (ER) stress, a condition in which eIF2α phosphorylation reduces the availability of ternary complexes and uORFs upstream the ATF4-coding ORF are skipped (Barbosa et al., 2013).

Cap-dependent translation initiation of specific mRNAs can also be inhibited by microRNAs. These small RNA molecules can exert this inhibitory effect by interfering with the 43S pre-initiation complex scanning (mediated by the locking of eIF4A2 onto the target's 5'-UTR) and by the recruitment of the CCR4-NOT complex, a deadenylation machinery that promotes removal of the poly(A) tail and decapping (Bartel, 2009; Jonas and Izaurralde, 2015). Notably, mechanisms targeting the length of poly(A) tails (miRNAs, 3'-UTR-binding RBPs...) impact on translation initiation, possibly through the stability of the closed-loop conformation and/or affecting ribosome recycling.

Translational control at the elongation step can also be mediated by *cis* features found in the CDS of the regulated mRNAs. For instance, certain aminoacid sequences can cause ribosome stalling, either because of the poor reaction kinetics of some aminoacids or from inhibitory conformations of the nascent peptides in the exit tunnel (Schuller and Green, 2018). In addition to it, mRNA sequences rich in codons of lowly expressed

cognate tRNAs can also elicit ribosomal pausing, a phenomenon that has been observed through ribosome profiling experiments and that is known as codon optimality (Richter and Coller, 2015). Additionally, the ribosome can also encounter strong mRNA secondary structures that can arrest elongation (Riba et al., 2019).

Remarkably, in recent years it has been shown that the composition of the ribosomes in a cell is heterogeneous, which endows them with differential selectivity for translating subsets of transcripts, including those controlling metabolism, cell cycle and development (Shi et al., 2017; Simsek et al., 2017).

mRNA localization

Transcript localization is a key step in the regulation of gene expression. From an energetic point of view, localization of an mRNA template optimizes energy expenditure, as it is far cheaper than mobilizing a myriad of protein molecules to the desired location. In addition, regional targeting of mRNAs can serve to prevent proteins from reaching the wrong subcellular compartment, as well as it can assist in complex formation, by bringing together the respective transcripts (Chin and Lécuyer, 2017).

While docking of certain mRNAs to the membranes of some cellular compartments (endoplasmic reticulum, mitochondria…) occurs co-translationally, upon emergence of signal sequences in the nascent peptides (Walter et al., 1981), several transcripts harbor *cis*-localization elements within their sequences that modulate their subcellular distribution and fate early from transcription (Smith, 2004; Lécuyer et al., 2007; Martin and Ephrussi, 2009). Indeed, there is growing evidence that gene promoters can dictate the behavior of the transcribed products by the recruitment and handover of trans-regulators to the nascent mRNA (Zander et al., 2016).

The most prevalent mechanism modulating mRNA localization involves the transport

of transcripts along the cytoskeleton through the interaction of mRNPs with motor proteins that favor directional movement. Alternatively, mRNAs can also be distributed asymmetrically in the cell due to diffusion-entrapment and selective stabilization mechanisms (Chin and Lécuyer, 2017).

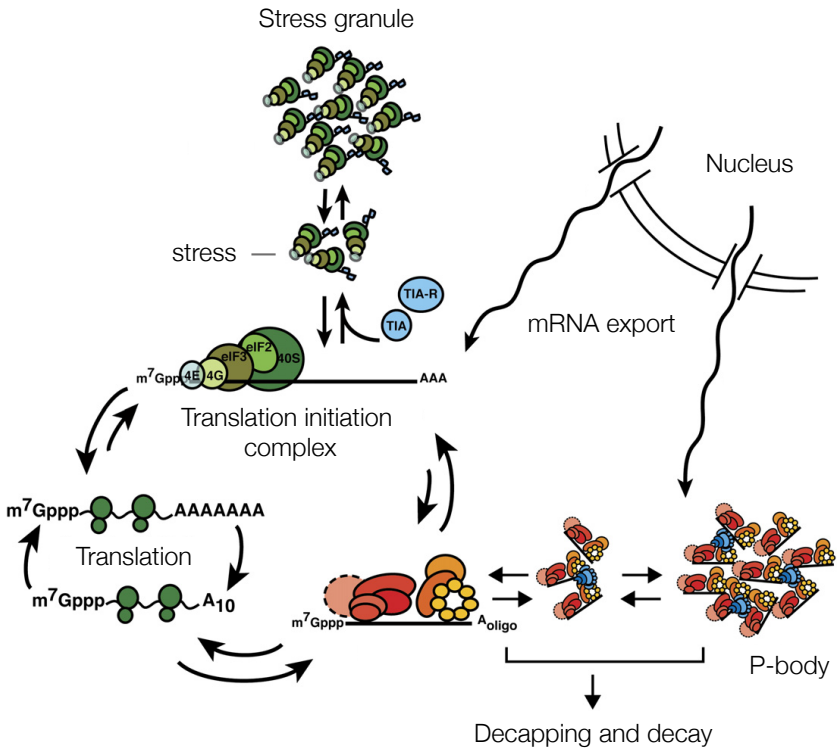

Figure 10: mRNA localization in stress granules and processing bodies. mRNAs can be localized in membraneless organelles in order to provide spatial and temporal control over their expression. Paradigmatic examples of these ensembles are stress granules, which assemble upon stress and contain polyadenylated mRNAs and stalled ribosomes, and P-bodies, which are assembled constitutively and are potential sites of mRNA storage. Picture adapted from Parker and Sheth (2007).

In normal conditions, but especially under stress, mRNAs can be detected at microscopic assemblies that are membraneless. In the cytoplasm, two kinds of biomolecular condensates have been extensively studied: processing bodies (P-bodies, PBs) and stress

granules (SGs) (Decker and Parker, 2012). Stress granules appear under acute or chronic stress conditions, which induce the phosphorylation of eIF2α, and consist of stalled pre-initiation complexes that include the 40S subunit, translation initiation factors eIF4F, eIF3 and PABP, as well as polyadenylated mRNAs that cannot be translated. On the contrary, Processing-bodies can be found constitutively in cells and are composed of proteins associated with mRNA silencing and decay as well as deadenylated mRNA (Luo et al., 2018). Despite the historical conception of P-bodies as mRNA decay centers, it is now becoming widely considered the possibility that the sequestration of mRNAs in processing-bodies may instead allow their rapid mobilization into the translationally active pool to ensure fast temporal and/or spatial control over gene expression (Standart and Weil, 2018).

Noteworthy, P-bodies and SGs are dynamic structures with partially overlapping functions. Accordingly, some of their components are shared and both proteins and mRNAs move between these compartments in an equilibrium with polysomes (Balagopal and Parker, 2009; Youn et al., 2018; Hondele et al., 2019).

Mechanisms of mRNA decay

The last step in the mRNA lifecycle is mRNA decay. Regulation of mRNA turnover is essential for controlling the abundance of cellular transcripts and thus protein expression levels (Garneau et al., 2007). Broadly, cellular mRNA decay can be divided into two pathways: basal mRNA decay and quality control decay.

Degradation of mRNAs at the end of their translational life, also known as basal mRNA decay, occurs in several stages, but initiates with the rate-limiting gradual shortening of the poly(A) tail, termed deadenylation, by cellular decay factors including the CCR4-NOT complex and poly(A)-specific ribonuclease (PARN) (Abernathy and Glaunsinger, 2015). Transcript deadenylation triggers removal of the cap by the decapping complex

DCP1/2 and its activators (Tharun, 2009; Nishimura et al., 2015). These events expose the mRNA to rapid exonucleolytic degradation, primarily from the 5'-end by XRN1 (Jinek et al., 2011), but also from the 3'-end by the exosome and DIS3L2 (Tomecki et al., 2010).

Besides basal mRNA decay, cells require a quality control system to maintain the transcriptome fidelity, thereby destroying cytoplasmic mRNAs recognized as aberrant. In such cases, deadenylation-indepenent mechanisms operate to degrade mRNAs with premature termination codons, a process known as nonsense-mediated decay (Parker and Song, 2004; Popp and Maquat, 2013), or mRNAs with stalled ribosomes or non-terminating ribosomes, processes known as no-go decay (Doma and Parker, 2006) and nonstop decay respectively (van Hoof, 2002). All these mechanisms start with the endonucleolytic cleavage of the affected mRNAs followed by the gradual trimming from either end (Gallouzi and Wilusz, 2013).

Prunning the 3'-end: mRNA deadenylation

The length of a poly(A) tail is a critical determinant of mRNA stability and translation efficiency (Chen and Shyu, 2011). Generally, poly(A) tails undergo partial deadenylation following mRNA transport to the cytoplasm. There is, then, a default deadenylation that occurs regardless of transcript lability or stability.

As mentioned above, nearly all major mRNA decay pathways are initiated by deadenylation, with the predominant deadenylase being the CCR4-CAF1 complex. Many studies have demonstrated that deadenylation is biphasic, involving the sequential actions of PAN2/3 (initial trimming up to 110nt) and CCR4-CAF1 complexes in mammalian cells (Yamashita et al., 2005; Webster et al., 2018; Yi et al., 2018). Apart from these deadenylases, many others can also be found in eukaryotes, such as Nocturnin, ANGEL and 2'PDE (Yan, 2014).

Importantly, poly(A) tail shortening is not exclusively linked to mRNA decay. As previously stated, deadenylated mRNAs can be stably stored in processing bodies and can then resume translation upon re-elongation of their poly(A) tail in the cytoplasm. Therefore, deadenylation is an important mechanism also in translational repression or silencing (Kim and Richter, 2006; Standart and Weil, 2018).

Several RNA-binding proteins can regulate the length of the poly(A) tail of their targets, thereby promoting their silencing or degradation. These RBPs recognize specific sequences at the 3'-UTR of the targets, among which the best characterized examples are AU-rich elements and the cytoplasmic polyadenylation elements. These sequences are bound by proteins such as TTP and CPEBs respectively, and are known to recruit deadenylases to their targets (Goldstrohm and Wickens, 2008).

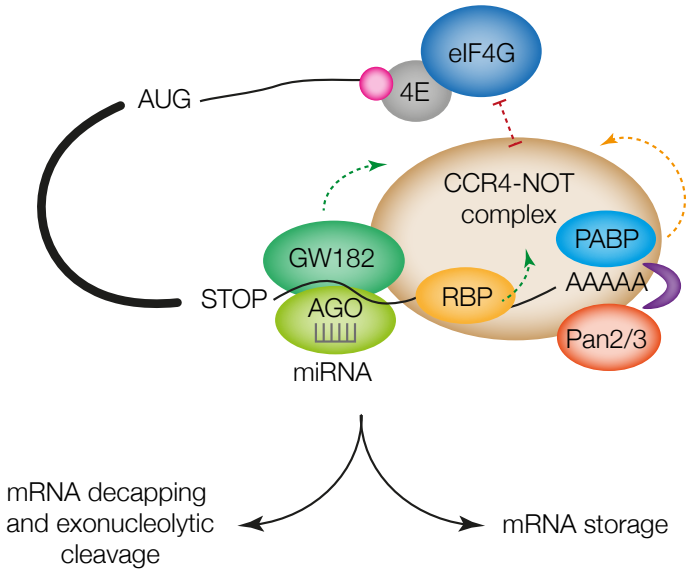

Figure 11: Overview of mRNA-specific deadenylation. poly(A) tail shortening or deadenylation is mediated by several deadenylases (PARN, CCR4/CAF1, PAN2/3...) and can be triggered by specific *cis* elements in the mRNA 3'-UTR and their cognate *trans*-acting factors. Depending on the context, deadenylation can drive either mRNA degradation or storage.

Notably, miRNA-mediated repression and decay involves poly(A) tail shortening as well, generally through recruitment of the CCR4-NOT complex. Alternatively, when miRNAs are fully complementary to their targets, deadenylation is bypassed and degradation is attained by direct endonucleolytic processing (Fabian et al., 2011; Yan, 2014).

Remarkably, deadenylation may also be regulated by translation through a yet unknown mechanism (Lima et al., 2017; Heck and Wilusz, 2018). It has been shown that PABP influences translation by interacting with eIF4G and eRF3 while, at the same time, promotes mRNA deadenylation (Bresson and Tollervey, 2018). Accordingly, it has been proposed that PABP might mediate the putative coupling between translation rate and deadenylation, which would ensure the coordination of translation, storage and decay. According to Lima et al. (2017), this coupling might explain why poly(A) tail length is not associated with translational efficiency in nonembryonic cells (Park et al., 2016).

Cytoplasmic polyadenylation

Cytoplasmic polyadenylation is the elongation of the poly(A) tail of an mRNA after it has been exported to the cytoplasm. Typically, this process increases protein expression from specific transcripts by the translational activation of stored mRNAs with short poly(A) tails, especially as a response to a specific signal (Villalba et al., 2011; Weill et al., 2012; Charlesworth et al., 2013). This process was first discovered in the 1970s in sea urchin embryos (Wilt, 1973) and since then it has been observed not only in the oocytes and early embryos of many animal species including insects, amphibians (Fox et al., 1989) and mammals (Yang et al., 2020b), but also in somatic cells (Du, 2005).

Regulation of translation by cytoplasmic polyadenylation allows mRNA nuclear export to be separated from the synthesis of the encoded proteins in space and time. Consequently, many of the mRNAs that are regulated by this process are localized to specific positions in the cell and/or are only translated upon certain stimuli (Eliscovich et al.,

2008; Radford et al., 2008; Martin and Ephrussi, 2009; Darnell and Richter, 2012). Notably, cytoplasmic polyadenylation itself is only one function of a family of RNP complexes that can also mediate translational repression, deadenylation and mRNA localization, as the same sequence elements and RBPs mediating the control of poly(A) tail size normally contribute to these other processes as well.

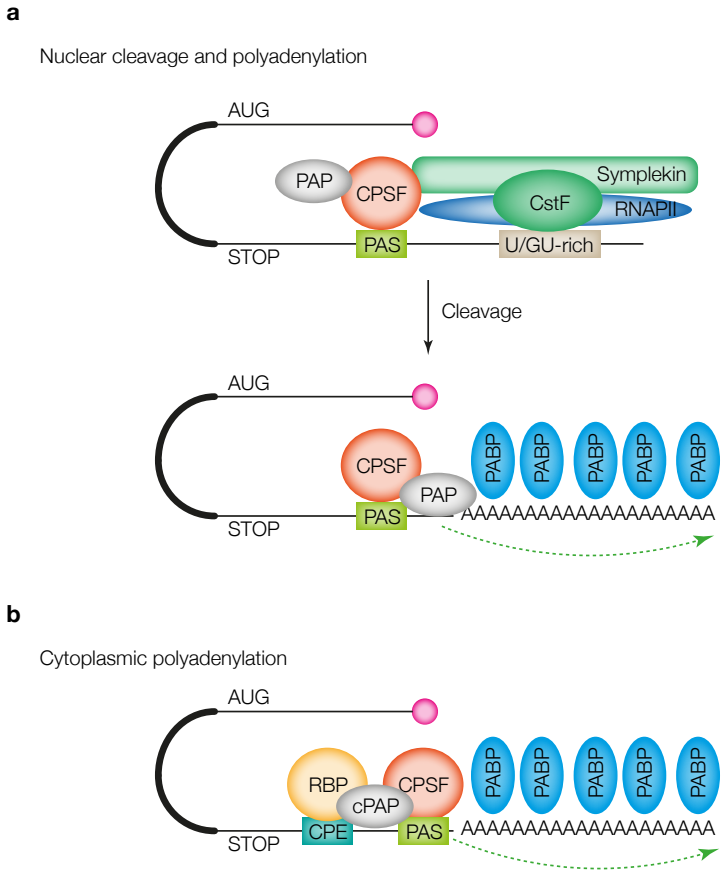

Figure 12: Overview of nuclear and cytoplasmic polyadenylation. (a) mRNAs are cleaved and polyadenylated co-transcriptionally in the nucleus. This process requires two *cis* elements in the 3'-UTR, namely the PAS and the U/GU-rich sequence recognized by CPSF and CstF complexes respectively. After cleavage, a poly(A)-polymerase elongates the poly(A) tail to favor mRNA export and transcript stability. (b) Elongation of the poly(A) tail in the cytoplasm upon a stimulus requires not only the PAS but also *cis* elements recognized by RBPs that mediate the recruitment of polyadenylation factors. Picture adapted from Weill et al. (2012).

Cytoplasmic polyadenylation requires not only the poly(A) signal that is needed for polyadenylation in the nucleus, which is recognized by the CPSF machinery (Colgan and Manley, 1997), but also specific *cis* elements at the 3'-UTR of the target mRNA, which allow regulation of this process. The sequence elements described to be mediating cytoplasmic polyadenylation are few : TCS (Wang et al., 2008), MBE (Charlesworth et al., 2006), PBE (Suh et al., 2009), DAZL binding sequence…, and the best-characterized is the cytoplasmic polyadenylation element, henceforth the CPE (Paris and Richter, 1990).

The set of poly(A)-polymerases that have been related in different organisms and cellular contexts to cytoplasmic polyadenylation is limited to five proteins, namely Gld2, Gld2, ZCCHC6, ZCCHC11 and POLS (Shin et al., 2017a). These proteins are only recruited to specific mRNAs by certain RBPs under certain stimuli (Rouhana, 2005; Kim and Richter, 2006; Charlesworth et al., 2013).

Intriguingly, there have also been described instances of translational activation independent of cytoplasmic polyadenylation, as it is the case of some studies with DAZL in *Xenopus laevis* oocytes (Padmanabhan, 2006).

The paradigm of translational activation upon cytoplasmic polyadenylation might be revisited considering the findings of Yang et al. (2020b). Their work with high-throughput approaches suggests that poly(A) tail length changes rather than raw length correlate better with changes in translation and, on top of that, poses the density and spacing of U-rich motifs in the 3'-UTR as critical determinants for controlling translation. Taking into account these observations, cytoplasmic polyadenylation would only have an impact on translation provided the transcript 3'-UTR has also an optimal U-rich motif composition. According to the authors, this cooperative fashion of promoting translation could be attributed to DAZL, though other proteins such as CPEB, FUBP1 or ELAV are possible candidates.

We will devote the following section to describe a family of RNA binding proteins, the CPEBs, focusing on the molecular principles by which they exert their dual function as translational regulators.

Translational control by the CPEBs

The CPEB family of proteins

The cytoplasmic polyadenylation element-binding family of proteins (CPEBs) are essential regulators of post-transcriptional gene expression. Even though they were initially described to have a role in early embryogenesis and germ cells development (Paris et al., 1991; Lantz et al., 1994; Hake and Richter, 1994; Walker et al., 1999; Stebbins-Boaz et al., 1999), it is now clear that these proteins are also key mediators of cellular homeostasis in a variety of somatic tissues, regulating important biological processes such as cell proliferation, senescence, cell polarity and synaptic plasticity (Novoa et al., 2010; Fernández-Miranda and Méndez, 2012). Hence, when misregulated, they contribute to the development of several pathological manifestations, including tumor development, memory defects... (Ortiz-Zapater et al., 2012; Calderone et al., 2016; Maillo et al., 2017; Villanueva et al., 2017; Parras et al., 2018).

In vertebrates, this family is composed of four members, namely CPEB1-4, where CPEB1 is the more distant paralog and CPEB2-4 are more closely related (Wang and Cooper, 2010). In other species, CPEBs can be found in different numbers, such as Orb and Orb2 in *Drosophila* (Lantz et al., 1992; Walker et al., 1999; Hasegawa et al., 2006). Notably, knock-out mouse models for CPEB1-4 display different phenotypes, thereby underscoring that these proteins are not functionally redundant (Ivshina et al., 2014).

All four paralogs harbor a highly conserved C-terminal region comprised of two RNA

recognition motifs (RRMs) in tandem and a ZZ-box, responsible for the binding of CPE-containing RNAs (Hake et al., 1998). Importantly, the RRMs are required for sequence-specific recognition of the CPE sequence, whereas the ZZ domain only contributes to the affinity (Afroz et al., 2014). On the other hand, the N-terminal domains of the four CPEBs are highly variable in length and composition across orthologs and paralogs, and lack any recognizable structure, which renders them as putative intrinsically disordered sequences. Nonetheless, this region has been shown to contain the regulatory elements of CPEB1 and CPEB4 and more evidence is appearing for the other members (Mendez et al., 2000b; Setoyama et al., 2007; Pavlopoulos et al., 2011; Guillén-Boixet et al., 2016).

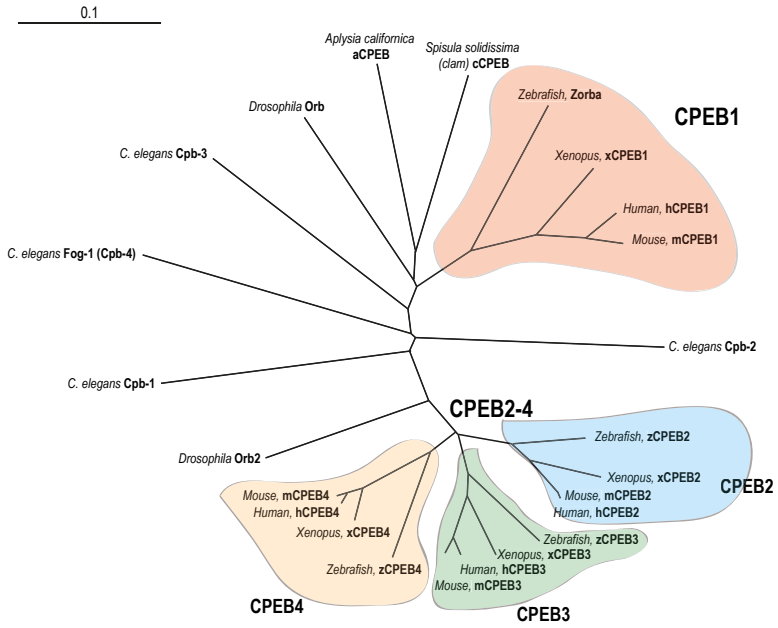

Figure 13: Phylogenetic tree of the CPEB family. Unrooted phylogenetic tree of the most representative CPEB proteins based on a multiple sequence analysis using complete protein sequences. As depicted, distances between orthologs are significantly shorter than those between paralogs. CPEB1 vertebrate orthologs are the most distant members, whereas those of CPEB2-4 are evolutionarily closer. Picture from Fernández-Miranda and Méndez (2012).

The cytoplasmic polyadenylation element

The CPE is a sequence that was originally characterized as conferring cytoplasmic polyadenylation during *Xenopus* oocyte maturation (Fox et al., 1989; McGrew and Richter, 1990). Essentially, it is a U-rich element containing a stretch of at least four uridines, defined by the consensus sequence 5'-UUUUA$_{1-3}$U-3', though several non-consensus CPEs have also been identified (Piqué et al., 2008).

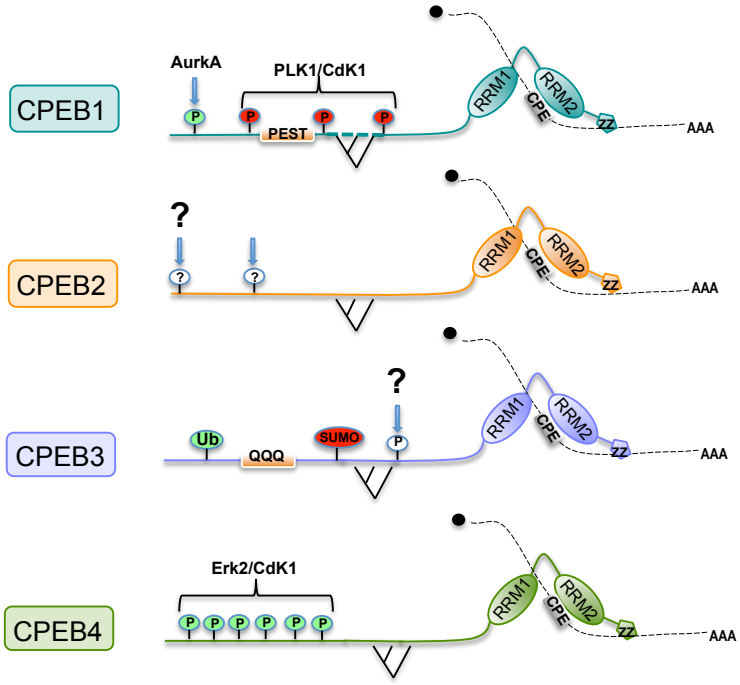

Figure 14: CPEBs domains and regulation. All four CPEBs share a similar structure: a highly ordered C-terminal domain comprising two RNA-recognition motifs (RRMs) in tandem and a ZZ-box, responsible for the binding to the targets, and a highly variable N-terminal domain which presumably contains the regulatory sites. Specially for CPEB1, CPEB3 and CPEB4, post-translational modifications affecting their function and/or stability have been identified. CPEBs can also be alternatively spliced, giving rise to isoforms with potential different behaviors and functions.

Importantly, most of the work on the interaction between CPEBs and CPEs has been

performed with CPEB1. For CPEB3-4, a distinct U-rich loop motif, not recognized by CPEB1, was identified by SELEX, though more recent studies show that CPEB2 and CPEB4 also recognize the same CPE as CPEB1 (Novoa et al., 2010; Igea and Méndez, 2010). CLIP experiments with the *Drosophila* orthologs Orb and Orb2b showed different binding motifs, suggesting that CPEBs can bind more elements than the canonical CPEs (i.e. Orb2 seems to have affinity for CPEs with a G at the fifth position) and that, despite sharing overlapping targets, some mRNAs might be preferentially bound by one CPEB subfamily (Stepien et al., 2016). This last statement is underscored by the fact that while the RNA-binding domain (RBD) of Orb2 can be functionally replaced by that of mouse CPEB2, it cannot be replaced by the RBD of Orb or mouse CPEB1.

Solution NMR studies suggest that structural differences in the RRMs of CPEB1 and CPEB4 in recognizing a CPE may explain why CPEB1 could be more permissive for non-consensus CPEs as compared to CPEB2-4, based on the recognition of A5. Nonetheless, the same work shows that both paralogs can bind to the CPEs with comparable affinities (Afroz et al., 2014).

Several studies in *Xenopus laevis* oocytes have established the principles of CPE-mediated translational control in the context of meiosis (Piqué et al., 2008; Belloc and Méndez, 2008). These seminal works demonstrated that CPE-mediated repression requires a cluster of at least two CPEs, irrespective of its position along the 3'-UTR, where the distance between the pair of CPEs defines the repression efficiency. More recently, other studies have confirmed these observations (Luong et al., 2020; Yang et al., 2020b). In addition, the Pumilio binding element (PBE) was also shown to enhance repression, possibly through stabilization of CPEB binding to the target mRNA.

Regarding the role of the CPEs in translational activation, Piqué et al. (2008) demonstrated that CPE-mediated cytoplasmic polyadenylation and the subsequent activation of translation require a single consensus CPE, proposing also that the distance between

this element and the PAS modulates the extent of polyadenylation, with an optimal separation of 25 nucleotides. Notably, only for the case of non-consensus CPEs the PBE would be a requirement.

Another recent work with mouse oocytes poses a different paradigm. CPE-mediated repression would be attained by preclusion of the binding of CPSF4 with the PAS by CPEB1, even for mRNAs with single CPEs (Dai et al., 2019). Therefore, translational repression requires a relative close distance between PASs and CPEs, though it varies among different 3'-UTRs. In brief, the numbers and positions of CPEs in relation to PASs within the 3'-UTR of a given transcript determine its repression efficiency in GV oocytes. About translation activation after germinal vesicle breakdown, the same work shows that it requires at least one CPE adjacent to the PAS.

Irrespective of the models proposed, it is widely accepted that in *Xenopus laevis* oocytes a combinatorial code of CPE, PAS, PBE, ARE and possibly other *cis* elements, ensures a fine-tuned control of meiosis, which has recently been related to APA in mouse oocytes (Yang et al., 2020b).

CPEBs role in translational repression

Translational control by cytoplasmic changes in the length of the poly(A) tail of the mRNAs was originally discovered as a key mechanism governing gene expression during meiotic progression in transcriptionally silent *Xenopus laevis* oocytes. As mentioned above, control mediated by CPEB1 is the best-characterized example of this mechanism of regulation.

Stage VI or fully-grown oocytes store huge amounts of silent mRNAs required for meiotic resumption upon progresterone stimulation (LaMarca et al., 1973; Rodman and Bachvarova, 1976; Schmitt and Nebreda, 2002). While CPEB1 itself doesn't have any

intrinsic catalytic activity, it is presumed that its main function is to recruit effector proteins to mRNAs that are intended for repression or masking. So far, three models have been proposed to explain CPEB1-mediated repression.

The first model contemplates the recruitment of Maskin to the CPEB1 particle (Stebbins-Boaz et al., 1999). This protein contains a peptide sequence that is conserved among eIF4E-binding proteins and would compete with eIF4G for binding to the cytoplasmic cap-binding complex, in a similar manner eIF4E-BPs exert their function. As a consequence, translation initiation would be precluded by impairment of the eIF4E-eIF4G interaction.

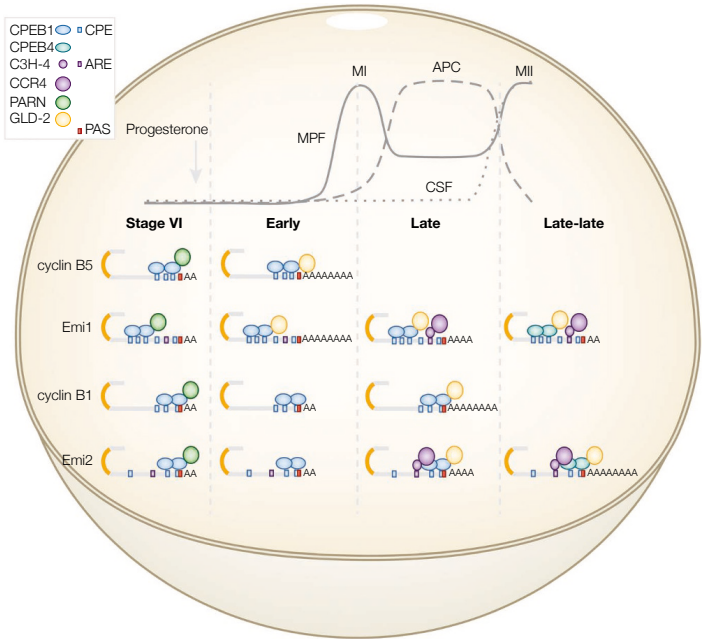

Figure 15: Sequential waves of polyadenylation determined by the CPE combinatorial code. Upon progesterone stimulation, CPEBs regulate the three key activities that drive meiotic progression by establishing three sequential waves of cytoplasmic polyadenylation. The CPE combinatorial code endows the oocytes with the capacity to fine-tune translation in a temporal fashion. Picture from Weill et al. (2012).

The second model is built on the proteins with opposite roles PARN and Gld2 (Barnard et al., 2004; Kim and Richter, 2006, 2007). PARN, as mentioned earlier, has deadenylase activity and would be responsible for the cytoplasmic poly(A) tail shortening of CPEB1 targets in *Xenopus laevis* oocytes. On the contrary, Gld2 is a poly(A)-polymerase that elongates the poly(A) tail of its targets. As the model suggests, the activity of PARN overtakes that of Gld2, hence ensuring short poly(A) tails. However, for PARN to be active it requires binding to the cap, which would not be possible as long as Maskin is bound to eIF4E. Consequently, these two models are mutually exclusive by definition.

Finally, a third work proposes a model without Maskin and PARN. Rather, CPEB1 targets would be translationally inactive due to the interaction of an ovary-specific isoform of eIF4E, termed eIF4E-1b, with the cap (Andrei, 2005; Minshall et al., 2007). According to this model, this isoform has less affinity for eIF4G and this would prevent translation initiation. In addition, translational repressors like eIF4E-T (EIF4ENIF1), p54 (DDX6), RAP55 (LSM14 family of proteins) and PAT1 would be also present in the complex. This model, though, would not explain how the mRNAs repressed by CPEB1 would have their poly(A) tails shortened.

Despite the implications that these models arise, there still lacks a study which determines, in a holistic manner, if all these models coexist in *Xenopus laevis* oocytes, if they represent different repression complexes for specific mRNAs or specific phases of the cell cycle, or if any of them predominates over the others (Rouhana, 2005). In any case, CPEB1 mediated repression seems to require both poly(A) tail shortening and eIF4F complex formation impairment, which are key steps in the circularization of mRNAs necessary for translation initiation. Nevertheless, it remains unknown as to which of these models may apply to somatic mammalian cells. For instance, the mammalian ortholog of Maskin (TACC3) does not contain the eIF4E-binding motif and, according to the third model, repression requires an ovary-specific isoform of eIF4E.

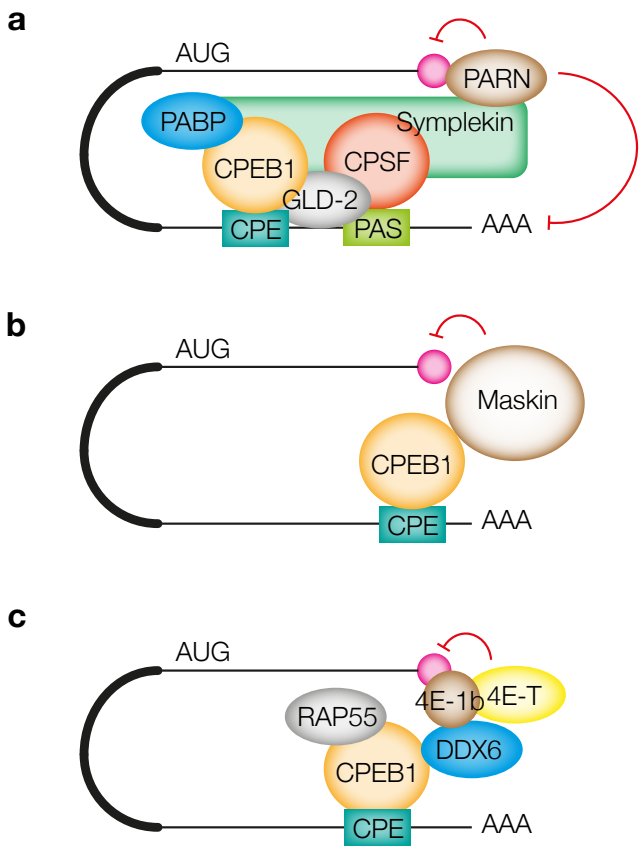

Figure 16: Proposed models for CPEB1-mediated repression in stage VI *Xenopus laevis* oocytes. (a) Repression complex mediated by the interaction between CPEB1 and PARN, which results in shortening of the poly(A) tail and cap-blockade. (b) Repression complex mediated by CPEB1 interaction with Maskin, which masks the cap-binding protein 4E, thus precluding the formation of the cap-binding complex. (c). Repression complex mediated by CPEB1 interaction with DDX6, eIF4E-T and eIF4E1-b, an isoform of 4E with reduced affinity for eIF4G. Picture adapted from Fernández-Miranda and Méndez (2012).

At the same time, alternative repression mechanisms have been described for the other CPEBs in somatic cells. CPEB2, for instance, has been observed to repress translation elongation by interacting with the eEF2, impairing eEF2/ribosome-triggered GTP hydrolysis (Chen and Huang, 2012). In another study CPEB3 was shown to mediate translational repression by the recruitmet of the deadenylase CAF1 to *GluR2* mRNA by dir-

ect interaction with Tob, which promotes the destabilization of the target mRNA in neurons (Hosoda et al., 2011). Finally, CPEB4 has been proposed to repress translation during terminal erythropoiesis in an eIF3-dependent fashion (Hu et al., 2014).

CPEBs role in translational activation

CPEB1 inhibits translation of its targets during oocyte development and in stage VI oocytes, which are arrested at Prophase I, yet it is also required for the efficient translation of the CPE containing mRNAs upon progesterone stimulation (Mendez et al., 2000b).

Oocytes that have been stimulated with progesterone activate signaling cascades that trigger the activation of Aurora Kinase A, which in turn phosphorylates CPEB1 at Ser174, thereby eliciting a rearrangement of the repression complex (Andresson, 1998; Cao, 2002; Cao et al., 2006). The single phosphorylation of CPEB1 engages the first polyadenylation wave, necessary for the synthesis of important cell cycle regulators (Emi1, Mos, cyclin B2 and cyclin B5 among others) and CPEB4. This first wave allows the proper entry into metaphase I (MI).

At metaphase I, CPEB1 is targeted for degradation by phosphorylation at multiple proline-directed sites conducted by Cdk1 and Plk1 (Reverte et al., 2001; Mendez, 2002; Setoyama et al., 2007). At this stage, CPEB1 engages the second polyadenylation wave, or late polyadenylation, which is necessary for the synthesis of proteins such as cyclin B1 and cyclin B5 (Hake and Richter, 1994; Mendez and Richter, 2001).

Finally, from interkinesis until the metaphase II (MII) arrest, CPEB4 takes over CPEB1 and, when hyperphosphorylated by ERK2 and Cdk1, is responsible for the translation of the mRNAs required for oocyte fecundation (Igea and Méndez, 2010; Guillén-Boixet et al., 2016). Importantly, translation at this late-late phase, is ensured by the presence of AREs at the 3'-UTRs of certain mRNAs and the negative feed-back loop established

by C3H-4 (Belloc and Méndez, 2008).

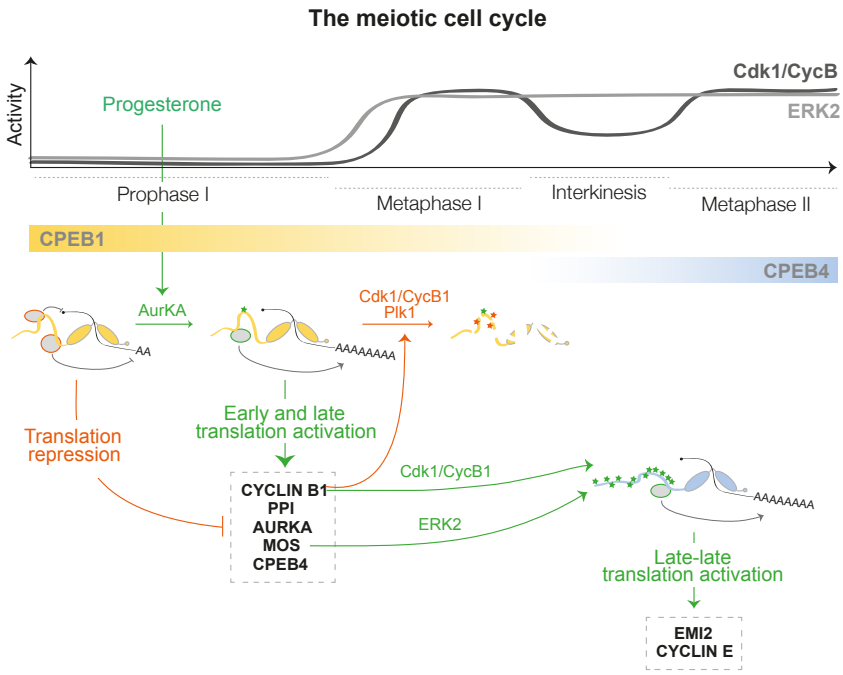

Figure 17: CPEB1 and CPEB4 concerted functions in the meiotic cell cycle. Upon progesterone stimulation, AurKA phosphorylates CPEB1 and switches its role from translational repressor to activator. During this first polyadenylation wave which drives the progression to Metaphase I, proteins such as Mos and CPEB4 are synthesized. Transition from MI to MII is facilitated by a late wave of polyadenylation mediated by Plk1/Cdk1-phosphorylated CPEB1 which, in turn, poises it for degradation. Once at MII, CPEB4 takes over CPEB1 and sustains the late-late polyadenylation wave. Picture adapted from Guillén-Boixet et al. (2016).

At the molecular level, Aurora A kinase phosphorylation of CPEB1 increases its affinity for CPSF, hence favoring the recognition of the PAS and, in turn, stabilizing the binding of Gld2 to elongate the poly(A) tail (Mendez et al., 2000b; Barnard et al., 2004). In addition, CPEB1 phosphorylation decreases the affinity of the complex for PARN, thereby inducing its exclusion and, consequently, facilitating poly(A) tail lengthening (Kim and Richter, 2006). Concomitantly, CPEB1 phosphorylation also helps dissociating ePAB (embryonic PABP) from the core, which allows its binding to the poly(A)

tail, a key step for mRNA circularization (Kim and Richter, 2007). On the other hand, it has also been proposed that Maskin phosphorylation upon progesterone stimulation would be necessary for breaking its interaction with eIF4E, hence favoring the recruitment of eIF4G to the cap (Barnard et al., 2005).

There are also some evidences of translation activation mediated by the CPEBs in mammalian somatic cells. CPEB1, for instance, represses *NR2A* mRNA in neurons when assembled with PARN, SYMPK, Gld2 and Neuroguidin, while it dissociates from PARN and NGD upon neuronal stimulation (Udagawa et al., 2012). Regarding CPEB2, it has been proposed that ablation of its interaction with eEF2 releases *HIF1a* mRNA from elongation blockage (Chen and Huang, 2012). As for CPEB3, Pavlopoulos et al. (2011) showed that, when mono-ubiquitinated by the E3-ligase activity of Neuralized, it is able of increasing the translation of *GluA1* and *GluA2* mRNAs.

We will finish the introduction talking about phase separation, an old concept applied very recently to Cell Biology, and will link it to the CPEBs.

CPEBs and phase separation

Principles of phase separation

Cells have exploited component compartmentalization to optimize spatiotemporal control over cellular materials, metabolic processes and signaling pathways (Ditlev et al., 2018; Mittag and Parker, 2018; Langdon and Gladfelter, 2018). Whereas component partitioning by membrane-bound organelles has been long understood, less was known about the membraneless counterparts (e.g., P-bodies, SGs, the Balbiani body, the nucleolus, germ granules...) until a seminal paper from Anthony Hyman's lab showed that *C. elegans* P-granules have liquid-like properties and form by a process known as liquid-liquid phase separation (Brangwynne et al., 2009).

Phase separation is a physical phenomenon that occurs when a supersaturated homogeneous solution of macromolecular components spontaneously separates (or demixes) into two phases, a dense phase and a dilute one, that then stably coexist. From a thermodynamic point of view, liquid-liquid phase separation (LLPS) occurs when the interactions of components for each other are sufficiently more energetically favorable than interactions with the solvent such that the total free energy of the system is favorable for demixing. Importantly, this process depends on the volume fractions of the components and environmental factors such as pH, temperature, ionic strength and the presence of other solutes (Banani et al., 2017; Boeynaems et al., 2018).

From this paper on, more evidences have been provided on this regard. Now, it is broadly considered that phase separation underlies many biological processes, including heterochromatin formation (Strom et al., 2017; Sanulli et al., 2019), nucleocytoplasmic transport (Schmidt and Görlich, 2016) and the formation of membraneless compartments (Sachdev et al., 2019; Kriwacki et al., 2019). Among the features of this kind of compartmentalization there is the selective enrichment of components into the condensates, the generation of microenvironments amenable for certain biochemical reactions, buffering of protein concentrations, the formation of signaling compartments and the nucleation of cytoskeletal structures (Langdon and Gladfelter, 2018).

Proteomic and genetic studies have identified protein components of several membraneless organelles (Fong et al., 2013; Boke et al., 2016; Jain et al., 2016; Youn et al., 2018). These studies suggest that the most important step towards forming a condensate is the establishment of a dense network of interacting molecules, which relies in the multivalency of adhesive domains and/or linear motifs between proteins and/or nucleic acids. In essence, phase separation results from weak multivalent interactions that form highly cooperatively and hence have the necessary properties to form large and dynamic assemblies (Oldfield and Dunker, 2014; Pak et al., 2016).

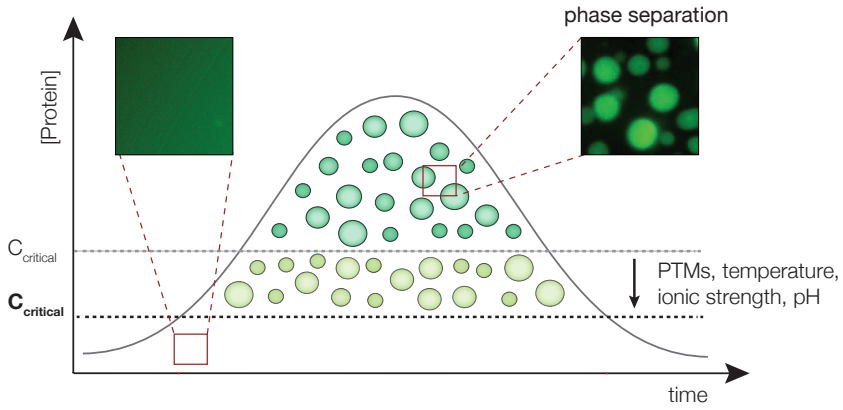

Figure 18: Schematic representation of a phase diagram over time. As depicted, dense liquid droplet formation occurs upon reaching a critical concentration, over which these condensates are stable and dynamic. The critical concentration can be affected by PTMs in the protein sequence and environmental cues such as pH, ionic strength and temperature. Noteworthy, droplet formation is a reversible process. Picture adapted from Alberti (2017).

At the conceptual level, the components of these membraneless compartments can be divided in scaffolds and clients (Banani et al., 2016). While scaffold proteins drive the formation of condensates and are critically required for their integrity, client proteins only partition into condensates after they have been formed. In general, scaffold proteins are present at higher concentrations and have many valences, whereas client proteins are typically less abundant and have a lower number of valences.

Multivalency can occur by a number of different manners, including oligomerization of proteins with folded domains, proteins with multiple interaction sites and proteins with intrinsically disordered regions (Langdon and Gladfelter, 2018).

Intrinsically disordered regions (IDRs) display a sequence-intrinsic preference for conformational heterogeneity (i.e., disorder), which is generally promoted by low-complexity domains (LCDs) found in these regions. LCDs have a biased aminoacid composition (specially enriched in polar small chain aminoacids such as G,S,N,Q,R) and may be

repetitive in sequence. These residues are often found as short linear interaction motifs (SLiMs), alternating charge blocks or degenerate repeats. Interestingly, aromatic residues are essential for the phase separation of intrinsically disordered proteins (IDPs), as they drive most of the intermolecular interactions mainly through cation-π and π-π systems (Kato et al., 2012; Tompa et al., 2014; Vernon et al., 2018).

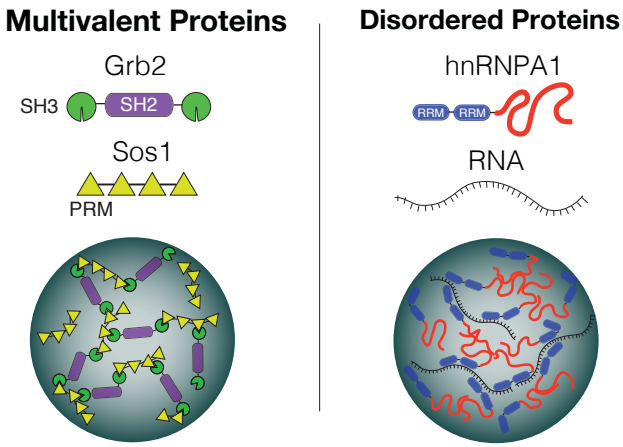

Figure 19: Features of phase separating proteins. Proteins that undergo liquid-liquid phase separation are able to establish several interactions with other proteins and/or nucleic acids, either via multiple folded domains (mutivalent proteins) or via linear motifs found in intrinsically disordered regions. Picture adapted from Shin and Brangwynne (2017).

A property of liquids is their ability to fastly rearrange in short timescales, which is critical for membraneless organelles function. This is achieved mostly by the network of weak interactions that stabilizes the condensates but also through regulation of the protein and RNA components by reversible post-translational/transcriptional modifications, which fine-tune the valence of scaffold or client proteins to drive condensate formation or client partitioning respectively (Guillén-Boixet et al., 2016; Hofweber and Dormann, 2019).

Recent work suggests the presence of stronger interactions in cellular granules such as RNP granules, whose dynamics would be regulated by ATP-driven machines, raising

the question as to which extent cellular phase separation is a passive phenomenon and, therefore, which active processes could be playing important roles (Jain et al., 2016; Falahati and Wieschaus, 2017; Hondele et al., 2019).

Accumulating data underscores the variety of different phases that can derive from phase separation. So far, we have focused on liquid condensates, but transitions to gel and solid compartments have also been characterized (Boke et al., 2016; Jain et al., 2016; Boeynaems et al., 2018).

Phase separation and disease

Several proteins associated with neurodegenerative disorders are components of membraneless organelles (Ramaswami et al., 2013; Li et al., 2013). Experimental evidence suggests that these organelles may be metastable or inherently unstable, as they tend to maturate to solid aggregates *in vitro* and *in vivo*. Indeed, there is increasing evidence that disease mutations affect the properties of condensates, generally by accelerating liquid-to-solid phase transitions (Murakami et al., 2015; Molliex et al., 2015). Among the phase separation-related mechanisms leading to disease we can find:

1. Mutation of beta-zippers in IDRs, which make them more prone to fold into stable amyloid structures (Thompson et al., 2006)

2. Generation of aberrant RNA or protein species, with repeat expansions that can lead to RBPs loss of function (Wojciechowska and Krzyzosiak, 2011)

3. Mutations in autophagy genes necessary for granules clearance (Renton et al., 2014)

4. Mitochondrial dysfunction, leading to a reduction in ATP levels required for the regulation of membraneless organelles (Lin and Beal, 2006)

5. Affected PTMs in tau protein (Wegmann et al., 2018)

Nevertheless, it is important to note that there is currently no direct evidence that pathological protein aggregates in patient brains result from solidification of SGs or other membraneless organelles.

State-of-the-art of CPEBs phase separation

There is growing evidence that CPEBs can form oligomers with biological activity that can be found in certain subcellular compartments or regions.

CPEB1 has long been linked to stress granules and P-bodies (Wilczynska, 2005). It is not only present in these structures but it also seems to be able to assemble them in non-stressed conditions or increase their number upon ectopic expression. The formation of CPEB1 bodies is dependent on translation, as they are assembled or disassembled upon cycloheximide or puromycin treatments respectively, and seems to require competent RRMs. Other members of the family, specially CPEB4, have been repeatedly identified as P-bodies and stress granules components as well (Youn et al., 2018).

CPEB3 and its *Aplysia* and *Drosophila* orthologs (ApCPEB and Orb2) have been shown to form amyloidogenic oligomers *in vitro* and *in vivo* (Si et al., 2003, 2010; Majumdar et al., 2012; Joag et al., 2019). For these proteins it has been shown that they are critical for the persistence of long term synaptic facilitation and behavioral memory, as they are thought to maintain memory through sustained and regulated protein synthesis (Si and Kandel, 2016). The best characterized mechanism has been established for CPEB3: while the SUMOylated version of CPEB3 is responsible for translation repression in the dendrites of basal state neurons, mono-ubiquitinyation and deSUMOylation-driven oligomerizaton of CPEB3 would favor translation activation upon neuronal stimulation (Raveendra et al., 2013; Stephan et al., 2015; Fioriti et al., 2015; Drisaldi et al., 2015).

Finally, a recent work from our lab has demonstrated that CPEB4 activity is regulated

by hyperphosphorylation, which impacts on the ability of this protein to phase separate into liquid-like droplets. On this regard, unphosphorylated CPEB4 forms condensates that are not competent for cytoplasmic polyadenylation and thereby repress the target mRNAs by sequestration, while phosphorylated and monomeric CPEB4 acquires a diffuse distribution that renders it for translational activation.

Notably, phase separation of CPEB4 relies on its intrinsically disordered NTD, and is affected by phosphorylation due to changes in the negative charge patterning (Guillén-Boixet et al., 2016).

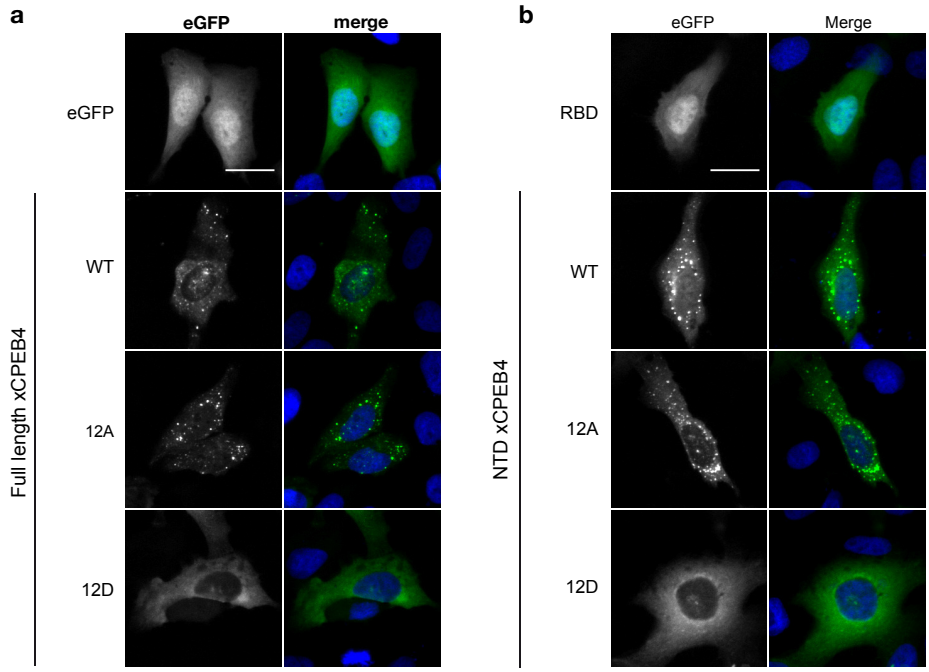

Figure 20: CPEB4 LLPS in U2-OS cells. Unphosphorylated CPEB4 undergoes liquid-liquid phase separation and represses translation of its target mRNAs. When hyperphosphorylated by ERK2 and Cdk1, changes in the charge pattern trigger condensate disassembly, thus facilitating translational activation of CPEB4 targets. In this case, phase separation properties rely on the intrinsically disordered N-terminal domain. Picture from Guillén-Boixet et al. (2016).

Objectives

Research aim and objectives

Since their discovery, several incompatible models have been proposed for the molecular mechanisms underlying translational regulation mediated by the CPEBs. Moreover, recent work on the phase separation properties of several RNA-binding proteins (including CPEB4) is adding yet another layer of complexity to the field of translational control. Consequently, the main goal of our work is to study the CPEBs mRNP composition and remodeling from a high-throughput and *in vivo* perspective, providing also new insights into the principles controlling their dynamic condensation inside the cell.

With this aim, we have dedicated our work to the *in vivo* study of the CPEBs repression and activation complexes in *Xenopus laevis* oocytes through proximity-dependent biotinylation methodologies. Additionally, we have provided a characterization of the *in vivo* liquid-liquid phase separation properties of the *Xenopus laevis* othologs, putting emphasis on CPEB1-3, which had not been previously studied in this regard.

Overall, our specific objectives are:

1. To adapt the BioID methodology to *Xenopus laevis* oocytes
2. To characterize the CPEB1 repression complex in stage VI oocytes
3. To determine the role of RNA in the formation of the repression complex
4. To determine the role of the NTD in the formation of the repression complex
5. To compare the complexes assembled by the four CPEBs in *Xenopus laevis* oocytes
6. To characterize the CPEB1 activation complex in response to progesterone
7. To test the ability of CPEB1-3 to undergo LLPS *in vivo*
8. To compare the features of CPEB1-4 liquid-liquid phase separation

Results

Development of a BioID protocol for frog oocytes

To study the complexes that CPEBs assemble and their remodeling in an *in vivo* scenario we decided to make use of a recent approach, based on proximity-dependent biotinylation, called BioID. This methodology was initially developed for cultured cells (Roux et al., 2012, 2013) and, from then on, its use has been expanded to other systems such as yeasts (Opitz et al., 2017) or plants (Khan et al., 2018). Briefly, BioID consists of fusing to a protein of interest a promiscuous biotin ligase (BirA* or BirA(R118G)), henceforth termed BirA that, upon biotin exposure, will biotinylate any surrounding protein in a radius of 10-20nm, leaving an irreversible mark that will serve as a readout of proximity. After a controlled exposure to biotin, cells are lysed and the modified proteins are purified using streptavidin columns and identified through mass spectrometry.

BioID offers two main advantages over other interactomic approaches: first, it allows the high-throughput identification of interactors (direct or indirect) of a protein of interest *in vivo* and, second, its experimental design permits the detection of transient or weak interactions, which are generally missed in other settings such as co-immunoprecipitations.

For these reasons, we decided to adapt the original protocol to *Xenopus laevis* oocytes, a system in which there are two clearly distinct scenarios: translational repression in stage VI oocytes and translational activation upon hormone stimulation. By these means, we expected to obtain a detailed description of the components of the CPEBs mRNP before and after exposure to progesterone, being able to build up a model for the dual role of this family of proteins.

Extensive biotinylation is achieved after 40h incubation

A schematic representation of the protocol we designed for the BioID in *Xenopus laevis* oocytes is depicted in figure 21a. In brief, oocytes are microinjected with *in vitro* transcribed RNAs coding for a protein of interest fused to BirA and then incubated with

biotin until they are collected. Streptavidin-HRP western blots are used to monitor biotinylation over time and to check the specificity of the labeling.

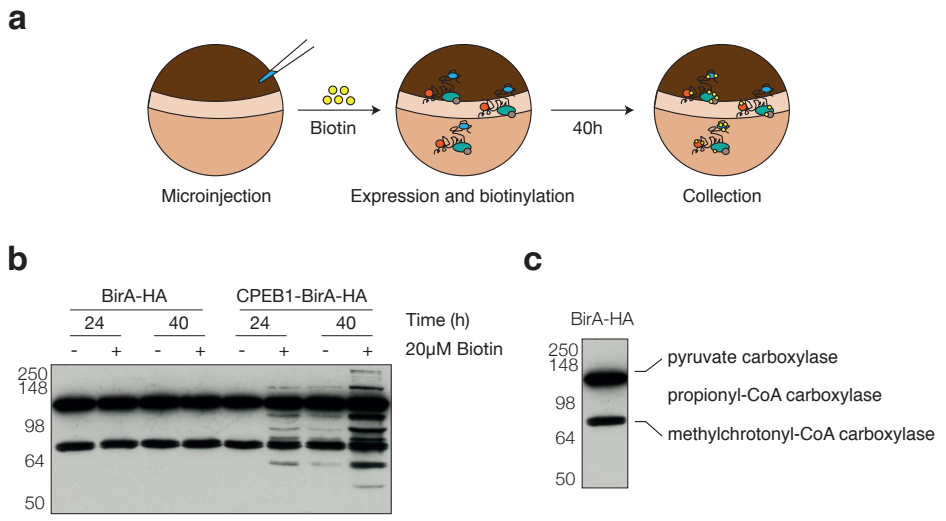

Figure 21: Setting up the conditions for efficient biotin labeling. (a) Schematic representation of the protocol for BioID in *Xenopus laevis* stage VI oocytes: oocytes are microinjected with capped and polyadenylated RNA coding for the BirA fusion protein and are then incubated with 20 μM biotin for 40h prior to collection. (b) Streptavidin-HRP western blot showing the biotinylation attained by CPEB1-BirA over time. Maximum biotinylation signal is achieved after 40h incubation, demonstrating high specificity. C) Streptavidin-HRP Western Blot showing the constitutively biotinylated proteins, later identified using mass spectrometry.

While in cultured cells the labeling step requires typically incubation for 24 hours, in the case of stage VI *Xenopus laevis* oocytes we observed that efficient labeling required around 40 hours. This increased exposure time may be explained by a reduced cellular permeability for biotin (Said et al., 1990) and, most likely, to the incubation temperature (18ºC). In fact, Kim et al. (2016) showed that outside the optimal temperature of the BirA enzyme (37ºC) its activity decreases dramatically, yielding poorer biotinylation.

Even though these slower kinetics might be bypassed by increasing the incubation time, the viability of *Xenopus laevis* oocytes once extracted from the frog ovaries is a limiting

factor. Consequently, we concluded that 40 hours of biotin exposure would allow the agreement between the enzymatic activity of the BirA enzyme and the oocytes lifespan.

As shown in figure 21b, 40h incubation with 20μM biotin at 18ºC allows efficient labeling of several proteins, presumably in a CPEB1-specific fashion. Not surprisingly, even in the absence of free biotin in the medium there is biotinylation, as oocytes have constitutive levels of this vitamin.

Notably, there are already biotinylated proteins that are expressed at high levels (fig. 21c), which can potentially affect the affinity purification step. Through mass spectrometry we determined the identity of these proteins, which contain at their active center a biotinyl group: propionyl-CoA carboxylase, methylchrotonyl-CoA carboxylase and pyruvate carboxylase (Tong, 2013).

It is important to stress that the performance of this approach in identifying the components of the CPEBs mRNPs highly depends on the extent of biotinylation achieved by the fusion proteins. In this regard, even though we have been able to set a condition in which extensive and specific biotinylation occurs for the desired fusions but not in the controls, we speculate that other approximations could help increase the biotin signal and reduce the incubation time (Kim et al., 2016; Branon et al., 2018).

On-bead digestion facilitates release from streptavidin columns

After oocytes have been incubated with biotin, they are collected and lysed. To purify the biotinylated proteins streptavidin-coated beads are used. Since the biotin-streptavidin interaction is incredibly stable (it is one of the strongest non-covalent interactions in nature, with a $k_d = 10^{-15}$M (Weber et al., 1989)), stringent washes can be used to remove the non-specifically bound proteins, a feature that is desirable for purification purposes. However, when we tried to elute the bound proteins from the beads follow-

ing the manufacturer's indications we did not observe clear differences with the control when checked by silver staining, not even for more stringent elution buffers containing biotin, thiourea or NH_4HCl (data not shown). Consequently, identification of CPEB mRNPs components through band excision was not a possible option.

Similarly, we tested an alternative proposed by Schiapparelli et al. (2014), based on the tryptic digestion of the samples before the streptavidin column (pre-bead digestion protocol). According to the authors, digestion of the proteins increases peptide solubility in an aqueous phase, which enhances the retention of biotinylated peptides in the beads, and then these can be efficiently eluted using 80% acetonitrile. Accordingly, this strategy increases the direct detection of biotinylated peptides, which serves as a double-check of the interaction of the protein of interest with the candidates. Despite our expectations, in our hands this approach had a really low yield of biotinylated peptides, despite the organic-phase elution (data not shown).

Most likely, the inefficient elution of these two protocols results from the strength of the biotin-streptavidin interaction. Therefore, with the aim to improve the affinity purification step, we decided to try a different approximation, independent of breaking the biotin-streptavidin interaction. Following an on-bead digestion protocol (Schiapparelli et al., 2014), instead of eluting intact proteins, these are treated with trypsin (or any other protease) while bound to the beads so that the non-biotinylated peptides are eluted whereas the modified ones are retained in the column. Consequently, biotinylation of the enriched proteins is inferred rather than direct. Besides, in order to increase the specificity we adopted new washing steps, introducing a combination of harsh buffers containing high concentrations of urea, SDS and Gdn-HCl (Pirone et al., 2017). Following this new protocol we were able to detect a greater number of proteins and with higher spectral counts. In turn, the number of potential hits could be increased as well.

Data analysis and hits selection

All the BioID experiments in the present work have been performed using four biological replicates. Since the frogs that we use in the lab are not inbred nor littermates, there is an important biological variability associated to our data that on the one hand increases the biological relevance and coverage of our findings but on the other restricts the statistical power of the data. For the identification of potential candidates we tested three label-free quantification methods.

At the beginning we used the MStats software, based on Top3, which takes the average intensity of the three peptides (or less, if fewer are detected) with the highest intensity, and uses this value for pairwise comparisons (Krey et al., 2014). A limitation of this quantification method is that, if peptides are not detected in the control (which indeed is desirable), the program cannot calculate statistics such as fold-change (FC) or p-value. In order to minimize this limitation, imputation of the missing values for a near-zero value allows calculation of *ad hoc* FC and p-values.

We also tried the Significant Analysis of Interactome (SAINT) algorithm, which has been broadly used for analyzing affinity purification and BioID data (Choi et al., 2011; Youn et al., 2018). SAINT models the spectral counts of each prey-bait pair into a mixed distribution of two components: true and false interactions. The SAINT version that we have been using, SAINTv2, estimates the spectral count distribution for false interactions from negative controls and the spectral count distribution for true interactions from the spectral counts for all interactions that involve this specific prey and bait. Importantly, SAINT normalizes the spectral counts to the length of the proteins and to the total number of spectra in the purification.

Compared with MStats, SAINT has higher specificity but lower sensitivity, since it is heavily dependent on spectral count number, which has a smaller order of magnitude

and does not fully correlate with peptide intensity. In order to get the maximum number of interactions, the union of SAINT and MStats hits is a good approach. Nonetheless, these two label-free quantification methods have three main drawbacks. First, they are, in general, not adequate for the detection of smaller proteins or for proteins that yield a small number of tryptic peptides. Second, they are not fully recommended for comparing between baits, which was important for our experiments and third, they treat missing values as 0 or near zero, which can accentuate slight differences.

For these reasons, together with the Proteomics and Biostatistics Core Facilities of the IRB, an *ad hoc* pipeline was developed to overcome these limitations. This method uses $\log_{10}$iBAQ as the quantitative variable. The iBAQ value corresponds to the sum of all the peptides intensities of a given protein divided by the number of observable peptides (Krey et al., 2014). By using iBAQ, sensitivity is increased in comparison to the use of spectral counts and, moreover, this value is normalized for protein length or *observability*, hence favoring the detection of smaller proteins as well. Commonly, this value is considered a proxy for relative abundance of a protein in the sample, which makes it amenable for comparisons between different conditions. To minimize batch effects across studies, a percentile normalization was included.

As it happens with MStats and SAINT, the presence of missing values hinders the analysis. Missing values can come from peptides that are not detected due to their low abundance in the sample but can also be due to common spectrometer-derived and/or random errors. In our case, we observed a negative correlation between the number of missings and the $\log_{10}$iBAQ value, which means that low abundance proteins were more likely not to be detected (figure 22a).

In order to solve this limitation as much as possible, an imputation method was developed: for those conditions for which one or two missing values had been identified in the four replicates, the remaining two or thee non-missing values were used for imputa-

tion using a k-nearest-neighbors approximation according to the iBAQ distributions of each replicate. For these bait-prey pairs, candidate interactions can be determined through a differential expression analysis using linear models.

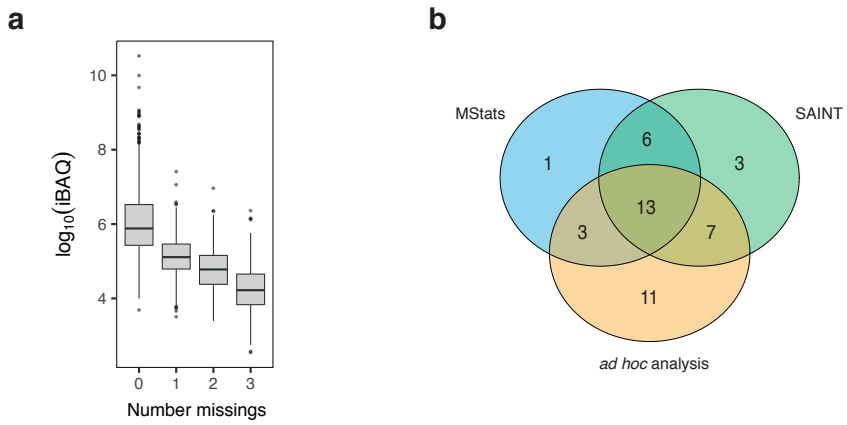

Figure 22: Analysis of BioID data. (a) Boxplot showing the distribution of mean $\log_{10}$iBAQ values depending on the number of missings for the proteins identified in the four replicates of a CPEB1-BirA condition. As observed, the number of missing values anticorrelates with the iBAQ, thus suggesting that less abundant proteins are detected worse. (b) Comparison of the hits identified for CPEB1-BirA using the three alternative methods.

Another scenario that can be found with this data are those conditions with more than two missing values, for which imputation cannot be performed, as it would be less accurate. From this subset of cases, we just considered proteins with 3 or 4 missing values in the control and 0 or 1 missing value in the desired condition, as we want to detect enrichment over the controls. In these cases there are no statistics provided and the arbitrary selection criteria that we chose was to take those proteins whose $\log_{10}$iBAQ was above the first quartile of the $\log_{10}$iBAQ values distribution in the desired conditions and below this threshold in the control condition. Importantly, the use of an arbitrary threshold entails the inherent possibility that true interactors appear as false negatives, though allows a systematic and uniform selection criteria.

With this quantification method we were able to identify most of the hits that had been detected using MStats or SAINT (fig. 22b). In addition, a subset of new potential hits was identified. Importantly, while the hits selection using MStats required a dedicated manual curation and the selection with SAINT required increasing the FDR threshold, lowering the strength of the conclusions, the analysis with the *ad hoc* method is more powerful statistically, allows the comparison between conditions and, as we will observe in the next section, provides true hits as validated by co-immunoprecipitation.

To sum up this section, we have described for the first time the BioID pipeline adapted for *Xenopus laevis* oocytes, emphasizing its caveats and the strategies we have adopted to bypass or control some of its limitations. By these means we have not only obtained novel results in the CPEB field but we have also provided a valuable contribution to the cell and molecular biology fields, by making frog oocytes (transcriptionally silent cells that undergo an incredible translational reprogramming upon hormone stimulation) a system amenable for *in vivo* interactomics.

CPEB1 repression complex in stage VI oocytes

In stage VI *Xenopus laevis* oocytes, CPEB1 is the highest expressed member, which explains why it is, by far, the most studied paralog in this context. Accordingly, several works modeling the molecular mechanism behind CPEB-mediated translational repression and activation have been built using CPEB1 as reference (Stebbins-Boaz et al., 1999; Kim and Richter, 2006; Minshall et al., 2007). For these reasons, we decided to set up and test the performance of the BioID using this paralog. To start with, the context of translational repression was preferred, as more stable complexes were expected.

BioID of wild-type CPEB1

In stage VI *Xenopus laevis* oocytes, it is well known that CPEB1 is exerting a translational repressor function. In contrast to other repressor proteins such as DDX6 (Hondele

et al., 2019), which have a well-characterized enzymatic activity, CPEB1 is considered to have a role in the recruitment of effector proteins to its target mRNAs. For the *in vivo* identification of these recruited proteins we adapted the BioID methodology to stage VI oocytes and fused CPEB1 to the BirA enzyme. In order to control for fusion effects, we performed all the experiments with fusions at the N- and C-termini (fig. 23a). Henceforth, we will refer to the proteins detected in our BioID, which can either be CPEB1 interactors or proteins in close proximity, as the CPEB1 proximome.

By using the thresholds described in the previous section (adjusted p-value < 0.05 when statistics can be performed or $\log_{10}\text{iBAQ}_{\text{protein}} > \text{Q1}_{\text{condition}}$), a total of 30 proteins were identified in the CPEB1 proximome for both fusion proteins (fig. 23b).

Despite the big overlap between CPEB1-BirA and BirA-CPEB1, there are some potential candidates that have been detected only with one fusion, which may reflect a slight change in the structure of CPEB1 or, more possibly, differences in the spatial architecture that can be acquainted by positioning the BirA at one terminus or at the other. Comparing appendix tables 1 and 2, in terms of protein enrichment (surrogate for protein biotinylation), C-terminal BirA constructs tend to work better, possibly due to the fact that this domain is highly ordered and, thus, could be less affected by the fusion.

To assess if there is evidence that these proteins can form a complex or, otherwise, they have been spuriously related in our experiment, we took data from a database of curated protein-protein interactions (Szklarczyk et al., 2017) and checked the network that these proteins form according to works on *Xenopus* species (*Xenopodinae*). As it is depicted in figure 23c, these proteins form a highly connected and significant network, providing evidence that the proximome we have identified through our BioID adaptation has robust biological meaning.

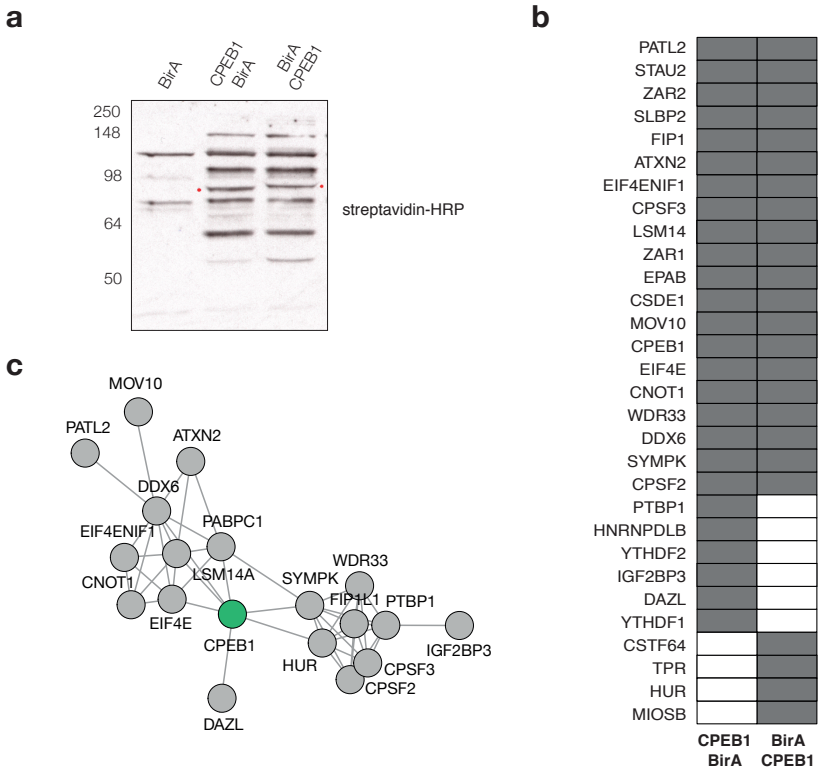

Figure 23: CPEB1 BioID provides bona fide repression complex components. (a) Streptavidin-HRP western blot showing the biotinylation attained by the BirA alone and fused to CPEB1 at both termini. After 40h of biotin exposure, extensive and highly specific biotinylation is observed for the CPEB1 fusions. (b) Table of proteins identified as potential CPEB1 interactors, in gray. Despite some unique hits for each fusion, most of the putative CPEB1 proximal proteins are common in the two conditions. (c) Network graph with *Xenopodinae* data for the CPEB1 hits using string-db. As observed, most of the hits identified in the CPEB1-BioID form a highly connected network. Only interactions with score > 0.6 have been depicted.

This list of proteins is enriched in biological processes related to regulation of translation, post-transcriptional control and mRNA metabolism, which is expected for CPEB1 interactors. Interestingly, at the level of cellular component, the proximome of CPEB1 is highly connected to non-membrane bound organelles such as P-bodies, stress granules and, in general, mRNA ribonucleoprotein complexes (fig. 24).

While some of these proteins had already been associated to CPEB1 (Minshall et al., 2007), we have identified a plethora of new interactions (i.e. YTHDF1, ATXN2, SLBP2, MOV10, PTBP1, IGF2BP3...), providing new insights into CPEB1-mediated translational repression. Interestingly, described interactors such as Maskin, PARN and Gld2 (Stebbins-Boaz et al., 1999; Kim and Richter, 2006) did not appear in our BioID data, which can either mean that they are not real partners of CPEB1 or that they cannot be detected with our experimental setting.

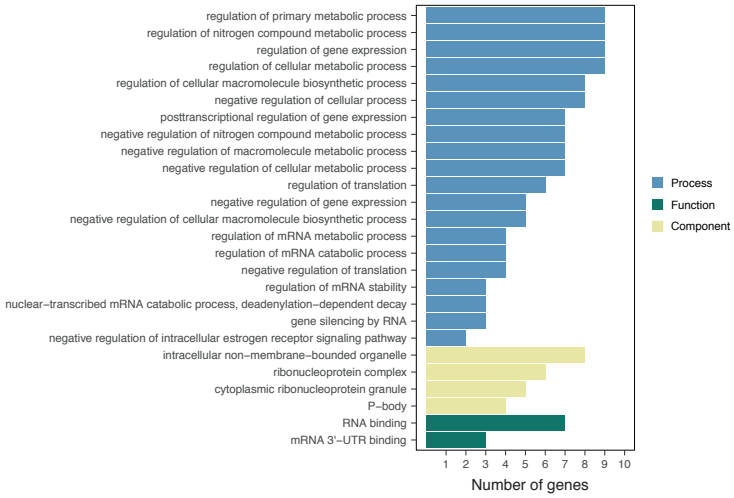

Figure 24: GO categories enriched for the CPEB1 proximome. Barplot displaying the gene ontology categories enriched for components, functions and processes by the number of genes found in our dataset. Only categories with FDR < 0.0001 are shown.

Co-immunoprecipitation experiments (co-IPs) were performed for validating some of the candidates. For these assays we either immunoprecipitated overexpressed HA-CPEB1 and checked the co-immunoprecipitation of endogenous candidates or immunoprecipitated HA-candidates and checked co-precipitation of endogenous CPEB1. Since we could not overexpress CNOT1, we decided to perform the validation with other CCR4-NOT complex components, namely CCR4, CNOT2 and CNOT10.

As shown in figure 25, HA-CPEB1 efficiently co-precipitates endogenous HUR, DDX6,

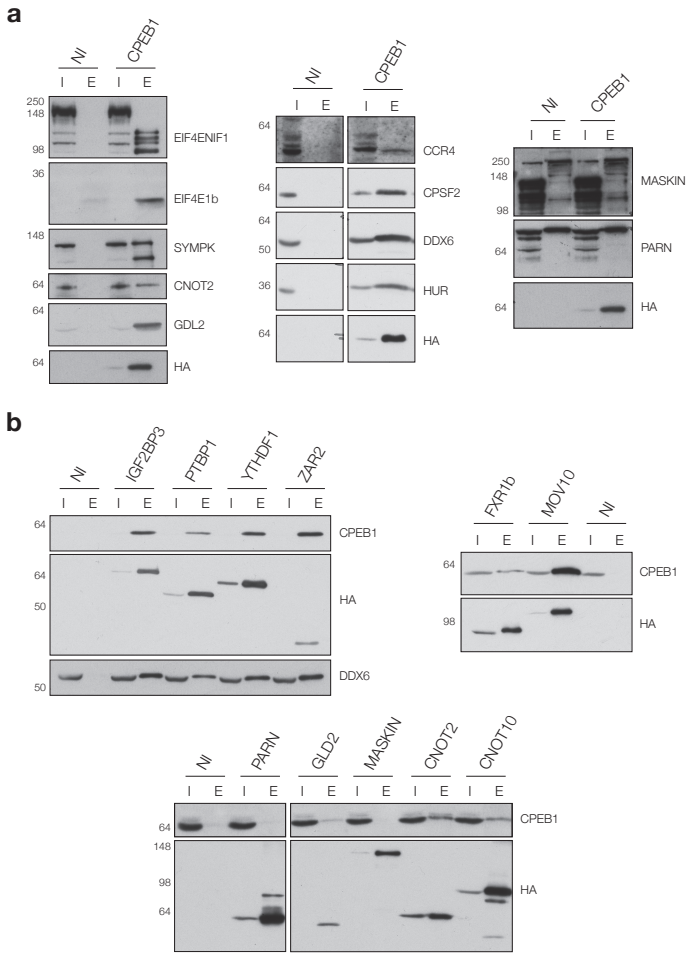

Figure 25: Validation of CPEB1 BioID data through co-immunoprecipitation. (a) Western blots showing HA-CPEB1 co-immunoprecipitation (I, input; E, elution) of: (left) EIF4ENIF1 (eIF4E-T), EIF4E1b, SYMPK, CNOT2 and Gld2; (middle) CCR4, CPSF2, DDX6 and HUR; (right) Maskin and PARN. Except for Maskin and PARN, all the candidates tested co-precipitate with CPEB1, validating the results obtained with BioID. For each candidate, three independent experiments were performed. (b) Western blots showing HA-candidate co-immunoprecipitation of: (top left) IGF2BP3, PTBP1, YTHDF1 and ZAR2; (top right) FXR1b and MOV10; (bottom) PARN, Gld2, Maskin, CNOT2 and CNOT10. Interaction with CPEB1 is confirmed for all tested proteins except PARN, Maskin and Gld2. For each candidate, two independent experiments were performed. HA-IP with not injected oocytes (NI) were performed as controls.

eIF4E-T, eIF4E-1b, CNOT2, CPSF2 and SYMPK. Apart from these proteins, we also tested some that did not appear in our BioID data but had been previously identified in the CPEB1 repression complex: Maskin, PARN and Gld2. While Gld2 was efficiently co-immunoprecipitated with HA-CPEB1, PARN and Maskin were not. In addition, co-immunoprecipitation of a catalytical subunit of the CCR4-NOT complex, CCR4, was observed as well, suggesting that PARN may not be the deadenylase of the CPEB1 repression complex but, instead, it is the CCR4-NOT complex.

Regarding the HA-candidate co-immunoprecipitations, we observed robust interaction with CNOT2, CNOT10, ZAR2, PTBP1, YTHDF1, IGF2BP3 and MOV10. Again, no interaction was observed for PARN and Maskin, supporting our prior observations. Intriguingly, no significant association was detected between HA-Gld2 and CPEB1 with this experimental setting, a result possibly due to the inefficient overexpression of HA-Gld2 achieved in oocytes. Remarkably, FXR1b, which was just below the BioID threshold, also interacts with CPEB1 but to a lower extent than MOV10.

Considering our results, Maskin is not a component of the main cytoplasmic pool of CPEB1 repression complexes, since it has not been identified either by BioID or co-IP. We speculate that, in fact, this interaction may occur only in a fraction of complexes found in the centrosome or the mitotic spindle, based on the literature (Groisman et al., 2000; O'Brien et al., 2005; Minshall et al., 2007). On the other hand, our data indicates that CPEB1 recruits the CCR4-NOT machinery instead of PARN, hence ensuring that the targets have short poly(A) tails. Indeed, as we will further discuss, several works suggest that PARN is a nuclear enzyme with little, if none, activity on the cytoplasmic pool of mRNAs (Yamashita et al., 2005; Wühr et al., 2015; Yi et al., 2018).

Apparently, the interaction of CPEB1 with proteins such as PTBP1, MOV10, HUR, FXR1b and ATXN2 suggests that CPEBs may act synergistically with the miRISC to efficiently recruit the CCR4-NOT complex to their targets. Moreover, our findings es-

tablish for the first time a putative connection between the CPEBs and the m^6A mark, as interaction with methylation readers such as YTHDF1, YTHDF2 and IGF2BP3 has been observed in our BioID experiments and then further validated through co-immunoprecipitation.

Importantly, our results prove the specificity of the BioID methodology adapted to *Xenopus laevis* oocytes. By means of this *in vivo* approach we have portrayed a more physiological approximation of the CPEB1 repression complex, providing an interesting set of new interactions that pave the way for a new conception of the molecular mechanism underlying CPEBs-mediated translational repression.

CPEB1 repression complex formation requires RNA binding

Several studies have used RNase treatments to discern the nature of the CPEB1-candidate interactions (Mendez et al., 2000a; Minshall et al., 2007; Lin et al., 2010). However, these experiments are performed *in vitro*, which can hinder the real nature of these interactions. To understand the requirements of these bindings and, in a more fundamental way, to what extent the CPEB1 complex assembly relies on its target mRNA, we conducted a BioID experiment using an RNA-binding mutant of CPEB1. This mutant consists of a Y365A substitution, designed from the CPEB1 C-terminus solved structure and validated functionally through competition assays (Afroz et al., 2014).

Our results indicate that a high number of interactions are reduced (tiles in red) or even lost in the mutant condition compared to the wild-type (fig.26b), suggesting that the interactions between these proteins depend on CPEB1 RNA binding competency *in vivo*. To validate these findings we proceeded with co-IPs of some of the candidates. For all the proteins tested, we observed a reduction in the co-immunoprecipitation with the RNA-binding mutant (fig.26c), even in the case of candidates for which the BioID did not detect any difference (e.g. SYMPK, eIF4E and HUR).

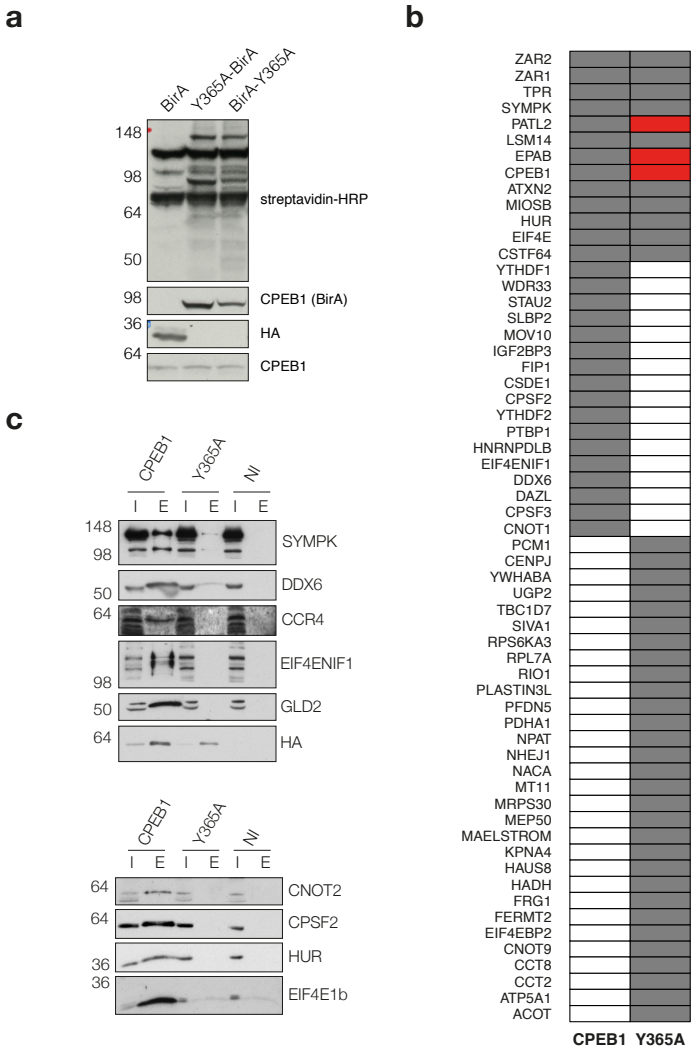

Figure 26: CPEB1 RNA-binding mutant is not able to form a repression complex. (a) Western blot showing biotinylation and expression (CPEB1 and HA) of the Y365A-mutants. Endogenous CPEB1 was used as loading control. (b) Table of CPEB1 and Y365A mutant hits. For each condition, the union of the N- and C-terminal fusion hits is depicted. Tiles in red indicate a significant reduction in the interaction compared to the wild-type (p-value < 0.05). As shown, most of the interactions are lost or reduced in the mutant condition, yet unique interactions for the Y365A-mutant also appear. (c) Western blots showing HA-CPEB1 and HA-Y365A co-immunoprecipitation of: (top) SYMPK, DDX6, CCR4, EIF4ENIF1, Gld2; (bottom) CNOT2, CPSF2, HUR and EIF4E1b (n = 2). HA-IP with not injected oocytes served as controls. As shown, Y365A mutant fails to co-immunoprecipitate CPEB1 partners.

Considering the differences between the BioID data, which captures transient and weak interactions *in vivo* and the co-IPs, in which these interactions can be affected by lysis and are less stable kinetically, discrepancies between methodologies are expected. Nonetheless, both approaches share the same interpretation: the interactions between CPEB1 and its partners are lost in general upon RNA-binding capacity ablation.

It is noteworthy that some new hits appear in the proximome of the mutant. Notwithstanding, this set of proteins do not form a highly connected network according to string database data, since only isolated functional groups appear to be significant and none of the GO terms enriched for these proteins can be related to a role in translational control (data not shown). We attribute this appearance of interactions to a less hindered CPEB1 molecule, as it would not be coated by the components of the repression complex.

Overall, from this data we conclude that the CPEB1 repression complex, and potentially those assembled by the other CPEBs, does not stably form unless it is bound to a target mRNA, which ensures specificity and the persistent repression required for maintaining the quiescence of cells.

Even though we cannot rule out the possibility that some interactions may occur independent of RNA binding, as has been pointed out by RNase treatment assays (Mendez et al., 2000a; Minshall et al., 2007; Lin et al., 2010), we speculate that the discrepancies with previous studies may be attributed to kinetic considerations: while the Y365A mutation is likely affecting complex nucleation in our experiments, RNase treatment is probably triggering complex disassembly, a process that might be RNA-independent once protein-protein interactions form a stable network.

CPEB1 potentially recruits repression factors through the NTD

The structure of the CPEBs, highly ordered at the CTD and intrinsically disordered at the NTD, is suggestive of modularity: while the CTD is responsible for binding the target mRNA, the NTD is a hub of regulatory elements (Mendez et al., 2000a; Pavlopoulos et al., 2011; Guillén-Boixet et al., 2016) and a platform for protein-protein interactions (Schelhorn et al., 2015). This assumption is apparently confirmed by experimental observations carried out by Afroz et al. (2014), which showed that the CTDs of CPEB1 and CPEB4 are able to compete polyadenylation mediated by their full-length counterparts, possibly because they are not able to recruit the polyadenylation machinery despite binding to the target.

Considering this hypothesis we decided to perform the BioID using a truncated version, expecting to observe an NTD-dependence for the vast majority of interactions that we had identified for the full-length. Since we had observed that the formation of the repression complex requires RNA binding and we suspected that the intrinsic disorder of the NTD may be affected by the fusion of the BirA enzyme, we chose to perform the BioID with an NTD-truncated version. Accordingly, the information of which interactions are mediated by the NTD itself would be obtained by subtraction comparing the CTD to the full-length CPEB1.

As shown in figure 27b, the BioID data points to a general reduction in the interaction of CPEB1 with its partners if it lacks its NTD. These results are consistent with observations from Tsvetkov et al. (2020), who observed loss of CPEB2 and CPEB3 interactors upon truncation of their prion-like domains, which are found in the NTD. Consequently, the formation of the repression complex does not only require binding to RNA, as we mentioned in the previous section, but it also seems to require the motifs that lie in the N-terminal domain to establish additional stabilizing contacts.

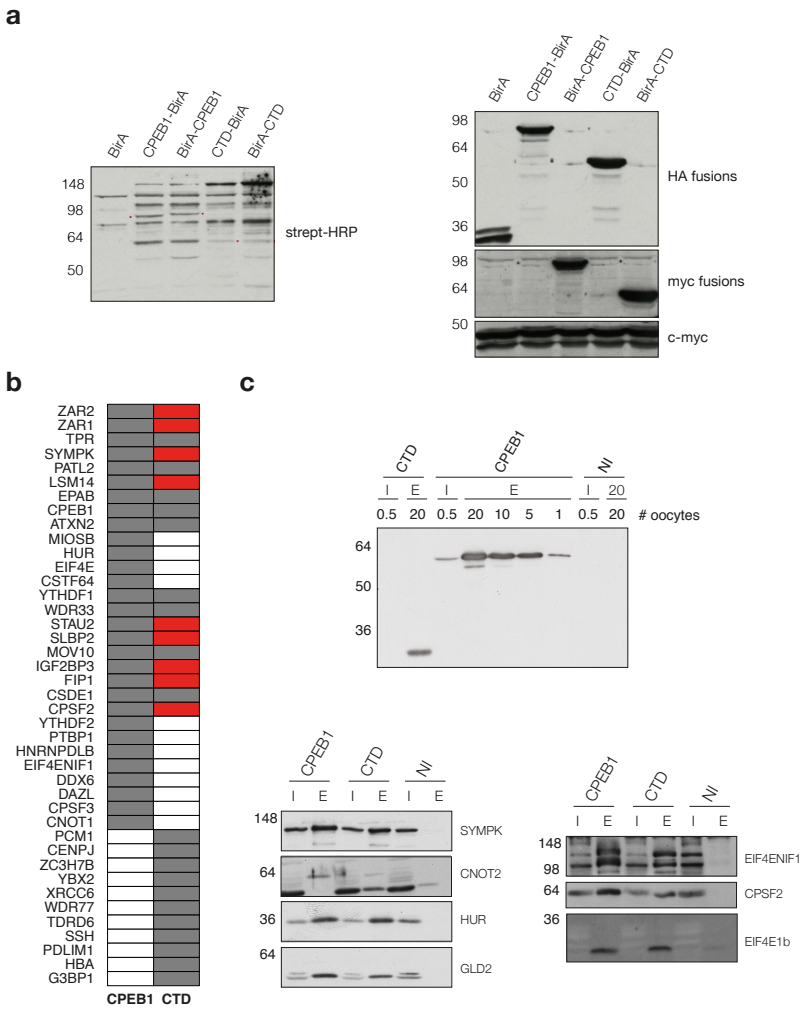

Figure 27: CPEB1 potentially recruits its partners through the NTD. (a) Western blot showing biotinylation and expression of the CTD variants. Endogenous c-myc was used as loading control. (b) Table of CPEB1 and CTD hits. For each condition, the union of the two fusions' hits is depicted. Red tiles indicate a significant reduction compared to full-length (p-value $<$ 0.05). As shown, most of the interactions are lost or reduced upon truncation, yet CTD-specific partners also appear. (c) (top) HA western blot showing the ratio 20:5 (20 oocytes CTD : 5 oocytes full-length) used for loading the co-IP gels. (bottom) Western blots showing HA-CPEB1 and HA-CTD co-IP (I, input; E, elution) of: (left) SYMPK, CNOT2, HUR and Gld2; (right) EIF4ENIF1, EIF4E1b and CPSF2. As shown in the figure, CPEB1 interaction with the tested partners seems not to be compromised by NTD truncation. Only one replicate was performed. HA-IP with not injected oocytes was used as control.

To validate this observation, we performed co-immunoprecipitation experiments with the full-length CPEB1 and the NTD-truncated version. As the expression of HA-CTD is lower than that of the full-length, we loaded a ratio of 20:5 oocytes, to have a similar amount of precipitated protein in both conditions (fig.27c). Contrary to what we expected from the BioID data, co-immunoprecipitation of most of the tested CPEB1 partners seemed not to be significantly compromised by the truncation of its N-terminal domain (fig.27c). From the tested candidates, only a potential reduction is observed for CNOT2, though more replicates and a curated quantification are still pending.

The discordance between these two alternative approaches may arise from the interpretation of the results: while the BioID data indicates changes in the local environment of the CTD-BirA protein (the biotinylation radius spans to just 10-20nm, (Varnaitė and MacNeill, 2016)), the co-IPs may be capturing a much bigger complex that would be less affected by the truncation as it can still interact with RNA. For this reason, we still consider the hypothesis that the NTD mediates an important fraction of the protein-protein interactions that take place in the CPEB1 repression complex.

From the results obtained for the two variants, the RNA-binding mutant and the NTD-truncated CPEB1, we propose that both RNA binding and the NTD are important for the assembly of the CPEB1 repression comple. We hypothesize that the formation of a competent repression complex only occurs once the CPEBs are bound to their targets: this contact would serve as the nucleation step, in order to ensure specificity. However, the stability and functionality of the complex would be guaranteed by additional contacts, most likely established by the NTD, which may explain why some interactions are RNase-resistant (Mendez et al., 2000b; Minshall et al., 2007) and the ability of the CTD to compete polyadenylation.

With these experiments, the data from the Y365A mutant and the characterization of the wild-type CPEB1 proximome, we have not only verified the feasibility of the BioID

in *Xenopus* oocytes but we have also explored the ability of this approach to detect interactomic changes upon mutation or truncation. Considering this, we next decided to use the BioID for CPEB2-4 to assess to which extent the four CPEBs assemble similar complexes.

Even though the experiments addressing the RNA and NTD dependence of CPEB2-4 are yet to be performed, we speculate that the same principles described for CPEB1 may apply to them, in view of their structural similarity (Afroz et al., 2014; Tsvetkov et al., 2020).

CPEB1-4 share a core of interactors in stage VI oocytes

In stage VI oocytes, CPEB1 is the highest expressed CPEB (Igea and Méndez, 2010; Peuchen et al., 2017). However, the fact that the other paralogs are also present in this scenario, yet at lower levels (Duran (2020), unpublished), poses the question whether the four CPEBs act seemingly as translational repressors or, conversely, they exert different or non-redundant functions. To address this question we performed BioID of CPEB2-4 in collaboration with Berta Duran from our lab. Importantly, these experiments were carried out with the two fusion positions as well and, for each condition, four biological replicates were used. Venn diagrams of the BirA-fusion variants show less hits overlap for CPEB2-4, which proves the need to work with both constructions in order to increase the scope of the technique (fig.28b).

As we can observe in figure 28c, the proximomes of the four CPEBs have a certain degree of overlap but, at the same time, show exclusive interactions. The more dissimilar condition seems to be CPEB2, with fewer targets than its counterparts. This observation could allegedly be attributed to the lower expression of CPEB2-BirA, which results in less biotinylation of its vicinal proteins and, ultimately, poorer detection of them, though there could be other explanations, as despite being BirA-CPEB2 highly

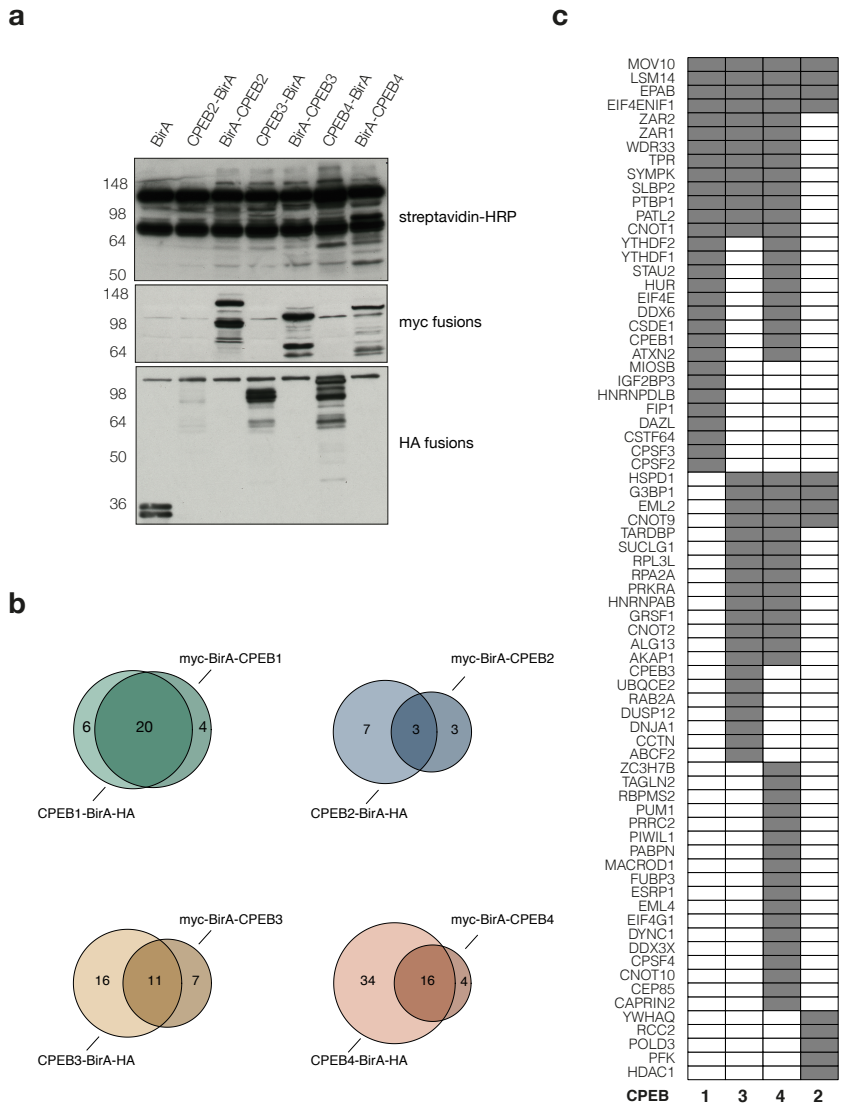

Figure 28: CPEB1-4 BioID results suggest functional similarities in stage VI oocytes. (a) Western blot showing biotinylation (streptavidin-HRP) and expression (HA and myc) of the CPEB2-4 BioID fusion proteins. (b) Venn diagrams depicting the overlap between fusion variants for each condition. While there is a high overlap between CPEB1 versions, a poorer overlap is observed for CPEB2-4. (c) Table of CPEB1-4 targets identified using the *ad hoc* analysis. For each condition, the union of the N- and C-terminal fusion hits is depicted. As shown, though CPEB1-4 share a core of proximal proteins, there are CPEB-specific interactors that suggest possible functional differences among the paralogs.

expressed it has yielded few hits as well. Taking into account the profiles of CPEB1, CPEB3 and CPEB4, we speculate that CPEB2 has a broader scope than what we have been able to detect. Nonetheless, there are a few CPEB2-specific hits that do not appear for the other CPEBs in spite of their higher expression, which suggests that they may be actual CPEB2-specific partners. These specific hits, however, have not yet been related in the literature according to the string-db database (data not shown).

Looking at the proximomes of CPEB1, CPEB3 and CPEB4 there seems to be a conserved core of interactions (MOV10, LSM14, EPAB, eIF4E-T, ZAR proteins, SYMPK, PTBP1, CNOT1...), which we speculate is bigger if we take into account that CNOT2 and CNOT10, that appear as candidates for CPEB3 and/or CPEB4, co-precipitated with CPEB1 despite not appearing as BioID hits.

For validating the BioID results through co-IPs we used candidates that appeared only for CPEB1 (CPSF2), for all of them (SYMPK, EIF4ENIF1) and hits that appeared for both CPEB1 and CPEB4 (HUR, EIF4E1b, CPEB1, DDX6). Interaction with Gld2 was also tested, yet it did not appear as a hit for any CPEB. Even though the expression of the HA proteins is not the same and the efficiency of the HA-IPs differs among conditions, all four CPEBs apparently interact with all the tested candidates (fig.29b). The interaction between CPEB2 and CPSF2 or EIF4E1b was validated in other replicates, and also the interaction of CPEB4 with EIF4ENIF1.

These observations suggest that complexes assembled by CPEB1-4 may have more in common than the BioID results indicate and, additionally, may be physically in contact, as CPEB2-4 efficiently co-immunoprecipitated the endogenous CPEB1. Notwithstanding, there is a significant number of CPEB-specific interactions that we have not tested yet and may be actually exclusive, raising the question as to which extent are the four CPEBs exerting a similar function in the oocyte.

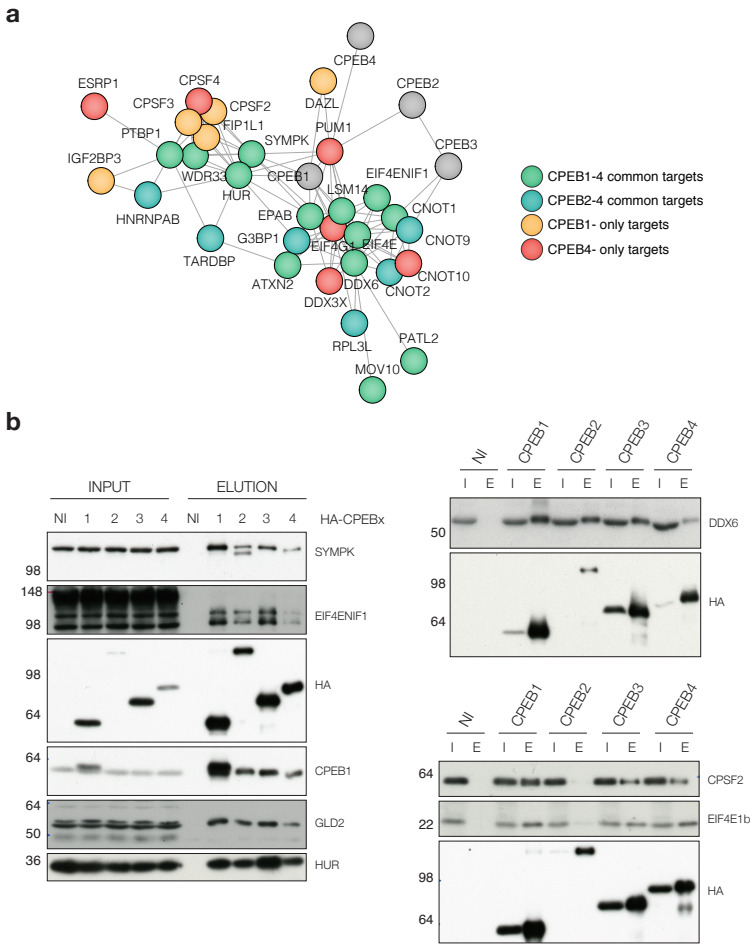

Figure 29: CPEB1-4 candidates interaction network and validation through co-immunoprecipitation. (a) Network graph with *Xenopodinae* data from string-db.org for the CPEB1-4 hits. Only interactions with score > 0.6 have been depicted. Dots in green indicate targets found for CPEB1 and the union of CPEB2-4, dots in blue are CPEB2-4 common targets and yellow and red indicate CPEB1-only and CPEB4-only targets respectively. As shown, CPEB1-4 targets form a highly connected network of functionally related proteins, which indicates the similarity between the complexes they can potentially assemble. (b) Western blots showing HA-CPEB1-4 co-immunoprecipitation (I, input; E, elution) of: (left) SYMPK, EIF4ENIF1, CPEB1, Gld2 and HUR; (right top) DDX6; (right bottom) CPSF2 and EIF4E1b. As shown in the figure, all four CPEBs interact seemingly with the tested candidates. For each condition, three independent experiments were performed. In all experiments, HA-IP with not injected oocytes (NI) were performed as controls.

Notably, these specific interactors of CPEB3 and CPEB4 have also been implicated in the regulation of mRNA stability, localization and translation, as is the case of G3BP1 and PRRC2 (Youn et al., 2018), TARDBP and PRKRA (Kok et al., 2007), DDX3X (Phung et al., 2019), ESRP1 (Fagoonee et al., 2013) and CAPRIN2 (Konopacka et al., 2015). In addition, these proteins are tightly connected to CPEB1 interactors according to the string database (fig.29a), which suggests that the function of CPEB2-4 may not differ much from that of CPEB1.

Considering all these findings, we speculate that all four CPEBs may act as translational repressors in stage VI oocytes, possibly through the assembly of partially different complexes. However, we propose that this inhibition of translation would be achieved by a similar mechanism: preclusion of translation initiation by targeting the adoption of the closed-loop conformation. Accordingly, cap-blockage is hinted by the interactions with eIF4E-1b and eIF4E-T and poly(A) tail shortening is expected from the interactions with the CCR4-NOT complex components, which had already been observed for CPEB3 (Hosoda et al., 2011).

Remarkably, to this general mechanism other complementary regulators are also added for the CPEB2-4 branch: interaction with the miRNA-induced silencing complex (MOV10, PTBP1, ATXN2), m^6A readers (YTHDF1/2) and master translational regulators such as CSDE1, STAU2 or HUR.

CPEB1 activation complex in maturing oocytes

As previously mentioned, CPEBs have been described to have a dual role in translational control: they can both repress and activate translation of their targets by controlling the length of their poly(A) tails (Kim and Richter, 2006; Fernández-Miranda and Méndez, 2012; Hu et al., 2014). While for CPEB4 it has been suggested that the switch from repressor to activator is not a consequence of changes in the complex composition, but

rather by a change in its condensation status (Guillén-Boixet et al., 2016), for CPEB1 this switch entails a remarkable complex remodeling (Stebbins-Boaz et al., 1999; Mendez et al., 2000b; Kim and Richter, 2006, 2007). So far, the reorganization of the CPEBs repression complex has not been addressed by any high-throughput *in vivo* approximation, and for this purpose BioID stands as a useful approach, specially because it was developed with the aim to capture transient and/or weak interactions in live cells (Roux et al., 2012), which we assume will be predominant in a complex that favors translation of a target mRNA. To set up the methodology we decided to start with CPEB1, for which there is more knowledge in this regard.

Notably, during meiosis resumption CPEB1 not only gets phosphorylated by Aurora A kinase for the early polyadenylation wave but then gets also hyperphosphorylated by Cdk1 and Plk1, triggering its degradation. Consequently, for the study of the CPEB1 activation complex we decided to use a 6-alanine mutant (Cdk1 and Plk phosphonull), which had been described to prevent CPEB1 degradation in canonical maturation experiments while not compromising its role as an activator (Mendez, 2002; Setoyama et al., 2007).

In our hands, even though this mutant was not fully degraded as the endogenous CPEB1 upon progesterone stimulation, its levels were reduced (fig.30a), possibly due to longer incubation times with the hormone. As a consequence, the detection range of the stage VI and MII samples was different, being the progesterone-stimulated conditions those that rendered fewer hits. In addition, since we did not control for the global proteomic changes between stage VI and MII oocytes, a quantitative comparison between the two conditions was not possible.

To reduce the impact of these limitations and get the most out of our data, we considered taking the hits of both conditions, ranking them according to their fold-changes, and then compare them in the two scenarios. Accordingly, proteins that are more import-

ant in the context of translational repression will have lower ranks in the MII samples, while those necessary for translational activation will appear in higher ranks. In any case, changes in these ranks may be attributed to proteomic and/or interactomic reasons.

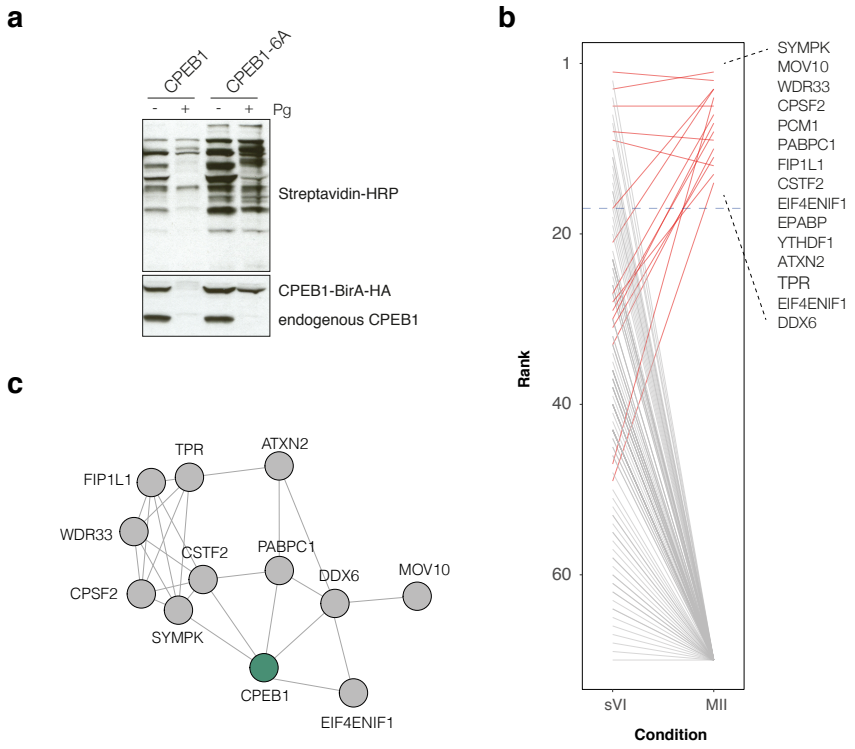

Figure 30: Determination of the CPEB1 activation complex through BioID. (a) Streptavidin-HRP western blot showing biotinylation attained by CPEB1-BirA and CPEB1-6A-BirA with and without progesterone stimulation. Overexpression was monitored using CPEB1 western blot. As depicted, CPEB1-6A gets partially degraded upon hormone incubation, compromising the extent of biotinylation in these samples. (b) Plot showing the rank comparison of the SAINT data (BFDR < 0.15) for CPEB1-6A samples with and without progesterone. While some interactions seem to be kept or favored in terms of rank, others are lowered or even not detected upon progesterone stimulation. (c) Network graph with *Xenopodinae* data from string-db.org for the CPEB1 activation hits. Interactions with score > 0.6 are depicted.

With these considerations, we found upregulation of factors related to polyadenylation, namely WDR33, CPSF2, FIP1L1, CSTF2 and PABPC1 (Sun et al., 2018), and also

translational regulators such as YTHDF1 (Shi et al., 2018) and DDX6 (Weston, 2006; Wang et al., 2015b), as expected (fig.30b). Accordingly, the identified proteins form a highly connected network (fig.30c). Symplekin, though not upregulated compared to stage VI conditions, still acts as a scaffold protein for the activation complex, as it had been observed previously (Kim and Richter, 2006). In this scenario, MOV10 and ATXN2 seem to be important, which provides more evidence to their possible dual role controlling translation of certain mRNAs (Lim and Allada, 2013; Kenny and Ceman, 2016; Kute et al., 2019). Interestingly, the BioID detected association with PCM1, a component of the pericentriolar material, supporting the role of CPEB1 in mediating spindle-localized translation (Eliscovich et al., 2008).

Other proteins with a relevant role in translational repression such as the CCR4-NOT components, PATL2 and the LSM14 family, have not been detected, which can indicate that the interaction with CPEB1 has been reduced, though other scenarios are also possible. PATL2, for instance, gets degraded upon maturation (Nakamura et al., 2010). On the other hand, with this approach we have not been able to detect new interactions (even not a poly(A) polymerase), which, as mentioned above, may be a combination of lack of biotinylation and more labile or transient interactions.

Albeit preliminary, these findings indicate that the translational activation mediated by CPEB1 is assisted by other RNA binding proteins, such as MOV10, YTHDF1 and ATXN2, which paradoxically also play a role in the context of translational repression. It is tempting to speculate that protein-protein interactions may not be sufficient to account for a univocal biological function but, rather, there are extra layers of regulation that ultimately decide the role a complex is exerting.

Considering that CPEB4 and many components of the CPEBs mRNPs undergo liquid-liquid phase separation, a process generally regulated by PTMs, we speculate that phosphorylation of some CPEB repression complex components triggered by progesterone

stimulation will affect the LLPS properties of the whole particle which, in turn, may also affect the activity of components such as the CCR4-NOT machinery, as it has been recently described *in vitro* (Sheu-Gruttadauria and MacRae, 2018; Kim et al., 2019).

In line with this hypothesis, the following Results sections will be devoted to the study of the liquid-liquid phase separation properties of the CPEB family since we believe that, as an increasing number of other RNA-binding proteins, all four CPEBs have their function regulated or exert their function through this principle.

Sequence analysis suggests different features for the CPEBs

Previous work from our lab demonstrated that CPEB4 is able to phase separate *in vitro* and *in vivo* in an RNA-independent fashion. Accordingly, CPEB4 LLPS relies solely on its NTD intrinsic properties, possibly through the multivalency conferred by the IDRs found in this region (Guillén-Boixet et al., 2016). On the other hand, little is known about the phase separation properties of the remaining CPEBs, for which only the ability to form cytoplasmic foci or amyloid deposits has been addressed for CPEB1 and CPEB2-3 respectively (Wilczynska, 2005; Stephan et al., 2015; Tsvetkov et al., 2020).

The ability of a protein to undergo liquid-liquid phase separation is determined by its sequence. As previously mentioned, the concept of multivalency explains the condensation properties of proteins *in vivo* or in potential physiological conditions (Banani et al., 2016; Wang et al., 2018). Motifs mediating protein-protein interactions (PPI) found in intrinsically disordered regions provide multivalency to proteins that lack multiple ordered protein-binding domains, and this is the principle that we speculate explains CPEBs phase separation, as they only have one ordered region, responsible for a single valency (the RRMs bind to RNA in a fly-trap conformation) (Afroz et al., 2014).

With these assumptions, we used on-line predictors to check the extent of intrinsic dis-

order and the potential PPI-mediating motifs in the CPEBs sequences.

Prediction of order/disorder using the metapredictor PONDR-FIT algorithm (Xue et al., 2010) shows clear differences between the highly structured CTDs and the more unstructured NTDs (fig.31a, black line), as expected. Remarkably, CPEB1 was the only member of the family without long disordered stretches.

Disordered proteins are enriched in SLiMs (Mooney et al., 2012) and MoRFs (Mohan et al., 2006), which are motifs with the ability to fold upon binding and mediate protein-protein interactions. Theoretically, these sequences increase the valency of the IDPs they lie at, hence favoring the formation of phase separated compartments. We checked the presence of these kind of motifs through open source predictors, namely SLIMPred v0.9 and MoRFchibi (Malhis et al., 2016). As depicted below, these motifs accumulate at the NTD of all four CPEBs, specially in the case of CPEB2-4 (fig.31a, highlighted stretches). Interestingly, some motifs can be found at the CTD of CPEB1-4, for example in regions in the vicinity of the ZZ-box, which indeed has also been suggested to mediate protein-protein interactions (Merkel et al., 2013).

Charge content and patterning has been established as a modulator of protein solvation properties and, therefore, contributes enthalpically to phase separation (Martin and Mittag, 2018). Accordingly, we checked the net charge distribution along the NTDs of CPEB1-4 at pH 7.4 in 9-amino acids windows (fig.31b). Charge distribution in IDRs is critical for phase separation: charge *blockiness* increases the propensity for LLPS whereas charge alternation severely impairs this phenomenon (Das and Pappu, 2013; Elbaum-Garfinkle et al., 2015). Using these settings, we observed a clear difference between CPEB1 and CPEB3-4, having CPEB1 an alternate pattern and CPEB3-4 a more *blocky* one, with long patches of negatively and positively charges residues. Notably, CPEB2 has an in-between profile.

Altogether, these analyses strongly suggest that, from the CPEB family, CPEB1 would have the lowest propensity for phase separation while CPEB2-4 would be more prone to undergo LLPS. To validate this hypothesis, which could help us propose an evolutionary purpose for the splitting of CPEB1 and CPEB2-4 branches, we conducted *in vivo* phase separation experiments using overexpression of GFP-tagged versions in U-2 OS cells.

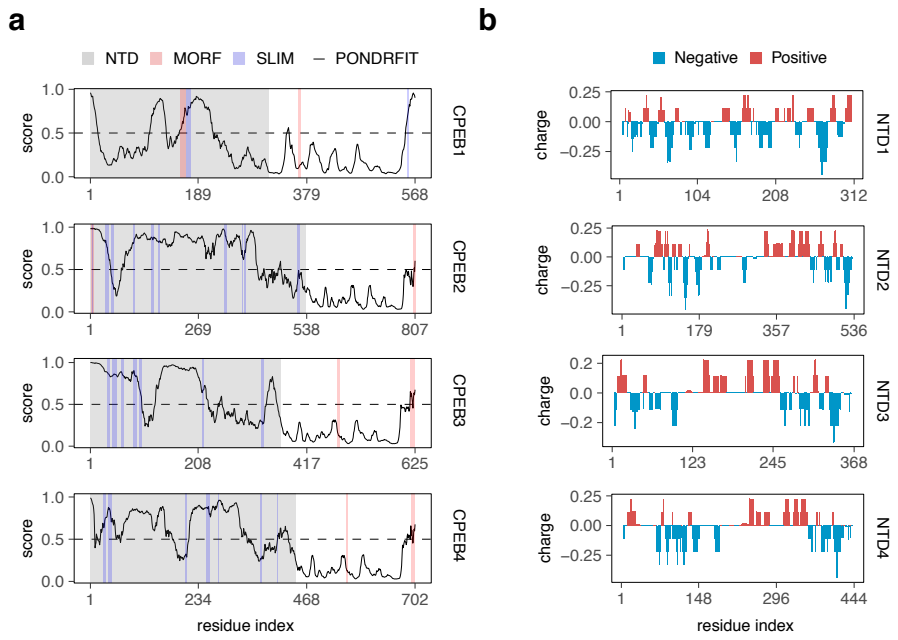

Figure 31: Comparative analysis of the CPEB sequences. (a) Plots displaying the disorder score obtained using PONDR-FIT for the four CPEB sequences in *Xenopus laevis*. Stretches with values over 0.5 are predicted as disordered and are concentrated at the N-terminal domain. Motifs predicted to mediate protein-protein interactions are depicted in light pink (MoRFs, predicted with MoRFchibi) and light blue (SLiMs, predicted with SLiMPred). Only significant MoRFs (legth over 5 residues and score cut-off of 0.66) and SLiMs (length between 3-12 residues and score cut-off of 0.25) are displayed. (b) Plots displaying the net charge of the NTD sequences at pH 7.4 in 9-amino-acid windows. Positively charged windows are coloured in red and negatively charged ones in blue. For these analyses we used the annotated sequences more similar to our cloned proteins.

CPEB1 biomolecular condensation in vivo

We dedicated our first experiments to address whether CPEB1 is able to undergo phase separation *in vivo* and how it is affected by the variations (RNA-binding mutant and NTD-truncated versions) that we used in our BioID experiments.

CPEB1 forms round cytoplasmic foci in U-2 OS cells

To test whether CPEB1 is able to phase separate *in vivo* we transfected U-2 OS cells with a plasmid coding for CPEB1-GFP. To minimize structural perturbations on its IDRs, we fused the GFP next to the ordered domain of CPEB1 (Alberti et al., 2018).

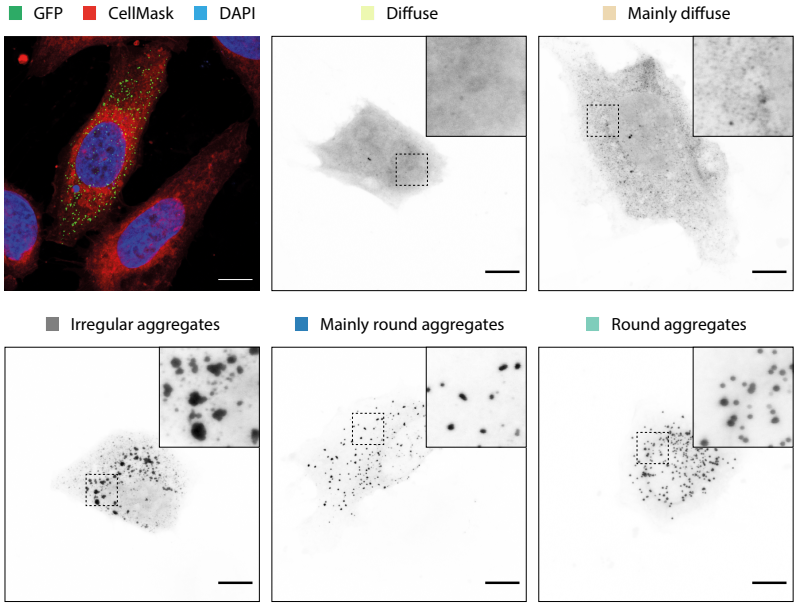

Figure 32: GFP-tagged proteins distribution in U-2 OS cells. Overexpressed GFP-tagged proteins adopt a variety of patterns in U-2 OS cells. To make the analysis simpler, cells were classified into five main categories: diffuse, mainly diffuse, irregular aggregates, mainly round aggregates and round aggregates. Patterns can be better appreciated in the cropped and zoomed sample. For this classification, only GFP signal from the cytoplasm was considered (determined using CellMask and DAPI as cytoplasmic and nuclear dyes, respectively). Pictures correspond to Z-projections. Scale bar = 10 μm.

According to the distribution of the GFP signal in the cytoplasm (reference pictures in figure 32) we categorized the cells in the following patterns: a) diffuse, when no structures could be identified in the cytoplasm, b) mainly diffuse, when either very few and small aggregates were detected or a granular but uniform cytoplasm was observed, c) irregular aggregates, when condensates with an irregular shape were spotted, d) round aggregates, when roundish foci were observed in the cytoplasm and e) mainly round aggregates, when only a small fraction of the cytoplasmic foci did not have an spherical shape. Additionally, in order to control for protein expression levels, images for low, medium and high CPEB1-GFP expressing cells were acquired (fig. 33).

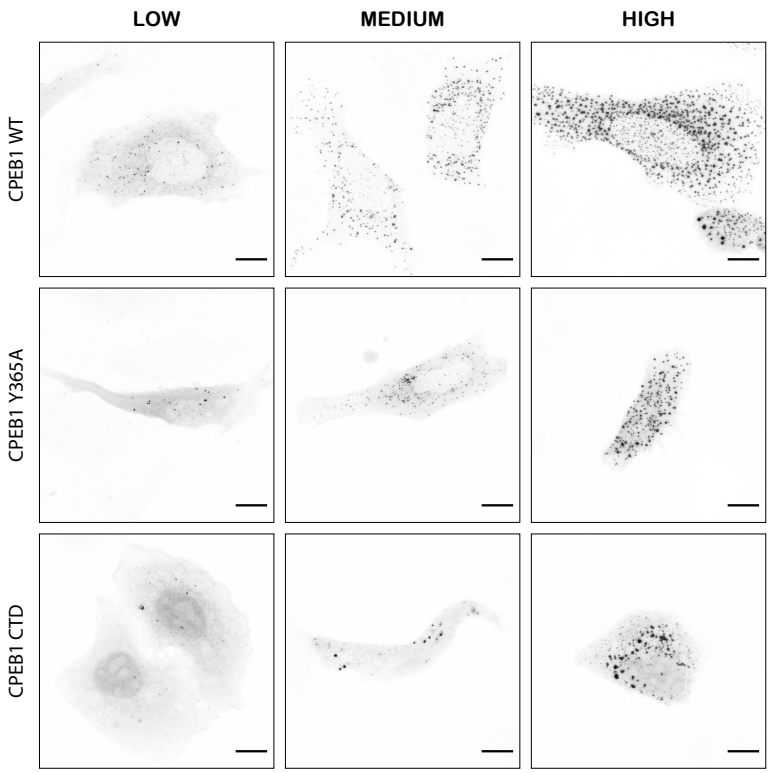

Figure 33: CPEB1 forms cytoplasmic foci in U-2 OS cells. Representative images of cells expressing CPEB1, the Y365A mutant and the CTD version fused to GFP. Cells were classified by intensities through arbitrary thresholds into three categories: low, medium and high. CPEB1 is able to form cytoplasmic foci regardless of RNA binding. Remarkably, CTD-GFP has a tendency towards irregularly-shaped aggregates. Scale bar = 10 μm.

As we expected from the work of Wilczynska (2005), cells expressing CPEB1-GFP displayed cytoplasmic foci when observed by confocal microscopy (fig.33). As shown in the sample images of figure 33, the condensed protein fraction correlates with the GFP signal, which means that there is a concentration dependency in CPEB1 condensation.

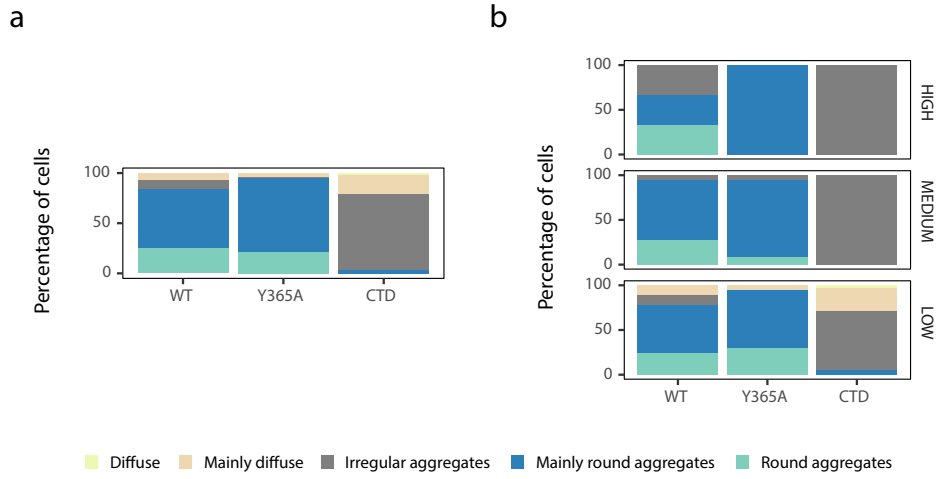

Figure 34: Distribution of the aggregation patterns for CPEB1 variants. (a) Barplot displaying the frequency of each aggregation pattern for CPEB1-GFP, Y365A-GFP and CTD-GFP in three independent experiments (n = 62 for CPEB1-GFP, n = 59 for Y365A-GFP and n = 57 for CTD-GFP). CPEB1-GFP tends to aggregate forming round condensates, which is not affected by RNA-binding impairment, while the CTD-GFP variant has more tendency for irregular aggregates. (b) Distribution of the aggregation patterns by intensities, suggesting a concentration dependency (n = 11, for high intensity cells, n = 53 for medium intensity and n = 114 for low).

The vast majority of cells expressing CPEB1-GFP have round aggregates in a wide range of protein concentrations, whose shape is reminiscent of liquid-like droplets (fig. 34a). As expected, some lower CPEB1-GFP expressing cells adopt a more diffuse pattern, while the higher expressing cells seem to form irregular aggregates, which would be indicative of less liquid-like nature (fig. 34b). Interestingly, CPEB1-GFP foci seem not to be dependent on the RNA binding capacity, since the mutant Y365A-GFP also forms these condensates, with a behavior that resembles that of the wild-type.

In opposition to what has been described for CPEB4 (Guillén-Boixet et al., 2016), the over-expressed CTD of CPEB1 does not adopt a diffuse distribution in the cytoplasm of U-2 OS cells but, rather, has the ability to condensate into irregular aggregates that, as we will discuss below, do not have liquid-like properties.

Considering the BioID and co-IPs data, we speculated that foci assembled by the RNA-binding mutant would not co-localize with those formed by the wild-type, as this mutation impaired its ability to recruit the repression complex components, which are presumably found in CPEB1 condensates. To address this hypothesis, the GFP fusions were co-transfected with a plasmid coding for CPEB1-mCherry and both fluorescent fusion proteins were detected by confocal microscopy.

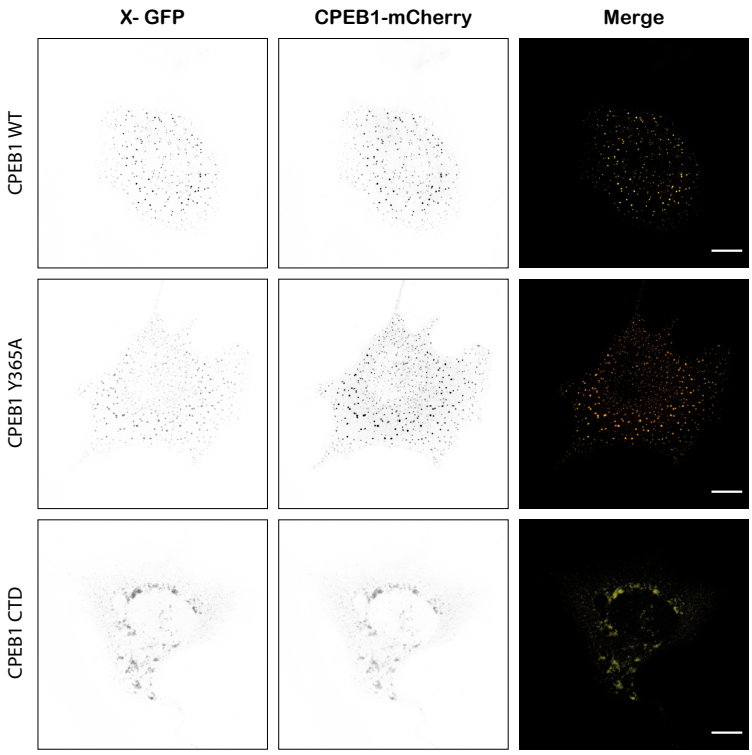

Figure 35: CPEB1 co-localizes with the Y365A mutant and the CTD in U-2 OS cells. Representative images of the green (GFP fusion) and red (CPEB1-mCherry) channels, as well as the resulting merge. Perfect co-localization is observed in all conditions. Scale bar = 10μm.

Preliminary data shown in figure 35 indicates that CPEB1-mCherry perfectly co-localizes with the mutant, suggesting that both variants can partition into the same condensates regardless of RNA. Even though these results may be in conflict with those from the BioID and co-IP, these discrepancies could be explained considering the resolution of both approaches: while the BioID has a resolution below 10-20nm, the confocal microscope we have used has a resolution of around 300-400nm. Consequently, despite observing proximity at the microscopic level, at the molecular level these two CPEB1 variants may not be interacting and, indeed, may even be found in different compartments within the same foci, as happens for other systems such as the nucleolus (Feric et al., 2016). To address this, super-resolution and even *in vitro* approaches would be highly useful.

Additionally, wild-type CPEB1 also co-localizes with the CTD, which means that, even though RNA is not essential for CPEB1 condensation in the cytoplasm, it may serve as a phase separated scaffold onto which CPEB1 will land. Conversely, there is also the possibility that CPEB1 condensation depends on a region of the CTD, which is not mediating RNA-binding, common for the three variants. In this scenario, the role of the NTD, as we will discuss below, would be to grant fluidity to these condensates, providing them with more liquid-like properties. To address these inquiries, *in vitro* experiments should be performed with a set of mutants and truncated versions, in presence and absence of RNA, in order to better map the regions implicated in CPEB1 condensation.

Overall, these results strongly suggest that CPEB1 is able to form round cytoplasmic foci in a concentration-dependent fashion, possibly through liquid-liquid phase separation. Despite not requiring RNA-binding for partitioning into these aggregates, the CTD would still be an essential requisite, as we will show in the following sections.

CPEB1 foci are formed by liquid-liquid phase separation

Considering that CPEB4 can undergo liquid-liquid phase separation (Guillén-Boixet et al., 2016), we speculated that CPEB1 foci would be assembled on a similar basis. Though still in debate (McSwiggen et al., 2019), compartments with the ability to fuse and fission, and that can recover their fluorescence after photobleaching are potentially formed by LLPS. Accordingly, we checked if CPEB1-GFP foci have the aforementioned properties.

As expected, CPEB1-GFP foci display features of compartments formed by phase separation, such as the ability to fuse and fission. An example of a fusion event is shown in figure 36: two separated droplets become one with time, which can be followed using the respective fluorescence intensities. However, we plan to capture fusion events in an unbiased manner using automatic image analysis pipelines in order to get a quantitative perspective of this event, which can be useful for comparing between conditions. Remarkably, in some cases we observed incomplete fusions (data not shown), or even kiss-and-run contacts between droplets, which is reminiscent of a phase transition towards a gel-like state (Shin et al., 2017b).

Apart from the ability to fuse/fission, we also measured the exchange dynamics of the condensates with molecules from the soluble phase by FRAP. As shown in figure 37a-c, CPEB1-GFP foci are in a constant exchange with molecules from the soluble pool, as their fluorescence recovers with time until it reaches a plateau.

Interestingly, nearly 50% of the molecules found in the droplet are immobile in the timescale of the experiment, which suggests that the behavior of these aggregates is not completely liquid-like. Unfortunately, given the size of the droplets, smaller regions could not be photobleached to discern if these two components (fast recovering and immobile molecules) are indeed separated into subcompartments, as it happens in other

more complex systems (Jain et al., 2016; Weber, 2017), which have a viscoelastic or elastic solid core.

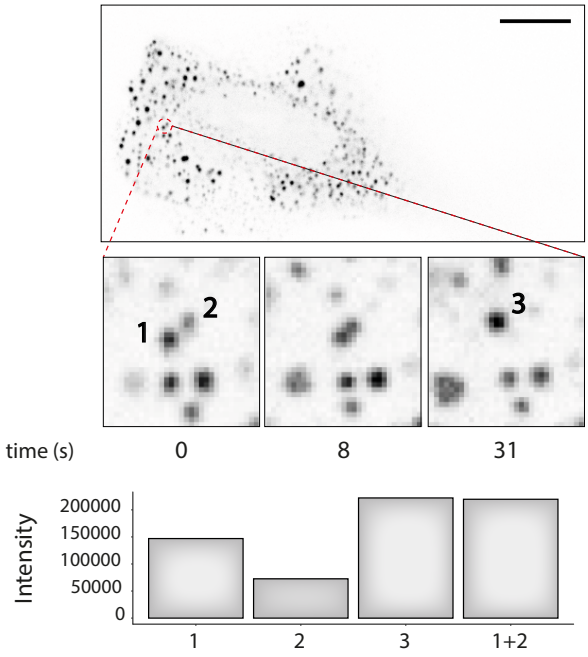

Figure 36: CPEB1 condensates experience fusion events. Representative crops for a time-lapse of a fusion event of CPEB1-GFP foci are depicted. The sum of the intensities of the isolated droplets is similar to that of the resulting one, an indication of fusion. Scale bar = 10 μm. Rate = 11.36 frames/second.

Surprisingly, the dynamic exchange in and out the droplets is independent of RNA-binding capacity, as the Y365A mutation does not affect significantly the recovery kinetics. Conversely, as intuited by the irregular shape of the CTD-GFP cytoplasmic aggregates, these have a solid-like behavior, being unable to recover after photobleaching in the timescale of the experiment (fig. 37a-c). Thus, these findings indicate a role for the CPEB1-NTD in preventing the transition from a liquid state to a solid one, as we speculated before.

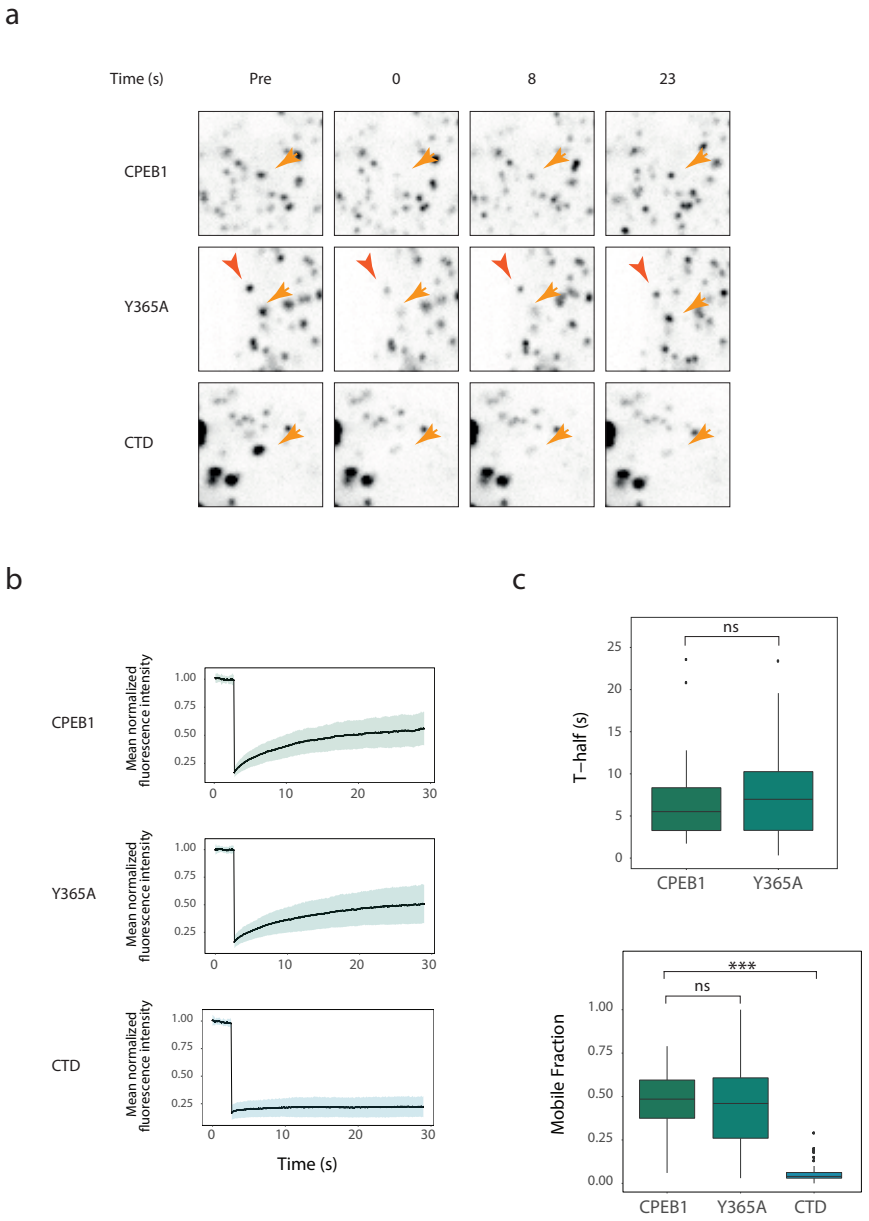

In this section we have provided the first evidence that CPEB1 can undergo liquid-liquid phase separation *in vivo*, and we have determined that this ability is, at least in our experimental setting of overexpression, independent of RNA-binding.

Figure 37: CPEB1 foci dynamically exchange molecules between the dense and the light phases. (a) Representative crops of a time-lapse of a FRAP experiment. Foci with a given intensity (frame 50, Pre) are photobleached (frame 51, time 0) and the fluorescence recovery is tracked over time (frames 89 and 261, 8 and 23s respectively). While CPEB1-GFP foci recover with time, in an RNA independent fashion, the CTD-GFP irregular aggregates do not, suggesting that the liquid-like nature of the CPEB1 droplets is provided by its NTD. (b) FRAP recovery curves for the CPEB1 variants fitted to a single exponential model. Mean fluorescence intensity is depicted for each time point as well as the standard deviation. (c) Boxplots showing the distributions of the t-half and mobile fraction for each variant after double normalization. As depicted, CPEB1-GFP recovery kinetics seem not to be affected by the RNA-binding ablating mutation and, compared to the full-length variants, the CTD-GFP version does not recovery at all. Data coming from three independent experiments (n = 48 for CPEB1-GFP, n = 66 for Y365A-GFP, n = 60 for CTD-GFP). Comparison between groups was carried out using a Kruskal-Wallis test (significance level of 5%) and then post-hoc Dunn's test with a Bonferroni correction to account for multiple testing (***, p-value < 0.001; **, p-value < 0.01 and *, p-value < 0.05).

These results, though, would not be expected considering the sequence analysis data, which implies that the determinants governing liquid-liquid phase separation are not fully understood yet and, consequently, there is still room for improvement in the predictive algorithms. On the other hand, we also speculate that the NTD of CPEB1 is required to prevent aberrant phase transitions, as has been suggested for other proteins such as Ded1p (Iserman et al., 2020).

The next section covers some experiments addressing the phase separation properties of CPEB2 and CPEB3 and preliminary data comparing the four CPEBs. The aim of the following studies is to provide comparative data for four related proteins in the same biological scenario which, along with the BioID data and unpublished work from Berta Duran (Duran, 2020), will help establishing a conceptual framework to the question: why four CPEBs are required in the same cell?

Comparison of CPEB1-4 phase separation properties

CPEB2 and CPEB3 phase separate in U-2 OS cells

Considering that CPEB1 and CPEB4 have the ability to phase separate *in vivo* and the fact that analysis of the CPEB2 and CPEB3 sequences pointed to a similar behavior for these proteins, we checked this hypothesis in the same experimental conditions. As expected, both proteins form cytoplasmic foci when overexpressed in U-2 OS cells, seemingly in a wide range of concentrations (fig. 38a-c). Apparently, CPEB3 seems to have a higher tendency to form irregularly shaped aggregates in the cytoplasm, possibly due to the presence of a prion-like domain in its NTD (Si and Kandel, 2016).

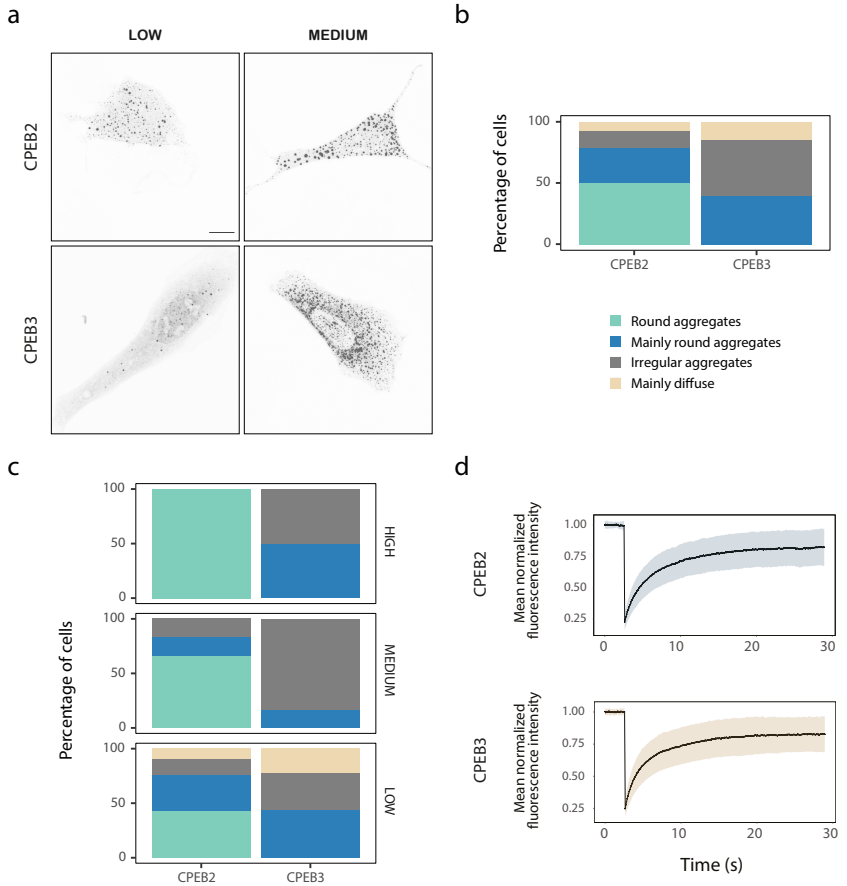

Figure 38: CPEB2 and CPEB3 undergo phase separation in vivo. (a) Representative images of cells expressing CPEB2-GFP and CPEB3-GFP at low and medium intensity levels. Cytoplasmic foci are observed for both fusion proteins, which are higher in number and size as protein concentration increases. Scale bar = 10 μm. (b) Barplot displaying the percentage of each aggregation pattern for CPEB2-GFP and CPEB3-GFP in two independent experiments (n = 28 and n = 28 respectively). CPEB2 and CPEB3 form cytoplasmic foci with mainly round shape. Apparently, CPEB3 has also tendency to aggregate into irregular foci. (c) Distribution of the aggregation patterns by intensities, suggesting a concentration dependency (n = 5, for high intensity cells, n = 12 for medium intensity and n = 39 for low). (d) FRAP recovery curves for the CPEB2 and CPEB3 fitted to a single exponential model. Mean fluorescence intensity is depicted for each time point as well as the standard deviation. Droplets formed by either protein show a fast and almost complete recovery after photobleaching.

These observations are in line with recent work from Kandel's lab, which indicate that CPEB3 partitions into P-bodies in a SUMOylation dependent-manner (Fioriti et al., 2015; Drisaldi et al., 2015; Ford et al., 2019). In addition, other studies with the CPEB2-4 orthologs Orb2A and Orb2B indicate that this branch of the CPEB family forms functional cytoplasmic foci with properties ranging from liquid-like to more solid-like (Li et al., 2016; Stepien et al., 2016; Joag et al., 2019; Hervas et al., 2020).

To address the material properties of the CPEB2-3 condensates we performed FRAP experiments. Both proteins displayed fast and complete recovery kinetics (fig. 38d). Indeed, CPEB2-GFP and CPEB3-GFP have faster and more complete recovery than CPEB1-GFP, which suggests that the droplets assembled by these paralogs have more liquid-like behavior (fig. 39a-b). These results are consistent with the sequence analysis data, which indicated that CPEB2-4 have more propensity for LLPS than CPEB1.

Remarkably, even though aggregates with irregular shapes have generally gel-like or solid-like properties, as observed for CTD-GFP, those of CPEB2 and CPEB3 recovered surprisingly fast, which indicates that they are not as gel or solid as it may seem from their

shape. This observation implies that as many features of these biomolecular condensates as possible should be analyzed to fully understand their material properties and be able to better compare between proteins.

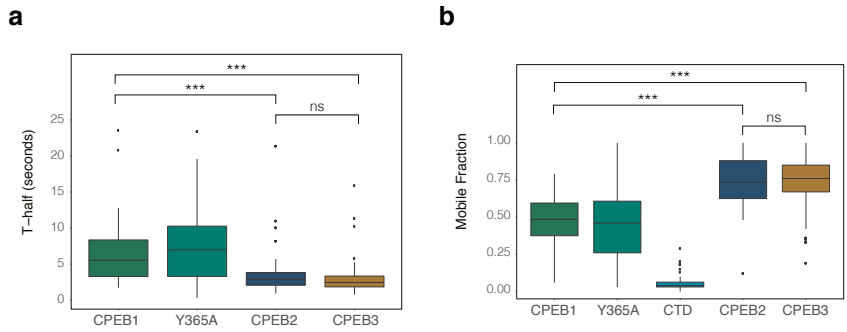

Figure 39: CPEB1 and CPEB2-3 droplets have different recovery kinetics. (a) Boxplots showing the distributions of the t-half for each fusion protein after double normalization. Remarkably, CPEB1 recovers slower than CPEB2-3, which suggests a less liquid-like behavior of these droplets. (b) Boxplots showing the distributions of the mobility fraction for each fusion protein after double normalization. Remarkably, CPEB1 recovers significantly less than CPEB2-3, meaning that molecules in CPEB1 droplets are retained longer, which indicates a more solid-like behavior. Data coming from three independent experiments (n = 48 for CPEB1-GFP, n = 66 for Y365A-GFP, n = 60 for CTD-GFP, n = 78 for CPEB2-GFP and n = 84 for CPEB3-GFP). Comparison between groups was carried out using a Kruskal-Wallis test (significance level of 5%) and then post-hoc Dunn's test with a Bonferroni correction to account for the multiple testing (***, p-value < 0.001; **, p-value < 0.01 and *, p-value < 0.05).

Altogether, these results strongly suggest that all four *Xenopus* CPEBs can undergo LLPS *in vivo*, a phenomenon only demonstrated thus far for CPEB4 (Guillén-Boixet et al., 2016) and proposed for human CPEB3 (Ford et al., 2019). Consistent with the sequence analysis data, CPEB1 forms less dynamic condensates, as they recover worse after photobleaching. Evolution might have selected the development of these two main biophysical behaviors for the CPEBs (by separating CPEB1 from CPEB2-4), in order to allow a differential regulation of CPEB targets based on mechanisms or principles yet to be characterized.

CPEB1-4 NTDs have different propensity to undergo phase separation

Sequence analysis of the four CPEBs indicates that the regions promoting phase separation most likely reside in their NTDs, since this domain is rich in intrinsically disordered stretches and linear motifs possibly mediating protein-protein interactions. Consistent with this hypothesis, Guillén-Boixet et al. (2016) showed that the NTD of CPEB4 is sufficient for its liquid-liquid phase separation. To address this question for the remaining CPEBs, we checked foci formation of their NTD-GFP variants in fixed U-2 OS.

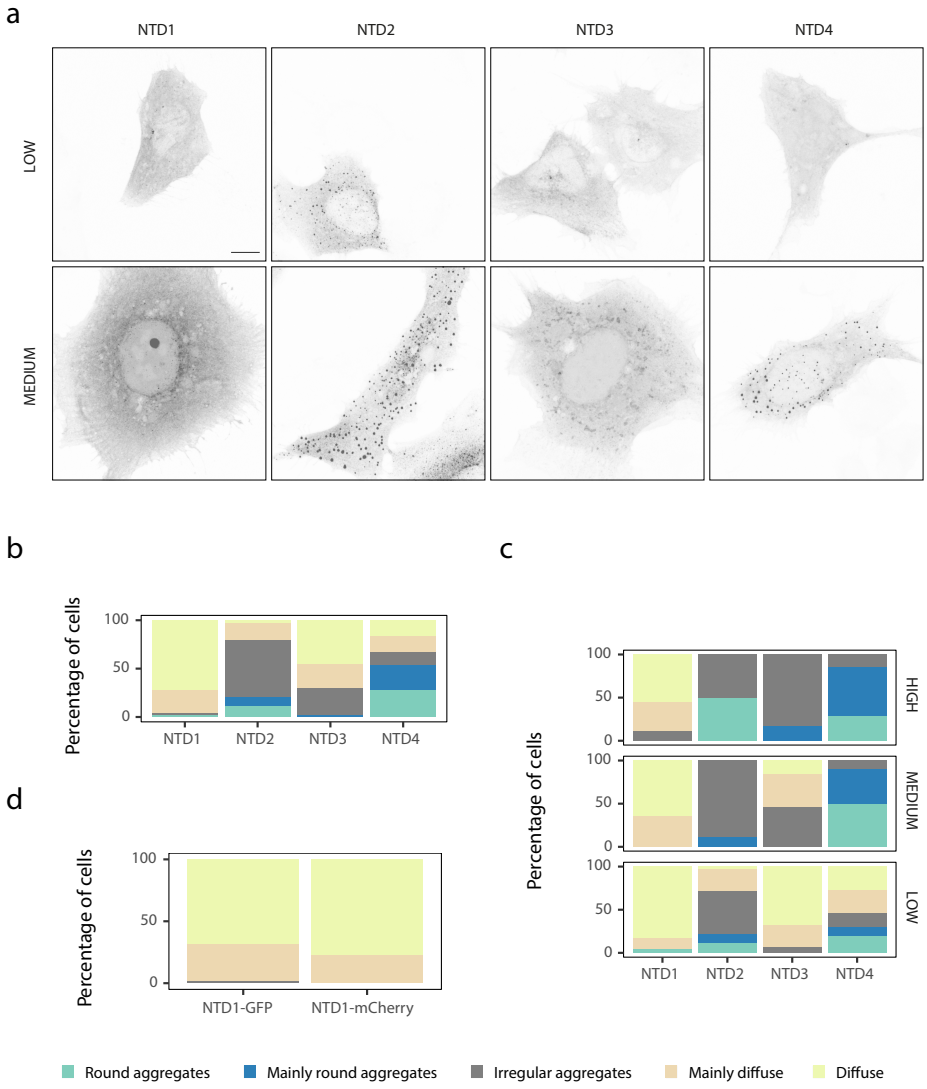

Figure 40: CPEB1-4 NTDs have different propensities for phase separation. (a) Representative images of cells expressing NTD1-4-GFP at low and medium intensity levels. Scale bar = 10 μm. (b) Barplot displaying the percentage of each aggregation pattern for NTD1-4 in two independent experiments (n = 49, n = 43, n = 47 and n = 43 respectively). (c) Distribution of the aggregation patterns by intensities, suggesting a concentration dependency both in the formation of round and irregular aggregates for NTD2-4 (n = 24, for high intensity cells, n = 49 for medium intensity and n = 102 for low). While NTD1 does not undergo liquid-liquid phase separation at any concentration, the NTD of the other members of the family have, to a certain extent, the ability to form LLPS condensates, specially at higher protein levels. More specifically, NTD2 and NTD3 have a high tendency to form irregular aggregates whilst NTD4 has a significant propensity for condensing into round aggregates. (d) Barplot displaying the percentage of each aggregation pattern for NTD1-GFP and NTD1-mCherry in two independent experiments (n = 47 and n = 43 respectively). Irrespective of the fluorescent tag, NTD1 remains soluble in a wide range of protein concentrations.

As shown in figure 40, the NTD of CPEB1 (NTD1) cannot undergo liquid-liquid phase separation, even at high protein concentrations or with another tag (mCherry), which was expected from the sequence analysis data and also observed by Wilczynska (2005). As previously mentioned, the lack of long disorder stretches, the few predicted SLiMs and MoRFs and the alternate charge patterning, are potential reasons explaining its soluble behavior.

Consequently, the fact that the full-length CPEB1 can form liquid-like droplets entails that its CTD is crucial for LLPS, which indeed has been recently suggested by other authors (Tsvetkov et al., 2020). Nonetheless, the NTD seems to be necessary for providing liquid-like properties, as the CTD alone has a tendency to transition to solid-like states (Patel et al., 2015; Shin et al., 2017b; Weber, 2017). We speculate that either contacts with the NTD or the physicochemical properties of the full-length protein are responsible of tuning down the propensity of the CTD of CPEB1 to phase transition.

Similarly, the NTD of CPEB3 adopts a diffuse distribution at low protein concentrations. However, at high protein levels it has increased propensity for condensing into irregular aggregates, probably driven by its prion-like domain. These findings are partially in line with observations from Ford et al. (2019), who showed that full-length CPEB3 condensates in HeLa cells while NTD3-GFP does not. Conversely, NTD2 and NTD4 can form round aggregates with potential liquid-like properties, yet NTD2 has higher tendency for irregular foci, even at low concentrations. These findings are supported by data from Tsvetkov et al. (2020), who observed that CPEB2 oligomerization relied on the prion-like domain present in its NTD.

In conclusion, overexpression of the NTDs supports our speculations from the sequence analysis data: CPEB2-4 seem to have evolved to undergo LLPS more easily than CPEB1, even though their CTD still has an important role determining the final material properties of the condensates they assemble, as the pattern distributions from CPEB2-3 and NTD2-3 also differ significantly. In this regard, the fact that only CPEB1 requires its CTD for phase separating (at least in the range of concentrations tested), establishes an orthogonality between CPEB1 and CPEB2-4 that may facilitate their differential regulation, behavior and effect on their targets.

CPEBs co-localize in the same biomolecular condensates

As we have described so far, all four CPEBs can form cytoplasmic foci in a process most likely driven by liquid-liquid phase separation. We have also shown that the condensates they form have different morphological distributions, different dynamics (as addressed by FRAP) and different structural requirements (as addresed by CTD truncation). Despite these differences, data coming from BioID experiments and work from other labs (Youn et al., 2018; Ford et al., 2019) suggests that, at least in some cellular systems, all four CPEBs are found in compartments with similar compositions (most likely P-bodies) and are, indeed, in close proximity. Even though it may seem counter-intuitive that all

of them coexist in a condensate while behaving differently, there is evidence of other systems in which proteins with different LLPS properties and dynamics co-condense into isotropic or anisotropic aggregates (Kedersha et al., 2005; Feric et al., 2016; Weber, 2017; Sheu-Gruttadauria and MacRae, 2018; Shiina, 2019; Kim et al., 2019; Neil et al., 2020).

In order to address the degree of co-localization between the four CPEBs we decided to co-expresses CPEB1-mCherry with the other family members fused to GFP, since CPEB1 has the more dissimilar behavior according to the FRAP data. Importantly, CPEB1-mCherry does not fully recapitulate CPEB1-GFP phase separation behavior, meaning that the fluorescent tag has a confounding effect on CPEB1 condensation properties (fig. 41a). To circumvent this issue we just considered for co-localization quantification those cells showing an aggregated patttern (round, mainly round and irregular aggregates). Co-localization was assessed using Pearson's correlation coefficient.

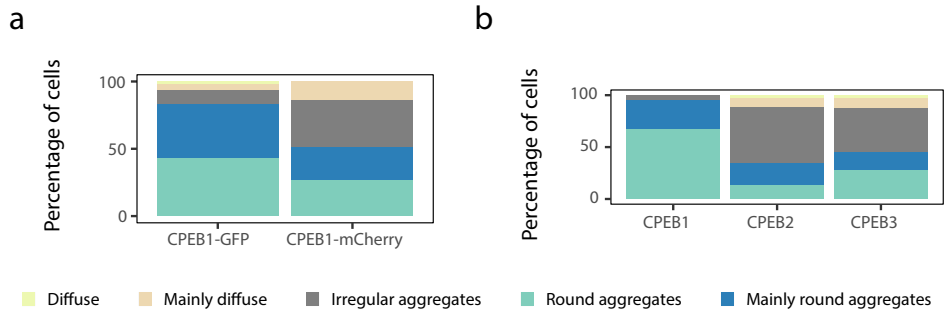

Figure 41: CPEBs cytoplasmic distribution upon co-transfection with CPEB1-mCherry. (a) Barplot displaying the percentage of each aggregation pattern for CPEB1-GFP and CPEB1-mCherry in three independent experiments (n = 49 and n = 37 respectively). Importantly, only one replicate contained both fusions. Even though the pattern distributions are not completely similar, both fusions are able to undergo LLPS *in vivo*. (b) Barplot displaying the percentage of each aggregation pattern for CPEB1-3-GFP upon co-expression with CPEB1-mCherry. While CPEB1-GFP phase separates mainly into round droplets, CPEB2 and CPEB3 also undergo transition into irregular aggregates. Data coming from two independent experiments (n = 44 for CPEB1-GFP, n = 43 for CPEB2-GFP and n = 42 for CPEB3-GFP).

As shown in figure 41b, all the CPEBX-GFP constructs are able to form cytoplasmic foci when co-transfected with CPEB1-mCherry. Interestingly, even though we cannot completely compare these results with the experiments expressing the GFP constructs alone since they have been performed separately (different transfection replicates), this data seems to indicate that CPEB1-mCherry would increase the propensity of CPEB2 to form aggregates with irregular shapes. In any case, it is important to highlight that, for all conditions tested, both CPEBX-GFP and CPEB1-mCherry proteins adopt the same pattern in the cell and, remarkably, co-localize almost perfectly (figs. 42 and 43).

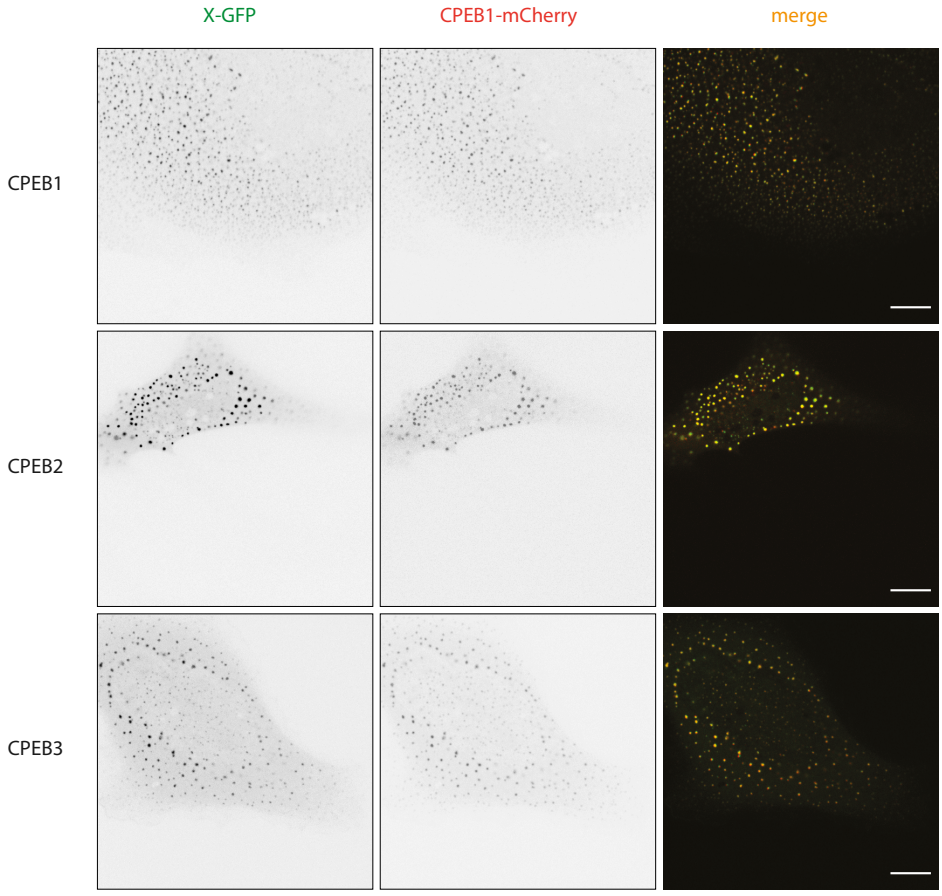

Figure 42: CPEBs co-localize in cytoplasmic puncta. Representative images of U-2 OS cells co-expressing CPEB1-mCherry with CPEB1-3 fused to GFP. In cells with an aggregate mCherry pattern, co-localization with the GFP signal is almost complete. Scale bar = 10 µm.

The fact that, at least for the conditions tested, CPEBs can co-localize into the same condensates, poses the question as to which are the factors determining that these four paralogs coalesce together. We speculated that RNA could be a possible determinant, as all four CPEBs recognize CPE elements and, therefore, could be binding to the same mRNAs. To address this possibility we have conducted a pilot experiment testing if NTDs-GFP co-localize with CPEB1-mCherry.

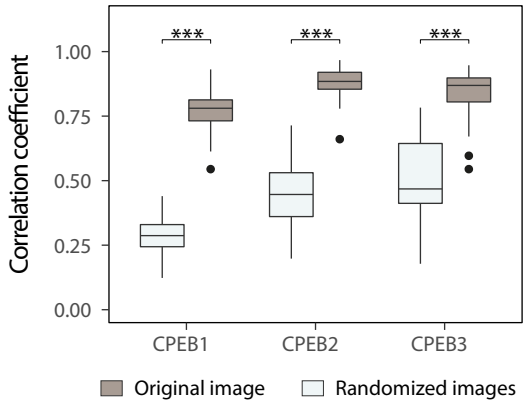

Figure 43: CPEBs co-localize in the same biomolecular condensates. Boxplots showing the distribution of the Pearson correlation coefficients of the original images and the average of 75 randomized versions. As depicted, there is a significant co-localization of CPEB1-mCherry aggregates and those of the GFP-fused proteins. Importantly, for this analysis only cells with an aggregate pattern (round or irregular) were used. Data coming from two independent experiments (n = 44 for CPEB1-GFP, n = 38 for CPEB2-GFP and n = 37 for CPEB3-GFP). For the statistical analysis, paired samples were compared using a Wilcoxon signed-rank test using a Bonferroni correction to account for multiple testing (***, p-value < 0.001; **, p-value < 0.01 and *, p-value < 0.05).

As shown in figure 44, the NTDs of CPEB1-4 co-localize almost completely with CPEB1-mCherry in cells displaying an aggregated pattern (quantification in figure 45b). These results strongly suggest that co-localization of the four CPEBs in the same granules is, potentially, independent of RNA binding. To further corroborate this hypothesis, co-expression of two NTDs could help discern it better. Nonetheless, we should not ex-

clude the possibility that scaffold RNAs may have a role in CPEBs phase separation irrespective of a binding through the RRMs.

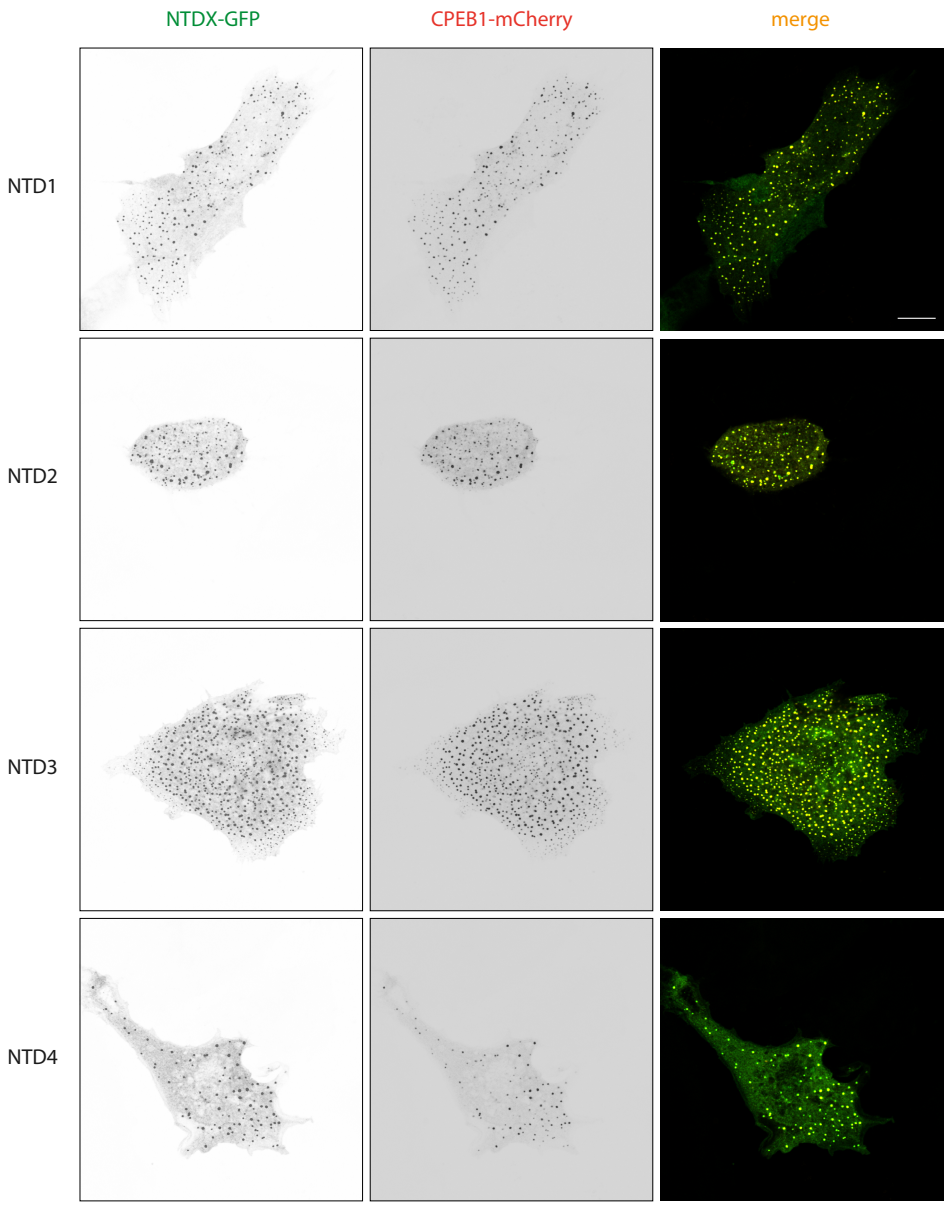

Figure 44: CPEBs co-localization is independent of RNA-binding. Representative images of U-2 OS cells co-expressing CPEB1-mCherry with NTD1-4 fused to GFP. In cells with aggregated mCherry pattern, co-localization with GFP is almost complete. Scale bar = 10 µm.

On the other hand, it was surprising to observe that even NTD1, which we demonstrated to be unable to undergo phase separation in a wide range of concentrations, is recruited to the foci assembled by its full-length counterpart. Therefore, these results suggest that this domain can condense if an appropriate environment is present in the cell.

Similarly, this preliminary data hints that CPEB1 reduces the propensity of NTD2-3 to condense into irregular aggregates (fig.45a), which we speculate may reflect a cross-talk between different species of the same condensate to define its overall properties.

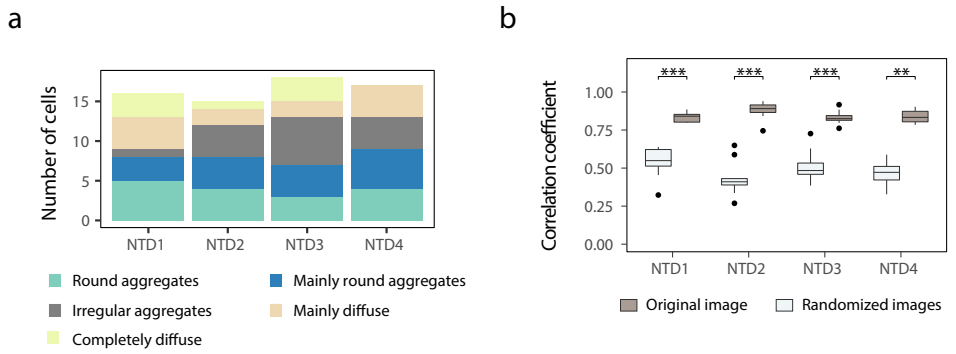

Figure 45: CPEBs co-localization is independent of the CTD. (a) Barplot displaying the number of cells for each aggregation pattern for NTD1-4-GFP upon co-expression with CPEB1-mCherry. Data coming from a single experiment (n = 16 for NTD1, n = 15 for NTD2, n = 18 for NTD3, n = 17 for NTD4). Co-expression of the NTDs with full-length CPEB1 increases their ability to phase separate into round and/or irregular aggregates. Importantly, both fusion proteins adopt the same pattern in the same cell. (b) Boxplots showing the distribution of the Pearson correlation coefficients for the original images and the average of 75 randomized versions. As depicted, there is a significant co-localization of CPEB1-mCherry aggregates and those of the GFP-fused NTDs. Importantly, for this analysis only cells with an aggregate pattern (round or irregular) were used. Data coming from a single experiment (n = 9 for NTD1, n = 11 for NTD2, n = 13 for NTD3, n = 13 for NTD4) . For the statistical analysis, paired samples were compared using a Wilcoxon signed-rank test using a Bonferroni correction to account for the multiple testing (***, p-value < 0.001; **, p-value < 0.01 and *, p-value < 0.05)

Since RNA-binding seems not to be the key determinant in CPEB1 and CPEB2-4 co-localization, we speculate that other factors such as sequence composition, may be driving the condensation of these proteins into the same droplets. As an example, it has been recently proposed that proteins composed exclusively of arginine-aspartic acid dipeptide repeats are specifically incorporated to nuclear speckles (Greig et al., 2020), which suggests that a specific grammar may exist for CPEB-enriched compartments. Alternatively, certain protein-protein interactions occurring at the NTDs may be promoting the observed co-condensation.

Overall, our findings indicate that the four CPEBs are potentially found in the same biomolecular condensates, as the BioID data suggested. Interestingly, this co-localization is potentially independent of RNA-binding, as concluded from the experiments with the NTDs. In addition, we have shown that the properties of one species can be affected by the phase separation of others.

Despite these observations, we cannot belittle the possibility that these proteins are sub-compartmentalized in smaller volumes within the microscopically-detected foci (Feric et al., 2016; Shiina, 2019). Accordingly, imaging the condensates with super-resolution and *in vitro* studies with purified recombinant proteins could bring light in this regard.

CPEB1-4 droplets move differently within the cytoplasm

While performing FRAP experiments in live cells we observed that the condensates the CPEBs assemble displayed a variety of movement trajectories and, interestingly, there seemed to be differences between paralogs. To better characterize the particle movements we recorded them for long time-periods, in two Z-stacks, and tracked them using Imaris particle tracking algorithms. As variable of interest we measured the ratio between the track displacement and the track length, henceforth track straightness.

Using this approach, we observed that most of CPEB2 and CPEB3 droplets, though being in constant movement, barely displaced from their position; accordingly, their droplets had low straightness values. Conversely, droplets formed by CPEB1 and CPEB4 had more tendency to move freely in the cytoplasm, covering wide territories and, remarkably, some of these foci showed fast and geometrically straight displacements.

Notably, we observed a clear association between the size of a droplet and its straightness (fig. 46). In this regard, smaller droplets (below percentile 15%) displayed more freedom in their movements and, in addition, were more prone to experience these fast and straight displacements. Oppositely, bigger droplets (above percentile 85%) had their movements more restricted and seemed to be confined in determined positions.

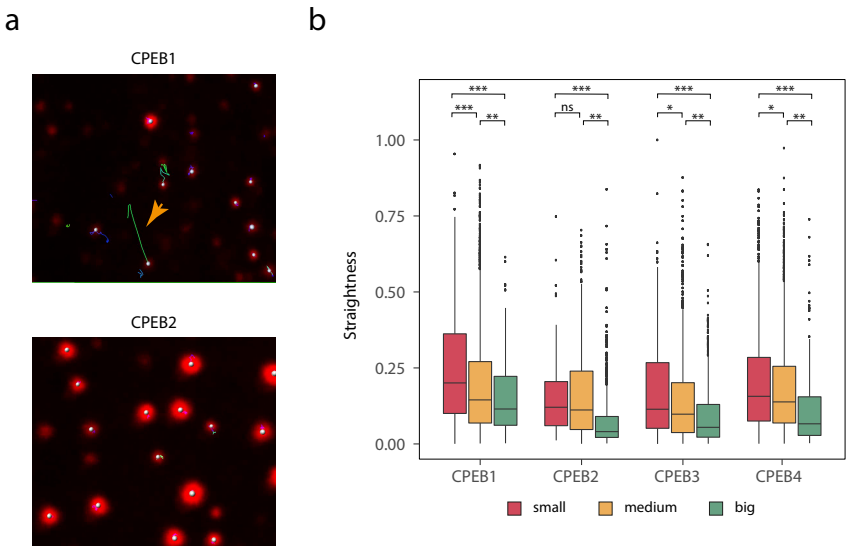

Figure 46: Differential droplets movement within the cytoplasm. (A) Representative crops showing CPEB1 and CPEB2 droplets trajectories. Arrow = displacement with high straightness. (B) Boxplots showing the relation between droplet size and straightness. Data coming from 10 cells for each condition, with a total of 9576 identified droplets (n = 3485 for CPEB1, n = 1179 for CPEB2, n = 1678 for CPEB3, n = 3234 for CPEB4). Comparison between groups using Kruskal-Wallis test (5% significance) and then post-hoc Dunn's test with a Bonferroni correction (***, p-value < 0.001; **, p-value < 0.01 and *, p-value < 0.05).

We hypothesize that these differences are explained by a differential association to elements of the cytoskeleton. In fact, Aizer et al. (2008) identified three patterns for P-bodies dynamics in the cell: confined motion, complete motionless and rapid-directional displacement, which they related to microtubules, actin bundles and motor proteins/organelle hitchhiking respectively.

Consequently, considering our observations CPEB2 and CPEB3 droplets would be more associated to actin bundles while those of CPEB1 and CPEB4 would be more associated to microtubules and, sporadically, to organelles or motor proteins that drag them in rapid and directional trajectories. Future work in this regard will be performed, assessing co-localization with cytoskeletal structures and also using agents affecting the polymerization/depolymerization dynamics of microtubules and actin.

Discussion

In eukaryotes, the nucleus physically separates transcription from translation, thus permitting the development of several regulatory mechanisms that control the expression of multiple genes in time and space. One of these mechanisms is governed by the CPEBs, a family of RNA-binding proteins with the ability to regulate up to 30% of the human genome. Accordingly, the role of the CPEBs has been studied in a plethora of systems and cellular processes. Even though many of these studies have addressed mechanistic inquiries about this family of proteins, there are still several open questions and limitations arising from these data.

In the present work we have studied the composition and remodeling of the CPEB mRNP in *Xenopus laevis* oocytes by means of *in vivo* interactomics, proposing a new model explaining the mechanism underlying the translational control attained by CPEBs. Additionally, we have characterized their liquid-liquid phase separation dynamics and properties, redefining our conception about the biophysical nature of these proteins.

We will dedicate this chapter to discuss several issues and open questions that arise from this work.

Revisiting CPEB1-mediated translational control

Novel players in CPEB1-mediated repression

Since the identification of CPEB1 as the protein binding the CPE, much effort has been put to propose a molecular mechanism for its functions. So far, it is well-established that CPEBs do not possess any catalytic activity and, therefore, their role as translational regulators derives from their ability to recruit certain factors to their target mRNAs.

From the studies covering the CPEB1 repression complex, three main models have been proposed. However, several evidences point to inconsistencies and contradictions between

them. For instance, the role of PARN as the deadenylase of the CPEB1 mRNP is difficult to conceive considering the growing evidence that this enzyme is predominantly found in the nucleus (Yamashita et al., 2005; Minshall et al., 2007; Wühr et al., 2015) and that it does not have a crucial role in cytoplasmic mRNA deadenylation, but rather participates in the maturation of nuclear non-coding RNAs (Yamashita et al., 2005; Montellese et al., 2017; Son et al., 2018; Yi et al., 2018).

In order to provide a model that overcomes the limitations of the others, we decided to undertake an approach that not only is high-throughput, hence removing any hypothesis bias, but also is based on *in vivo* molecular labeling, which allows to take more accurate snapshots of the interactomic landscape of the CPEBs.

On one hand, factors such as PARN and Maskin have not been detected in any of our experiments (figs 23 and 25). However, we do not rule out the possibility that the interaction of CPEB1 with these two proteins occurs in other cellular locations, such as the nucleus in the case of PARN, or for a small fraction of the cytoplasmic CPEB, which could be the case of Maskin, a protein that mainly localizes to the centrosomes (Groisman et al., 2000; Peset et al., 2005; O'Brien et al., 2005).

On the other hand, the CPEB mRNP conceived by Minshall et al. (2007) is based on the interaction of eIF4E-1b and eIF4E-T with the cap, which inhibits translation initiation. This model, though, has not been further discussed in the field and, importantly, lacks a deadenylase. In this regard, while our BioID data confirms the presence of the eIF4E1b and eIF4E-T duplex in the CPEB1 mRNP it also identifies the CCR4-NOT complex as the deadenylation machinery acting on CPEB targets in stage VI *Xenopus laevis* oocytes. Notably, this finding is supported by other studies in which the association between CPEBs and the CCR4-NOT complex has been observed in cell lines (Hosoda et al., 2011; Ogami et al., 2014) or hinted in frog oocytes Waghray et al. (2015).

In addition to these factors, our results establish novel associations with other machineries that mediate translational control (fig 23 and 25). We have defined with higher precision the link between CPEB1 and the polyadenylation complex in the context of translational repression, by incorporating WDR33, FIP1L1 and CSTF64 to the mRNP and confirming the presence of Gld2. Importantly, this finding suggests that polyadenylation of CPEB1 targets may not be triggered by the recruitment of polyadenylation factors but rather by activation and/or rearrangement of these (i.e. by phosphorylation).

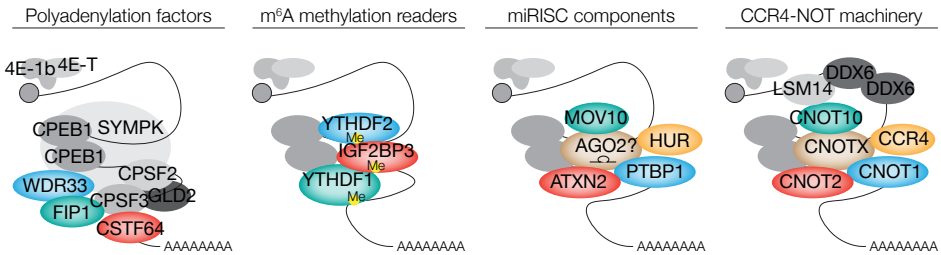

Figure 47: Cellular machineries associated to CPEB1-mediated translational repression. Families of factors that appear to be associated to CPEB1 according to the BioID data. We speculate that CPEB function is attained with the synergistic contribution of machineries mediating cytoplasmic polyadenylation, RNA methylation, microRNA-induced silencing and transcript deadenylation. In color, novel interactors are highlighted.

Considering the appearance of the methylation readers YTHDF1/2 and IGF2BP3 in our results, we propose a connection between CPEB1 and the m^{6}A modification of the RNA body. An indirect evidence of this hypothesis comes from the work of Takahashi et al. (2014), who observed that IGF2BP3 represses translation with CPEB1 and Pumilio in zebrafish oocytes. It is tempting to address also the possibility that m^{6}A may affect directly the CPEs (consensus CPE: 5'-UUUUA$_{1\text{-}3}$U-3') and the impact of this modification on the RNA phase separation properties (Ries et al., 2019).

We have also identified factors related to miRNA-induced silencing such as PTBP1, MOV10, HUR and ATXN2, which are thought to both facilitate and impair the func-

tion of the miRISC through interaction or competition with AGO2 (McCann et al., 2011; Liu et al., 2012; Kundu et al., 2012; Cui and Placzek, 2018; Nawalpuri et al., 2020). It is tempting to speculate that CPEB1 acts synergistically with the miRISC to efficiently recruit the CCR4-NOT complex to its targets. So far, there have only been evidences of functional associations between CPEB1 and miRNAs (Wilczynska et al., 2016; Kratassiouk et al., 2016), but we cannot belittle the possibility that CPEBs may act as seeds onto which the miRISC machinery could land, independent of a miRNA. However, this last mechanism has not been described for any other protein yet.

Finally, our data confirms the interaction of CPEB1 with ZAR1/2 and DAZL, which had been suggested previously but had not been proven (Charlesworth et al., 2012; Sousa Martins et al., 2016; Yang et al., 2020a). Remarkably, these are germ-line-specific proteins, which means that they are dispensable for somatic translational repression but, for reasons yet unknown, indispensable during oocyte maturation.

Altogether, these findings suggest that CPEB1-mediated translational control is not an isolated phenomenon but it is part of a more complex machinery, resulting from the additive, synergistic or antagonistic integration of the *trans*-acting factors recruited by the combinatorial code of *cis*-acting elements of a given mRNA in a given context. The composition of this particle, then, dictates the fate of the mRNA.

Liquid-liquid phase separation ensures CPEB-mediated repression

Cells exploit liquid-liquid phase separation to optimize spatiotemporal control over cellular materials, metabolic processes and signalling pathways. Despite the list of functions that have been attributed to this phenomenon, the precise mechanism by which these are exerted is still subject of speculation.

In the present work we have provided strong evidence that all four CPEBs can undergo

LLPS *in vivo* (figs 33 and 38) and we propose that this property is essential for their dual function as repressors and activators. Accordingly, we speculate that CPEBs form condensates in stage VI oocytes, which favor translational repression, and dissolve in response to progesterone to facilitate transcript polyadenylation and translation.

Indeed, the model we propose has been suggested for other proteins such as FMRP. It has been shown that phosphorylation-dependent LLPS of the low-complexity region of FMRP is sufficient to inhibit translation and, remarkably, reversion of the condensation by methylation alleviates translational repression (Tsang et al., 2019). Additionally, these condensates are not only able to sequester repression factors such as 4E-BP proteins and miRNAs but they have also been proven to stimulate deadenylation mediated by the CCR4-NOT machinery (Kim et al., 2019), an effect also observed for AGO2 and TNRC6B condensates (Sheu-Gruttadauria and MacRae, 2018).

These findings indicate that LLPS, somehow, creates a chemical environment that allows specific reactions that are necessary for translational control and, more interestingly, establishes a framework for quick regulation: CCR4-NOT deadenylase activity dramatically decreases upon droplet dissolution. Most likely, mRNAs regulated by the CPEBs also exploit this principle to control translation in space and time. To test this hypothesis we could employ rabbit reticulocyte translation systems as in Kim et al. (2019).

On the other hand, even though several studies have addressed the LLPS properties of RNA and its possible role controlling size and composition of phase separated compartments (Garcia-Jove Navarro et al., 2019), it is still not known how RNA condensation affects to its translation. We speculate that CPEBs facilitate condensation and compaction of their targets, which may hinder translation initiation. This hypothesis is supported by observations from Adivarahan et al. (2018), who showed that mRNAs found in stress granules, which assemble by LLPS, are more compacted than translating ones.

Finally, the association between CPEBs and methylation readers can also have an impact in the phase separation properties of the target mRNA and, altogether, of the whole particle. This hypothesis is supported by data from Ries et al. (2019), who have shown that polymethylation correlates with repression in ribosome-profiling assays and that this behavior is linked to increased YTHDF2 condensation, thus establishing a potential connection between RNA modification, condensate formation and translational repression. In this regard, it would be interesting to address the effect of the CPEB family of proteins in the condensation of polymethylated transcripts and vice versa.

In conclusion, translational repression mediated by the CPEBs is inherently linked to liquid-liquid phase separation. As we will discuss below, we hypothesize that LLPS ensures the repressed state of the CPEB targets and warrants an accurate timing for translational activation in response to hormone stimulation.

Extensive modification of CPEB mRNP factors ensures the switch to translational activation

Upon hormone stimulation, CPEB1 gets phosphorylated and switches its function from repressor to activator, which has been linked to a remodeling of the repression complex. Considering our activation BioID data, we propose that CPEB1-mediated repression may be alleviated by the release of CCR4-NOT from the complex, similar to what had been previously described for PARN (Kim and Richter, 2006). Accordingly, transcript deadenylation would be inhibited and polyadenylation by Gld2 would be favored.

In addition to the release of the CCR4-NOT complex, we have identified new factors participating in CPEB1 translational activation such as YTHDF1 (fig. 30). This connection is supported by the observation that m^6A methylation occurring upon hormonal stimulation in *Xenopus laevis* oocytes correlates with higher protein levels (Qi et al., 2016). It is tempting to speculate that the increased translation of the m^6A-regulated

transcripts may be facilitated by CPEB1 through a mechanism yet to be described.

Similarly, our data suggests a link between CPEB1 and ATXN2. Ataxin-2 has been described to bind PABP and to protect poly(A) tails by regulating negatively the activity of deadenylases such as PAN, thus increasing translation of its targets (Ostrowski et al., 2017). Considering these evidences, we speculate that ATXN2 assists CPEB1 in translational activation by warranting stability of the newly synthesized poly(A) tails.

Another factor that appeared in our data is MOV10, which has been proposed to stimulate translation in neurons in response to NMDA by dissociating AGO2 from its targets (Kute et al., 2019). In view of these findings, we hypothesize that progesterone stimulation may have a similar effect in *Xenopus* oocytes and, consequently, MOV10 would assist CPEB1 translational activation by facilitating the release of inhibitory factors.

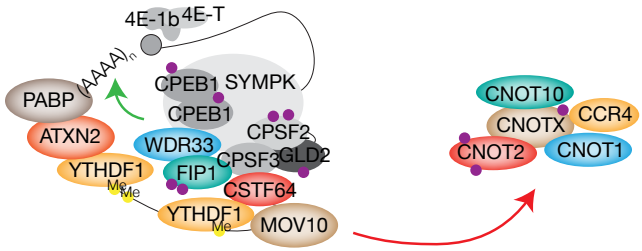

Figure 48: Model for CPEB1-mediated translational activation. Upon progesterone stimulation, proteins of the CPEB1 repression complex are post-translationally modified (purple dots), which affects their activity and/or phase separation properties. Remarkably, CPEB targets are potentially modified epigenetically, which may favor their translation. Additionally, the CCR4-NOT deadenylase is released from the complex, favoring polyadenylation.

Intriguingly, all of the identified proteins in the activation complex were also identified in stage VI oocytes. Indeed, some of them have been proposed, as CPEB1, to have a dual role in translational control, specially the YTHDF proteins (Shi et al., 2019), ATXN2 (Lim and Allada, 2013), MOV10 (Kute et al., 2019), DDX6 (Wang et al., 2015a) and

IGF2BP3 (Suvasini et al., 2011). It is conceivable that this switch in activity results from post-translational modifications, in a similar manner to CPEB1 regulation. In fact, we observed changes in mobility of proteins such as Gld2, YTHDF1, CNOT2 and IGF2BP3 and data from Peuchen et al. (2017) indicates that, overall, the proteins that we have identified in our BioID experiments tend to get phosphorylated upon progesterone stimulation (fig. 49). Conclusively, these observations suggest that the functional switch of the CPEB1 repression complex relies not only on the phosphorylation of CPEB1 but also on wide-spread modifications affecting other proteins in the complex, altogether contributing to the re-elongation of the poly(A)-tail of CPEB1 targets.

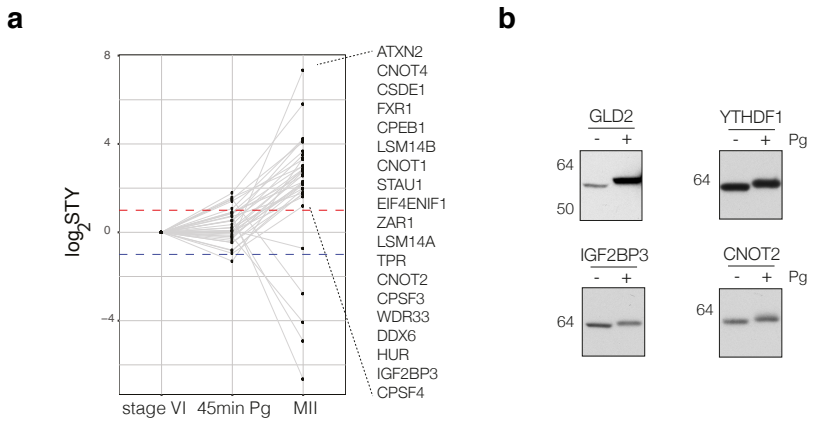

Figure 49: Widespread phosphorylation in CPEB partners upon progesterone stimulation. (a) Plot showing the average log_2STY phosphorylation for CPEB1-4 hits in three states: stage VI oocytes, 45 minutes after progesterone stimulation and MII oocytes. In general, CPEB interactors tend to get phosphorylated with meiotic progression. Data from Peuchen et al. (2017). (b) HA-western blots of oocytes with and without progesterone stimulation. Gld2, CNOT2, YTHDF1 and IGF2BP3 shift in MII oocytes compared with stage VI oocytes.

Post-translational modification of proteins found in these mRNPs could have an impact on their catalytic activity, as is the case of Gld2 (Chung et al., 2019), interactome, protein levels and, as suggested more recently, in their aggregation status (Rai et al., 2018). In this regard, it has been shown that *cyclinB1*, a CPEB1 target, forms granules in the animal pole of mouse and zebrafish oocytes that disassemble upon meiosis resumption,

in a Pum1 phosphorylation-dependent manner (Kotani et al., 2013; Saitoh et al., 2018). Consequently, it is tempting to speculate that this mechanism operates during *Xenopus laevis* oocyte maturation as well, in which extensive protein modification (e.g. by means of phosphorylation) may occur to dissolve many sorts of RNA granules, including those in which CPEBs are found. Notably, the fact that the activity of the CCR4-NOT deadenylase is enhanced by LLPS raises the possibility that CPEB granule dissolution is a mechanism controlling its localization and function.

Remarkably, Kotani et al. (2013) observed that *cyclin B1* granule dissolution in zebrafish oocytes by cytochalasin B treatment did not relieve the repressed state of this CPEB1 target. In view of this observation, we hypothesize that granule dissolution is required but not sufficient to promote translation. Accordingly, translational activation may require additional post-translational modifications that trigger catalytic, stoichiometric and interactomic changes on the CPEB repression complex.

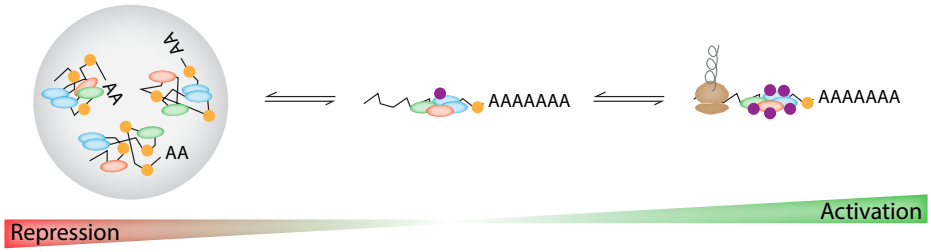

Figure 50: Granule assembly and disassembly participate in CPEB-mediated translational control. Repressed CPEB targets are found in granules formed by LLPS. Upon hormone stimulation, these condensates dissolve and cytoplasmic polyadenylation is promoted. However, translational activation requires additional cues, possibly resulting from the effect of post-translational modifications (purple dots) on key regulatory RNA-binding proteins.

In conclusion, we consider that progesterone stimulation triggers a signaling cascade that tackles RNA granules from different angles to ensure a fast and complete disassembly and reprogramming, necessary for cytoplasmic polyadenylation and, ultimately,

translation activation. However, recent evidence proposes that poly(A) tail re-elongation is not enough to sustain translation (Saitoh et al., 2018; Yang et al., 2020b), which implies that still more work needs to be done to fully understand how CPEBs activate translation beyond cytoplasmic polyadenylation.

Phase separation exerts evolutionary pressure on CPEBs

In this work we have shown that the LLPS properties of the CPEBs differ, specially of CPEB1. Interestingly, this pattern resembles the dichotomy established by evolution. In this regard, we have predicted the LLPS potential of multiple CPEB homologs using CatGranule (Bolognesi et al., 2016) and, as expected, this preliminary analysis suggests that evolution has favored the distancing between a low phase separation propensity protein (CPEB1 orthologs) and the high LLPS propensity paralogs CPEB2-4.

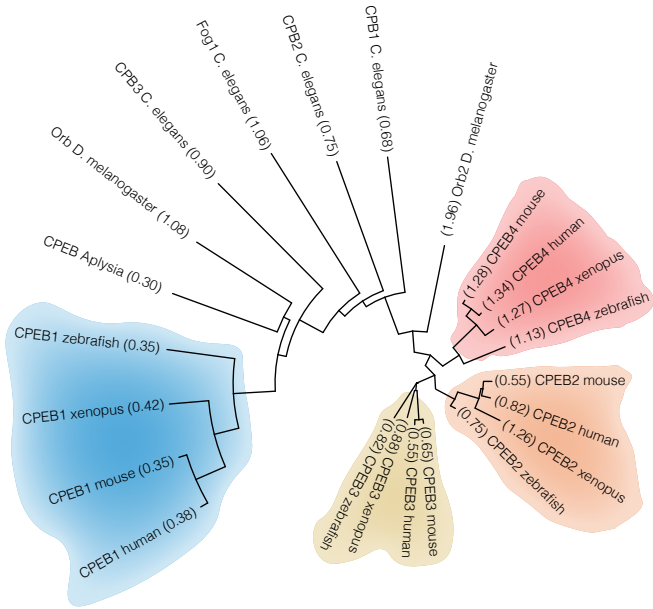

Figure 51: Distinct evolutionary branches of the CPEB family of proteins have different LLPS propensities. Phylogenetic tree depicting the relative evolutionary distance between several CPEB homologs. As shown in the picture, CPEB1 orthologs are the most distant members of the family and, additionally have lower predicted LLPS potential (value in parentheses).

We hypothesize that this evolutionary pressure results from the need to specialize the CPEBs into two complementary behaviors. One one hand CPEB1 orthologs would have evolved for ensuring robust and long-lasting translational repression, required for the control of genes related to irreversible and/or tightly regulated processes such as the cell cycle, and on the other the CPEB2-4 branch would have evolved to take control of more dynamic processes. According to our speculation, this functional diversity would be attained by the different exchange dynamics of molecules between the dense and the light phases, which is the feature that distinguishes best CPEB1 from CPEB2-4.

CPEBs phase separate in the oocyte as clients of other factors

As we mentioned, imaging of post-vitellogenic oocytes is technically difficult due to pigmentation of the shell and ubiquitous presence of yolk droplets. Consequently, we do not know to what extent our data with U-2 OS cells applies to frog germ cells. However, we believe that CPEBs are found in phase separated compartments in *Xenopus laevis* oocytes as well. A piece of data supporting this hypothesis comes from the work of a former member of the lab, Maria Piqué, who performed a size-exclusion chromatography of stage VI oocyte extracts and observed that CPEB1 eluted at high-molecular weight fractions, far from its own molecular weight (fig. 52a, unpublished data), which can be an indirect observation of CPEB1 condensation in these cells.

We also speculate that in these cellular conditions phase separation of the CPEBs might be facilitated by other scaffold proteins. Generally, scaffold proteins are present at higher concentrations and have many valences, while client proteins are less abundant and have more valences (Banani et al., 2016). In this regard, Xing et al. (2020) have shown that yeast P-bodies are composed of mainly seven proteins, which barely recover upon FRAP, and which they propose have scaffold-like properties.

Using quantitative proteomic data from *Xenopus laevis* stage VI oocytes (Peuchen et al.,

2017) we have checked the concentration of proteins common or related with our BioID datasets and have observed that, from the analyzed proteins, CPEB1 is one of the lower expressed (fig. 52b). Accordingly, we propose that CPEBs in the oocyte are clients of structures assembled by other more abundant proteins like PUM1, CNOT1 or DDX6.

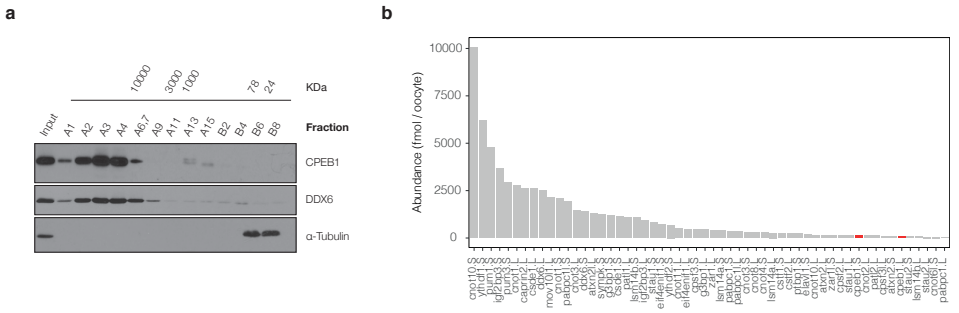

Figure 52: CPEBs are found in condensates assembled by scaffold proteins in stage VI oocytes. (a) Western blot showing the detection of CPEB1, DDX6 and tubulin in fractions of a size-exclusion chromatography of Murray's extracts. As expected, CPEB1 and DDX6 elute in high-molecular weight fractions, possibly in form of liquid-like condensates, while tubulin elutes as a monomer. (b) Barplot showing the abundance of several proteins of the oocyte. Highlighted in red are the two CPEB1 genes. As shown, CPEBs are lowly expressed compared to other proteins such as CNOT1. Proteomic data from Peuchen et al. (2017).

CPEB1-4 may not be redundant in stage VI oocytes

Among the whole family, CPEB1 is the member for which more mechanistic studies have been conducted, specially in *Xenopus laevis* oocytes. While little is known about the role of CPEB2 and CPEB3 in stage VI oocytes or in meiosis progression, a couple of studies have focused on CPEB4 and have demonstrated that it overtakes CPEB1 polyadenylation in the late-late phase. Beyond this context, roles for CPEB2-4 have been proposed in both translational repression and activation, through mechanisms distinct from what has been described for CPEB1 in frogs: CPEB2 can block elongation by binding to eEF2, and CPEB4 can block translation initiation in an eIF3-dependent manner.

Considering the lack of comparative studies, we decided to address the functional similarity or disparity of the four CPEBs by studying them in the same cellular system. In this regard, we have studied the interactomic landscape of the whole family and their LLPS properties. Combining our findings with data from Duran (2020) (unpublished), who has addressed the same question by studying the expression, regulation and targets of CPEB1-4, we aim to provide a broad picture of this family of proteins in the oocyte.

Taking into account that our interactomic studies suggest that all four CPEBs bind to similar translational control machineries (fig. 28), we speculate that all of them exert translational repression in the oocyte. However, these experiments show also CPEB-specific interactions that make us consider the possibility that the functional properties of the complexes the CPEBs assemble differ between members. This idea is supported by data from Youn et al. (2018), who observed that CPEB1, CPEB2 and CPEB4, despite being found in proximal protein hubs, have a slightly different interactomic environment (data not shown). In this sense, we propose that even though the four CPEBs can act as repressors in frog oocytes, their functions may not be completely redundant, and key interactors would be involved in ensuring this functional specificity.

RIP-Seq data from Duran (2020) suggests that not only the complexes the CPEBs assemble in the oocyte are different but also they exert translational control on different mRNA subsets. Remarkably, in a similar way to the LLPS data, the greatest difference comes from the comparison CPEB1 *versus* CPEB2-4, while most of the CPEB2-4 targets are shared between the three paralogs (fig. 53a).

A functional characterization of these targets indicates that CPEB1 is responsible for regulating cytoplasmic-associated processes whereas CPEB2-4 would have a bias towards genes that have functions in the nucleus (fig. 53b). Although the analysis of the RIP-Seq data is still ongoing, we aim to discern not only the role of each CPEB controlling certain cellular processes but also the molecular features of the targets that determine by which

CPEB subfamily are they regulated and, ultimately, the implications of this differential regulation in terms of cellular localization and temporal control of expression.

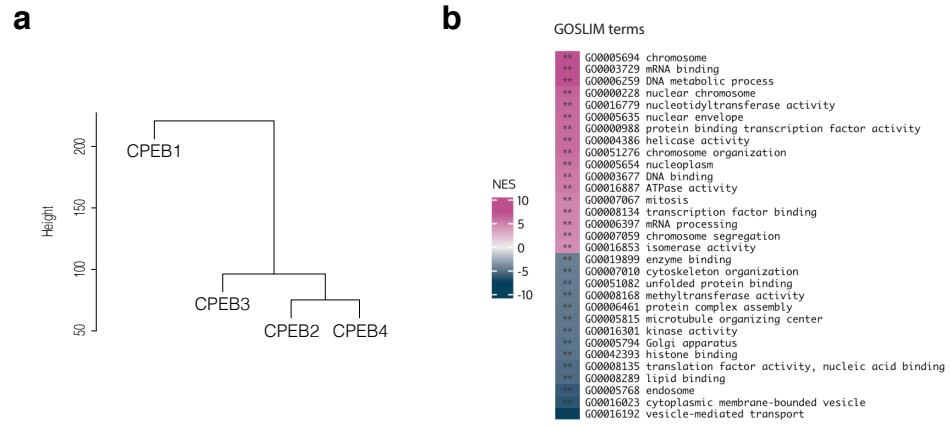

Figure 53: CPEB targets cluster into functionally differerent groups. (a) Dendrogram showing a hierarchical clustering of the DESeq2 data for all CPEBs. As shown, CPEB1 targets are the more dissimilar. (b) Heatmap showing the enrichment of GOSLIM categories in the comparison CPEB2-4 vs CPEB1 targets. Differential categories are enriched in both datasets, suggesting functional differences between the two CPEB branches. Data from Duran (2020).

Further results from Duran (2020) suggest that CPEB2-4 are not degraded upon progesterone stimulation, while CPEB1 does. This finding supports the aforementioned hypothesis that CPEB1 may have evolved to control irreversible processes (i.e. transcript localization, regulation of mRNAs implicated in the re-entry into meiosis, etc) while the other CPEBs may have been devoted to the control of reversible ones (i.e processes occurring periodically during the sequential embryonic divisions).

In conclusion, in collaboration with Berta Duran we have performed for the first time a comparative study of all four CPEBs in the same scenario and have shown that the two main CPEB families defined by evolution (possibly in an LLPS-associated manner) are also similarly separated in terms of function and regulation. However, the fact that CPEB2-4 bind to highly similar mRNA populations and are regulated by the same kinases raises the question as to which extent are these paralogs redundant. We hypo-

thesize that the answer lies in a more profound analysis of their specific interactomes and the different material properties of the LLPS granules into which they condense.

Indeed, we observed differences in the behavior of the droplets they assemble in U-2 OS cells. The most remarkable discriminatory feature we identified was the ability of the CPEB1 and CPEB4 droplets to move freely in the cytoplasm and describe straight trajectories (fig. 46). As we mentioned in the Results section, these differences in the movement profiles can be attributed to a differential association to cytoskeletal structures or organelles (Huang, 2003; Aizer et al., 2008), even though further studies should be conducted for the specific case of the CPEBs, for which only sparse data has been collected (Groisman et al., 2000; Stephan et al., 2015; Chen et al., 2016).

Limitations and perspectives

Limitations studying the CPEB mRNP composition and remodeling

Despite the fact that the BioID protocol we adapted for *Xenopus laevis* oocytes helped us to identify new components of the CPEB mRNPs and was useful for addressing the effect of an RNA-binding mutation, this methodology has still a main caveat: the rate at which proteins are biotinylated in the oocyte is too low to ensure a good signal-to-noise ratio. For this reason, we speculate that we have mainly been able to detect the most abundant components of the complexes we have addressed. Additionally, as biotinylation requires long incubations, this approach is limited if we want to study fast rearrangements. Considering these facts, we propose that use of faster biotinylating enzymes, such as APEX (Rhee et al., 2013; Chen and Perrimon, 2017) or TurboID (Branon et al., 2018), would allow to increase the signal-to-noise ratio. Unfortunately, we tried to adapt an APEX2 protocol in oocytes, as this methodology also allows temporal induction, but we did not manage to set it up.

Another important consideration of our work is that the methodology used does not allow to discern whether what we are observing is a unique repression complex or, conversely, is a combination of complexes assembled on different target mRNAs with potentially different compositions (Rouhana, 2005; O'Brien et al., 2005; Minshall et al., 2007; Fernández-Miranda and Méndez, 2012; Yang et al., 2020a). To address this question, we have tried to adapt the BioID for single 3'-UTRs by considering an RNA-pull down step with the λN peptide, aiming to unravel the relationship between the motifs found in these sequences and the complexes they can assemble. Even though the protocol looks promising (data not shown), we have not been able to optimize the enrichment of the biotinylation signal over the controls yet.

Finally, to functionally validate the importance or participation of the newly identified CPEB1-4 complex proteins and the relevance of the specific interactors, we consider performing a reporter assay in cells knock-down for these candidates. For these experiments, a bi-cistronic plasmid coding for two secretable luciferases will be transfected into a human cell line and relative luminescence will be measured from the medium. Importantly, one luciferase will be under the control of the CPEBs (cDNA fused to a 3'-UTR contaning CPEs), and the other will serve as the negative control (mutated CPEs). Consequently, upon knocking-down the candidate, relief of translational repression would be expected provided this protein is exerting a function in CPEB-medited repression. Unfortunately, the development of this assay is still incomplete as the cloning of the bi-cistronic plasmid is being incredibly cumbersome.

Limitations in the study of the CPEB mRNP dynamics

The study of liquid-liquid phase separation in *Xenopus laevis* oocytes has been restricted to stage I-II, since at these stages they are amenable for imaging due to the lack of pigment and yolk granules that make the cytoplasm opaque (Neil et al., 2020). The presence of these substances in stage VI oocytes make immunofluorescence nearly im-

possible. For this reason we decided to carry out our experiments in cultured cells, which are ideal for imaging, even for live acquisition. However, we still consider that novel methodological approximations should be developed for allowing imaging protocols in stage VI oocytes in order to the study of LLPS directly in these cells.

An important consideration of our work is that we have performed the LLPS experiments in an over-expression setting and, therefore, most likely above the physiological concentration of the analyzed proteins. As a consequence, it is possible that some of our data may be confused by supersaturation effects, which trigger gelation of the tested proteins and, with time, a liquid-to-solid transition (Patel et al., 2015; Shin et al., 2017b). In fact, even though we managed to detect some fusion events in our droplets, these were rare. Accordingly, we speculate that this static behavior (in terms of fusion and fission) and the presence of aggregates with irregular shapes in some cells may be attributed to the fact that cells are imaged 24h after transfection, which may favor supersaturation. In order to get rid of the limitations inherent to over-expression, we plan on generating CPEBX-GFP-expressing cells by endogenous tagging using CRISPR.

On the other hand, we still lack more details about the material properties of the droplets assembled by the four CPEBs. Experiments such as inverse capillary velocity, microrheology, half-FRAP and fluorescence correlation spectroscopy could help us understand better the droplets and get to known how much similar or different they are (Alberti et al., 2019). Even though these experiments should ideally be carried out *in vivo*, it is eventually easier to work *in vitro* with recombinant protein since it provides more controlled conditions and the system is closer to equilibrium (Martin and Mittag, 2018).

Finally, we would like to unravel the importance of LLPS for the function of the CPEBs. We speculate that treating oocytes or cultured cells with drugs that affect the LLPS properties of these proteins might render a phenotype that explains the role of their condensation. Accordingly, molecules such as 1,6-hexanediol could be used in this regard.

Conclusions

The present study provides new insights into the interactomic landscape of all four CPEBs in the same biological scenario, *Xenopus laevis* oocytes, with an special emphasis on the requirement of RNA binding and the N-terminal domain for CPEB1 repression complex formation. In line with this, we have also provided new players in the CPEB1-mediated translational activation occurring upon hormone stimulation. At the same time, we have generated the first systematic comparison of the LLPS properties of the *Xenopus laevis* CPEB sequences, putting an special focus on CPEB1, CPEB2 and CPEB3, which had not been studied before.

The main conclusions of the work are the following:

1. BioID allows the identification, quantification and comparison of proteins proximal to a protein of interest in *Xenopus laevis* stage VI oocytes.

2. The repression complex of CPEB1 in stage VI oocytes does not contain PARN. Instead, interactions with components of the CCR4-NOT machinery suggest it is the deadenylase of the complex.

3. The repression complex of CPEB1 in stage VI oocytes does not contain Maskin. Instead, the cap is blocked by EIF4E1b and repression is attained with proteins found in P-bodies such as DDX6, PATL2 and EIF4ENIF1.

4. CPEB1-mediated repression acts in synergy with other mechanisms including miRNA-induced silencing, adenosine methylation and repression mediated by other RBPs such as DAZL, ZAR1/2 and STAU2.

5. Formation of the repression complex requires RNA binding and, most likely, the NTD of the CPEBs.

6. All four CPEBs seem to assemble highly similar repression complexes with P-body associated proteins. Nonetheless, there are potential CPEB-specific components that may explain the non-redundancy of these paralogs.

7. BioID allows the identification of proteins proximal to a protein of interest in maturing *Xenopus laevis* oocytes. However, this methodology needs further improvement.

8. CPEB1-mediated translational activation potentially acts in synergy with other mechanisms including adenosine methylation and miRNA-induced translation.

9. CPEB1-mediated translational activation potentially requires wide-spread phosphorylation (and other PTMs) of the repression complex components, possibly to ensure changes in activity and condensation state.

10. All four CPEBs undergo phase separation *in vivo* when overexpressed, even though the complexes they assemble have different material properties (droplet size, number, FRAP curves, movement...).

11. Only phase separation of CPEB1 seems to rely on its CTD. Surprisingly, it does not depend on RNA binding. Phase separation of the other CPEBs, despite not requiring the respective CTD, depends on this domain for determining the overall biophysical properties of the condensate.

12. CPEBs phase separate into the same compartments, presumably in an RNA-independent manner. Co-condensation seems to affect the LLPS properties of the individual proteins.

Materials and Methods

Cloning strategies and RNA production

Cloning, subcloning and mutagenesis

Common cloning strategies have been used for generating most of the constructs. Plasmid amplification and manipulation techniques involve vector transformation into *E. coli* DH5α cells (Invitrogen, ref: 18265017), small or large scale plasmid DNA preparations with NucleoSpin Plasmid (Macherey-Nagel, ref: 740588) and NucleoBond Xtra Maxi (Macherey-Nagel, ref: 740414) kits respectively, amplicon generation with Phusion High-Fidelity DNA Polymerase (Thermo Fisher Scientific, ref: F530L) and ligation with T4 DNA ligase (Werfen, ref: M0202M). For mutagenesis, the QuickChange Lightning Multi Site-Directed Mutagenesis Kit (Agilent Technologies, ref: 210513) was used. Constructs that were used in phase separation experiments were produced by in-Fusion cloning reaction (BD Clontech trademark) following the protocol described in Berrow et al. (2007). The vectors used, pPEU4 and pPEU5, contain a C-terminal eGFP or mCherry tag respectively, which make them suitable for fluorescence microscopy.

Plasmid	Substitution	Mutagenesis oligo	LE
pcDNA-3.1-MCS-CPEB1_6A	S138A	ctttagcatgctgaacgcccccatggggaagcc	PmeI
	S144A	cccatggggaagccagccccctgggctttctg	
	S184A	gattctcgctccagcgcccctctgactctgac	
	S210A	caagtcttcgcatcgctcctccgctgcatttcc	
	S248A	ggcggcagcaactgtcgctccacttggcataac	
	S423A	gcaactttgtgcgtgctccatcacaacggctgg	
pcDNA-3.1-CPEB1(Y365A)-BirA(R118G)-HA	Y365A	gcccaaaggttatgttgctctggtatttgaatcagag	PmeI
pcDNA-3.1-mycBioID-CPEB1(Y365A)	Y365A	gcccaaaggttatgttgctctggtatttgaatcagag	Acc65I

Table 1: Oligos used for mutagenesis. Table of the oligos used for mutagenesis, showing the resulting plasmid construct, the mutations introduced and the linearization enzyme (LE). Unless otherwise specified, the residues follow the *Xenopus laevis* homolog index numbering.

For those genes of interest that were not in our library, total RNA from *Xenopus laevis* oocytes was extracted with TRIzol (Life Technologies, ref: 15596026) and then retrotranscribed with RevertAid First Strand cDNA synthesis kit (Thermo Fisher Scientific,

K1622) using oligodT(20). For the specific cDNA amplification, BioTaq DNA polymerase was used (Bioline, ref: BIO21040). Finally, some plasmids were either generated by other members in the lab or purchased (tables 2 and 3).

Plasmid description	Reference	From
pcDNA-3.1-mycBioID	35700	Addgene
pcDNA-3.1-MCS-BirA(R118G)-HA	36047	Addgene
pCMV-SPORT6-MOV10	IMAGp998B2214632Q	Source Bioscience
pCMV-SPORT6-FXR1B	IRBHp990B105D	Source Bioscience

Table 2: Purchased plasmids. Table of purchased plasmids and empty vectors.

Plasmids
pBSK(-)-HA
pET30a-His-CPEB1
pBSK(-)-FLAG-GLD2
pLuc + artificial 3'UTR CPE
pGL-5Bbox
pBSK(-)-His-HA-GST-Lambda
pET30a-His-MASKIN
pDEST32-CNOT10
pDonor-CNOT2

Table 3: Plasmids from former members. Table of plasmids that were already in our stock.

In vitro transcription and polyadenylation

RNAs for microinjection into *Xenopus laevis* oocytes were synthesized and capped *in vitro* using mMESSAGE mMACHINE T7 or T3 Transcription kits (Ambion, refs: AM1344 and AM1348 respectively) following manufacturer's instructions. RNAs for protein production in oocytes were also polyadenylated *in vitro* using Poly(A) Tailing Kit (Ambion, ref: AM1350). Synthesized RNAs were isolated regular by LiCl purification.

Plasmid	Forward oligo	Reverse oligo	RE1	RE2	LE3
pcDNA-3.1-CPEB1_NTD-BirA-HA	cccaccggtatggccttccactgaaag	cccgaattccacaggatttttgtagtttc	AgeI	EcoRI	PmeI
pcDNA-3.1-CPEB1-BirA-HA	cccaccggtatggccttccactgaaag	cccgaattcgctggagtcacgactttc	AgeI	EcoRI	PmeI
pcDNA-3.1-CPEB1_CTD-BirA-HA	cccgggcccttattcctgcaaagtctttctc	cccgaattcgctggagtcacgactttc	ApaI	EcoRI	PmeI
pcDNA-3.1-mycBioID-CPEB1	cccctcgaggtggcctcccactgaaag	cccgaattctagctggagtcacgactttc	XhoI	EcoRI	Acc65I
pcDNA-3.1-mycBioID-CPEB1_CTD	cccgctcgagtattcctgcaaagtctttctc	cccgaattctagctggagtcacgactttc	XhoI	EcoRI	Acc65I
pcDNA-3.1-CPEB2-BirA-HA	cccgctagcatgggggattacggcttcg	cccaccggtcgttccagcggaaagtggatc	NheI	HpaI	PmeI
pcDNA-3.1-CPEB3-BirA-HA	cccgctagcatgcaggatgatttactgatg	cccaccggtcgctccagcggaaaggaac	NheI	AgeI	PmeI
pcDNA-3.1-CPEB4-BirA-HA	cccgctagcatgggggattacgggttg	cccaccgggcgttccagcggaatgaaatatg	NheI	HpaI	PmeI
pcDNA-3.1-mycBioID-CPEB2	cccgcggccgctgggggattacgggcttcg	cccgatatctagttccagcggaagtggatc	NotI	EcoRV	PmeI
pcDNA-3.1-mycBioID-CPEB3	cccgcggccgctgcaggatgatttactgatg	cccgatatctcagctccagcggaaaggaac	NotI	EcoRV	Acc65I
pcDNA-3.1-mycBioID-CPEB4	cccgcggccgctgggggattacgggtttgg	cccgatatctcagttccagcggaatgaaatatg	NotI	EcoRV	Acc65I
pBSK(-)-HA-MASKIN	cccgcggccgcagccttcaaatcataaacgatg	ccccccgggtcagatcttctccatcttaaaataaaatc	NotI	XmaI	EcoRI
pBSK(-)-HA-PARN	cccgcggccgcatggaaatcaccaggagc	ccccccgggctaccaagtatctggaacttc	NotI	XmaI	EcoRI
pBSK(-)-HA-GLD2	cccgcggccgcatgtaccctaactccccag	ccccccgggtcataacgagtgcatttttttc	NotI	XmaI	EcoRI
pBSK(-)-HA-CNOT2	cccgcgggccgcatgtttggtgcttcaagaaag	ccccccgggttagaaggctgctgagcag	NotI	XmaI	HindIII
pBSK(-)-HA-CNOT10	cccgcgggccgcgctgcagacaaagcaggag	ccccccgggtcatttctctgaacagcag	NotI	XmaI	XhoI
pBSK(-)-HA-ZAR2	ccctctagagcgggtttgtgtattctcc	cccgaattctcagacgatgtattgtagc	XbaI	EcoRI	EcoRV
pBSK(-)-HA-YTHDF1	cccgcggccgctctgctactagcgtggatcc	cccgaattcttagcatgagtcgggtttagg	NotI	EcoRI	HindIII
pBSK(-)-HA-PTBP1	cccgcggccgcgcgaaggcattgttcaagatataac	cccccccgggttaaattgtggatttggaaaagg	NotI	XmaI	XhoI
pBSK(-)-HA-IGF2BP3	cccggatccaacaagctgtatattggaaacc	cccgaattcttatttcttctttggttgggg	BamHI	EcoRI	HindIII
pBSK(-)-HA-MOV10	cccgcggccgcatgtattgttctgcaagtaaag	cccccccgggtcagtgttcatgtctccaatttg	NotI	XmaI	XhoI
pBSK(-)-HA-FXR1B	cccgcggccgcgaggacctgacggtgggaag	cccgatatcttaagacacccccattcagtatg	NotI	EcorV	XhoI

Table 4: Plasmids and subcloning oligos. Table of the plasmids used in our experiments and the oligos required for subcloning. Restriction enzymes are also shown (RE1 and RE2) as well as the plasmid linearization enzyme (LE).

Plasmid	Forward oligo	Reverse oligo	RE1	RE2	LE3
pcDNA-3.1-MCS-BirA(R118G)-HA					PmeI
pcDNA-3.1-mycBioID					Acc65I
pBSK(-)-FLAG-GLD2					Acc65I
pPEU4-CPEB1-GFP	aggagatataccatggccttcccactgaaagatgat	cttccagaccgcttgagctggagtcacgacttttctga			
pPEU4-CPEB1(Y365A)-GFP	aggagatataccatggccttcccactgaaagatgat	cttccagaccgcttgagctggagtcacgacttttctga			
pPEU4-CPEB1_CTD-GFP	aggagatataccatgtattcctgcaaagtctttctcgg	cttccagaccgcttgagctggagtcacgacttttctga			
pPEU4-CPEB1_NTD-GFP	aggagatataccatggccttcccactgaaagatgat	cttccagaccgcttgacacaggatttttgtagtttctagg			
pPEU5-CPEB1-mCherry	aggagatataccatggccttcccactgaaagatgat	cttccagaccgcttgagctggagtcacgacttttctga			
pPEU5-CPEB1_NTD-mCherry	aggagatataccatggccttcccactgaaagatgat	cttccagaccgcttgacacaggatttttgtagtttctagg			
pPEU4-CPEB2-GFP	aggagatataccatgggggattacggcttcgggtta	cttccagaccgcttgagttccagcggaagtggatctggcg			
pPEU4-CPEB3-GFP	aggagatataccatgcaggatgatttactgatggac	cttccagaccgcttgagctccagcggaaaggaac			
pPEU4-CPEB4-GFP	aggagatataccatgggggattacgggtttggagtgc	cttccagaccgcttgagttccagcggaatgaaatatgcctc			
pPEU4-CPEB2_NTD-GFP	aggagatataccatgggggattacggcttcgggtta	cttccagaccgcttgaatagcaattgggagaattcagaaccc			
pPEU4-CPEB3_NTD-GFP	aggagatataccatgcaggatgatttactgatggac	cttccagaccgcttgattctattccttcaccgttctg			
pPEU4-CPEB4_NTD-GFP	aggagatataccatgggggattacgggtttggagtgc	cttccagaccgcttgattccattggaaagagagagg			

Table 4: Plasmids and subcloning oligos (continuation). Table of the plasmids used in our experiments and the oligos required for subcloning. Restriction enzymes are also shown (RE1 and RE2) as well as the plasmid linearization enzyme (LE).

Oocyte manipulation and samples immunoblotting

Oocyte obtention, microinjection and enucleation

Ovarian tissue was isolated from female *Xenopus laevis* frogs by surgery and kept in Modified Bath Saline media (MBS: 88 mM NaCl, 1 mM KCl, 1 mM $MgSO_4$, 2.5 mM $NaHCO_3$, adjusted to pH 7.8 and supplemented with fresh 0.7 mM $CaCl_2$). The ovary with multiple lobes was snipped off using blunt-end forceps and then incubated with a mixture of 0.8 mg/mL collagenase type IA (Sigma Aldrich, ref: C9891) and 0.48 mg/mL dispase II (Dispase II; Sigma Aldrich, ref: D4693) in MBS for 2 h at 22 ºC to allow for oocyte defolliculation and isolation.

After digestion, isolated oocytes were thoroughly washed with MBS and then placed in a Petri dish for manual selection of stage VI oocytes under the microscope (Leica MZ95; Modular high-performance stereomicroscope with 9.5:1 zoom).

For overexpression experiments, selected fully-grown oocytes were microinjected with *in vitro* transcribed RNAs (or the corresponding vehicles) using a Nanoject II Drummond microinjector and 3.5" Drummond 3-000-203-G/X replacement glass capillaries. When required, maturation of stage VI oocytes was induced with 10μM progesterone (Sigma Aldrich, P0130) in MBS at 18ºC or room temperature.

For experiments requiring nuclei, oocytes were placed in Gall's medium (83 mM KCl, 17 mM NaCl, 1 mM $MgCl_2$, 10 mM Tris-HCl, adjusted to pH 7.2), snipped with forceps and squeezed to release the nuclei. Nuclei were then transferred to an Eppendorf tube containing 0.5mL ice-cold nucleus medium (100 mM pH 5.2 Sodium Acetate and 5 mM EDTA) and then centrifuged for 5 minutes at 100g. Pelleted nuclei were resuspended in the desired buffer.

Immunoblotting

Protein extracts were separated by SDS-polyacrylamide gel electrophoresis (PAGE).

Protein target	Obtained from	Reference	Supplier	Dilution
CPEB1	rabbit polyclonal	Custom antibody (#R1010)	Abbyntek	1:1000
PARN	rabbit polyclonal	20R-1155	Fitzgerald	1:1000
CNOT2	rabbit polyclonal	ABIN1106729	Antibodies online	1:1000
EIF4E1B	rabbit polyclonal	Custom antibody (Xe4)	Abbyntek	1:1000
EIF4ET	rabbit polyclonal	Custom antibody (Xe3)	Abbyntek	1:1000
MASKIN	rabbit polyclonal	Custom antibody	Richter's lab	1:1000
GLD2	rabbit polyclonal	Custom antibody (Xe7)	Abbyntek	1:1000
HUR	mouse monoclonal	sc-5261	Santa Cruz	1:1000
CPSF2	rabbit polyclonal	Custom antibody (Xe2)	Abbyntek	1:1000
SYMPK	mouse monoclonal	610644	BD Transduction Lab	1:1000
CCR4	rabbit polyclonal	Custom antibody (#1827A)	Invitrogen	1:500
DDX6	rabbit polyclonal	Custom antibody (Xe5)	Abbyntek	1:1000
alpha tubulin	mouse monoclonal	T9026	Sigma	1:10000
histone3	Rabbit polyclonal	9715	Cell Signaling	1:2000
DDX6	rabbit polyclonal	PD009	MBL Int Corp	1:1000
GST	mouse monoclonal	sc-138	Santa Cruz	1:1000
FLAG	mouse monoclonal	F1804	Sigma	1:1000
GFP	rabbit polyclonal	A6455	Invitrogen	1:1000
HA	rat monoclonal	11867431001	Roche	1:2000
HIS	mouse monoclonal	H 1029	Sigma	1:1000
MYC	goat polyclonal	ab9132	Abcam	1:1000
anti-rabbit HRP	goat polyclonal	G21234	ThermoFisher	1:3000
anti-goat HRP	donkey polyclonal	ab6885	abcam	1:3000
anti-rat HRP	goat polyclonal	G31471	ThermoFisher	1:3000
anti-mouse HRP	goat polyclonal	G31430	ThermoFisher	1:3000
Alexa Fluor 647 anti rabbit	goat polyclonal	A21245	Invitrogen	1:400

Table 5: Table of primary and secondary antibodies. Antigen, source species, product reference, commercial supplier and working dilutions are depicted.

After separation, proteins were transferred onto nitrocellulose membranes (Amersham Protran 0.45 NC Nitrocellulose Western blotting membranes, GE Healthcare Life Sciences, ref: 10600002) for 1 h at 400 mA.

Membranes were blocked with 5% milk for 1h at room temperature and then incubated with primary antibodies from 1 h room temperature to overnight at 4 ºC. For detection of biotinylated proteins, streptavidin-HRP (Invitrogen, ref: S911) was used (table 5).

BioID approach methods

Identification of endogenously biotinylated proteins

All the mass spectrometry (MS) experiments have been performed at the IRB Barcelona Mass Spectrometry and Proteomics Core Facility.

Fully-grown stage VI oocytes were lysed in 10 µL/oocyte H1 kinase solution (80 mM sodium β-glycerophosphate pH 7.4, 0.5 mM sodium orthovanadate, 15 mM $MgCl_2$ and 20 mM EGTA) supplemented with 1 mM PMSF (Sigma, ref:78830) and EDTA-free protease inhibitors (Roche, ref: 11836170001) and then centrifuged twice for clarification at 16000g for 15 minutes at 4 ºC. Protein lysates were mixed with Laemmli buffer 2X (60 mM Tris-HCl pH 6.8, 10% glycerol, 4% SDS, 0.01% bromophenol blue) and run in a 4–20% Criterion TGX Precast Gel (BioRad, ref: 567-1093) for 1 h at 150 V. Afterwards, gels were stained with Pierce Silver Stain kit for Mass Spectrometry (Thermo Fisher Scientific, ref: 10404005) following manufacturer's instructions. After staining, the bands of interest were excised and sent to the proteomics core facility.

Stained electrophoretic protein bands were reduced with 10 mM DTT for 45 min at 56 ºC and alkylated for 30 min in the dark with 55 mM iodoacetamide (Sigma, ref: A3221). Then, in-gel digestion was performed with trypsin (0.1 µg/µL) in 50 mM NH_4HCO_3 at 37 ºC overnight. Digestion was stopped by addition of 1% formic acid. Peptides were extracted with 100% acetonitrile and completely evaporated. Samples were reconstituted in 1% formic acid aqueous solution for MS analysis. For the nano-LC-MS/MS,

20% of the samples volume was used.

Samples were loaded to a 180 μm x 2 cm C18 Symmetry trap column (Waters) at a flow rate of 15 μL/min using a nanoAcquity Ultra Performance LCTM chromatographic system (Waters Corp., Milford, MA). Peptides were separated using a C18 analytical column (BEH130 C18 75 μm x 25 cm, 1.7 μm, Waters Corp.) with a 120 minutes run, comprising three consecutive steps with linear gradients from 1 to 35% B in 180 minutes, from 35 to 50% B in 10 minutes (A = 0.1% formic acid in water, B = 0.1% formic acid in acetonitrile). The column outlet was directly connected to an Advion TriVersa NanoMate (Advion) fitted on an LTQ-FT Ultra mass spectrometer (Thermo). The mass spectrometer was operated using the data-dependent acquisition mode. Survey MS scans were acquired in the FT with the resolution (defined at 400 m/z) set to 100.000. Up to six of the most intense ions per scan were fragmented and detected in the linear ion trap. The ion count target value was 1.000.000 for the survey scan and 50.000 for the MS/MS scan. Target ions already selected for MS/MS were dynamically excluded for 30 seconds. Spray voltage in the NanoMate source was set to 1.70 kV. Capillary voltage and tube lens on the LTQ-FT were tuned to 40 V and 120 V. Minimal signal required to trigger MS to MS/MS switch was set to 1.000 and activation Q was 0.250. The spectrometer was working in positive polarity mode and singly charge state precursors were rejected for fragmentation.

A database search was performed with Proteome Discoverer software v1.4 (Thermo) using Sequest HT search engine and SwissProt database (*Xenopodinae*, release 2016_03 and the contaminants database). Searches were run against targeted and decoy databases to determine the false discovery rate (FDR). Search parameters included trypsin enzyme specificity, allowing for two missed cleavage sites, carbamidomethyl in cysteine as static modification and methionine oxidation and biotin in lysine as dynamic modifications. Peptide mass tolerance was 10 ppm and the MS/MS tolerance was 0.6 Da. Peptides with an FDR $<$ 1% were considered as positive identifications with a high confidence level.

BioID labeling and affinity purification

Fully-grown oocytes were incubated with 20 μM biotin for 40 h after RNA microinjection for efficient BirA labeling at 18 ºC. For experiments requiring progesterone stimulation, the hormone was added 16h after microinjection.

For each experimental condition, around 100 oocytes were lysed in 6 μL/oocyte cold lysis buffer (50 mM Tris-HCl pH 7.4, 100 mM NaCl supplemented with EDTA-free protease inhibitors and 1 mM PMSF) and then centrifuged twice for clarification at 16000g for 15 minutes at 4 ºC. Later, 300 μL of prechilled 50 mM Tris-HCl pH 7.4 supplemented with protease inhibitors and 1 mM PMSF were added to 200 μL of cleared extracts for further clearing with PD MiniTrap G-25 columns (GE Healthcare Life Sciences, ref: 28-9180-07) and then reagents were added to a final concentration of 50 mM Tris-HCl pH 7.4, 100 mM NaCl, 1.6% Triton-X100, 0.04% SDS, 1X EDTA-free protease inhibitors and 1 mM PMSF in a final volume of 1 mL.

Cleared extracts were incubated with 200 μL MyOne Dynabeads Streptavidin C1 (Invitrogen, ref: 65001) for 20 h at 4 ºC with orbital shaking. After incubation, beads were washed thrice with wash buffer 1 (8 M Urea and 0.25% SDS in PBS), twice with wash buffer 2 (6 M Guanidine-HCl in PBS), once with wash buffer 3 (6.4 M Urea, 1 M NaCl and 0.2% SDS in PBS), thrice with wash buffer 4 (4 M Urea, 1 M NaCl, 10% isopropanol, 10% ethanol, 0.2% SDS in PBS), once with wash buffer 1, once with wash buffer 5 (8 M Urea and 1% SDS in PBS) and thrice with wash buffer 6 (2% SDS in PBS). After the beads had been washed, they were further rinsed with 50 mM Tris-HCl pH 7.4 to remove detergents that could interfere with Mass Spectrometry. Finally, beads were washed with 50 mM NH_4HCO_3 pH 8 to eliminate the traces of Tris.

Beads bound to biotinylated proteins were then resuspended in 500 μL of 3 M urea and 50 mM NH_4HCO_3 pH 8.0 in water and incubated with 5 mM DTT for 1 h with

orbital shaking at room temperature for disulfide bond reduction. After, incubation in the dark for 30 minutes at room temperature with 10 mM iodoacetamide was carried out for blocking thiol groups. Alkylation was stopped by addition of 5 mM DTT, sample volumes were raised to 1.5 ml with 50mM NH_4HCO_3 pH 8 to reduce urea concentration and then proteins were digested on-bead with 2 µg trypsin (Promega, ref: V5111) for 16 h at 37 ºC with orbital shaking. Digestion was stopped by adding 1% formic acid and the supernatant enriched in biotinylated peptides was retrieved.

Mass spectrometry of BioID samples

Digested samples from BioID affinity purifications were desalted using PolyLC tips C18 and peptides were eluted with 80% acetonitrile and 1% formic acid. Next, samples were diluted to 20% acetonitrile and 0.1% formic acid and loaded into strong cation exchange columns and peptides were eluted in 5% NH_4OH and 30% methanol. Finally, samples were evaporated to dry and reconstituted in 3% acetonitrile and 1% formic acid. For the nano-LC-MS/MS, 10% of the samples volume was used.

Samples were loaded to a 300 µm x 5 mm PepMap100, 5 µm, 100Å, C18 µ-precolumn (Thermo Scientific) at a flow rate of 15µL/minute using a Thermo Scientific Dionex Ultimate 3000 chromatographic system. Peptides were separated using a C18 analytical column (Acclaim PepMap RSLC (75 µm x 50 cm, nanoViper, C18, 2 µm, 10Å, Thermo Scientific) with a 120 minutes run, comprising three consecutive steps with linear gradients from 1 to 35% B in 90 min, from 35 to 50% B in 5 min, and from 50% to 85% B in 2 min, followed by isocratic elution at 85% B in 5 min and stabilization to initial conditions (A = 0.1%formic acid in water, B = 0.1% formic acid in acetonitrile). The column outlet was directly connected to an Advion TriVersa NanoMate (Advion) fitted on an Orbitrap Fusion Lumos Tribrid (Thermo Scientific).

The mass spectrometer was operated in a data-dependent acquisition mode. Survey

MS scans were acquired in the orbitrap with the resolution (defined at 200 m/z) set to 120000. The lock mass was user-defined at 445.12 m/z in each Orbitrap scan. The top speed (most intense) ions per scan were fragmented and detected in the linear ion trap. The ion count target value was 400000 for the survey scan and 10000 for the MS/MS scan. Target ions already selected for MS/MS were dynamically excluded for 15 seconds. Spray voltage in the NanoMate source was set to 1.60 kV. RF Lenses were tuned to 30%. Minimal signal required to trigger MS to MS/MS switch was set to 5000 and activation Q was 0.250. The spectrometer was working in positive polarity mode and singly charge state precursors were rejected for fragmentation.

A database search was performed with Proteome Discoverer software v2.1.0.81 using Sequest HT search engine and UniProt *Xenopodinae* release 2017_02, contaminants database and user proteins manually introduced. Search was run against targeted and decoy database to determine the FDR. Search parameters included trypsin specificity, allowing for two missed cleavage sites, oxidation in methionine and acetylation in protein N-terminus as dynamic modifications.

When specified, biotin in lysine was included as a dynamic modification. Peptide mass tolerance was 10 ppm and the MS/MS tolerance was 0.6Da. Peptides with a q-value lower than 0.1 and a FDR $< 1\%$ were considered as positive identifications with a high confidence level.

BioID data analysis

For the identification of BioID hits percentile normalization of $\log_{10}$iBAQ was used. For those conditions for which one or two missing values had been identified in the four replicates, the remaining two or thee non-missing values were used for imputation using a k-nearest-neighbors approximation according to the $\log_{10}$iBAQ distributions of each replicate (k = 10 nearest neighbors). For these bait-prey pairs, a differential expression

analysis was performed using linear models (lmFit and eBayes from limma R package).

Only when the control had more than two missing values and the condition none or just one , we also considered as potential hits those proteins whose log_{10}iBAQ value was above the first quantile of the log_{10}iBAQ values distribution in the respective conditions and below this threshold in the control condition. Alternatively, as described in the Results section, other label-free quantification approaches were also tested (Top3 from MStats software and the SAINT algorithm).

Validation of BioID candidate proximal proteins

Overexpressed HA-tagged constructs were precipitated using Pierce Anti-HA Magnetic Beads (Thermo Fisher cientific, ref: 88836). Fifty to a hundred oocytes expressing HA-tagged proteins were lysed in 10 µL/oocyte cold immunoprecipitation lysis buffer (20 mM TrisHCl pH 8, 100 mM NaCl, 0.5% NP-40, 1 mM EDTA, 1 mM $MgCl_2$ supplemented with 1 mM PMSF and EDTA-free protease inhibitors). Oocyte lysates were centrifuged twice for clarification at 16000g for 15 minutes at 4 ºC and then incubated with orbital shaking for 20 h at 4 ºC with anti-HA magnetic beads in a ratio 1.25 µL beads/oocyte. After incubation, beads were washed 6 times with 1 volume of lysis buffer and then the bound fraction was eluted with Laemmli buffer 2x and heating for 20 minutes at 60 ºC. Finally, eluates were recovered, supplemented with 160 mM DTT and run in a PAGE gel.

Cells manipulation

Cell culture and transfection

U-2 OS cells were grown in Dulbecco's Modified Eagle Medium (DMEM, Gibco, ref: 10938-025) with 10% fetal bovine serum (FBS, Gibco, ref: 10270106), 1% Gln and 1% penicillin/streptomycin (Gibco, ref: 15140122). Twenty-four hours before transfec-

tion, cells were seeded onto 12mm ⌀ glass coverslips (Marienfeld Superior, ref: 0111550) coated with poly-lysine to be 70% confluent by the time of transfection. Transfection was performed with Lipofectamine LTX and Plus Reagent (Invitrogen, ref: 15338100) following manufacturer's indications. Briefly, 2.5 μg of plasmid DNA were incubated with 2.5 μl Plus Reagent in Opti-MEM (Invitrogen, ref: 11058021) for 10 minutes and then with 6 μl of Lipofectamine LTX in Opti-MEM for 30 minutes. Cells were incubated with Lipofectamine-DNA complexes for 24h before fixation or harvesting. For mCherry co-localization experiments, two plasmids were transfected at the same time using the protocol described above. In this case, for the preparation of the DNA-LTX complexes 1.25 μg of each plasmid were used so as to keep the ratio DNA:well surface.

For live-cell imaging experiments, cells were seeded in μ-Slide 8 Well ibiTreat plates (Ibidi, ref: 80826) 24 hours before transfection to be 70% confluent by the time of transfection. DNA and lipofectamine preparations were scaled-down to 250 ng DNA, 0.6 μl Lipofectamine LTX and 0.3 μl Plus Reagent. For acquisition, medium was changed to FluoroBrite DMEM (Thermo Fisher Scientific, ref: A1896701) + 10% FBS + 1% penicillin/streptomycin + 1% Glutamine, suitable for fluorescence microscopy.

Cell harvesting

U-2 OS cells grown in 6-well plates (Labclinics, ref: 140675) were transfected as described above. Twenty-four hours after exposure to DNA-lipid complexes, cells from each well were harvested for protein extraction. Briefly, cells were washed twice with PBS, scraped off the plate gently in the presence of 1 mL cold PBS (Invitrogen, ref: 14190169) and then recovered in Eppendorf tubes. Tubes were centrifuged at 0.5 g for 5 minutes at 4 ºC and cell pellets were resuspended in 50 μL lysis buffer (50 mM Tris-HCl pH 7.5, 150 mM NaCl, 1% NP-40, 5 mM EGTA and 5 mM EDTA supplemented with fresh 20 mM NaF, 10 mM β-glycerophosphate, 1 mM DTT, 1 mM PMSF, EDTA-free protease inhibitors, Phosphatase inhibitors cocktail 2 (Sigma Aldrich, ref: P5726) and

phosphatase inhibitors cocktail 3 (Sigma Aldrich, ref: P0044)), lysed by pipetting, sonicated 5 minutes at M2 settings (Bioruptor XL, Diagenode), centrifuged 5 minutes at 16000g at 4ºC and then the supernatant was kept in a new tube. Samples were quantified with BSA standard curves using DC Protein Assay kit (BioRad, ref: 500-0116) following manufacturer's instructions on a 96-well plate reader (ELx808 Absorbance Microplate Reader, Biotek) measuring absorbance at 750 nm.

Cell fixation and mounting

After 24 h of exposure to DNA-lipid complexes, medium was removed and the coverslips were rinsed twice with PBS and then incubated with 4% para-formaldehyde (Aname, ref: 15710) in PBS for 10 minutes at room temperature. Next, cells were washed twice with PBS and incubated with 0.5 μg/μL DAPI (Sigma, ref: D9542) for 10 minutes in the dark. After staining, coverslips were rinsed with PBS again in the dark, dried and transferred to a 76 mm x 26 mm slide (Thermo Fisher Scientific, ref: AGAB000002) for mounting with Prolong Gold Antifade Mountant (Invitrogen, ref: P36934). For experiments were fluorescent labeling of the cytoplasm was required, cells were stained before fixation. Coverslips were incubated with fresh 1:2000 CellMask Deep Red Plasma membrane stain (ThermoFisher, ref: C10046) in DMEM for 5 minutes at 37 ºC and then washed twice with PBS for fixation.

Imaging methodologies

GFP distribution in fixed cells

Images of GFP plasmid-transfected cells were acquired with Spectral Confocal Microscope Leica SP5 at size 1024x1024 pixels and zoom factor 3.3. The objective that was used was 63X (63x/1.40-0.60 Oil Lbd BL) with immersion oil. For acquisition of DAPI the 405nm Diode excitation laser was set at 9% and the HyD2 detector was set at 415-480nm with gain 21% and for acquisition of GFP the Argon 488nm excitation laser was

set at 20% and the HyD2 detector was set at 500-550nm with gain 20%. When required, far-red fluorescence was acquired with the HeNe 633nm laser set at 15% and the HyD2 detector was set at 636-700nm with 10% gain. For each cell, 15-25 stacks were acquired at slices of 0.2μm. Cell coordinates were marked and the multiposition setting of the microscope (Mark and Find) was used to acquire stacks cell by cell.

Co-localization

For mCherry co-localization experiments, the red signal was acquired with the DPSS561 excitation laser set at 12% and the HyD2 detector set at 578-565nm with gain 10%. DAPI and GFP signals were acquired using the aforementioned settings. On the other hand, for co-localization experiments using far-red signal from immunofluorescence (Alexa Fluor 647nm secondary antibody), excitation was set at 15% intensity of 633nm HeNe laser and detection was set at 737-779nm using the HyD2 detector.

In both experimental approaches 15-25 stacks were acquired per cell at slices of 0.2 μm. Cell coordinates were marked and the multiposition setting of the microscope was used to acquire stacks cell by cell.

Fixed cells image analysis

For the GFP pattern analysis, cells were first stratified according to the mean fluorescence intensity of the green channel. Background signal was removed by thresholding and then images with a mean below 70 units were classified as low-intensity cells, those above 100 units were classified as high-intensity cells and those between 70 and 100 units were classified as medium-intensity cells. Next, for each cell the cytoplasmic distribution of the GFP-tagged product was categorized between: diffuse, mainly diffuse, irregular aggregates, mainly round aggregates and round aggregates.

For co-localization analysis, channels were split and thresholded before applying the

Colocalization Test (https://imagej.net/Colocalization_Test) from Fiji (ImageJ, version 2.0.0-rc-69/1.52p). From each image, the observed Pearson correlation coefficient and the average coefficient from 100 randomized versions (background) were retrieved.

Live cell imaging

Cells expressing GFP-tagged proteins were monitored to track fusion and fission events as well as to observe the particles movement using a Spinning Disk Microscope (Andor Revolution xD, Andor). A total of 800 images were taken by experiment, with a size of 140x140 pixels and acquiring two Z-stacks with a slice of 0.5 μm. Typical frame rate was set to 8 images per second (125 ms/frame) and the exposure time of the EMCCD camera (Andor) was set to 50 ms. For acquisition, AOTF 488 nm laser intensity was set at 12%. Fluorescence intensity of fusion events was quantified using Fiji software.

Imaris software was used (https://imaris.oxinst.com) for particle tracking analysis. Images were rescaled setting the voxel size to (x = 1, y = 1, z = 1) units and particles were segmented using an estimated size of 2 units, automatic quality threshold and local contrast using the diameter obtained from the region border. For track selection, the following parameters were set: maximum frame distance of 6 frames, maximum gap size of 0 frames, and track duration minimum of 7 seconds. From each track, data regarding particle size, track length, track displacement and straightness was collected for subsequent analysis.

Fluorescence recovery after photobleaching

Fluorescence Recovery After Photobleaching (FRAP) of GFP constructs-expressing cells was performed with a Spinning Disk Microscope equipped with a FRAPPA module allowing fast switching between FRAP and imaging with the same 488 nm laser set. A total of 350 images with a size of 512x512 pixels were taken by experiment, 50 before the bleaching and 300 after, with a typical frame rate of 11 images per second (88 ms)

with an exposure time of 50 ms on an EMCCD camera. For acquisition, AOTF 488 nm laser intensity was set at 12% while for bleaching laser was set at 60% intensity in two repeats with a dwell time of 40ms each.

For the analysis of FRAP data mean fluorescence intensity was obtained for the bleached region, the whole cell area and the background in each time frame using Fiji software. Double normalization of these data and curve-fitting to a single exponential was performed using the open-source easyFRAPweb (easyfrap.vmnet.upatras.gr/), previously discarding the 20 first acquired frames. From the data obtained with easyFRAP, observations not fitting to a curve or with recovery dynamics out of the range of the experimental settings were neglected for further analysis. Finally, for each condition the mean curve was calculated as well as the distribution of t-halves and mobile fractions.

References

Abernathy, E. and Glaunsinger, B. (2015). Emerging roles for RNA degradation in viral replication and antiviral defense. *Virology*, 479-480:600–608.

Adivarahan, S., Livingston, N., Nicholson, B., Rahman, S., Wu, B., Rissland, O. S., and Zenklusen, D. (2018). Spatial Organization of Single mRNPs at Different Stages of the Gene Expression Pathway. *Molecular Cell*, 72(4):727–738.e5.

Afroz, T., Skrisovska, L., Belloc, E., Guillen-Boixet, J., Mendez, R., and Allain, F. H.-T. (2014). A fly trap mechanism provides sequence-specific RNA recognition by CPEB proteins. *Genes & Development*, 28(13):1498–1514.

Aguilera, A. (2005). Cotranscriptional mRNP assembly: from the DNA to the nuclear pore. *Current Opinion in Cell Biology*, 17(3):242–250.

Aizer, A., Brody, Y., Ler, L. W., Sonenberg, N., Singer, R. H., and Shav-Tal, Y. (2008). The dynamics of mammalian P body transport, assembly, and disassembly in vivo. *Chemtracts*, 19(10):4154–4166.

Alberti, S. (2017). Phase separation in biology. *Current Biology*, 27(20):R1097–R1102.

Alberti, S., Gladfelter, A., and Mittag, T. (2019). Considerations and Challenges in Studying Liquid-Liquid Phase Separation and Biomolecular Condensates. *Cell*, 176(3):419–434.

Alberti, S., Saha, S., Woodruff, J. B., Franzmann, T. M., Wang, J., and Hyman, A. A. (2018). A User's Guide for Phase Separation Assays with Purified Proteins. *Journal of Molecular Biology*, 430(23):4806–4820.

Amrani, N., Ghosh, S., Mangus, D. A., and Jacobson, A. (2008). Translation factors promote the formation of two states of the closed-loop mRNP. *Nature*, 453(7199):1276–1280.

Andersen, D. S. and Leevers, S. J. (2007). The Essential Drosophila ATP-binding Cassette Domain Protein, Pixie, Binds the 40 S Ribosome in an ATP-dependent Manner and Is Required for Translation Initiation. *Journal of Biological Chemistry*, 282(20):14752–14760.

Andrei, M. A. (2005). A role for eIF4E and eIF4E-transporter in targeting mRNPs to mammalian processing bodies. *RNA*, 11(5):717–727.

Andresson, T. (1998). The kinase Eg2 is a component of the Xenopus oocyte progesterone-activated signaling pathway. *The EMBO Journal*, 17(19):5627–5637.

Balagopal, V. and Parker, R. (2009). Polysomes, P bodies and stress granules: states and fates of eukaryotic mRNAs. *Current Opinion in Cell Biology*, 21(3):403–408.

Banani, S. F., Lee, H. O., Hyman, A. A., and Rosen, M. K. (2017). Biomolecular condensates: organizers of cellular biochemistry. *Nature Reviews Molecular Cell Biology*, 18(5):285–298.

Banani, S. F., Rice, A. M., Peeples, W. B., Lin, Y., Jain, S., Parker, R., and Rosen, M. K. (2016). Compositional Control of Phase-Separated Cellular Bodies. *Cell*, 166(3):651–663.

Baralle, F. E. and Giudice, J. (2017). Alternative splicing as a regulator of development and tissue identity. *Nature Reviews Molecular Cell Biology*, 18(7):437–451.

Barbosa, C., Peixeiro, I., and Romão, L. (2013). Gene Expression Regulation by Upstream Open Reading Frames and Human Disease. *PLoS Genetics*, 9(8):e1003529.

Barnard, D. C., Cao, Q., and Richter, J. D. (2005). Differential Phosphorylation Controls Maskin Association with Eukaryotic Translation Initiation Factor 4E and Localization on the Mitotic Apparatus. *Molecular and Cellular Biology*, 25(17):7605–7615.

Barnard, D. C., Ryan, K., Manley, J. L., and Richter, J. D. (2004). Symplekin and xGLD-2 Are Required for CPEB-Mediated Cytoplasmic Polyadenylation. *Cell*, 119(5):641–651.

Barreau, C. (2005). AU-rich elements and associated factors: are there unifying principles? *Nucleic Acids Research*, 33(22):7138–7150.

Bartel, D. P. (2009). MicroRNAs: Target Recognition and Regulatory Functions. *Cell*, 136(2):215–233.

Bava, F.-A., Eliscovich, C., Ferreira, P. G., Miñana, B., Ben-Dov, C., Guigó, R., Valcárcel, J., and Méndez, R. (2013). CPEB1 coordinates alternative 3'-UTR formation with translational regulation. *Nature*, 495(7439):121–125.

Belloc, E. and Méndez, R. (2008). A deadenylation negative feedback mechanism governs meiotic metaphase arrest. *Nature*, 452(7190):1017–1021.

Beringer, M. and Rodnina, M. V. (2007). The Ribosomal Peptidyl Transferase. *Molecular Cell*, 26(3):311–321.

Berrow, N. S., Alderton, D., Sainsbury, S., Nettleship, J., Assenberg, R., Rahman, N., Stuart, D. I., and Owens, R. J. (2007). A versatile ligation-independent cloning method suitable for high-throughput expression screening applications. *Nucleic Acids Research*, 35(6):e45–e45.

Boeynaems, S., Alberti, S., Fawzi, N. L., Mittag, T., Polymenidou, M., Rousseau, F., Schymkowitz, J., Shorter, J., Wolozin, B., Van Den Bosch, L., Tompa, P., and Fuxreiter, M. (2018). Protein Phase Separation: A New Phase in Cell Biology. *Trends in Cell Biology*, 28(6):420–435.

Boke, E., Ruer, M., Wühr, M., Coughlin, M., Lemaitre, R., Gygi, S. P., Alberti, S., Drechsel, D., Hyman, A. A., and Mitchison, T. J. (2016). Amyloid-like Self-Assembly of a Cellular Compartment. *Cell*, 166(3):637–650.

Bolognesi, B., Lorenzo Gotor, N., Dhar, R., Cirillo, D., Baldrighi, M., Tartaglia, G. G., and Lehner, B. (2016). A Concentration-Dependent Liquid Phase Separation Can Cause Toxicity upon Increased Protein Expression. *Cell Reports*, 16(1):222–231.

Brangwynne, C. P., Eckmann, C. R., Courson, D. S., Rybarska, A., Hoege, C., Gharakhani, J., Julicher, F., and Hyman, A. A. (2009). Germline P Granules Are Liquid Droplets That Localize by Controlled Dissolution/Condensation. *Science*, 324(5935):1729–1732.

Branon, T. C., Bosch, J. A., Sanchez, A. D., Udeshi, N. D., Svinkina, T., Carr, S. A., Feldman, J. L., Perrimon, N., and Ting, A. Y. (2018). Efficient proximity labeling in living cells and organisms with TurboID. *Nature Biotechnology*, 36(9):880–887.

Bresson, S. and Tollervey, D. (2018). Tailing Off: PABP and CNOT Generate Cycles of mRNA Deadenylation. *Molecular Cell*, 70(6):987–988.

Buratowski, S. (2005). Connections between mRNA 3' end processing and transcription termination. *Current Opinion in Cell Biology*, 17(3):257–261.

Calderone, V., Gallego, J., Fernandez-Miranda, G., Garcia-Pras, E., Maillo, C., Berzigotti, A., Mejias, M., Bava, F.-A., Angulo-Urarte, A., Graupera, M., Navarro, P., Bosch, J., Fernandez, M., and Mendez, R. (2016). Sequential Functions of CPEB1 and CPEB4 Regulate Pathologic Expression of Vascular Endothelial Growth Factor and Angiogenesis in Chronic Liver Disease. *Gastroenterology*, 150(4):982–997.e30.

Cao, Q. (2002). Dissolution of the maskin-eIF4E complex by cytoplasmic polyadenylation and poly(A)-binding protein controls cyclin B1 mRNA translation and oocyte maturation. *The EMBO Journal*, 21(14):3852–3862.

Cao, Q., Kim, J. H., and Richter, J. D. (2006). CDK1 and calcineurin regulate Maskin association with eIF4E and translational control of cell cycle progression. *Nature Structural & Molecular Biology*, 13(12):1128–1134.

Carmody, S. R. and Wente, S. R. (2009). mRNA nuclear export at a glance. *Journal of Cell Science*, 122(12):1933–1937.

Carvalho, M. D. G. D. C., Carvalho, J. F., and Merrick, W. C. (1984). Biological characterization of various forms of elongation factor 1 from rabbit reticulocytes. *Archives of Biochemistry and Biophysics*, 234(2):603–611.

Charlesworth, A., Meijer, H. A., and de Moor, C. H. (2013). Specificity factors in cytoplasmic polyadenylation. *Wiley Interdisciplinary Reviews: RNA*, 4(4):437–461.

Charlesworth, A., Wilczynska, A., Thampi, P., Cox, L. L., and MacNicol, A. M. (2006). Musashi regulates the temporal order of mRNA translation during Xenopus oocyte maturation. *The EMBO Journal*, 25(12):2792–2801.

Charlesworth, A., Yamamoto, T. M., Cook, J. M., Silva, K. D., Kotter, C. V., Carter, G. S., Holt, J. W., Lavender, H. F., MacNicol, A. M., Ying Wang, Y., and Wilczynska, A. (2012). Xenopus laevis zygote arrest 2 (zar2) encodes a zinc finger RNA-binding protein that binds to the translational control sequence in the maternal Wee1 mRNA and regulates translation. *Developmental Biology*, 369(2):177–190.

Chen, C.-L. and Perrimon, N. (2017). Proximity-dependent labeling methods for proteomic profiling in living cells. *Wiley Interdisciplinary Reviews: Developmental Biology*, 6(4):e272.

Chen, C.-Y. A. and Shyu, A.-B. (2011). Mechanisms of deadenylation-dependent decay. *Wiley Interdisciplinary Reviews: RNA*, 2(2):167–183.

Chen, M., Zheng, W., and Wolynes, P. G. (2016). Energy landscapes of a mechanical prion and their implications for the molecular mechanism of long-term memory. *Proceedings of the National Academy of Sciences*, 113(18):5006–5011.

Chen, P.-J. and Huang, Y.-S. (2012). CPEB2-eEF2 interaction impedes HIF-1α RNA translation. *The EMBO Journal*, 31(4):959–971.

Chin, A. and Lécuyer, E. (2017). RNA localization: Making its way to the center stage. *Biochimica et Biophysica Acta (BBA) - General Subjects*, 1861(11):2956–2970.

Choi, H., Larsen, B., Lin, Z.-Y., Breitkreutz, A., Mellacheruvu, D., Fermin, D., Qin, Z. S., Tyers, M., Gingras, A.-C., and Nesvizhskii, A. I. (2011). SAINT: probabilistic scoring of affinity purification–mass spectrometry data. *Nature Methods*, 8(1):70–73.

Chung, C. Z., Balasuriya, N., Manni, E., Liu, X., Li, S. S.-C., O'Donoghue, P., and Heinemann, I. U. (2019). Gld2 activity is regulated by phosphorylation in the N-terminal domain. *RNA Biology*, 16(8):1022–1033.

Colgan, D. F. and Manley, J. L. (1997). Mechanism and regulation of mRNA polyadenylation. *Genes & Development*, 11(21):2755–2766.

Crick, F. (1970). Central Dogma of Molecular Biology. *Nature*, 227(5258):561–563.

Cui, J. and Placzek, W. J. (2018). PTBP1 enhances miR-101-guided AGO2 targeting to MCL1 and promotes miR-101-induced apoptosis. *Cell Death & Disease*, 9(5):552.

Dai, X.-X., Jiang, J.-C., Sha, Q.-Q., Jiang, Y., Ou, X.-H., and Fan, H.-Y. (2019). A combinatorial code for mRNA 3'-UTR-mediated translational control in the mouse oocyte. *Nucleic Acids Research*, 47(1):328–340.

Darnell, J. C. and Richter, J. D. (2012). Cytoplasmic RNA-Binding Proteins and the Control of Complex Brain Function. *Cold Spring Harbor Perspectives in Biology*, 4(8):a012344–a012344.

Darnell, J. E. (2013). Reflections on the history of pre-mRNA processing and highlights of current knowledge: A unified picture. *RNA*, 19(4):443–460.

Das, R. K. and Pappu, R. V. (2013). Conformations of intrinsically disordered proteins are influenced by linear sequence distributions of oppositely charged residues. *Proceedings of the National Academy of Sciences*, 110(33):13392–13397.

Decker, C. J. and Parker, R. (2012). P-Bodies and Stress Granules: Possible Roles in the Control of Translation and mRNA Degradation. *Cold Spring Harbor Perspectives in Biology*, 4(9):a012286–a012286.

Desterro, J., Bak-Gordon, P., and Carmo-Fonseca, M. (2020). Targeting mRNA processing as an anticancer strategy. *Nature Reviews Drug Discovery*, 19(2):112–129.

Dever, T. E. and Green, R. (2012). The Elongation, Termination, and Recycling Phases of Translation in Eukaryotes. *Cold Spring Harbor Perspectives in Biology*, 4(7):a013706–a013706.

Di Giammartino, D. C., Nishida, K., and Manley, J. L. (2011). Mechanisms and Consequences of Alternative Polyadenylation. *Molecular Cell*, 43(6):853–866.

Ditlev, J. A., Case, L. B., and Rosen, M. K. (2018). Who's In and Who's Out—Compositional Control of Biomolecular Condensates. *Journal of Molecular Biology*, 430(23):4666–4684.

Doma, M. K. and Parker, R. (2006). Endonucleolytic cleavage of eukaryotic mRNAs with stalls in translation elongation. *Nature*, 440(7083):561–564.

Dong, J., Lai, R., Nielsen, K., Fekete, C. A., Qiu, H., and Hinnebusch, A. G. (2004). The Essential ATP-binding Cassette Protein RLI1 Functions in Translation by Promoting Preinitiation Complex Assembly. *Journal of Biological Chemistry*, 279(40):42157–42168.

Drisaldi, B., Colnaghi, L., Fioriti, L., Rao, N., Myers, C., Snyder, A. M., Metzger, D. J., Tarasoff, J., Konstantinov, E., Fraser, P. E., Manley, J. L., and Kandel, E. R. (2015). SUMOylation Is an Inhibitory Constraint that Regulates the Prion-like Aggregation and Activity of CPEB3. *Cell Reports*.

Du, L. (2005). Activity-dependent polyadenylation in neurons. *RNA*, 11(9):1340–1347.

Duran, B. (2020). *Combinatorial perspective on the gene expression circuits established by the CPEB-family of proteins*. PhD thesis, Universitat de Barcelona.

Eckmann, C. R., Rammelt, C., and Wahle, E. (2011). Control of poly(A) tail length. *Wiley Interdisciplinary Reviews: RNA*, 2(3):348–361.

Edery, I. and Sonenberg, N. (1985). Cap-dependent RNA splicing in a HeLa nuclear extract. *Proceedings of the National Academy of Sciences*, 82(22):7590–7594.

Elbaum-Garfinkle, S., Kim, Y., Szczepaniak, K., Chen, C. C.-H., Eckmann, C. R., Myong, S., and Brangwynne, C. P. (2015). The disordered P granule protein LAF-1 drives phase separation into droplets with tunable viscosity and dynamics. *Proceedings of the National Academy of Sciences*, 112(23):7189–7194.

Eliscovich, C., Peset, I., Vernos, I., and Méndez, R. (2008). Spindle-localized CPE-mediated translation controls meiotic chromosome segregation. *Nature Cell Biology*, 10(7):858–865.

Elkon, R., Ugalde, A. P., and Agami, R. (2013). Alternative cleavage and polyadenylation: extent, regulation and function. *Nature Reviews Genetics*, 14(7):496–506.

Fabian, M. R., Cieplak, M. K., Frank, F., Morita, M., Green, J., Srikumar, T., Nagar, B., Yamamoto, T., Raught, B., Duchaine, T. F., and Sonenberg, N. (2011). miRNA-mediated deadenylation is orchestrated by GW182 through two conserved motifs that interact with CCR4–NOT. *Nature Structural & Molecular Biology*, 18(11):1211–1217.

Fagoonee, S., Bearzi, C., Di Cunto, F., Clohessy, J. G., Rizzi, R., Reschke, M., Tolosano, E., Provero, P., Pandolfi, P. P., Silengo, L., and Altruda, F. (2013). The RNA Binding Protein ESRP1 Fine-Tunes the Expression of Pluripotency-Related Factors in Mouse Embryonic Stem Cells. *PLoS ONE*, 8(8):e72300.

Falahati, H. and Wieschaus, E. (2017). Independent active and thermodynamic processes govern the nucleolus assembly in vivo. *Proceedings of the National Academy of Sciences*, 114(6):1335–1340.

Feric, M., Vaidya, N., Harmon, T. S., Mitrea, D. M., Zhu, L., Richardson, T. M., Kriwacki, R. W., Pappu, R. V., and Brangwynne, C. P. (2016). Coexisting Liquid Phases Underlie Nucleolar Subcompartments. *Cell*, 165(7):1686–1697.

Fernández-Miranda, G. and Méndez, R. (2012). The CPEB-family of proteins, translational control in senescence and cancer. *Ageing Research Reviews*, 11(4):460–472.

Fioriti, L., Myers, C., Huang, Y.-Y., Li, X., Stephan, J. S., Trifilieff, P., Colnaghi, L., Kosmidis, S., Drisaldi, B., Pavlopoulos, E., and Kandel, E. R. (2015). The Persistence of Hippocampal-Based Memory Requires Protein Synthesis Mediated by the Prion-like Protein CPEB3. *Neuron*, 86(6):1433–1448.

Fischer, P. M. (2009). Cap in hand: Targeting eIF4E. *Cell Cycle*, 8(16):2535–2541.

Fong, K.-w., Li, Y., Wang, W., Ma, W., Li, K., Qi, R. Z., Liu, D., Songyang, Z., and Chen, J. (2013). Whole-genome screening identifies proteins localized to distinct nuclear bodies. *The Journal of Cell Biology*, 203(1):149–164.

Fong, N. (2001). Capping, splicing, and 3' processing are independently stimulated by RNA polymerase II: different functions for different segments of the CTD. *Genes & Development*, 15(14):1783–1795.

Ford, L., Ling, E., Kandel, E. R., and Fioriti, L. (2019). CPEB3 inhibits translation of mRNA targets by localizing them to P bodies. *Proceedings of the National Academy of Sciences*, 116(36):18078–18087.

Fox, C. A., Sheets, M. D., and Wickens, M. P. (1989). Poly(A) addition during maturation of frog oocytes: distinct nuclear and cytoplasmic activities and regulation by the sequence UUUUUAU. *Genes & Development*, 3(12b):2151–2162.

Frolova, L. Y., Tsikovskii, R. Y., Sivolobova, G. F., Oparina, N. Y., Serpinsky, O. I., Blinov, V. M., Tatkov, S. I., and Kisselev, L. L. (1999). Mutations in the highly conserved GGQ motif of class 1 polypeptide release factors abolish ability of human eRF1 to trigger peptidyl-tRNA hydrolysis. *RNA*, 5(8):S135583829999043X.

Gallie, D. R. (1991). The cap and poly(A) tail function synergistically to regulate mRNA translational efficiency. *Genes & Development*, 5(11):2108–2116.

Gallouzi, I. E. and Wilusz, J. (2013). A DIStinctively novel exoribonuclease that really likes U. *The EMBO Journal*, 32(13):1799–1801.

Garcia-Jove Navarro, M., Kashida, S., Chouaib, R., Souquere, S., Pierron, G., Weil, D., and Gueroui, Z. (2019). RNA is a critical element for the sizing and the composition of phase-separated RNA–protein condensates. *Nature Communications*, 10(1):3230.

Garneau, N. L., Wilusz, J., and Wilusz, C. J. (2007). The highways and byways of mRNA decay. *Nature Reviews Molecular Cell Biology*, 8(2):113–126.

Gebauer, F. and Hentze, M. W. (2004). Molecular mechanisms of translational control. *Nature Reviews Molecular Cell Biology*, 5(10):827–835.

Ghosh, A. and Lima, C. D. (2010). Enzymology of RNA cap synthesis. *Wiley Interdisciplinary Reviews: RNA*, 1(1):152–172.

Gingras, A.-C., Raught, B., and Sonenberg, N. (1999). eIF4 Initiation Factors: Effectors of mRNA Recruitment to Ribosomes and Regulators of Translation. *Annual Review of Biochemistry*, 68(1):913–963.

Goldstrohm, A. C. and Wickens, M. (2008). Multifunctional deadenylase complexes diversify mRNA control. *Nature Reviews Molecular Cell Biology*, 9(4):337–344.

Goodfellow, I. G. and Roberts, L. O. (2008). Eukaryotic initiation factor 4E. *The International Journal of Biochemistry & Cell Biology*, 40(12):2675–2680.

Greig, J. A., Nguyen, T. A., Lee, M., Holehouse, A. S., Posey, A. E., Pappu, R. V., and Jedd, G. (2020). Arginine-Enriched Mixed-Charge Domains Provide Cohesion for Nuclear Speckle Condensation. *Molecular Cell*, 77(6):1237–1250.e4.

Groisman, I., Huang, Y.-S., Mendez, R., Cao, Q., Theurkauf, W., and Richter, J. D. (2000). CPEB, Maskin, and Cyclin B1 mRNA at the Mitotic Apparatus. *Cell*, 103(3):435–447.

Guillén-Boixet, J., Buzon, V., Salvatella, X., and Méndez, R. (2016). CPEB4 is regulated during cell cycle by ERK2/Cdk1-mediated phosphorylation and its assembly into liquid-like droplets. *eLife*, 5(NOVEMBER2016).

Haimov, O., Sinvani, H., and Dikstein, R. (2015). Cap-dependent, scanning-free translation initiation mechanisms. *Biochimica et Biophysica Acta (BBA) - Gene Regulatory Mechanisms*, 1849(11):1313–1318.

Hake, L. E., Mendez, R., and Richter, J. D. (1998). Specificity of RNA Binding by CPEB: Requirement for RNA Recognition Motifs and a Novel Zinc Finger. *Molecular and Cellular Biology*, 18(2):685–693.

Hake, L. E. and Richter, J. D. (1994). CPEB is a specificity factor that mediates cytoplasmic polyadenylation during Xenopus oocyte maturation. *Cell*, 79(4):617–627.

Hasegawa, E., Karashima, T., Sumiyoshi, E., and Yamamoto, M. (2006). C. elegans CPB-3 interacts with DAZ-1 and functions in multiple steps of germline development. *Developmental Biology*, 295(2):689–699.

Heck, A. M. and Wilusz, J. (2018). The Interplay between the RNA Decay and Translation Machinery in Eukaryotes. *Cold Spring Harbor Perspectives in Biology*, 10(5):a032839.

Hervas, R., Rau, M. J., Park, Y., Zhang, W., Murzin, A. G., Fitzpatrick, J. A. J., Scheres, S. H. W., and Si, K. (2020). Cryo-EM structure of a neuronal functional amyloid implicated in memory persistence in Drosophila. *Science*, 367(6483):1230–1234.

Hinnebusch, A. G. and Lorsch, J. R. (2012). The Mechanism of Eukaryotic Translation Initiation: New Insights and Challenges. *Cold Spring Harbor Perspectives in Biology*, 4(10):a011544–a011544.

Hofweber, M. and Dormann, D. (2019). Friend or foe—Post-translational modifications as regulators of phase separation and RNP granule dynamics. *Journal of Biological Chemistry*, 294(18):7137–7150.

Holcik, M. and Sonenberg, N. (2005). Translational control in stress and apoptosis. *Nature Reviews Molecular Cell Biology*, 6(4):318–327.

Hondele, M., Sachdev, R., Heinrich, S., Wang, J., Vallotton, P., Fontoura, B. M. A., and Weis, K. (2019). DEAD-box ATPases are global regulators of phase-separated organelles. *Nature*, 573(7772):144–148.

Horowitz, N. H., Bonner, D., Mitchell, H. K., Tatum, E. L., and Beadle, G. W. (1945). Genic Control of Biochemical Reactions in Neurospora. *The American Naturalist*, 79(783):304–317.

Hosoda, N., Funakoshi, Y., Hirasawa, M., Yamagishi, R., Asano, Y., Miyagawa, R., Ogami, K., Tsujimoto, M., and Hoshino, S.-i. (2011). Anti-proliferative protein Tob negatively regulates CPEB3 target by recruiting Caf1 deadenylase. *The EMBO Journal*, 30(7):1311–1323.

Hu, W., Yuan, B., and Lodish, H. F. (2014). Cpeb4-Mediated Translational Regulatory Circuitry Controls Terminal Erythroid Differentiation. *Developmental Cell*, 30(6):660–672.

Huang, Y.-S. (2003). Facilitation of dendritic mRNA transport by CPEB. *Genes & Development*, 17(5):638–653.

Igea, A. and Méndez, R. (2010). Meiosis requires a translational positive loop where CPEB1 ensues its replacement by CPEB4. *The EMBO Journal*, 29(13):2182–2193.

Iserman, C., Desroches Altamirano, C., Jegers, C., Friedrich, U., Zarin, T., Fritsch, A. W., Mittasch, M., Domingues, A., Hersemann, L., Jahnel, M., Richter, D., Guenther, U.-P., Hentze, M. W., Moses, A. M., Hyman, A. A., Kramer, G., Kreysing, M., Franzmann, T. M., and Alberti, S. (2020). Condensation of Ded1p Promotes a Translational Switch from Housekeeping to Stress Protein Production. *Cell*, 181(4):818–831.e19.

Ivshina, M., Lasko, P., and Richter, J. D. (2014). Cytoplasmic Polyadenylation Element Binding Proteins in Development, Health, and Disease. *Annual Review of Cell and Developmental Biology*, 30(1):393–415.

Jackson, R. J., Hellen, C. U. T., and Pestova, T. V. (2010). The mechanism of eukaryotic translation initiation and principles of its regulation. *Nature Reviews Molecular Cell Biology*, 11(2):113–127.

Jain, S., Wheeler, J. R., Walters, R. W., Agrawal, A., Barsic, A., and Parker, R. (2016). ATPase-Modulated Stress Granules Contain a Diverse Proteome and Substructure. *Cell*, 164(3):487–498.

Jinek, M., Coyle, S. M., and Doudna, J. A. (2011). Coupled 5' Nucleotide Recognition and Processivity in Xrn1-Mediated mRNA Decay. *Molecular Cell*, 41(5):600–608.

Joag, H., Ghatpande, V., Sarkar, M., Raina, A., Desai, M., Shinde, M., Bose, T., and Majumdar, A. (2019). A role of cellular translation regulation associated with toxic Huntingtin protein. *bioRxiv*, page 687764.

Jonas, S. and Izaurralde, E. (2015). Towards a molecular understanding of microRNA-mediated gene silencing. *Nature Reviews Genetics*, 16(7):421–433.

Jurado, A. R., Tan, D., Jiao, X., Kiledjian, M., and Tong, L. (2014). Structure and Function of Pre-mRNA 5'-End Capping Quality Control and 3'-End Processing. *Biochemistry*, 53(12):1882–1898.

Kato, M., Han, T. W., Xie, S., Shi, K., Du, X., Wu, L. C., Mirzaei, H., Goldsmith, E. J., Longgood, J., Pei, J., Grishin, N. V., Frantz, D. E., Schneider, J. W., Chen, S., Li, L., Sawaya, M. R., Eisenberg, D., Tycko, R., and McKnight, S. L. (2012). Cell-free Formation of RNA Granules: Low Complexity Sequence Domains Form Dynamic Fibers within Hydrogels. *Cell*, 149(4):753–767.

Kaul, G., Pattan, G., and Rafeequi, T. (2011). Eukaryotic elongation factor-2 (eEF2): its regulation and peptide chain elongation. *Cell Biochemistry and Function*, 29(3):227–234.

Kedersha, N., Stoecklin, G., Ayodele, M., Yacono, P., Lykke-Andersen, J., Fritzler, M. J., Scheuner, D., Kaufman, R. J., Golan, D. E., and Anderson, P. (2005). Stress granules and processing bodies are dynamically linked sites of mRNP remodeling. *Journal of Cell Biology*, 169(6):871–884.

Kenny, P. and Ceman, S. (2016). RNA Secondary Structure Modulates FMRP's Bi-Functional Role in the MicroRNA Pathway. *International Journal of Molecular Sciences*, 17(6):985.

Khan, M., Youn, J.-Y., Gingras, A.-C., Subramaniam, R., and Desveaux, D. (2018). In planta proximity dependent biotin identification (BioID). *Scientific Reports*, 8(1):9212.

Khong, A. and Parker, R. (2018). mRNP architecture in translating and stress conditions reveals an ordered pathway of mRNP compaction. *Journal of Cell Biology*, 217(12):4124–4140.

Kim, D. I., Jensen, S. C., Noble, K. A., KC, B., Roux, K. H., Motamedchaboki, K., and Roux, K. J. (2016). An improved smaller biotin ligase for BioID proximity labeling. *Molecular Biology of the Cell*, 27(8):1188–1196.

Kim, J. H. and Richter, J. D. (2006). Opposing Polymerase-Deadenylase Activities Regulate Cytoplasmic Polyadenylation. *Molecular Cell*, 24(2):173–183.

Kim, J. H. and Richter, J. D. (2007). RINGO/cdk1 and CPEB mediate poly(A) tail stabilization and translational regulation by ePAB. *Genes & Development*, 21(20):2571–2579.

Kim, T. H., Tsang, B., Vernon, R. M., Sonenberg, N., Kay, L. E., and Forman-Kay, J. D. (2019). Phospho-dependent phase separation of FMRP and CAPRIN1 recapitulates regulation of translation and deadenylation. *Science*, 365(6455):825–829.

Kok, K. H., Ng, M.-H. J., Ching, Y.-P., and Jin, D.-Y. (2007). Human TRBP and PACT Directly Interact with Each Other and Associate with Dicer to Facilitate the Production of Small Interfering RNA. *Journal of Biological Chemistry*, 282(24):17649–17657.

Komar, A. A. (2009). A pause for thought along the co-translational folding pathway. *Trends in Biochemical Sciences*, 34(1):16–24.

Konopacka, A., Greenwood, M., Loh, S.-Y., Paton, J., and Murphy, D. (2015). RNA binding protein Caprin-2 is a pivotal regulator of the central osmotic defense response. *eLife*, 4.

Kornblihtt, A. R. (2004). Multiple links between transcription and splicing. *RNA*, 10(10):1489–1498.

Kotani, T., Yasuda, K., Ota, R., and Yamashita, M. (2013). Cyclin B1 mRNA translation is temporally controlled through formation and disassembly of RNA granules. *The Journal of Cell Biology*, 202(7):1041–1055.

Kotovic, K. M., Lockshon, D., Boric, L., and Neugebauer, K. M. (2003). Cotranscriptional Recruitment of the U1 snRNP to Intron-Containing Genes in Yeast. *Molecular and Cellular Biology*, 23(16):5768–5779.

Kozak, M. (2002). Pushing the limits of the scanning mechanism for initiation of translation. *Gene*, 299(1-2):1–34.

Kratassiouk, G., Pritchard, L. L., Cuvellier, S., Vislovukh, A., Meng, Q., Groisman, R., Degerny, C., Deforzh, E., Harel-Bellan, A., and Groisman, I. (2016). The WEE1 regulators CPEB1 and miR-15b switch from inhibitor to activators at G2/M. *Cell Cycle*, 15(5):667–677.

Krey, J. F., Wilmarth, P. A., Shin, J.-B., Klimek, J., Sherman, N. E., Jeffery, E. D., Choi, D., David, L. L., and Barr-Gillespie, P. G. (2014). Accurate Label-Free Protein Quantitation with High- and Low-Resolution Mass Spectrometers. *Journal of Proteome Research*, 13(2):1034–1044.

Kriwacki, R., Mitrea, D., Ferrolino, M., Gibbs, E., Phillips, A. H., Tolbert, M., Stanley, C. B., Nourse, A., Onuchic, P. L., Banerjee, P. R., and Deniz, A. A. (2019). The Ins and Outs of Phase Separation in Nucleolar Biology. *Biophysical Journal*, 116(3):454a.

Kuge, H. (1998). Cap ribose methylation of c-mos mRNA stimulates translation and oocyte maturation in Xenopus laevis. *Nucleic Acids Research*, 26(13):3208–3214.

Kundu, P., Fabian, M. R., Sonenberg, N., Bhattacharyya, S. N., and Filipowicz, W. (2012). HuR protein attenuates miRNA-mediated repression by promoting miRISC dissociation from the target RNA. *Nucleic Acids Research*, 40(11):5088–5100.

Kute, P. M., Ramakrishna, S., Neelagandan, N., Chattarji, S., and Muddashetty, R. S. (2019). NMDAR mediated translation at the synapse is regulated by MOV10 and FMRP. *Molecular Brain*, 12(1):65.

LaMarca, M. J., Smith, L., and Strobel, M. C. (1973). Quantitative and qualitative analysis of RNA synthesis in stage 6 and stage 4 oocytes of Xenopus laevis. *Developmental Biology*, 34(1):106–118.

Langdon, E. M. and Gladfelter, A. S. (2018). A New Lens for RNA Localization: Liquid-Liquid Phase Separation. *Annual Review of Microbiology*, 72(1):255–271.

Lantz, V., Ambrosio, L., and Schedl, P. (1992). The Drosophila orb gene is predicted to encode sex-specific germline RNA-binding proteins and has localized transcripts in ovaries and early embryos. *Development*, 115(1):75–88.

Lantz, V., Chang, J. S., Horabin, J. I., Bopp, D., and Schedl, P. (1994). The Drosophila orb RNA-binding protein is required for the formation of the egg chamber and establishment of polarity. *Genes & Development*, 8(5):598–613.

Lécuyer, E., Yoshida, H., Parthasarathy, N., Alm, C., Babak, T., Cerovina, T., Hughes, T. R., Tomancak, P., and Krause, H. M. (2007). Global Analysis of mRNA Localization Reveals a Prominent Role in Organizing Cellular Architecture and Function. *Cell*, 131(1):174–187.

Leppek, K., Das, R., and Barna, M. (2018). Functional 5' UTR mRNA structures in eukaryotic translation regulation and how to find them. *Nature Reviews Molecular Cell Biology*, 19(3):158–174.

Li, L., Sanchez, C. P., Slaughter, B. D., Zhao, Y., Khan, M. R., Unruh, J. R., Rubinstein, B., and Si, K. (2016). A Putative Biochemical Engram of Long-Term Memory. *Current Biology*, 26(23):3143–3156.

Li, Y. R., King, O. D., Shorter, J., and Gitler, A. D. (2013). Stress granules as crucibles of ALS pathogenesis. *The Journal of Cell Biology*, 201(3):361–372.

Lim, C. and Allada, R. (2013). ATAXIN-2 Activates PERIOD Translation to Sustain Circadian Rhythms in Drosophila. *Science*, 340(6134):875–879.

Lima, S. A., Chipman, L. B., Nicholson, A. L., Chen, Y.-H., Yee, B. A., Yeo, G. W., Coller, J., and Pasquinelli, A. E. (2017). Short poly(A) tails are a conserved feature of highly expressed genes. *Nature Structural & Molecular Biology*, 24(12):1057–1063.

Lin, C.-L., Evans, V., Shen, S., Xing, Y., and Richter, J. D. (2010). The nuclear experience of CPEB: Implications for RNA processing and translational control. *RNA*, 16(2):338–348.

Lin, M. T. and Beal, M. F. (2006). Mitochondrial dysfunction and oxidative stress in neurodegenerative diseases. *Nature*, 443(7113):787–795.

Liu, C., Zhang, X., Huang, F., Yang, B., Li, J., Liu, B., Luo, H., Zhang, P., and Zhang, H. (2012). APOBEC3G Inhibits MicroRNA-mediated Repression of Translation by Interfering with the Interaction between Argonaute-2 and MOV10. *Journal of Biological Chemistry*, 287(35):29373–29383.

Liu, N., Dai, Q., Zheng, G., He, C., Parisien, M., and Pan, T. (2015). N6-methyladenosine-dependent RNA structural switches regulate RNA–protein interactions. *Nature*, 518(7540):560–564.

Luo, Y., Na, Z., and Slavoff, S. A. (2018). P-Bodies: Composition, Properties, and Functions. *Biochemistry*, 57(17):2424–2431.

Luong, X. G., Daldello, E. M., Rajkovic, G., Yang, C.-R., and Conti, M. (2020). Genome-wide analysis reveals a switch in the translational program upon oocyte meiotic resumption. *Nucleic Acids Research*, 48(6):3257–3276.

Ma, W. and Mayr, C. (2018). A Membraneless Organelle Associated with the Endoplasmic Reticulum Enables 3'UTR-Mediated Protein-Protein Interactions. *Cell*, 175(6):1492–1506.e19.

Machnicka, M. A., Milanowska, K., Osman Oglou, O., Purta, E., Kurkowska, M., Olchowik, A., Januszewski, W., Kalinowski, S., Dunin-Horkawicz, S., Rother, K. M., Helm, M., Bujnicki, J. M., and Grosjean, H. (2012). MODOMICS: a database of RNA modification pathways—2013 update. *Nucleic Acids Research*, 41(D1):D262–D267.

Maillo, C., Martín, J., Sebastián, D., Hernández-Alvarez, M., García-Rocha, M., Reina, O., Zorzano, A., Fernandez, M., and Méndez, R. (2017). Circadian- and UPR-dependent control of CPEB4 mediates a

translational response to counteract hepatic steatosis under ER stress. *Nature Cell Biology*, 19(2):94–105.

Majumdar, A., Cesario, W. C., White-Grindley, E., Jiang, H., Ren, F., Khan, M. R., Li, L., Choi, E. M.-L., Kannan, K., Guo, F., Unruh, J., Slaughter, B., and Si, K. (2012). Critical Role of Amyloid-like Oligomers of Drosophila Orb2 in the Persistence of Memory. *Cell*, 148(3):515–529.

Malhis, N., Jacobson, M., and Gsponer, J. (2016). MoRFchibi SYSTEM: software tools for the identification of MoRFs in protein sequences. *Nucleic Acids Research*, 44(W1):W488–W493.

Martin, E. W. and Mittag, T. (2018). Relationship of Sequence and Phase Separation in Protein Low-Complexity Regions. *Biochemistry*, 57(17):2478–2487.

Martin, K. C. and Ephrussi, A. (2009). mRNA Localization: Gene Expression in the Spatial Dimension. *Cell*, 136(4):719–730.

Marzluff, W. F., Wagner, E. J., and Duronio, R. J. (2008). Metabolism and regulation of canonical histone mRNAs: life without a poly(A) tail. *Nature Reviews Genetics*, 9(11):843–854.

Mayr, C. (2016). Evolution and Biological Roles of Alternative 3'UTRs. *Trends in Cell Biology*, 26(3):227–237.

Mayr, C. (2017). Regulation by 3'-Untranslated Regions. *Annual Review of Genetics*, 51(1):171–194.

McCann, C., Holohan, E. E., Das, S., Dervan, A., Larkin, A., Lee, J. A., Rodrigues, V., Parker, R., and Ramaswami, M. (2011). The Ataxin-2 protein is required for microRNA function and synapse-specific long-term olfactory habituation. *Proceedings of the National Academy of Sciences*, 108(36):E655–E662.

McGrew, L. L. and Richter, J. D. (1990). Translational control by cytoplasmic polyadenylation during Xenopus oocyte maturation: characterization of cis and trans elements and regulation by cyclin/MPF. *The EMBO Journal*, 9(11):3743–3751.

McSwiggen, D. T., Mir, M., Darzacq, X., and Tjian, R. (2019). Evaluating phase separation in live cells: diagnosis, caveats, and functional consequences. *Genes & Development*, 33(23-24):1619–1634.

Mendez, R. (2002). Differential mRNA translation and meiotic progression require Cdc2-mediated CPEB destruction. *The EMBO Journal*, 21(7):1833–1844.

Mendez, R., Hake, L. E., Andresson, T., Littlepage, L. E., Ruderman, J. V., and Richter, J. D. (2000a). Phosphorylation of CPE binding factor by Eg2 regulates translation of c-mos mRNA. *Nature*, 404(6775):302–307.

Mendez, R., Murthy, K. G., Ryan, K., Manley, J. L., and Richter, J. D. (2000b). Phosphorylation of CPEB by Eg2 Mediates the Recruitment of CPSF into an Active Cytoplasmic Polyadenylation Complex. *Molecular Cell*, 6(5):1253–1259.

Mendez, R. and Richter, J. D. (2001). Translational control by CPEB: a means to the end. *Nature Reviews Molecular Cell Biology*, 2(7):521–529.

Merkel, D. J., Wells, S. B., Hilburn, B. C., Elazzouzi, F., Pérez-Alvarado, G. C., and Lee, B. M. (2013). The C-Terminal Region of Cytoplasmic Polyadenylation Element Binding Protein Is a ZZ Domain with Potential for Protein–Protein Interactions. *Journal of Molecular Biology*, 425(11):2015–2026.

Mignone, F., Gissi, C., Liuni, S., and Pesole, G. (2002). Untranslated regions of mRNAs. *Genome biology*, 3(3):REVIEWS0004.

Millevoi, S. and Vagner, S. (2010). Molecular mechanisms of eukaryotic pre-mRNA 3' end processing regulation. *Nucleic Acids Research*, 38(9):2757–2774.

Minshall, N., Reiter, M. H., Weil, D., and Standart, N. (2007). CPEB Interacts with an Ovary-specific eIF4E and 4E-T in Early Xenopus Oocytes. *Journal of Biological Chemistry*, 282(52):37389–37401.

Mittag, T. and Parker, R. (2018). Multiple Modes of Protein–Protein Interactions Promote RNP Granule Assembly. *Journal of Molecular Biology*, 430(23):4636–4649.

Mohan, A., Oldfield, C. J., Radivojac, P., Vacic, V., Cortese, M. S., Dunker, A. K., and Uversky, V. N. (2006). Analysis of Molecular Recognition Features (MoRFs). *Journal of Molecular Biology*, 362(5):1043–1059.

Molliex, A., Temirov, J., Lee, J., Coughlin, M., Kanagaraj, A. P., Kim, H. J., Mittag, T., and Taylor, J. P. (2015). Phase Separation by Low Complexity Domains Promotes Stress Granule Assembly and Drives Pathological Fibrillization. *Cell*, 163(1):123–133.

Montellese, C., Montel-Lehry, N., Henras, A. K., Kutay, U., Gleizes, P.-E., and O'Donohue, M.-F. (2017). Poly(A)-specific ribonuclease is a nuclear ribosome biogenesis factor involved in human 18S rRNA maturation. *Nucleic Acids Research*, 45(11):6822–6836.

Montoya, J., Ojala, D., and Attardi, G. (1981). Distinctive features of the 5'-terminal sequences of the human mitochondrial mRNAs. *Nature*, 290(5806):465–470.

Mooney, C., Pollastri, G., Shields, D. C., and Haslam, N. J. (2012). Prediction of Short Linear Protein Binding Regions. *Journal of Molecular Biology*, 415(1):193–204.

Moteki, S. and Price, D. (2002). Functional Coupling of Capping and Transcription of mRNA. *Molecular Cell*, 10(3):599–609.

Muckenthaler, M., Gray, N. K., and Hentze, M. W. (1998). IRP-1 Binding to Ferritin mRNA Prevents the Recruitment of the Small Ribosomal Subunit by the Cap-Binding Complex eIF4F. *Molecular Cell*, 2(3):383–388.

Murakami, T., Qamar, S., Lin, J. Q., Schierle, G. S. K., Rees, E., Miyashita, A., Costa, A. R., Dodd, R. B., Chan, F. T., Michel, C. H., Kronenberg-Versteeg, D., Li, Y., Yang, S.-P., Wakutani, Y., Meadows, W., Ferry, R. R., Dong, L., Tartaglia, G. G., Favrin, G., Lin, W.-L., Dickson, D. W., Zhen, M., Ron, D., Schmitt-Ulms, G., Fraser, P. E., Shneider, N. A., Holt, C., Vendruscolo, M., Kaminski, C. F., and St George-Hyslop, P. (2015). ALS/FTD Mutation-Induced Phase Transition of FUS Liquid Droplets and Reversible Hydrogels into Irreversible Hydrogels Impairs RNP Granule Function. *Neuron*, 88(4):678–690.

Nakamura, Y., Tanaka, K. J., Miyauchi, M., Huang, L., Tsujimoto, M., and Matsumoto, K. (2010). Translational repression by the oocyte-specific protein P100 in Xenopus. *Developmental Biology*, 344(1):272–283.

Nawalpuri, B., Ravindran, S., and Muddashetty, R. S. (2020). The Role of Dynamic miRISC During Neuronal Development. *Frontiers in Molecular Biosciences*, 7.

Neil, C., Jeschonek, S., Cabral, S., O'Connell, L. C., Powrie, E., Wood, T., and Mowry, K. (2020). L-Bodies are Novel RNA-Protein Condensates Driving RNA Transport in Xenopus Oocytes. *SSRN Electronic Journal*.

Nelson, M. R., Leidal, A. M., and Smibert, C. A. (2004). Drosophila Cup is an eIF4E-binding protein that functions in Smaug-mediated translational repression. *The EMBO Journal*, 23(1):150–159.

Nishimura, T., Padamsi, Z., Fakim, H., Milette, S., Dunham, W. H., Gingras, A.-C., and Fabian, M. R. (2015). The eIF4E-Binding Protein 4E-T Is a Component of the mRNA Decay Machinery that Bridges the 5' and 3' Termini of Target mRNAs. *Cell Reports*, 11(9):1425–1436.

Novoa, I., Gallego, J., Ferreira, P. G., and Mendez, R. (2010). Mitotic cell-cycle progression is regulated by CPEB1 and CPEB4-dependent translational control. *Nature Cell Biology*, 12(5):447–456.

O'Brien, L. L., Albee, A. J., Liu, L., Tao, W., Dobrzyn, P., Lizarraga, S. B., and Wiese, C. (2005). The Xenopus TACC Homologue, Maskin, Functions in Mitotic Spindle Assembly. *Molecular Biology of the Cell*, 16(6):2836–2847.

Ogami, K., Hosoda, N., Funakoshi, Y., and Hoshino, S. (2014). Antiproliferative protein Tob directly regulates c-myc proto-oncogene expression through cytoplasmic polyadenylation element-binding protein CPEB. *Oncogene*, 33(1):55–64.

Oldfield, C. J. and Dunker, A. K. (2014). Intrinsically Disordered Proteins and Intrinsically Disordered Protein Regions. *Annual Review of Biochemistry*, 83(1):553–584.

Opitz, N., Schmitt, K., Hofer-Pretz, V., Neumann, B., Krebber, H., Braus, G. H., and Valerius, O. (2017). Capturing the Asc1p/ R eceptor for A ctivated C K inase 1 (RACK1) Microenvironment at the Head Region of the 40S Ribosome with Quantitative BioID in Yeast. *Molecular & Cellular Proteomics*, 16(12):2199–2218.

Ortiz-Zapater, E., Pineda, D., Martínez-Bosch, N., Fernández-Miranda, G., Iglesias, M., Alameda, F., Moreno, M., Eliscovich, C., Eyras, E., Real, F. X., Méndez, R., and Navarro, P. (2012). Key contribution of CPEB4-mediated translational control to cancer progression. *Nature Medicine*, 18(1):83–90.

Ostareck, D. H., Ostareck-Lederer, A., Shatsky, I. N., and Hentze, M. W. (2001). Lipoxygenase mRNA Silencing in Erythroid Differentiation. *Cell*, 104(2):281–290.

Ostrowski, L., Hall, A., and Mekhail, K. (2017). Ataxin-2: From RNA Control to Human Health and Disease. *Genes*, 8(6):157.

Padmanabhan, K. (2006). Regulated Pumilio-2 binding controls RINGO/Spy mRNA translation and CPEB activation. *Genes & Development*, 20(2):199–209.

Pak, C. W., Kosno, M., Holehouse, A. S., Padrick, S. B., Mittal, A., Ali, R., Yunus, A. A., Liu, D. R., Pappu, R. V., and Rosen, M. K. (2016). Sequence Determinants of Intracellular Phase Separation by Complex Coacervation of a Disordered Protein. *Molecular Cell*, 63(1):72–85.

Papasaikas, P., Tejedor, J. R., Vigevani, L., and Valcárcel, J. (2015). Functional Splicing Network Reveals Extensive Regulatory Potential of the Core Spliceosomal Machinery. *Molecular Cell*, 57(1):7–22.

Paris, J. and Richter, J. D. (1990). Maturation-specific polyadenylation and translational control: diversity of cytoplasmic polyadenylation elements, influence of poly(A) tail size, and formation of stable polyadenylation complexes. *Molecular and Cellular Biology*, 10(11):5634–5645.

Paris, J., Swenson, K., Piwnica-Worms, H., and Richter, J. D. (1991). Maturation-specific polyadenylation: in vitro activation by p34cdc2 and phosphorylation of a 58-kD CPE-binding protein. *Genes & Development*, 5(9):1697–1708.

Park, J.-E., Yi, H., Kim, Y., Chang, H., and Kim, V. N. (2016). Regulation of Poly(A) Tail and Translation during the Somatic Cell Cycle. *Molecular Cell*, 62(3):462–471.

Parker, R. and Sheth, U. (2007). P Bodies and the Control of mRNA Translation and Degradation. *Molecular Cell*, 25(5):635–646.

Parker, R. and Song, H. (2004). The enzymes and control of eukaryotic mRNA turnover. *Nature Structural & Molecular Biology*, 11(2):121–127.

Parras, A., Anta, H., Santos-Galindo, M., Swarup, V., Elorza, A., Nieto-González, J. L., Picó, S., Hernández, I. H., Díaz-Hernández, J. I., Belloc, E., Rodolosse, A., Parikshak, N. N., Peñagarikano, O., Fernández-Chacón, R., Irimia, M., Navarro, P., Geschwind, D. H., Méndez, R., and Lucas, J. J. (2018). Autism-like phenotype and risk gene mRNA deadenylation by CPEB4 mis-splicing. *Nature*, 560(7719):441–446.

Patel, A., Lee, H. O., Jawerth, L., Maharana, S., Jahnel, M., Hein, M. Y., Stoynov, S., Mahamid, J., Saha, S., Franzmann, T. M., Pozniakovski, A., Poser, I., Maghelli, N., Royer, L. A., Weigert, M., Myers, E. W., Grill, S., Drechsel, D., Hyman, A. A., and Alberti, S. (2015). A Liquid-to-Solid Phase Transition of the ALS Protein FUS Accelerated by Disease Mutation. *Cell*, 162(5):1066–1077.

Pause, A., Belsham, G. J., Gingras, A.-C., Donzé, O., Lin, T.-A., Lawrence, J. C., and Sonenberg, N. (1994). Insulin-dependent stimulation of protein synthesis by phosphorylation of a regulator of 5'-cap function. *Nature*, 371(6500):762–767.

Pavlopoulos, E., Trifilieff, P., Chevaleyre, V., Fioriti, L., Zairis, S., Pagano, A., Malleret, G., and Kandel, E. R. (2011). Neuralized1 Activates CPEB3: A Function for Nonproteolytic Ubiquitin in Synaptic Plasticity and Memory Storage. *Cell*, 147(6):1369–1383.

Pechmann, S. and Frydman, J. (2013). Evolutionary conservation of codon optimality reveals hidden signatures of cotranslational folding. *Nature Structural & Molecular Biology*, 20(2):237–243.

Peset, I., Seiler, J., Sardon, T., Bejarano, L. A., Rybina, S., and Vernos, I. (2005). Function and regulation of Maskin, a TACC family protein, in microtubule growth during mitosis. *Journal of Cell Biology*, 170(7):1057–1066.

Peuchen, E. H., Cox, O. F., Sun, L., Hebert, A. S., Coon, J. J., Champion, M. M., Dovichi, N. J., and Huber, P. W. (2017). Phosphorylation Dynamics Dominate the Regulated Proteome during Early Xenopus Development. *Scientific Reports*, 7(1):15647.

Phung, B., Cieśla, M., Sanna, A., Guzzi, N., Beneventi, G., Cao Thi Ngoc, P., Lauss, M., Cabrita, R., Cordero, E., Bosch, A., Rosengren, F., Häkkinen, J., Griewank, K., Paschen, A., Harbst, K., Olsson, H., Ingvar, C., Carneiro, A., Tsao, H., Schadendorf, D., Pietras, K., Bellodi, C., and Jönsson, G. (2019). The X-Linked DDX3X RNA Helicase Dictates Translation Reprogramming and Metastasis in Melanoma. *Cell Reports*, 27(12):3573–3586.e7.

Piqué, M., López, J. M., Foissac, S., Guigó, R., and Méndez, R. (2008). A Combinatorial Code for CPE-Mediated Translational Control. *Cell*, 132(3):434–448.

Pirone, L., Xolalpa, W., Sigurðsson, J. O., Ramirez, J., Pérez, C., González, M., de Sabando, A. R., Elortza, F., Rodriguez, M. S., Mayor, U., Olsen, J. V., Barrio, R., and Sutherland, J. D. (2017). A comprehensive platform for the analysis of ubiquitin-like protein modifications using in vivo biotinylation. *Scientific Reports*, 7(1):40756.

Pisarev, A. V., Skabkin, M. A., Pisareva, V. P., Skabkina, O. V., Rakotondrafara, A. M., Hentze, M. W., Hellen, C. U., and Pestova, T. V. (2010). The Role of ABCE1 in Eukaryotic Posttermination Ribosomal Recycling. *Molecular Cell*, 37(2):196–210.

Popp, M. W.-L. and Maquat, L. E. (2013). Organizing Principles of Mammalian Nonsense-Mediated mRNA Decay. *Annual Review of Genetics*, 47(1):139–165.

Prigogine, L., Nicolis, G., and Babloyantz, A. (1972). Thermodynamics of evolution. *Physics Today*, 25(12):38–44.

Proudfoot, N. J. (2011). Ending the message: poly(A) signals then and now. *Genes & Development*, 25(17):1770–1782.

Qi, S.-T., Ma, J.-Y., Wang, Z.-B., Guo, L., Hou, Y., and Sun, Q.-Y. (2016). N 6 -Methyladenosine Sequencing Highlights the Involvement of mRNA Methylation in Oocyte Meiotic Maturation and Embryo Development by Regulating Translation in Xenopus laevis. *Journal of Biological Chemistry*, 291(44):23020–23026.

Radford, H. E., Meijer, H. A., and de Moor, C. H. (2008). Translational control by cytoplasmic polyadenylation in Xenopus oocytes. *Biochimica et Biophysica Acta (BBA) - Gene Regulatory Mechanisms*, 1779(4):217–229.

Rai, A. K., Chen, J.-X., Selbach, M., and Pelkmans, L. (2018). Kinase-controlled phase transition of membraneless organelles in mitosis. *Nature*, 559(7713):211–216.

Ramanathan, A., Robb, G. B., and Chan, S.-H. (2016). mRNA capping: biological functions and applications. *Nucleic Acids Research*, 44(16):7511–7526.

Ramaswami, M., Taylor, J. P., and Parker, R. (2013). Altered Ribostasis: RNA-Protein Granules in Degenerative Disorders. *Cell*, 154(4):727–736.

Raveendra, B. L., Siemer, A. B., Puthanveettil, S. V., Hendrickson, W. A., Kandel, E. R., and McDermott, A. E. (2013). Characterization of prion-like conformational changes of the neuronal isoform of Aplysia CPEB. *Nature Structural & Molecular Biology*, 20(4):495–501.

Renton, A. E., Chiò, A., and Traynor, B. J. (2014). State of play in amyotrophic lateral sclerosis genetics. *Nature Neuroscience*, 17(1):17–23.

Reverte, C. G., Ahearn, M. D., and Hake, L. E. (2001). CPEB Degradation during Xenopus Oocyte Maturation Requires a PEST Domain and the 26S Proteasome. *Developmental Biology*, 231(2):447–458.

Rhee, H.-W., Zou, P., Udeshi, N. D., Martell, J. D., Mootha, V. K., Carr, S. A., and Ting, A. Y. (2013). Proteomic Mapping of Mitochondria in Living Cells via Spatially Restricted Enzymatic Tagging. *Science*, 339(6125):1328–1331.

Riba, A., Di Nanni, N., Mittal, N., Arhné, E., Schmidt, A., and Zavolan, M. (2019). Protein synthesis rates and ribosome occupancies reveal determinants of translation elongation rates. *Proceedings of the National Academy of Sciences*, 116(30):15023–15032.

Richter, J. D. and Coller, J. (2015). Pausing on Polyribosomes: Make Way for Elongation in Translational Control. *Cell*, 163(2):292–300.

Ries, R. J., Zaccara, S., Klein, P., Olarerin-George, A., Namkoong, S., Pickering, B. F., Patil, D. P., Kwak, H., Lee, J. H., and Jaffrey, S. R. (2019). m6A enhances the phase separation potential of mRNA. *Nature*, 571(7765):424–428.

Rodman, T. C. and Bachvarova, R. (1976). RNA synthesis in preovulatory mouse oocytes. *The Journal of Cell Biology*, 70(1):251–257.

Rouhana, L. (2005). Vertebrate GLD2 poly(A) polymerases in the germline and the brain. *RNA*, 11(7):1117–1130.

Roundtree, I. A., Evans, M. E., Pan, T., and He, C. (2017). Dynamic RNA Modifications in Gene Expression Regulation. *Cell*, 169(7):1187–1200.

Roux, K. J., Kim, D. I., and Burke, B. (2013). BioID: A Screen for Protein-Protein Interactions. *Current Protocols in Protein Science*, 74(1).

Roux, K. J., Kim, D. I., Raida, M., and Burke, B. (2012). A promiscuous biotin ligase fusion protein identifies proximal and interacting proteins in mammalian cells. *Journal of Cell Biology*, 196(6):801–810.

Roux, P. P. and Topisirovic, I. (2012). Regulation of mRNA Translation by Signaling Pathways. *Cold Spring Harbor Perspectives in Biology*, 4(11):a012252–a012252.

Rowlands, A. G., Panniers, R., and Henshaw, E. C. (1988). The catalytic mechanism of guanine nucleotide exchange factor action and competitive inhibition by phosphorylated eukaryotic initiation factor 2. *The Journal of biological chemistry*, 263(12):5526–33.

Sachdev, R., Hondele, M., Linsenmeier, M., Vallotton, P., Mugler, C. F., Arosio, P., and Weis, K. (2019). Pat1 promotes processing body assembly by enhancing the phase separation of the DEAD-box ATPase Dhh1 and RNA. *eLife*.

Said, H. M., Polenzani, L., Khorchid, S., Hollander, D., and Miledi, R. (1990). Uptake of biotin by native Xenopus laevis oocytes. *American Journal of Physiology-Cell Physiology*, 259(3):C397–C401.

Saitoh, A., Takada, Y., Horie, M., and Kotani, T. (2018). Pumilio1 phosphorylation precedes translational activation of its target mRNA in zebrafish oocytes. *Zygote*, 26(5):372–380.

Sanulli, S., Trnka, M. J., Dharmarajan, V., Tibble, R. W., Pascal, B. D., Burlingame, A. L., Griffin, P. R., Gross, J. D., and Narlikar, G. J. (2019). HP1 reshapes nucleosome core to promote phase separation of heterochromatin. *Nature*, 575(7782):390–394.

Schelhorn, C., Martín-Malpartida, P., Suñol, D., and Macias, M. J. (2015). Structural Analysis of the Pin1-CPEB1 interaction and its potential role in CPEB1 degradation. *Scientific Reports*, 5(1):14990.

Schiapparelli, L. M., McClatchy, D. B., Liu, H.-H., Sharma, P., Yates, J. R., and Cline, H. T. (2014). Direct Detection of Biotinylated Proteins by Mass Spectrometry. *Journal of Proteome Research*, 13(9):3966–3978.

Schmidt, H. B. and Görlich, D. (2016). Transport Selectivity of Nuclear Pores, Phase Separation, and Membraneless Organelles. *Trends in Biochemical Sciences*, 41(1):46–61.

Schmitt, A. and Nebreda, A. R. (2002). Signalling pathways in oocyte meiotic maturation. *Journal of cell science*, 115(Pt 12):2457–9.

Schuller, A. P. and Green, R. (2018). Roadblocks and resolutions in eukaryotic translation. *Nature Reviews Molecular Cell Biology*, 19(8):526–541.

Setoyama, D., Yamashita, M., and Sagata, N. (2007). Mechanism of degradation of CPEB during Xenopus oocyte maturation. *Proceedings of the National Academy of Sciences*, 104(46):18001–18006.

Shao, S., Murray, J., Brown, A., Taunton, J., Ramakrishnan, V., and Hegde, R. S. (2016). Decoding Mammalian Ribosome-mRNA States by Translational GTPase Complexes. *Cell*, 167(5):1229–1240.e15.

Shatkin, A. J. and Manley, J. L. (2000). The ends of the affair: Capping and polyadenylation. *Nature Structural Biology*, 7:838–842.

Shatsky, I. N., Terenin, I. M., Smirnova, V. V., and Andreev, D. E. (2018). Cap-Independent Translation: What's in a Name? *Trends in Biochemical Sciences*, 43(11):882–895.

Sheu-Gruttadauria, J. and MacRae, I. J. (2018). Phase Transitions in the Assembly and Function of Human miRISC. *Cell*, 173(4):946–957.e16.

Shi, H., Wei, J., and He, C. (2019). Where, When, and How: Context-Dependent Functions of RNA Methylation Writers, Readers, and Erasers. *Molecular Cell*, 74(4):640–650.

Shi, H., Zhang, X., Weng, Y.-L., Lu, Z., Liu, Y., Lu, Z., Li, J., Hao, P., Zhang, Y., Zhang, F., Wu, Y., Delgado, J. Y., Su, Y., Patel, M. J., Cao, X., Shen, B., Huang, X., Ming, G.-l., Zhuang, X., Song, H., He, C., and Zhou, T. (2018). m6A facilitates hippocampus-dependent learning and memory through YTHDF1. *Nature*, 563(7730):249–253.

Shi, Z., Fujii, K., Kovary, K. M., Genuth, N. R., Röst, H. L., Teruel, M. N., and Barna, M. (2017). Heterogeneous Ribosomes Preferentially Translate Distinct Subpools of mRNAs Genome-wide. *Molecular Cell*, 67(1):71–83.e7.

Shiina, N. (2019). Liquid- and solid-like RNA granules form through specific scaffold proteins and combine into biphasic granules. *Journal of Biological Chemistry*, 294(10):3532–3548.

Shimotohno, K., Kodama, Y., Hashimoto, J., and Miura, K. I. (1977). Importance of 5'-terminal blocking structure to stabilize mRNA in eukaryotic protein synthesis. *Proceedings of the National Academy of Sciences*, 74(7):2734–2738.

Shin, J., Paek, K. Y., Ivshina, M., Stackpole, E. E., and Richter, J. D. (2017a). Essential role for non-canonical poly(A) polymerase GLD4 in cytoplasmic polyadenylation and carbohydrate metabolism. *Nucleic Acids Research*, 45(11):6793–6804.

Shin, Y., Berry, J., Pannucci, N., Haataja, M. P., Toettcher, J. E., and Brangwynne, C. P. (2017b). Spatiotemporal Control of Intracellular Phase Transitions Using Light-Activated optoDroplets. *Cell*, 168(1-2):159–171.e14.

Shin, Y. and Brangwynne, C. P. (2017). Liquid phase condensation in cell physiology and disease. *Science*, 357(6357):eaaf4382.

Shoemaker, C. J. and Green, R. (2011). Kinetic analysis reveals the ordered coupling of translation termination and ribosome recycling in yeast. *Proceedings of the National Academy of Sciences*, 108(51):E1392–E1398.

Si, K., Choi, Y. B., White-Grindley, E., Majumdar, A., and Kandel, E. R. (2010). Aplysia CPEB Can Form Prion-like Multimers in Sensory Neurons that Contribute to Long-Term Facilitation. *Cell*, 140(3):421–435.

Si, K. and Kandel, E. R. (2016). The Role of Functional Prion-Like Proteins in the Persistence of Memory. *Cold Spring Harbor Perspectives in Biology*, 8(4):a021774.

Si, K., Lindquist, S., and Kandel, E. R. (2003). A Neuronal Isoform of the Aplysia CPEB Has Prion-Like Properties. *Cell*, 115(7):879–891.

Simsek, D., Tiu, G. C., Flynn, R. A., Byeon, G. W., Leppek, K., Xu, A. F., Chang, H. Y., and Barna, M. (2017). The Mammalian Ribo-interactome Reveals Ribosome Functional Diversity and Heterogeneity. *Cell*, 169(6):1051–1065.e18.

Smith, R. (2004). Moving Molecules: mRNA Trafficking in Mammalian Oligodendrocytes and Neurons. *The Neuroscientist*, 10(6):495–500.

Son, A., Park, J.-E., and Kim, V. N. (2018). PARN and TOE1 Constitute a 3' End Maturation Module for Nuclear Non-coding RNAs. *Cell Reports*, 23(3):888–898.

Sonenberg, N. and Hinnebusch, A. G. (2009). Regulation of Translation Initiation in Eukaryotes: Mechanisms and Biological Targets. *Cell*, 136(4):731–745.

Song, H., Mugnier, P., Das, A. K., Webb, H. M., Evans, D. R., Tuite, M. F., Hemmings, B. A., and Barford, D. (2000). The Crystal Structure of Human Eukaryotic Release Factor eRF1—Mechanism of Stop Codon Recognition and Peptidyl-tRNA Hydrolysis. *Cell*, 100(3):311–321.

Soop, T. (2003). A p50-like Y-box protein with a putative translational role becomes associated with pre-mRNA concomitant with transcription. *Journal of Cell Science*, 116(8):1493–1503.

Sousa Martins, J. P., Liu, X., Oke, A., Arora, R., Franciosi, F., Viville, S., Laird, D. J., Fung, J. C., and Conti, M. (2016). DAZL and CPEB1 regulate mRNA translation synergistically during oocyte maturation. *Journal of Cell Science*, 129(6):1271–1282.

Standart, N. and Weil, D. (2018). P-Bodies: Cytosolic Droplets for Coordinated mRNA Storage. *Trends in Genetics*, 34(8):612–626.

Stebbins-Boaz, B., Cao, Q., de Moor, C. H., Mendez, R., and Richter, J. D. (1999). Maskin Is a CPEB-Associated Factor that Transiently Interacts with eIF-4E. *Molecular Cell*, 4(6):1017–1027.

Stephan, J. S., Fioriti, L., Lamba, N., Colnaghi, L., Karl, K., Derkatch, I. L., and Kandel, E. R. (2015). The CPEB3 Protein Is a Functional Prion that Interacts with the Actin Cytoskeleton. *Cell Reports*, 11(11):1772–1785.

Stepien, B. K., Oppitz, C., Gerlach, D., Dag, U., Novatchkova, M., Krüttner, S., Stark, A., and Keleman, K. (2016). RNA-binding profiles of Drosophila CPEB proteins Orb and Orb2. *Proceedings of the National Academy of Sciences*, 113(45):E7030–E7038.

Strom, A. R., Emelyanov, A. V., Mir, M., Fyodorov, D. V., Darzacq, X., and Karpen, G. H. (2017). Phase separation drives heterochromatin domain formation. *Nature*, 547(7662):241–245.

Suh, N., Crittenden, S. L., Goldstrohm, A., Hook, B., Thompson, B., Wickens, M., and Kimble, J. (2009). FBF and Its Dual Control of gld-1 Expression in the Caenorhabditis elegans Germline. *Genetics*, 181(4):1249–1260.

Sun, Y., Zhang, Y., Hamilton, K., Manley, J. L., Shi, Y., Walz, T., and Tong, L. (2018). Molecular basis for the recognition of the human AAUAAA polyadenylation signal. *Proceedings of the National Academy of Sciences*, 115(7):E1419–E1428.

Suvasini, R., Shruti, B., Thota, B., Shinde, S. V., Friedmann-Morvinski, D., Nawaz, Z., Prasanna, K. V., Thennarasu, K., Hegde, A. S., Arivazhagan, A., Chandramouli, B. A., Santosh, V., and Somasundaram, K. (2011). Insulin Growth Factor-2 Binding Protein 3 (IGF2BP3) Is a Glioblastoma-specific Marker That Activates Phosphatidylinositol 3-Kinase/Mitogen-activated Protein Kinase (PI3K/MAPK) Pathways by Modulating IGF-2. *Journal of Biological Chemistry*, 286(29):25882–25890.

Szklarczyk, D., Morris, J. H., Cook, H., Kuhn, M., Wyder, S., Simonovic, M., Santos, A., Doncheva, N. T., Roth, A., Bork, P., Jensen, L. J., and von Mering, C. (2017). The STRING database in 2017: quality-controlled protein–protein association networks, made broadly accessible. *Nucleic Acids Research*, 45(D1):D362–D368.

Takahashi, K., Kotani, T., Katsu, Y., and Yamashita, M. (2014). Possible involvement of insulin-like growth factor 2 mRNA-binding protein 3 in zebrafish oocyte maturation as a novel cyclin B1 mRNA-binding protein that represses the translation in immature oocytes. *Biochemical and Biophysical Research Communications*, 448(1):22–27.

Tharun, S. (2009). Lsm1-7-Pat1 complex: A link between 3' and 5'-ends in mRNA decay? *RNA Biology*, 6(3):228–232.

Thompson, M. J., Sievers, S. A., Karanicolas, J., Ivanova, M. I., Baker, D., and Eisenberg, D. (2006). The 3D profile method for identifying fibril-forming segments of proteins. *Proceedings of the National Academy of Sciences*, 103(11):4074–4078.

Tomecki, R., Kristiansen, M. S., Lykke-Andersen, S., Chlebowski, A., Larsen, K. M., Szczesny, R. J., Drazkowska, K., Pastula, A., Andersen, J. S., Stepien, P. P., Dziembowski, A., and Jensen, T. H. (2010). The human core exosome interacts with differentially localized processive RNases: hDIS3 and hDIS3L. *The EMBO Journal*, 29(14):2342–2357.

Tomek, W. and Wollenhaupt, K. (2012). The "closed loop model" in controlling mRNA translation during development. *Animal Reproduction Science*, 134(1-2):2–8.

Tompa, P., Davey, N. E., Gibson, T. J., and Babu, M. M. (2014). A Million Peptide Motifs for the Molecular Biologist. *Molecular Cell*, 55(2):161–169.

Tong, L. (2013). Structure and function of biotin-dependent carboxylases. *Cellular and Molecular Life Sciences*, 70(5):863–891.

Tsang, B., Arsenault, J., Vernon, R. M., Lin, H., Sonenberg, N., Wang, L.-Y., Bah, A., and Forman-Kay, J. D. (2019). Phosphoregulated FMRP phase separation models activity-dependent translation through bidirectional control of mRNA granule formation. *Proceedings of the National Academy of Sciences*, 116(10):4218–4227.

Tsvetkov, P., Eisen, T. J., Heinrich, S. U., Brune, Z., Hallacli, E., Newby, G. A., Kayatekin, C., Pincus, D., and Lindquist, S. (2020). Persistent Activation of mRNA Translation by Transient Hsp90 Inhibition. *Cell Reports*, 32(6):108001.

Udagawa, T., Swanger, S. A., Takeuchi, K., Kim, J. H., Nalavadi, V., Shin, J., Lorenz, L. J., Zukin, R. S., Bassell, G. J., and Richter, J. D. (2012). Bidirectional Control of mRNA Translation and Synaptic Plasticity by the Cytoplasmic Polyadenylation Complex. *Molecular Cell*, 47(2):253–266.

Ulitsky, I., Shkumatava, A., Jan, C. H., Subtelny, A. O., Koppstein, D., Bell, G. W., Sive, H., and Bartel, D. P. (2012). Extensive alternative polyadenylation during zebrafish development. *Genome Research*, 22(10):2054–2066.

van Hoof, A. (2002). Exosome-Mediated Recognition and Degradation of mRNAs Lacking a Termination Codon. *Science*, 295(5563):2262–2264.

Varnaitė, R. and MacNeill, S. A. (2016). Meet the neighbors: Mapping local protein interactomes by proximity-dependent labeling with BioID. *PROTEOMICS*, 16(19):2503–2518.

Vernon, R. M., Chong, P. A., Tsang, B., Kim, T. H., Bah, A., Farber, P., Lin, H., and Forman-Kay, J. D. (2018). Pi-Pi contacts are an overlooked protein feature relevant to phase separation. *eLife*, 7.

Villalba, A., Coll, O., and Gebauer, F. (2011). Cytoplasmic polyadenylation and translational control. *Current Opinion in Genetics & Development*, 21(4):452–457.

Villanueva, E., Navarro, P., Rovira-Rigau, M., Sibilio, A., Méndez, R., and Fillat, C. (2017). Translational reprogramming in tumour cells can generate oncoselectivity in viral therapies. *Nature Communications*, 8(1):14833.

Waghray, S., Williams, C., Coon, J. J., and Wickens, M. (2015). Xenopus CAF1 requires NOT1-mediated interaction with 4E-T to repress translation in vivo. *RNA*, 21(7):1335–1345.

Wahl, M. C., Will, C. L., and Lührmann, R. (2009). The Spliceosome: Design Principles of a Dynamic RNP Machine. *Cell*, 136(4):701–718.

Walker, J., Minshall, N., Hake, L., Richter, J., and Standart, N. (1999). The clam 3' UTR masking element-binding protein p82 is a member of the CPEB family. *RNA*, 5(1):S1355838299981219.

Walter, P., Ibrahimi, I., and Blobel, G. (1981). Translocation of proteins across the endoplasmic reticulum. I. Signal recognition protein (SRP) binds to in-vitro-assembled polysomes synthesizing secretory protein. *The Journal of Cell Biology*, 91(2):545–550.

Wang, J., Choi, J.-M., Holehouse, A. S., Lee, H. O., Zhang, X., Jahnel, M., Maharana, S., Lemaitre, R., Pozniakovsky, A., Drechsel, D., Poser, I., Pappu, R. V., Alberti, S., and Hyman, A. A. (2018). A Molecular Grammar Governing the Driving Forces for Phase Separation of Prion-like RNA Binding Proteins. *Cell*, 174(3):688–699.e16.

Wang, X., Zhao, B. S., Roundtree, I. A., Lu, Z., Han, D., Ma, H., Weng, X., Chen, K., Shi, H., and He, C. (2015a). N6-methyladenosine Modulates Messenger RNA Translation Efficiency. *Cell*, 161(6):1388–1399.

Wang, X. P. and Cooper, N. G. (2010). Comparative in Silico analyses of Cpeb1-4 with functional predictions. *Bioinformatics and Biology Insights*, 4:61–83.

Wang, Y., Arribas-Layton, M., Chen, Y., Lykke-Andersen, J., and Sen, G. L. (2015b). DDX6 Orchestrates Mammalian Progenitor Function through the mRNA Degradation and Translation Pathways. *Molecular Cell*, 60(1):118–130.

Wang, Y. Y., Charlesworth, A., Byrd, S. M., Gregerson, R., MacNicol, M. C., and MacNicol, A. M. (2008). A novel mRNA 3' untranslated region translational control sequence regulates Xenopus Wee1 mRNA translation. *Developmental Biology*, 317(2):454–466.

Weber, P., Ohlendorf, D., Wendoloski, J., and Salemme, F. (1989). Structural origins of high-affinity biotin binding to streptavidin. *Science*, 243(4887):85–88.

Weber, S. C. (2017). Sequence-encoded material properties dictate the structure and function of nuclear bodies. *Current Opinion in Cell Biology*, 46:62–71.

Webster, M. W., Chen, Y.-H., Stowell, J. A., Alhusaini, N., Sweet, T., Graveley, B. R., Coller, J., and Passmore, L. A. (2018). mRNA Deadenylation Is Coupled to Translation Rates by the Differential Activities of Ccr4-Not Nucleases. *Molecular Cell*, 70(6):1089–1100.e8.

Wegmann, S., Eftekharzadeh, B., Tepper, K., Zoltowska, K. M., Bennett, R. E., Dujardin, S., Laskowski, P. R., MacKenzie, D., Kamath, T., Commins, C., Vanderburg, C., Roe, A. D., Fan, Z., Molliex, A. M., Hernandez-Vega, A., Muller, D., Hyman, A. A., Mandelkow, E., Taylor, J. P., and Hyman, B. T. (2018). Tau protein liquid–liquid phase separation can initiate tau aggregation. *The EMBO Journal*, 37(7).

Weill, L., Belloc, E., Bava, F.-A., and Méndez, R. (2012). Translational control by changes in poly(A) tail length: recycling mRNAs. *Nature Structural & Molecular Biology*, 19(6):577–585.

Wells, S. E., Hillner, P. E., Vale, R. D., and Sachs, A. B. (1998). Circularization of mRNA by Eukaryotic Translation Initiation Factors. *Molecular Cell*, 2(1):135–140.

Weston, A. (2006). Xp54 and related (DDX6-like) RNA helicases: roles in messenger RNP assembly, translation regulation and RNA degradation. *Nucleic Acids Research*, 34(10):3082–3094.

Wilczynska, A. (2005). The translational regulator CPEB1 provides a link between dcp1 bodies and stress granules. *Journal of Cell Science*, 118(5):981–992.

Wilczynska, A., Git, A., Argasinska, J., Belloc, E., and Standart, N. (2016). CPEB and miR-15/16 Co-Regulate Translation of Cyclin E1 mRNA during Xenopus Oocyte Maturation. *PLOS ONE*, 11(2):e0146792.

Wilt, F. H. (1973). Polyadenylation of Maternal RNA of Sea Urchin Eggs After Fertilization. *Proceedings of the National Academy of Sciences*, 70(8):2345–2349.

Wojciechowska, M. and Krzyzosiak, W. J. (2011). Cellular toxicity of expanded RNA repeats: focus on RNA foci. *Human Molecular Genetics*, 20(19):3811–3821.

Wühr, M., Güttler, T., Peshkin, L., McAlister, G. C., Sonnett, M., Ishihara, K., Groen, A. C., Presler, M., Erickson, B. K., Mitchison, T. J., Kirschner, M. W., and Gygi, S. P. (2015). The Nuclear Proteome of a Vertebrate. *Current Biology*, 25(20):2663–2671.

Xing, W., Muhlrad, D., Parker, R., and Rosen, M. K. (2020). A quantitative inventory of yeast P body proteins reveals principles of composition and specificity. *eLife*, 9.

Xue, B., Dunbrack, R. L., Williams, R. W., Dunker, A. K., and Uversky, V. N. (2010). PONDR-FIT: A meta-predictor of intrinsically disordered amino acids. *Biochimica et Biophysica Acta (BBA) - Proteins and Proteomics*, 1804(4):996–1010.

Yamashita, A., Chang, T.-C., Yamashita, Y., Zhu, W., Zhong, Z., Chen, C.-Y. A., and Shyu, A.-B. (2005). Concerted action of poly(A) nucleases and decapping enzyme in mammalian mRNA turnover. *Nature Structural & Molecular Biology*, 12(12):1054–1063.

Yan, Y.-B. (2014). Deadenylation: enzymes, regulation, and functional implications. *Wiley Interdisciplinary Reviews: RNA*, 5(3):421–443.

Yang, C.-R., Rajkovic, G., Daldello, E. M., Luong, X. G., Chen, J., and Conti, M. (2020a). The RNA-binding protein DAZL functions as repressor and activator of mRNA translation during oocyte maturation. *Nature Communications*, 11(1):1399.

Yang, F., Wang, W., Cetinbas, M., Sadreyev, R. I., and Blower, M. D. (2020b). Genome-wide analysis identifies cis -acting elements regulating mRNA polyadenylation and translation during vertebrate oocyte maturation. *RNA*, 26(3):324–344.

Yi, H., Park, J., Ha, M., Lim, J., Chang, H., and Kim, V. N. (2018). PABP Cooperates with the CCR4-NOT Complex to Promote mRNA Deadenylation and Block Precocious Decay. *Molecular Cell*, 70(6):1081–1088.e5.

Youn, J.-Y., Dunham, W. H., Hong, S. J., Knight, J. D., Bashkurov, M., Chen, G. I., Bagci, H., Rathod, B., MacLeod, G., Eng, S. W., Angers, S., Morris, Q., Fabian, M., Côté, J.-F., and Gingras, A.-C. (2018). High-Density Proximity Mapping Reveals the Subcellular Organization of mRNA-Associated Granules and Bodies. *Molecular Cell*, 69(3):517–532.e11.

Zander, G., Hackmann, A., Bender, L., Becker, D., Lingner, T., Salinas, G., and Krebber, H. (2016). mRNA quality control is bypassed for immediate export of stress-responsive transcripts. *Nature*, 540(7634):593–596.

Zhang, H., Wang, Y., and Lu, J. (2019). Function and Evolution of Upstream ORFs in Eukaryotes. *Trends in Biochemical Sciences*, 44(9):782–794.

Zhao, B. S., Roundtree, I. A., and He, C. (2017). Post-transcriptional gene regulation by mRNA modifications. *Nature Reviews Molecular Cell Biology*, 18(1):31–42.

Zhao, J. (2002). The mRNA export factor Dbp5 is associated with Balbiani ring mRNP from gene to cytoplasm. *The EMBO Journal*, 21(5):1177–1187.

Appendix

Appendix I: BioID tables

Accessions	Gene name	Grouped name	FC	Ctrl miss	Cond miss
Q4V7K4;A0A1L8HCH4	PATL2	PATL2	28.94	0	0
Q98SP8;A0A1L8EKZ2	EPABA	EPAB	21.16	2	0
A0A1L8HEX9	MOV10	MOV10	24.34	2	0
A0A1L8GFC1	CNOT1	CNOT1	17.19	2	0
A0A1L8GGX7;Q5EE04	TPR	TPR	10.63	0	0
A0A1L8ES55;Q6GR16;A0A1L8ES40	EPABB	EPAB	13.31	1	0
A0A1L8GT79;Q52KN7	CPEB1B	CPEB1	10.35	0	0
A0A1L8GUZ9;A0A1L8GY11	EIF4E	EIF4E	8.84	0	0
A0A1L8FLL9;P54824	DDX6	DDX6	12.46	0	0
A0A1L8HQ92;Q6DE09	EIF4ENIF	EIF4ENIF1	7.97	0	0
A0A1L8ESZ1;Q68FI1	LSM14BB-A	LSM14	NA	4	0
A0A1L8F0H9;Q9W799;A0A1L8F9H7	CPSF2	CPSF2	NA	3	0
A0A1L8F3F9;Q7ZYV9	SYMPK	SYMPK	NA	3	0
A0A1L8FVU1;A0A1L8FR11;Q5U5D4	MIOSB	MIOSB	NA	4	1
Q6NU42;A0A1L8G560	TPR	TPR	NA	4	0
A0A1L8G578	CPSF3	CPSF3	NA	4	1
A0A1L8GAN7;A0A1L8G4F1	WDR33	WDR33	NA	4	0
A0A1L8GL86;A0A1L8GL44;A0A8M2	LSM14A-A	LSM14	NA	3	0
A0A1L8GLF8	CNOT1	CNOT1	NA	4	0
B7ZQW3;A0A1L8GUY9;A0A1L8GUW5	SLBP2	SLBP2	NA	4	1
A0A1L8GZ04	MOV10	MOV10	NA	3	0
A0A1L8HBI7	ZAR1L	ZAR1	NA	4	0
A0A1L8HE42;Q505M1;A0A1L8H6C1	CSDE1	CSDE1	NA	4	0
A0A1L8HJK9	ZAR1L	ZAR1	NA	4	0
A0AUS9;Q63ZL7;A0A1L8HLC5	FIP1	FIP1	NA	4	0
A0A1L8HY91;A0A1L8HNY0;Q91903	ELAVL2	HUR	NA	4	0
A0A1L8HQR6	ATXN2L	ATXN2	NA	4	1
C0SPG1	ZAR2	ZAR2	NA	4	0
Q2VPF5;Q6DD72;Q7ZWR9;A0A1L8FT79	STAU2	STAU2	NA	4	0
Q68F10;Q7ZYT8;Q91581	CSTF64	CSTF64	NA	4	1
Q8AVJ2	LSM14A-B	LSM14	NA	4	0

Table A1: BirA-CPEB1 enriched proteins. BioID hits obtained with the *ad hoc* analysis pipeline. For each identified group of accession numbers (Uniprot), the gene name, grouped gene name, fold-change and missing values found in the control or conditions are depicted. We used the grouped gene names for Gene Ontology and network analyses.

Accessions	Gene name	Grouped name	FC	Ctrl miss	Cond miss
Q4V7K4;A0A1L8HCH4	PATL2	PATL2	37.88	0	0
Q98SP8;A0A1L8EKZ2	EPABA	EPAB	44.23	2	0
A0A1L8HEX9	MOV10	MOV10	35.14	2	0
A0A1L8GT79;Q52KN7	CPEB1B	CPEB1	29.15	0	0
A0A1L8ES55;Q6GR16;A0A1L8ES40	EPABB	EPAB	16.62	1	0
Q7ZXB4;Q4QR55;A0A1L8HNA9	PTBP1	PTBP1	20.87	1	0
A0A1L8GUZ9;A0A1L8GY11	EIF4E	EIF4E	12.96	0	0
A0A1L8GFC1	CNOT1	CNOT1	13	2	0
A0A1L8HQ92;Q6DE09	EIF4ENIF	EIF4ENIF1	11.31	0	0
A0A1L8FLL9;P54824	DDX6	DDX6	16.2	0	0
A0A1L8ELU2	YTHDF1	YTHDF1	NA	4	1
A0A1L8ESZ1;Q68FI1	LSM14B-A	LSM14	NA	4	0
A0A1L8F0H9;Q9W799;A0A1L8F9H7	CPSF2	CPSF2	NA	3	0
A0A1L8F3F9;Q7ZYV9	SYMPK	SYMPK	NA	3	0
A0A1L8FW10;O73932	IGF2BP3A	IGF2BP3	NA	4	1
A0A1L8G578	CPSF3	CPSF3	NA	4	0
A0A1L8GAN7;A0A1L8G4F1	WDR33	WDR33	NA	4	0
A0A1L8GL86;A0A1L8GL44;A0A8M2	LSM14A-A	LSM14	NA	3	0
A0A1L8GLF8	CNOT1	CNOT1	NA	4	1
A0A1L8GUY9;A0A1L8GUW5	SLBP2	SLBP2	NA	4	1
A0A1L8GZ04	MOV10	MOV10	NA	3	0
A0A1L8HBI7	ZAR1L	ZAR1	NA	4	0
A0A1L8HE42;Q505M1;A0A1L8H6C1	CSDE1	CSDE1	NA	4	1
Q6DCK2;A0A1L8HE82;A0A1L8HEE7	YTHDF2	YTHDF2	NA	4	1
A0A1L8HJK9	ZAR1L	ZAR1	NA	4	0
A0AUS9;Q63ZL7;A0A1L8HLC5	FIP1	FIP1	NA	4	0
A0A1L8HQR6	ATXN2L	ATXN2	NA	4	0
A0A1L8I198;Q4V7W4	ATXN2	ATXN2	NA	3	0
B7ZS12;Q4V7Y4	DAZLB	DAZL	NA	4	1
C0SPG1	ZAR2	ZAR2	NA	4	0
O57526	IGF2BP3B	IGF2BP3	NA	4	1
Q2VPF5;Q6DD72;Q7ZWR9	STAU2	STAU2	NA	4	0
Q498K9	LSM14B-B	LSM14	NA	4	1
Q5XGZ1	CPSF3	CPSF3	NA	4	0
Q6NU14	HNRNPDLB	HNRNPDLB	NA	4	1
Q8AVJ2	LSM14A-B	LSM14	NA	4	0

Table A2: CPEB1-BirA enriched proteins. BioID hits obtained with the *ad hoc* analysis pipeline. For each identified group of accession numbers (Uniprot), the gene name, grouped gene name, fold-change and missing values found in the control or conditions are depicted. We used the grouped gene names for Gene Ontology and network analyses.

Accessions	Gene name	Grouped name	FC	Ctrl miss	Cond miss
B7ZSB2;Q9PVV4;A0A1L8HTV8	PCM1	PCM1	62.53	0	0
A0A1L8GGX7;Q5EE04	TPR	TPR	92.8	0	0
A0A1L8GYM0	CCT2	CCT2	16.48	0	0
A0A1L8ES31;Q5XHK2;P29309	YWHABA	YWHABA	NA	4	0
A0A1L8EVQ1;Q6IP65	CNOT9	CNOT9	NA	4	1
A0A1L8EX65	MT11	MT11	NA	4	1
Q6GQB2;A0A1L8F1B9;Q6EE38	RPL7A	RPL7A	NA	4	1
A0A1L8F383	PLASTIN3L	PLASTIN3L	NA	4	1
A0A1L8FMH2;A0A1L8FGF3	ACOT	ACOT	NA	4	0
A0A1L8FVU1;A0A1L8FR11;Q5U5D4	MIOSB	MIOSB	NA	4	0
A0A1L8FS62	RIO1	RIO1	NA	3	0
A0A1L8FXY4;Q6NU66	TBC1D7	TBC1D7	NA	4	1
Q6NU42;A0A1L8G560	TPR	TPR	NA	3	0
Q6DEB6;A0A1L8G7J1;Q6PAX1	UGP2	UGP2	NA	3	0
Q6NS18;A0A1L8GA53	KPNA4	KPNA4	NA	4	1
A0A1L8H047;Q91572	CPEB1A	CPEB1	NA	3	0
Q63ZK6;A0A1L8HIL8;A0A1L8HAF1	PFDN5	PFDN5	NA	4	0
A0A1L8HC69	MAELSTROM	MAELSTROM	NA	4	0
A0A1L8HDJ9;Q6DEB0;A0A1L8HDN2	PDHA1	PDHA1	NA	4	1
A0A1L8HJA8	CENPJ	CENPJ	NA	3	0
Q68F10;Q7ZYT8;Q91581	CSTF64	CSTF64	NA	4	0
Q6DJI1	EIF4EBP2	EIF4EBP2	NA	4	1
Q7T0N8	HADH	HADH	NA	4	0
Q8AVJ2	LSM14A-B	LSM14	NA	4	0
Q9PTN1	RPS6KA3	RPS6KA3	NA	4	1

Table A3: BirA-CPEB1(Y365A) enriched proteins. BioID hits obtained with the *ad hoc* analysis pipeline. For each identified group of accession numbers (Uniprot), the gene name, grouped gene name, fold-change and missing values found in the control or conditions are depicted.

Accessions	Gene name	Grouped name	FC	Ctrl miss	Cond miss
B7ZSB2;Q9PVV4;A0A1L8HTV8	PCM1	PCM1	76.71	0	0
A0A1L8GGX7;Q5EE04	TPR	TPR	16.9	0	0
A0A1L8GYM0	CCT2	CCT2	15.34	0	0
Q7ZTL5;A0A1L8HCN3;Q4QR49	CCT8	CCT8	11.25	0	0
A0A1L8F3F9;Q7ZYV9	SYMPK	SYMPK	22.15	2	0
Q4V7K4;A0A1L8HCH4	PATL2	PATL2	9.65	1	0
K7SGN7;A0A1L8HIW5	ZAR2B	ZAR2	35	2	0
A0A1L8GUZ9;A0A1L8GY11	EIF4E	EIF4E	9.45	0	0
A0A1L8F002;A4FVE4	SIVA1	SIVA1	5.9	2	0
A0A1L8GT79;Q52KN7	CPEB1B	CPEB1	6.71	0	0
Q98SP8;A0A1L8EKZ2	EPABA	EPAB	8.61	1	0
Q6DD11;A0A1L8F062	FERMT2	FERMT2	5.31	1	0
A0A1L8ENT6;Q6DDL8	NHEJ1	NHEJ1	NA	4	1
A0A1L8ES31;Q5XHK2;P29309	YWHABA	YWHABA	NA	4	1
A0A1L8EVQ1;Q6IP65	CNOT9	CNOT9	NA	4	0
A0A1L8EX65	MT11	MT11	NA	4	1
Q6GQB2;A0A1L8F1B9;Q6EE38	RPL7A	RPL7A	NA	4	0
A0A1L8FMH2;A0A1L8FGF3	ACOT	ACOT	NA	4	0
A0A1L8FS62	RIO1	RIO1	NA	3	0
A0A1L8FXY4;Q6NU66	TBC1D7	TBC1D7	NA	4	1
Q6NU42;A0A1L8G560	TPR	TPR	NA	3	0
Q6DEB6;A0A1L8G7J1;Q6PAX1	UGP2	UGP2	NA	3	0
Q6NS18;A0A1L8GA53	KPNA4	KPNA4	NA	4	0
A0A1L8GL86;A0A1L8GL44;A0A8M2	LSM14A-A	LSM14	NA	4	1
A0A1L8H047;Q91572	CPEB1A	CPEB1	NA	3	0
A0A1L8H601	MEP50	MEP50	NA	4	1
A0A1L8H9Q1;A0A1L8HI21;Q6IP73	NACA	NACA	NA	4	0
Q63ZK6;A0A1L8HIL8;A0A1L8HAF1	PFDN5	PFDN5	NA	4	0
A0A1L8HAZ4;A2RRX6	NPAT	NPAT	NA	4	0
A0A1L8HBI7	ZAR1L	ZAR1	NA	4	1
A0A1L8HDJ9;Q6DEB0;A0A1L8HDN2	PDHA1	PDHA1	NA	4	0
A0A1L8HJA8	CENPJ	CENPJ	NA	3	0
A0A1L8HQR6	ATXN2L	ATXN2	NA	3	0
A0A1L8HS35;Q7SY94	ATP5A1	ATP5A1	NA	4	1
A0A1L8HTW2;A0A1L8HU14;Q6GLS8	FRG1	FRG1	NA	4	1
A0A1L8HXE0;Q0IHJ3	HAUS8	HAUS8	NA	4	1
A0A1L8I2F0;Q3B8C9	MRPS30	MRPS30	NA	4	0
C0SPG1	ZAR2	ZAR2	NA	4	1
Q5U259;A0A1L8HNJ9	ELAVL1B	HUR	NA	4	1
Q68F10;Q7ZYT8;Q91581	CSTF64	CSTF64	NA	4	0
Q8AVJ2	LSM14A-B	LSM14	NA	4	0

Table A4: CPEB1(Y365A)-BirA enriched proteins. BioID hits obtained with the *ad hoc* analysis pipeline. For each identified group of accession numbers (Uniprot), the gene name, grouped gene name, fold-change and missing values found in the control or conditions are depicted.

Accessions	Gene name	Grouped name	FC	Ctrl miss	Cond miss
A0A1L8HEX9	MOV10	MOV10	19.73	2	0
Q4V7K4;A0A1L8HCH4	PATL2	PATL2	15.02	0	0
A0A1L8GGX7;Q5EE04	TPR	TPR	20.79	0	0
Q98SP8;A0A1L8EKZ2	EPABA	EPAB	12.86	2	0
B7ZSB2;Q9PVV4;A0A1L8HTV8	PCM1	PCM1	11.25	0	0
Q6GQB6	G3BP1	G3BP1	6.86	1	0
A0A1L8ELU2	YTHDF1	YTHDF1	NA	4	1
A0A1L8ESZ1;Q68FI1	LSM14B-A	LSM14	NA	4	1
Q6GPP8;A0A1L8EXB9	HBA-L5	HBA	NA	4	0
A0A1L8F0H9;Q9W799;A0A1L8F9H7	CPSF2	CPSF2	NA	3	0
A0A1L8F3F9;Q7ZYV9	SYMPK	SYMPK	NA	3	0
A0A1L8FKQ9;Q6IVY4	SSH	SSH	NA	4	0
A0A1L8FW10;O73932	IGF2BP3A	IGF2BP3	NA	4	1
A0A1L8GAN7;A0A1L8G4F1	WDR33	WDR33	NA	4	0
A0A1L8GZ04	MOV10	MOV10	NA	3	0
A0A1L8H4N6;A0A1L8H4P1;P21574	YBX2	YBX2	NA	4	1
A0A1L8HBI7	ZAR1L	ZAR1	NA	4	0
A0A1L8HE42;Q505M1;A0A1L8H6C1	CSDE1	CSDE1	NA	4	0
A0A1L8HJA8	CENPJ	CENPJ	NA	3	0
A0A1L8HJK9	ZAR1L	ZAR1	NA	4	1
A0AUS9;Q63ZL7;A0A1L8HLC5	FIP1	FIP1	NA	4	0
A0A1L8HQR6	ATXN2L	ATXN2	NA	4	0
C0SPG1	ZAR2	ZAR2	NA	4	1
Q2VPF5;Q6DD72;Q7ZWR9	STAU2	STAU2	NA	4	0
Q7ZYS4	PDLIM1	PDLIM1	NA	3	0
Q8AVJ2	LSM14A-B	LSM14	NA	4	0
Q90WE3	TDRD6	TDRD6	NA	4	1

Table A5: BirA-CPEB1-CTD enriched proteins. BioID hits obtained with the *ad hoc* analysis pipeline. For each identified group of accession numbers (Uniprot), the gene name, grouped gene name, fold-change and missing values found in the control or conditions are depicted.

Accessions	Gene name	Grouped name	FC	Ctrl miss	Cond miss
Q4V7K4;A0A1L8HCH4	PATL2	PATL2	15.51	0	0
Q6NUD0	WDR77	WDR77	29.17	2	0
A0A1L8HEX9	MOV10	MOV10	15.14	2	0
A0A1L8GT79;Q52KN7	CPEB1B	CPEB1	7.39	0	0
B7ZSB2;Q9PVV4;A0A1L8HTV8	PCM1	PCM1	8.41	0	0
A0A1L8ELU2	YTHDF1	YTHDF1	NA	4	1
A0A1L8ESZ1;Q68FI1	LSM14B-A	LSM14	NA	4	0
Q6GPP8;A0A1L8EXB9	HBA-L5	HBA	NA	4	1
A0A1L8F3F9;Q7ZYV9	SYMPK	SYMPK	NA	3	0
A0A1L8FW10;O73932	IGF2BP3A	IGF2BP3	NA	4	1
Q6AZR6;A0A1L8GNA8;Q9W626	XRCC6	XRCC6	NA	3	0
Q6DCZ5;A0A1L8GNW3	ZC3H7B	ZC3H7B	NA	4	0
B7ZQW3;A0A1L8GUY9;Q9YGP6	SLBP2	SLBP2	NA	4	1
A0A1L8HBI7	ZAR1L	ZAR1	NA	4	0
A0A1L8HJA8	CENPJ	CENPJ	NA	3	0
A0A1L8HJK9	ZAR1L	ZAR1	NA	4	0
A0AUS9;Q63ZL7;A0A1L8HLC5	FIP1	FIP1	NA	4	1
A0A1L8HQR6	ATXN2L	ATXN2	NA	4	1
C0SPG1	ZAR2	ZAR2	NA	4	1
Q2VPF5;Q6DD72;Q7ZWR9	STAU2	STAU2	NA	4	1
Q8AVJ2	LSM14A-B	LSM14	NA	4	0

Table A6: CPEB1-CTD-BirA enriched proteins. BioID hits obtained with the *ad hoc* analysis pipeline. For each identified group of accession numbers (Uniprot), the gene name, grouped gene name, fold-change and missing values found in the control or conditions are depicted.

Accessions	Gene name	Grouped name	FC	Ctrl miss	Cond miss
A0A1L8HQ92;Q6DE09	EIF4ENIF	EIF4ENIF1	37.88	0	0
A0A1L8ES55;Q6GR16;A0A1L8ES40	EPABB	EPAB	NA	3	0
A0A1L8ESZ1;Q68FI1	LSM14B-A	LSM14	NA	4	1
A0A1L8EVQ1;Q6IP65	CNOT9	CNOT9	NA	4	0
A0A1L8HEX9	MOV10	MOV10	NA	4	0
Q6GQB6	G3BP1	G3BP1	NA	4	1
Q8AVJ2	LSM14A-B	LSM14	NA	4	0
Q98SP8;A0A1L8EKZ2	EPABA	EPAB	NA	4	0

Table A7: BirA-CPEB2 enriched proteins. BioID hits obtained with the *ad hoc* analysis pipeline. For each identified group of accession numbers (Uniprot), the gene name, grouped gene name, fold-change and missing values found in the control or conditions are depicted.

Accessions	Gene name	Grouped name	FC	Ctrl miss	Cond miss
A0A1L8ES55;Q6GR16;A0A1L8ES40	EPABB	EPAB	NA	3	0
A0A1L8ESZ1;Q68FI1	LSM14B-A	LSM14	NA	4	1
Q6NTK9;A0A1L8F893;A0A1L8F870	EML2	EML2	NA	4	1
B9VQ38;A0A1L8FPA6;Q52KW8	RCC2	RCC2	NA	4	1
A0A1L8HEX9	MOV10	MOV10	NA	4	0
A0A1L8HFI8;Q91695;Q7ZYT5	HDAC1	HDAC1	NA	4	1
A0A1L8HIB5	PFK	PFK	NA	4	1
Q52KS2;Q6DDT8	POLD3	POLD3	NA	3	0
Q6IP60;Q7ZTR6	HSPD1	HSPD1	NA	4	1
Q7ZXH6	YWHAQ	YWHAQ	NA	4	1
Q8AVJ2	LSM14A-B	LSM14	NA	4	0
Q98SP8;A0A1L8EKZ2	EPABA	EPAB	NA	4	1

Table A8: CPEB2-BirA enriched proteins. BioID hits obtained with the *ad hoc* analysis pipeline. For each identified group of accession numbers (Uniprot), the gene name, grouped gene name, fold-change and missing values found in the control or conditions are depicted.

Accessions	Gene name	Grouped name	FC	Ctrl miss	Cond miss
A0A1L8GGX7;Q5EE04	TPR	TPR	45.81	1	0
A0A1L8ES55;Q6GR16;A0A1L8ES40	EPABB	EPAB	NA	3	0
A0A1L8ESZ1;Q68FI1	LSM14B-A	LSM14	NA	4	1
A0A1L8EUL0	UBQE2	UBQE2	NA	4	1
A0A1L8EVQ1;Q6IP65	CNOT9	CNOT9	NA	4	0
Q640D7;A0A1L8EYM2	RPL3L	RPL3L	NA	4	1
A0A1L8GAN7;A0A1L8G4F1	WDR33	WDR33	NA	4	0
A0A1L8GL86;A0A1L8GL44;A0A8M2	LSM14A-A	LSM14	NA	4	1
A0A1L8GLF8	CNOT1	CNOT1	NA	4	1
A0A1L8GYK2	CNOT2	CNOT2	NA	4	1
A0A1L8HE73;Q6IP18;A0A1L8H7J6	RPA2A	RPA2A	NA	4	1
A0A1L8HEX9	MOV10	MOV10	NA	4	0
A0A1L8HSF1;A0A1L8HSG7	SUCLG1	SUCLG1	NA	4	1
Q8UWC3;B7ZQN6;A0A1L8GE11	CCTN	CCTN	NA	4	0
BirA-xCPEB3	CPEB3	CPEB3	NA	4	0
Q6GQB6	G3BP1	G3BP1	NA	4	0
Q6IP60;Q7ZTR6	HSPD1	HSPD1	NA	4	1
Q7ZWW5	ABCF2	ABCF2	NA	4	1
Q8AVG6	DNJA1	DNJA1	NA	4	1
Q8AVJ2	LSM14A-B	LSM14	NA	4	0
Q98SP8;A0A1L8EKZ2	EPABA	EPAB	NA	4	0

Table A9: BirA-CPEB3 enriched proteins. BioID hits obtained with the *ad hoc* analysis pipeline. For each identified group of accession numbers (Uniprot), the gene name, grouped gene name, fold-change and missing values found in the control or conditions are depicted.

Accessions	Gene name	Grouped name	FC	Ctrl miss	Cond miss
Q4V7K4;A0A1L8HCH4	PATL2	PATL2	35.47	1	0
C0SPG1	ZAR2	ZAR2	52.81	2	0
A0A1L8F7F0	ALG13	ALG13	9.58	1	0
A0A1L8HQ92;Q6DE09	EIF4ENIF	EIF4ENIF1	152.64	0	0
A0A1L8ES55;Q6GR16;A0A1L8ES40	EPABB	EPAB	NA	3	0
A0A1L8ESZ1;Q68FI1	LSM14B-A	LSM14	NA	4	1
A0A1L8EVQ1;Q6IP65	CNOT9	CNOT9	NA	4	0
A0A1L8EVQ5;B1H1Q2;A0A1L8ENU2	GRSF1	GRSF1	NA	4	1
A0A1L8EWC9;Q7ZYA5;Q91836	PRKRA	PRKRA	NA	4	0
A0A1L8F3F9;Q7ZYV9	SYMPK	SYMPK	NA	4	0
Q6NTK9;A0A1L8F893;A0A1L8F870	EML2	EML2	NA	4	1
A0A1L8FKV7;Q7ZXS6;A0A1L8FFB1	TARDBP	TARDBP	NA	4	0
A0A1L8FZ34;Q2VPM6;A0A1L8FT25	RAB2A	RAB2A	NA	4	1
Q0IH89;A0A1L8G7J0	DUSP12	DUSP12	NA	4	1
A0A1L8GAN7;A0A1L8G4F1	WDR33	WDR33	NA	4	0
A0A1L8GL86;A0A1L8GL44;A0A8M2	LSM14A-A	LSM14	NA	4	1
B7ZQW3;A0A1L8GUY9;Q9YGP6	SLBP2	SLBP2	NA	4	1
A0A1L8GYK2	CNOT2	CNOT2	NA	4	0
A0A1L8H8J4	AKAP1	AKAP1	NA	3	0
A0A1L8HBI7	ZAR1L	ZAR1	NA	3	0
A0A1L8HEX9	MOV10	MOV10	NA	4	0
Q6GM69;Q98UD3;Q7ZYE9	HNRNPAB	HNRNPAB	NA	4	1
Q6GQB6	G3BP1	G3BP1	NA	4	0
Q6IP60;Q7ZTR6	HSPD1	HSPD1	NA	4	1
Q7ZWW5	ABCF2	ABCF2	NA	4	1
Q7ZXB4;Q4QR55;A0A1L8HNA9	PTBP1	PTBP1	NA	3	0
Q8AVG6	DNJA1	DNJA1	NA	4	1
Q8AVJ2	LSM14A-B	LSM14	NA	4	0
Q98SP8;A0A1L8EKZ2	EPABA	EPAB	NA	4	0

Table A10: CPEB3-BirA enriched proteins. BioID hits obtained with the *ad hoc* analysis pipeline. For each identified group of accession numbers (Uniprot), the gene name, grouped gene name, fold-change and missing values found in the control or conditions are depicted.

Accessions	Gene name	Grouped name	FC	Ctrl miss	Cond miss
C0SPG1	ZAR2	ZAR2	54.43	2	1
A0A1L8HJK9	ZAR1L	ZAR1	29.64	2	1
A0A1L8FLL9;P54824	DDX6	DDX6	36.49	0	1
A0A1L8F032	DYNC1	DYNC1	7.66	0	1
A0A1L8H047;Q91572	CPEB1A	CPEB1	7.2	2	1
A0A1L8ESZ1;Q68FI1	LSM14B-A	LSM14	NA	4	1
A0A1L8EVQ1;Q6IP65	CNOT9	CNOT9	NA	4	1
A0A1L8F3F9;Q7ZYV9	SYMPK	SYMPK	NA	4	1
A0A1L8FCQ5;Q7ZWS8	TAGLN2	TAGLN2	NA	4	1
A0A1L8FWB8;Q6DE97	CNOT10A	CNOT10	NA	4	1
A0A1L8GAN7;A0A1L8G4F1	WDR33	WDR33	NA	4	1
A0A1L8GJT9	MACROD1	MACROD1	NA	4	1
A0A1L8GYK2	CNOT2	CNOT2	NA	4	1
A0A1L8HE63;A0A1L8HE74;Q66KI6	PUM1	PUM1	NA	4	1
A0A1L8HE73;Q6IP18;A0A1L8H7J6	RPA2A	RPA2A	NA	4	1
A0A1L8HEX9	MOV10	MOV10	NA	4	0
A0A1L8HQR6	ATXN2L	ATXN2	NA	4	1
A0A1L8I198;Q4V7W4	ATXN2	ATXN2	NA	4	1
Q6GM69;Q98UD3;Q7ZYE9	HNRNPAB	HNRNPAB	NA	4	1
Q6GQB6	G3BP1	G3BP1	NA	4	1
Q8AVJ2	LSM14A-B	LSM14	NA	4	1
Q98SP8;A0A1L8EKZ2	EPABA	EPAB	NA	4	1

Table A11: BirA-CPEB4 enriched proteins. BioID hits obtained with the *ad hoc* analysis pipeline. For each identified group of accession numbers (Uniprot), the gene name, grouped gene name, fold-change and missing values found in the control or conditions are depicted.

Accessions	Gene name	Grouped name	FC	Ctrl miss	Cond miss
C0SPG1	ZAR2	ZAR2	171.33	2	0
A0A1L8F7F0	ALG13	ALG13	26.35	1	0
A0A1L8GUZ9;A0A1L8GY11	EIF4E	EIF4E	28.17	0	0
A0A1L8HQ92;Q6DE09	EIF4ENIF	EIF4ENIF1	383.27	0	0
A0A1L8GT79;Q52KN7	CPEB1B	CPEB1	57.26	0	0
Q4V7K4;A0A1L8HCH4	PATL2	PATL2	101.52	1	0
A0A1L8HJK9	ZAR1L	ZAR1	102.51	2	0
A0A1L8H047;Q91572	CPEB1A	CPEB1	18.4	2	0
A0A1L8FLL9;P54824	DDX6	DDX6	99.83	0	0
A0A1L8G192;A0A1L8G1A2;Q2TAF3	EML4	EML4	12.48	0	1
A0A1L8GGX7;Q5EE04	TPR	TPR	15.52	1	0
A0A1L8G9T6	EIF4G1	EIF4G1	13.86	0	0
A0A1L8GWA6;B1WBD5	CAPRIN2	CAPRIN2	7.69	0	0
A0A1L8GZ04	MOV10	MOV10	11.89	2	0
A0A1L8ELU2	YTHDF1	YTHDF1	NA	4	1
A0A1L8EM14	CPSF4	CPSF4	NA	4	1
A0A1L8ES55;Q6GR16;A0A1L8ES40	EPABB	EPAB	NA	3	0
A0A1L8ESZ1;Q68FI1	LSM14B-A	LSM14	NA	4	0
Q6PA59;A0A1L8ET20	YTHDF1	YTHDF1	NA	4	0
A0A1L8EVQ1;Q6IP65	CNOT9	CNOT9	NA	4	0
A0A1L8EVQ5;B1H1Q2;A0A1L8ENU2	GRSF1	GRSF1	NA	4	0
A0A1L8EWC9;Q7ZYA5;Q91836	PRKRA	PRKRA	NA	4	0
Q640D7;A0A1L8EYM2	RPL3L	RPL3L	NA	4	1
Q6PAA0;A0A1L8F1K5	FUBP3	FUBP3	NA	4	1
A0A1L8F3F9;Q7ZYV9	SYMPK	SYMPK	NA	4	0
Q6NTK9;A0A1L8F893;A0A1L8F870	EML2	EML2	NA	4	0
Q7ZXS6;A0A1L8FFB1;Q8JJ42	TARDBP	TARDBP	NA	4	0
A0A1L8FTH7;A0A1L8FZJ1;Q7ZY29	ESRP1	ESRP1	NA	4	0
A0A1L8FWB8;Q6DE97	CNOT10A	CNOT10	NA	4	0
A0A1L8GAN7;A0A1L8G4F1	WDR33	WDR33	NA	4	0
A0A1L8GFC1	CNOT1	CNOT1	NA	4	0
A0A1L8GL86;A0A1L8GL44;A0A8M2	LSM14A-A	LSM14	NA	4	0
A0A1L8GLF8	CNOT1	CNOT1	NA	4	0

Continues next page.

Accessions	Gene name	Grouped name	FC	Ctrl miss	Cond miss
A0A1L8GN33	PRRC2	PRRC2	NA	4	0
Q6DCZ5;A0A1L8GNW3	ZC3H7B	ZC3H7B	NA	4	1
A0A1L8GT66;Q9YGP5;Q66IX3	RBPMS2	RBPMS2	NA	4	1
A0A1L8GUI7;Q6GPN8	CNOT2	CNOT2	NA	4	0
B7ZQW3;A0A1L8GUY9;Q9YGP6	SLBP2	SLBP2	NA	4	0
A0A1L8GYK2	CNOT2	CNOT2	NA	4	0
A0A1L8H7B4	CEP85	CEP85	NA	3	0
A0A1L8HE63;A0A1L8HE74;Q66KI6	PUM1	PUM1	NA	4	0
A0A1L8H8J4	AKAP1	AKAP1	NA	3	0
A0A1L8HBI7	ZAR1L	ZAR1	NA	3	0
A0A1L8HE42;Q505M1;A0A1L8H6C1	CSDE1	CSDE1	NA	4	0
Q6DCK2;A0A1L8HE82;A0A1L8HEE7	YTHDF2	YTHDF2	NA	4	0
A0A1L8HEX9	MOV10	MOV10	NA	4	0
A0A1L8HK01	PIWIL1	PIWIL1	NA	3	0
B7ZPG0;A0A1L8HL44;Q7T3U0	ZAR1	ZAR1	NA	4	1
A0A1L8HQR6	ATXN2L	ATXN2	NA	4	0
A0A1L8HSF1;A0A1L8HSG7	SUCLG1	SUCLG1	NA	4	1
A0A1L8HX08;A0A1L8HWX9;Q1JQ73	ELAVL1A	HUR	NA	4	0
A0A1L8I198;Q4V7W4	ATXN2	ATXN2	NA	4	0
B7ZRW2;B7ZRW4;Q6TY21	PABP1B	PABPN	NA	4	0
Q52L23;Q7ZXJ0;P24346	DDX3X	DDX3X	NA	3	0
Q2VPF5;Q6DD72;A0A1L8FT79	STAU2	STAU2	NA	4	0
Q5U259;A0A1L8HNJ9	ELAVL1B	HUR	NA	3	0
Q6GM69;Q98UD3;Q7ZYE9	HNRNPAB	HNRNPAB	NA	4	0
Q6GQB6	G3BP1	G3BP1	NA	4	0
Q6IP60;Q7ZTR6	HSPD1	HSPD1	NA	4	1
Q7ZXB4;Q4QR55;A0A1L8HNA9	PTBP1	PTBP1	NA	3	0
Q804A5	PABP1A	PABPN	NA	4	0
Q8AVJ2	LSM14A-B	LSM14	NA	4	0
Q98SP8;A0A1L8EKZ2	EPABA	EPAB	NA	4	0

Table A12: CPEB4-BirA enriched proteins (continuation). BioID hits obtained with the *ad hoc* analysis pipeline. For each identified group of accession numbers (Uniprot), the gene name, grouped gene name, fold-change and missing values found in the control or conditions are depicted.

Accessions	Gene name	Grouped name	FC	BFDR	Rank.PI	Rank.MII
A0A1L8HEX9	MOV10	MOV10	342.5	0	1	2
A0A1L8GZ04	MOV10	MOV10	215	0	2	NA
A0A1L8F3F9	SYMPK	SYMPK	205	0	3	1
K7SGN7	ZAR2	ZAR2	160	0	4	NA
A0A1L8ES55	EPABP–B	EPAB	147.5	0	5	5
C0SPG1	ZAR2	ZAR2	140	0	6	NA
A0A1L8GL86	LSM14A–A	LSM14	135	0	7	NA
Q98SP8	EPABP–A	EPA	115	0	8	9
A0A1L8GGX7	TPR	TPR	109	0	9	12
Q8AVJ2	LSM14A–B	LSM14	107.5	0	10	NA
A0A1L8ESZ1	LSM14–B–A	LSM14	85	0	11	NA
A0A1L8HJK9	ZAR1L	ZAR1	85	0	11	NA
A0A1L8G447	FXR1–B	FXR1	80	0	12	NA
Q7ZXB4	PTBP1	PTBP1	75	0	13	NA
B7ZQW3	SLBP2	SLBP2	72.5	0	14	NA
A0A1L8HBI7	ZAR1L	ZAR1	70	0	15	NA
Q498K9	LSM14B–B	LSM14	70	0	15	NA
B7ZPG0	ZAR1	ZAR1	65	0	16	NA
A0A1L8HE42	CSDE1	CSDE1	62.5	0	17	NA
Q9W799	CPSF2	CPSF2	62.5	0	17	3
Q4V7K4	PATL2	PATL2	62.33	0	18	NA
Q7ZXJ0	DDX3X	DDX3X	60	0	19	NA
Q2VPF5	STAU2	STAU2	57.5	0	20	NA
A0A1L8GAN7	WDR33	WDR33	55	0	21	3
A0A1L8FTH7	ESRP1	ESRP1	52.5	0	22	NA
A0A1L8EYG5	TNRC6A	TNRC6A	50	0	23	NA
A0A1L8FW10	IGF2BP3–A	IGF2BP3	50	0	23	NA
A0A1L8GN33	PRRC2	PRRC2	50	0	23	NA
A0A1L8I198	ATXN2	ATXN2	50	0	23	NA
Q6GM69	HNRNPAB	HNRNPA	50	0	23	NA
A0A1L8EQS4	TNRC6A	TNRC6A	47.5	0	24	NA
A0A1L8FPI2	HAUS5	HAUS5	47.5	0	24	NA
A0A1L8GT79	CPEB1–B	CPEB1	43	0	25	NA

Continues next page.

Accessions	Gene name	Grouped name	FC	BFDR	Rank.PI	Rank.MII
A0A1L8EVQ5	GRSF1	GRSF1	42.5	0	26	NA
A0A1L8FKV7	TARDBP	TARDBP	42.5	0	26	NA
A0A1L8GFC1	CNOT1	CNOT1	42.5	0	26	NA
A0A1L8EM14	CPSF4	CPSF4	37.5	0	27	NA
A0A1L8GH02	TNRC6B	TNRC6B	37.5	0.05	27	NA
A0AUS9	FIP1L1	FIP1L1	37.5	0	27	6
A0A1L8HQ92	EIF4ENIF1	EIF4ENIF1	36.2	0	28	13
A0A1L8I094	EIF4ENIF1	EIF4ENIF1	34	0	29	8
A0A1L8GBY1	PUM2	PUM2	32.5	0	30	NA
A0A1L8GLF8	CNOT1	CNOT1	32.5	0	30	NA
A0A1L8HY91	ELAVL2	HUB	32.5	0	30	NA
Q68F10	CSTF64	CSTF64	32.5	0.05	30	7
A0A1L8HQR6	ATXN2L	ATXN2	32	0	31	11
A0A1L8HE63	PUM1	PUM1	30	0	32	NA
B7ZRL0	FMR1–A	FMR1	30	0.05	32	NA
A0A1L8ELU2	YTHDF1	YTHDF1	27.5	0	33	10
A0A1L8H4E1	GIGY1F1	GIGY1F1	27.5	0.06	33	NA
A0A1L8HX08	ELAVL1–A	HUR	27.5	0.01	33	NA
Q5U259	ELAVL1–B	HUR	27.5	0	33	NA
A0A1L8FPW7	ZNF605	ZNF605	26	0	34	NA
Q6NUC6	RC3H1	RC3H1	25	0.06	35	NA
A0A1L8FLF8	HIST1H2AD	HIST1H2AD	22.5	0	36	NA
A0A1L8H6G5	USP9X	USP9X	22.5	0.08	36	NA
O57526	IGF2BP3B	IGF2BP3	22.5	0.07	36	NA
Q6IRC9	HNRNPH1	HNRNPH	22.5	0.01	36	NA
Q6NU42	TRAPPC	TRAPPC	22.5	0.01	36	NA
Q804A5	PABP1A	PABPC	22.5	0	36	NA
A0A1L8FWB8	CNOT10–A	CNOT10	20	0.07	37	NA
A0A1L8GG85	ROQUIN1	ROQUIN1	20	0.08	37	NA
A0A1L8H047	CPEB1–A	CPEB1	20	0.01	37	NA
Q6NUC0	TRIM25	TRIM25	20	0.09	37	NA
A0A1L8EVQ1	CNOT9	CNOT9	17.5	0.1	38	NA
A0A1L8G1G1	ZFP36L2	ZFP36	17.5	0.07	38	NA

Continues next page.

Accessions	Gene name	Grouped name	FC	BFDR	Rank.PI	Rank.MII
A0A1L8H8S9	TRAF2	TRAF2	17.5	0.1	38	NA
Q0IH89	DUSP12	DUSP12	17.5	0.01	38	NA
Q6DCZ5	ZC3H7B	ZC3H7B	17.5	0.01	38	NA
Q6NUD0	WDR77	WDR77	15.5	0	39	NA
A0A1L8FKP2	PATL1	PATL1	15	0.09	40	NA
A0A1L8GVJ2	ANKH1	ANKH1	15	0.06	40	NA
A0A1L8H7B4	CEP85	CEP85	15	0.1	40	NA
Q63ZK6	PFDN5	PFDN5	15	0.08	40	NA
Q642P5	DBT	DBT	15	0.1	40	NA
Q6PAA0	FUBP3	FUBP3	15	0.09	40	NA
A0A1L8FRG7	CNOT10–B	CNOT10	15	0.09	40	NA
Q7T0N9	CDC23	CDC23	15	0.09	40	NA
A4FVE0	42SP50	42SP50	14.67	0	41	NA
Q66IU7	MYCBP2	MYCBP2	13	0.01	42	NA
A0A1L8F917	HNRNPL	HNRNPL	12.5	0.14	43	NA
A0A1L8GRB6	SEC24A	SEC24A	12.5	0.14	43	NA
A0A1L8H6M8	MAKORIN1	MAKORIN1	12.5	0.14	43	NA
B7ZR49	P43	P43	12.5	0.1	43	NA
Q68ES9	RPL3	RPL3	12.5	0.1	43	NA
Q6AZM7	PPOX	PPOX	12.5	0.14	43	NA
Q6NTK2	YTHDF2	YTHDF2	12.5	0.1	43	NA
Q7ZWW5	ABCF2	ABCF2	12.5	0.1	43	NA
Q7ZXC7	G3BP1	G3BP1	12.5	0.1	43	NA
A0A1L8H1F1	TIA1	TIA1	12.5	0.14	43	NA
A0A1L8EL76	SMARCD3	SMARCD3	12.5	0.1	43	NA
A0A1L8HHY6	ATP5B	ATP5B	12.5	0.1	43	NA
Q6DCD3	HSP70	HSP70	12.5	0.1	43	NA
A0A1L8FDC8	MYO1E2	MYO1E2	11	0	44	NA
A0A1L8HK01	PIWIL1	PIWIL1	11	0	44	NA
A0A1L8F7F0	ALG13	ALG13	10.5	0	45	NA
Q6NU04	TDRD7	TDRD7	10.5	0.02	45	NA
Q5PPT1	PRDX4	PRDX4	10	0.08	46	NA
Q641C7	RNPEP	RNPEP	10	0.14	46	NA
B7ZSB2	PCM1	PCM1	9.8	0	47	4

Continues next page.

Accessions	Gene name	Grouped name	FC	BFDR	Rank.PI	Rank.MII
A0A1L8GUZ9	EIF4E	EIF4E	9.4	0	48	NA
A0A1L8FLL9	DDX6	DDX6	9.09	0	49	14
A0A1L8HC69	MAELSTROM	MAELSTROM	9	0.02	50	NA
Q6DD11	FERMT2	FERMT2	7.67	0.03	51	NA
A0A1L8HWM7	CIRBPA	CIRBP	7.25	0	52	NA
A0A1L8EV51	COIL	COIL	7	0.14	53	NA
A0A1L8HG63	RBBP7	RBBP7	7	0.14	53	NA
A0A1L8HTJ6	RFC1	RFC1	6.27	0	54	NA
A0A1L8EQN7	PLK1	PLK1	6	0.03	55	NA
Q6DDW1	TXNL1	TXNL1	6	0.04	55	NA
A0A1L8GXE6	ANKH1	ANKH1	5.8	0.04	56	NA
Q3KQ82	PFN1	PFN1	5.67	0.04	57	NA
A0A1L8HPG1	PCK2	PCK2	5.5	0.04	58	NA
A0A1L8HYG8	PSAT1	PSAT1	5.5	0.01	58	NA
A0A1L8F3P4	GNL1	GNL1	4.83	0.01	59	NA
A0A1L8EQ20	FSCN1	FSCN1	4.5	0.13	60	NA
A0A1L8EYC7	PLK1	PLK1	4.5	0.02	60	NA
A0A1L8FT46	CHD7	CHD7	4.33	0.03	61	NA
Q6DFJ1	GBE1	GBE1	4.33	0.03	61	NA
Q5XG28	SENP3	SENP3	4	0.02	62	NA
Q7ZTL5	CCT8	CCT8	4	0.01	62	NA
Q6DKM3	WBSCR22	WBSCR22	3.83	0.01	63	NA
A0A1L8GF35	PHKBS	PHKBS	3.43	0.13	64	NA
A0A1L8HCG6	HLCS	HLCS	3.43	0.13	64	NA
Q8QHA5	DNA2	DNA2	3.26	0.14	65	NA
A0A1L8GDJ8	FEN1–B	FEN1	3.25	0.15	66	NA
A0A1L8H0F8	MYO5	MYO5	3.24	0.01	67	NA
Q5U491	PRMT5	PRMT5	2.89	0.13	68	NA
A0A1L8FMH5	NOL9	NOL9	2.26	0.14	69	NA
Q2NLA5	GLNRS1	GLNRS1	1.92	0.13	70	NA

Table A13: CPEB1-6A-BirA enriched proteins (continuation). BioID hits obtained for CPEB1-6A-BirA samples with and without progesterone. SAINT algorithm was used for the analysis and proteins with BFDR below 0.15 were defined as hits. For each identified group of accession numbers (Uniprot), the gene name, grouped gene name, fold-change, BFDR and rank in prophase I and metaphase II oocytes are depicted.

Appendix II: Cloned CPEB1-4 sequences

Protein	Accession number	NTD
CPEB1	Q91572	1..312
CPEB2	Not annotated	1..536
CPEB2*	A0A5G3HI07	1..536
CPEB3	A0A1L8FJ58	1..367
CPEB4	A0A1L8GV75	1..444

Table A14: CPEB sequences used in our experiments. UniProtKN Accession numbers of the CPEB paralogs used for our clonings and experiments. For each protein, the interval of residues comprising the NTD is depicted as well. The sequence of CPEB2 we have in our lab is not annotated in UniProt, thus for some sequence analysis algorithms we used the more similar UniProt entry, specified with the asterisk.

```
>CPEB2_cloned
MGDYGFGLLQAANLSSGGTGSGGGSLFGGGSFRGSAGQFPSLSSSSSGSA
LFLSAGYQQQQQVMQDELLLGVSCAPGNKHSKSGRVSPPALLLLQEPAKR
KDFSPQEGDAFREELKKQQQQSGEMNQQPCTYQRHGSPAAEELESPDKNL
PVSPSSSSSSSSCCSAEEALVGEAHAATSPPALSHQHLPAKGKLCMEAQG
GHLPNLLGGPYPGSPELAQTPGGSPPALPGFGTPWSVQTSSPPPPPPALP
QQQHQQQQHQPTAPHPAAPNLNALHSPDPDSFYPGIPSSINPAFFQSFST
NPCPGINVPGFSSPFSAQINIPQQQQQSRRSPVSPQLNPQHHQAAAFLQQ
RNSYNHHQPLVKQSPWGGHQSSGWNTGSMSWGGIHARDHRRTANMGMPGS
MNQISPLKKAYSGNVIAPPKFTRSTPSLTPKSWIEDNVFRTDNNSNTLLP
LQDRSRMYDSLNMHSLENSLIEIMRAEHDPLKGRLNYPHPGTESLLMLNG
RSSLFPLDDGLLDDGHNDQVGVLNSPNCYSGHQNGERIERFSRKVFVGGL
PPDIDEDEITASFRRFGPLVVDWPHKAESKSYFPPKGYAFLLFQEETSVQ
ALIEACIEEEGKLYLCVSSPTIKDKPVQIRPWNLSDSDFVMDGSQPLDPR
KTIFVGGVPRPLRAVELAMIMDRLYGGVCYAGIDTDPELKYPKGAGRVAF
SNQQSYIAAISARFVQLQHGDIDKRVEVKPYVLDDQMCDECQGARCGGKF
APFFCANVTCLQYYCEFCWANIHSRAGREFHKPLVKEGADRPRQIHFRWN
```

CPEB2 cloned sequence. Protein sequence of the CPEB2 variant cloned in our lab.

Acknowledgements

Me gustaría dar las gracias a todas las personas que me han acompañado en este viaje. De no haber sido por vosotros estoy seguro de que no lo habría podido lograr; hubiera tirado la toalla antes de tiempo y no me lo hubiese perdonado nunca. Gracias a todos por haber sido una fuente de luz, esperanza y motivación.

En primer lugar me gustaría agradecerle a Raúl haberme dado la oportunidad de hacer investigación en su laboratorio y de haber podido conocer a las CPEBs, una fuente de preguntas, dudas, frustraciones y alegrías que no olvidaré. Asimismo, quiero agradecer a todo el grupo rméndez por el apoyo que me han dado en todo momento y por haberme guiado por los caminos de la ciencia.

Eulàlia, gràcies per haver-me ensenyat tot el que sé ara, per haver-me donat les eines que necessitava per poder treballar de forma autònoma. Si no fos per la teva ajuda, encara em perdrien els gels... Gonzalo, el codire, que ya me habrás firmado veinte hipotecas sin saberlo... Me ha encantado conocer el lado espiritual de la vida a través de nuestras conversaciones. Espero que nunca te compres un peluco pero sí que vivas la vida con la intensidad con la que lo haces, cada día en tu vida es un concierto de Pearl Jam donde alguien se destroza el cuello!

Annarita, nunca olvidaré que fuiste tú quien me enseñó a hacer Western Blots y me consoló la primera vez que tiré una alícuota de anticuerpo primario sin querer. Me da rabia que, pese a que sé que eres una gran cocinera, la mitad de tus platos no los pruebe porque llevan queso! Me queda pendiente ver tus habilidades en el volley... Alba! La noia de les mil activitats! M'encanta la passió i l'amor que li poses a les coses que t'agraden, n'hauria d'aprendre... Espero que el teu grup de dansa arribi lluny (no ho dubto pas) i que el projecte Afrovaca continui ajudant a la gent que realment ho necessita!

Chiara!! Ya sabes que muchas veces he pensado que somos muy iguales en muchas cosas..., pero la verdad es que tienes muchas otras que te hacen una persona única! Eres

increíblemente creativa, trabajas duro y consigues todo lo que te propones. Me encanta ver tu motivación a la hora de pensar talleres, juegos, proyectos de bricolaje... Me tendrías que dar algún cursillo! Me ha encantado compartir estos años a tu lado, pero esto no acaba aquí! Nos quedan room escapes por hacer y podríamos atrevernos con lo del bubble soccer...

Juditini!! Mi vecina del pasillo de los guays con quien comparto gustos musicales, películas, juegos, series, lenguaje de barrio, el preciado chocoflan... Que sepas que nunca se me quitará de la cabeza tu foto en Sudáfrica (o Madagascar?) intentando captar Wi-fi detrás de una cortina jajaja. Espero que me sigas descubriendo juegos nuevos y yo intentaré algún día hackearte el Spotify cuando lleves los cascos puestos....

Vero! Ya sabes que no incurriríamos... No sé cómo sigue la frase. Pero está claro que si algo ha marcado nuestra filosofía y lenguaje ha sido El Shrek. Bueno y los pasos de baile de Gru, y el Olaf... Creo que eres la única persona en el mundo que me sigue mis "escenas" típicas de películas malas y series de los 90s, y nos podríamos tirar 20 minutos con la bromita... jajaja. No me equivoco si digo que eres una de las personas que más ha influído en mi en estos años, y ha hecho que sea la persona que soy ahora. Me has motivado a ser una mejor versión de mí mismo en muchos aspectos, y por eso te estoy tremendamente agradecido. A algunos siempre les quedará París, a nosotros siempre nos quedará Calafell y el pollo de corral que nunca hicimos!

Los pinchis! Nada hubiera sido igual sin vosotros. Pese a que soy un rancio y no me he apuntado a nada y por ende apenas tenemos anécdotas, todo lo que me llevaré de vosotros serán buenos recuerdos. Conversaciones con Rosa ella en su poyata y yo jugando con el rollo del papel porque me incomoda hablar, conversaciones con Irene en la poyata de los paquetes o en su labo, cuando le llevaba donettes a Emi, o las veces que Clara me ha pedido que le contara algo, o que hablara más fuerte que desde su poyata no nos oye... Sin duda las dottoras habéis sido una referencia para mí, os admiro un montón y

creo que pocas personas son tan especiales y a la vez tan buenas científicas como vosotras.

En el lado opuesto tenemos a las más benjaminas, las Annas. La Barto me ha hecho reír como nadie, con sus geles que no polimerizan, las imitaciones a La Llamada o el miedo que pasamos cuando vamos a buscar células a los tanques de nitrógeno... Mi pequeña padawan ya se ha convertido en toda una maestra Jedi y no me cabe duda de que vas a tener una tesis genial y que la vas a disfrutar como nadie! La Ferrer ha venido para quedarse, pisando fuerte! Tomando las riendas de la calçotada i amb una iniciativa i motivació que meravellen! Ets una persona genial, amb mil i una inquietuds, però també amb petites inseguretats que desapareixeran quan siguis conscient de tot el que vals!

Kitus!! Alfáramir!! Una enciclopedia Larousse con patas y barba, mucha barba! El hombre de las dos caras, la de antes y después de pasar por la peluquera! Que se llama.... Sonia? Me has ayudado un montón con mis problemas, que no han sido pocos, acertando casi más que la psicóloga, sólo que a ti no te pago... Muchas gracias por haber estado siempre ahí, en esa esquina llena de órganos, PBS sucio, papeles con reacciones de PCR y, en ocasiones, una poco delimitada zona RNase-free... Sé que llegará un día en el que nos encontraremos y ya no serás un espejo para mí, ni tú ni nadie, y sé que te alegrarás por mí como el buen amigo que eres.

Last but not least, la personita que vino, me zarandeó la cabeza y revolvió todos los mecanismos apagados que había en mi interior. Sí Berta, vas ser tu! Fruït d'haver-te conegut es va engegar una reacció en cadena dintre meu que m'ha fet canviar. Les meves aspiracions, somnis, la imatge de mi mateix, la meva falsa seguretat, tot això va caure, i ho he estat qüestionant des d'aquell moment. Ja saps que no ho he passat bé, però no m'empenedeixo, ara sóc més jo que mai, i això en gran part és gràcies a tu. També saps que, tret de les meves punyalades traperes, t'estimo molt (tot i que els dos som força erizos) i viuria mil cops aquesta etapa amb tu. T'admiro molt i sé que arribaràs tot lo lluny que et proposis, i espero estar allà per veure-ho, o com a mínim que m'enviïs un

whastapp. Ànims que ja et queda ben poquet, versió evolucionada de la Marie Kondo!

I would also like to thank all the people in the IRB for these amazing years, I couldn't have learned what science is in a better place.

Gracias a toda la administración, en especial a Leyre, Carlos, Natàlia y Maria Aurora por haberme ayudado con la burocracia y las dichosas memorias de seguimiento. Sin vuestra ayuda hubiera estado perdido en un mar de papeleo...

Gracias a las facilities que me han ayudado con mis experimentos, no podría haber estado en mejores manos. Gràcies Marina i Gian per tota l'ajuda que m'heu proporcionat, tant científica com psicològica, al vostre despatx on sempre fa calor! Gràcies també a l'Anna i la Lídia, per haver-me ajudat a conèixer la cèl·lula des d'un punt de vista que desconeixia...

Ha sido un placer compartir mis días en el IRB con gente como Isa, Joel, Sara, Enric, Marta, Paloma, Celia, Laura, Cris, Carla, Ela, Busra, Susi, Rami, Inés, Cris Figueras, Muriel, Gemma, Marina. Espero que todo os vaya genial! A la Laura, la meva amiga Biomed, la persona més bona i més treballadora que conec, li desitjo lo millor, que segur que ho tindràs, i també que arribi el dia en què visquis a 5 minuts de la feina...

No puedo acabar de hablar de la gente del IRB sin mencionar a mis compañeros de viaje! Un megaviaje a todo tren en las islas griegas y otro más de chill pero en un casoplón en Ibiza me han sabido a poco. Siempre recordaré la barbacoa en Ibiza, cuando nos metimos en esa cueva con gente extraña, Alicia prou!, Imerogivli, los gyros, las canciones de Bebe en las discos y nosotros cantando La Playa volviendo de Antíparos... Cuando acabemos todos podríamos repetir no? Yo me he quedado con ganas de más, esta aventura no puede acabar aquí!

Por último, me gustaría agradecer a los miembros del TAC: Xavier Salvatella, Manuel Palacín y Manuel Irimia por el seguimiento que me han llevado durante estos años. Gràcies també a la Gemma Marfany per haver sigut la millor tutora que hagués pogut tenir mai, el teu suport m'ha ajudat a continuar y no tirar la toalla!

Fuera del ámbito científico, me gustaría dar las gracias a mis amigos y familia, que no han dejado de apoyarme en ningún momento.

Gracias a los javifueristas, que hacen que cada día con ellos sea el día de la marmota, lo cual no es malo, porque da la sensación de que no ha pasado el tiempo. Sois mis amigos de toda la vida ya, me conocéis prácticamente mejor que nadie y con vosotros puedo ser yo mismo. Os quiero un montón y nos quedan más comilonas en la Mola por compartir!

Gràcies al grup més heterogeni, el Primavera/Estiu/Tardor/Hivern 2015-actualitat... Hem compartit moltes coses, moltes nits a la Rasa, molts Sant Joans i estius al càmping, sopars, calçotades improvisades... Us estimo molt i espero que tornem de càmping aviat!

Gracias a los Nananá, que aunque nos veamos poco siempre son todo risas. Tal vez nunca os perdone lo de las falsas telas ignífugas, pero hay que admitir que hicieron el apaño y nos quedó una barbacoa de pm... La siguiente comida pa' cuándo? Mire y Fabi, la boda pa' cuándo?

Vaig tenir molta sort en poder compartir la carrera amb la millor classe que existeix al món. Els BQs sexys amb què he compartit les apassionants classes de BioCel, les diapositives del Daban, la follada de Bioquímica Clínica, nits a Mundo i 20000 sopars de Nadal que ja són sagrats. Sou els millors i sé que aconseguireu tot el que us proposeu! M'agradaria fer una especial menció a la penya croquetaire, amb qui he pogut compartir estiu rere estiu, acumulant experiències com les QSMs, l'strip-Pato, els mosquits del John i la Julie i posar-me gordo menjant crusants a Blanes...

Gràcies també als BBQs de verdat, aka doresilas. He redescobert el que és un grup d'amics amb vosaltres. M'he sentit estimat i acollit des del dia 1, i des d'aquell moment no hem parat de fer coses. Cercatasques, bbqs, dinars al Vil·lar, Alquézar x2, room escapes, prendre algo a la Sardana... No us vull perdre mai, encara ens queden moltes històries per escriure junts.

Gracias también a ti, que desde hace tres años me has hecho la persona más feliz del mundo. Puede que sólo sea una forma de hablar, porque ha sido en estos tres años en los que se ha desmoronado todo lo que creía cierto y he tenido que empezar a construirme a mí mismo, pero has estado siempre ahí, apoyándome y enseñándome el camino correcto. No ha sido fácil, no lo está siendo, y no lo será, para ninguno de los dos, pero si miramos hacia atrás nos está quedando un camino precioso, del cual tenemos que sentirnos muy orgullosos. Me muero de ganas por ver hacia dónde nos va a llevar... seguro que hacia una casa con un baño japonés! Es broooma... Te quiero.

Tú también me has traído una família política a la que adoro. Gracias Amparo por todo el amor y cariño que me das, por enseñarme a ver la vida con actitud desenfadada y desafiante, que a veces tanto necesito. De la misma manera, gracias Iván, Manolo, Maite, Cris, Noel, Bea, Pepe, Raquel, Danae, Gris, Wilson, Dani, Maruchi, Mayka, toda la família de Sant Carles, por haberme hecho sentir uno más. Os quiero mucho.

Y por último, mi familia. Lo que más quiero en el mundo. Si a algo le estoy agradecido a la vida es haber nacido rodeado de amor, de ejemplos de lucha y superación. Si tengo una aspiración en la vida, es parecerme a las mejores cosas de mis padres, y poderlas transmitir a mis hijos. Gracias a todos por haberme hecho tan feliz, por los viajes que hemos compartido, las comidas, los días en Calafell, las tardes de playa en Altafulla, los desayunos en Can Solà... No puedo volver al pasado, y menos mal porque sino me quedaría en él, siempre con 8 años, pero un futuro con vosotros también es maravilloso.